DOCTORAL THESIS

Development and Evaluation of Mechanical Joints for Composite Floor Elements with Cross Laminated Timber

Nicolas Jacquier

LULEÅ UNIVERSITY OF TECHNOLOGY

LULEÅ
TEKNISKA
UNIVERSITET

DOCTORAL THESIS

Development and Evaluation of Mechanical Joints for Composite Floor Elements with Cross Laminated Timber

Nicolas Jacquier

Luleå University of Technology
Department of Civil, Mining and Environmental Engineering
Division of Structural and Construction Engineering
–
Timber Structures

SE-97187 Luleå
Sweden

Printed by Luleå University of Technology, Graphic Production 2015

ISSN 1402-1544
ISBN 978-91-7583-307-1 (print)
ISBN 978-91-7583-308-8 (pdf)

Luleå 2015

www.ltu.se

Development and Evaluation of Mechanical Joints for Composite Floor Elements with Cross Laminated Timber

Nicolas Jacquier
Avdelning för byggkonstruktion och production
Instutitionen för samhälsbyggnad och naturresusrser

Som med vederbörligt tillstånd av Tekniska fakultetsnämnden vid Luleå Tekniska Universitet för avläggande av teknologie doktorsexamen kommer att offentligt försvaras:

Sal F1031, Luleå Tekniska Universitet
Torsdag den 7 maj 2015, 10.00

Opponent:	Tekn. Dr. Massimo Fragiacomo, Department of Architecture, Design and Urban Planning, University of Sassari, Alghero, Italy
Betygsnämnd:	Professor Robert Kliger, Department of Civil and Environmental Engineering, Structural Engineering, Chalmers University of Technology, Sweden
	Professor Annika Mårtensson, Department of Building and Environmental Technology, Structural Engineering, Lund Insitute of Technology, Sweden
	Professor Mats Ekevad, Department of Engineering Sciences and Mathematics, Wood Science and Engineering, Luleå University of Technology, Sweden
Huvudledare:	Professor Lars Stehn, Byggkonstruktion och produktion, Träbyggnad, Luleå Tekniska Universitet
Biträdande handledare:	Professor Ulf Arne Gihammar, Byggkonstruktion och produktion, Träbyggnad, Luleå Tekniska Universitet

Luleå April 2015

Preface

I gratefully acknowledge Stora Enso Timber, the County Administrative Board in Norrbotten, the Regional Council of Västerbotten, the European Union's Structural Funds – The Regional Fund, the centre for Lean Wood Engineering, and the Swedish governmental agency for innovation systems (VINNOVA) for their financial support to this project.

I warmly thank my supervisors Lars Stehn and Ulf Arne Girhammar for their continuous guidance during these five years. I am grateful to Helena Lidelöw for her advice and fruitful discussions. I am also grateful to Mattias Brännström for his involvement in this project from the research and development point of view. I would also like to thank the representatives of Stora Enso Timber, Janne Manninen, Hermann Kirchmayr and Mauri Konttila, for the industrial collaboration. I am thankful to Ari Kevarinmäki at VTT Expert Services laboratories and Lars Åström at LTU Complab laboratories concerning the experimental testing. Many thanks to all the people that I had the chance to meet and work with at the Timber Structures research group and at Luleå University of Technology during this period.

Last but not least, I am very thankful to my family and close friends for giving me all the moral support that I needed to complete this work. I really appreciated your encouragements. This was very important for me.

Luleå, April 2015

Abstract

One of the important issues in the development of a multi-storey timber construction system is the definition of the floor solution. This thesis focuses on the development of composite floor solutions where Cross Laminated Timber (CLT) panels are used as a base element. Preliminary investigations on shear connections between prefabricated concrete beams and CLT panels were performed. The focus is on investigations on glulam-CLT composite beam elements, and the mechanical shear connectors used to achieve composite action.

The new shear connections system evaluated in this thesis for glulam-CLT floor elements consists of double-sided punched metal plate fasteners. In order to secure the shear connection made with double-sided nail plates and to improve the shear behaviour of the joint, a combination with inclined self-tapping screws was evaluated through a shear test programme. It was found that the double-sided punched metal plate fasteners and inclined screws can effectively be combined.

Bending tests (6.4 m span) were carried out using double-sided nail plates as shear connectors, with and without combination with inclined screws. The double-sided nail plate connectors did behave satisfactorily in terms of strength and stiffness for the beam design considered, even when not combined with screws. It is however suggested that further research should be carried out before using double-sided nail plates as the sole shear connection in timber composite floor elements. It was found that, for the design and load case considered, the new shear connection system performs satisfactorily and could fulfil necessary design criteria. It is considered that the shear connection system may be suitable for floor spans up to 7 meters. Further research is necessary in order to assess the behaviour of double-sided nail plates under long term loadings and, combined shear and separation forces.

An analytical linear elastic model for the stiffness of inclined screw joints was derived. This model takes into account the dowel and withdrawal action of the screw as well as the friction between the timber members. The linear elastic model is general and allows prediction of the load-deformation behaviour of inclined screw joints in shear tension in the serviceability limit state for different angle inclinations. One of the advantages of this model is that different material properties and geometries can be used in each of the jointed members. The model is found to be appropriate for inclination angles between 30 and 60 degrees between the screw axis and the normal to the shear plane. Further material testing is necessary in order to obtain certain material parameters for this model.

Sammanfattning

En av de viktigaste frågeställningarna i utvecklingen av ett träbyggsystem för flervåningshus är lösningar och definition av bjälklagen. Denna avhandling fokuserar på utveckling av samverkansbjälklag där massivträ (Cross Laminated Timber, CLT) skivor används strukturellt. Preliminära undersökningar av beteendet hos ett skjuvförband mellan prefabricerade betongbalkar och CLT har utförts. Huvuddelen av avhandlingen behandlar undersökningar och analys av samverkanselement av limträ och CLT och speciellt de mekaniska skjuvförbindare som använts för att uppnå samverkan.

Det nya skjuvförbandet som utvärderas är ämnat för ett samverkansbjälklagselement av limträ och CLT och består av dubbelsidiga spikplåtar. För att säkra förbandet mot eventuella separationskrafter och för att utvärdera om och hur den skjuvupptagande förmågan förändras utvärderades en kombination av lutande skruvar och de dubbelsidiga spikplåtarna i experimentella tester. Det visade sig att de dubbelsidiga spikplåtarna och lutande skruvar effektivt kan kombineras.

Böjtester utfördes på bjälklagselement av limträ och CLT (6,4 m spännvidd) som var sammanfogade av de dubbelsidiga spikplåtarna, med eller utan en kombination med lutande skruvar. Det visade sig att förbandet betedde sig tillfredsställande, även utan lutande skruvar, ur hållfasthet och styvhetssynpunkt för de lastfall som beaktats. Resultaten pekar på att ett bjälklagselement sammanfogat av dubbelsidiga spikplåtar bör vara lämpligt för bjälklag med spännvidder upp till 7 m. Dock föreslås att ytterligare undersökningar bör genomföras innan dubbelsidiga spikplåtar kan föreslås som enskilt förband för att åstadkomma ett samverkansbjälklag i trä (limträ eller/och CLT). Ytterligare forskning behövs för att bedöma beteendet hos dubbelsidiga spikplåtar för långsiktig belastning och kombinationen skjuv- och separationskrafter.

En analytisk linjärelastisk modell för att bestämma styvheten för lutande skruvförband härleddes och presenteras i avhandlingen. Denna modell tar hänsyn till dymlingseffekter och utdragskrafter av skruven samt friktionen mellan träkomponenterna. Den linjärelastiska modellen är generell och beskriver last – deformationsbeteendet av lutande skruvförband utsatt för skjuvspänning i bruksgränstillstånd för olika lutningar på skruven. En av fördelarna med denna modell är att olika materialegenskaper och geometrier kan användas i var och en av de skarvade träkomponenterna. Modellen har visat sig vara tillämplig för lutningsvinklar mellan 30 och 60 grader mellan skruvaxeln och normalen till skjuvplanet. Ytterligare materialtestning krävs för att erhålla vissa kritiska materialvärden för denna modell.

Table of contents

Part I

1 Introduction

1.1 Background – Multi-storey timber construction

Timber construction has gained interest for the last decades due to political incentives aiming at reducing emissions of carbon dioxide in construction on one hand, and on the other hand due to the evolution of the building codes, the emergence of new engineered wood products, tools, and mechanical fasteners, which broaden the range of timber construction possibilities. The development of multi-storey timber construction is therefore increasing and is also driven by the perspectives of rapid erection using new assembly methods and prefabricated elements. Projects with 8 to 10 storeys have been completed in several places in the world during the last 10 years (Fig. 1) and projects with up to 14-storey are currently under construction.

Fig. 1: Recent multi-storey buildings made with Cross Laminated Timber

Multi-storey timber buildings are complex constructions due to demanding functional requirements in terms of safety and comfort of occupants. The main engineering issues are the building stabilisation, fire safety, vibration and acoustic performance. In addition, aspects such as prefabrication level, ease of assembly on site (buildability), or aesthetics have also to be considered in order to produce economically optimised building solutions. More than with other construction materials, these issues have a high interdependence. The conceptual design of the technical solutions for these construction systems should therefore be carried out considering these aspects simultaneously in order to obtain a satisfactory result (Kolb, 2008; Ringhofer & Schickhofer, 2014; Smith & Frangi, 2008).

Among the different actors in the timber construction industry, the company Stora Enso Timber has been developing different construction and building systems for the European markets using primarily Cross Laminated Timber (CLT) since 2008. The company developed integrated building system solutions based on the so-called “platform” construction system for Finland and Sweden from 2010. These were intended for multi-storey residential buildings, and possibly for other applications (office, hotel and public buildings). The present thesis focuses on structural aspects of prefabricated floors elements developed in this context and made with CLT, and with emphasis on the shear connection system. A more detailed description of the research context is presented in Chapter 2.

1.2 Timber composite floors

Timber composite structures have been built for decades using various kinds of mechanical fasteners (Fig. 2). Their behaviour started to be investigated thoroughly in the 1950s. Möhler (1956) presented the first solutions to the governing differential equations for deformation and internal stresses in mechanically jointed timber beams and columns. This work formed the basis for the so-called γ-method given in the Eurocode 5 (CEN, 2014) for the design of timber composite beams and columns with partial interaction.

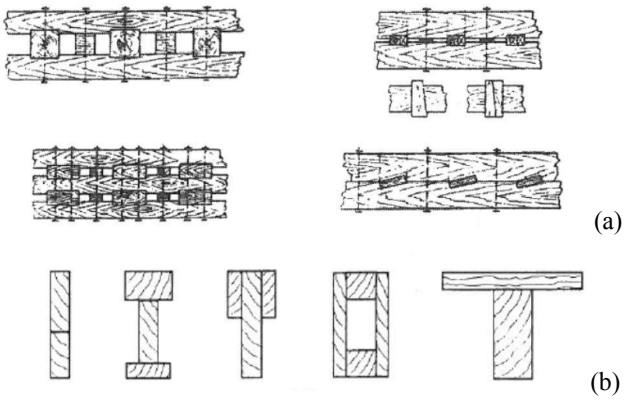

Fig. 2: (a) Old and (b) modern construction examples of timber composite structures (beams and columns) (Ceccotti, 2003)

The role of the mechanical fasteners (or shear connectors) in a composite structure is to transfer shearing forces between the different members while providing a certain level of composite action. The stiffer the shear connection, the higher the level of composite action and therefore the lower the vertical deformation of the floor structure under transverse loading (see Fig. 3). Knowledge on the behaviour of the shear connectors (strength and stiffness) is therefore crucial for the design of composite structures.

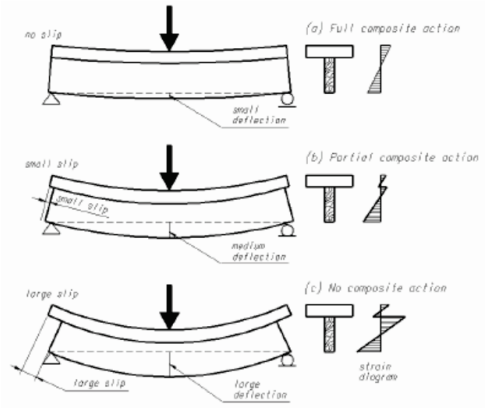

Fig. 3: Influence of the level of composite action on the deformation of composite elements in bending (Lukaszewska, 2009)

Modern timber composite structures are commonly made with structural glue or with mechanical fasteners (see Fig. 2-b). Even though modern glues allow the manufacture of strong and reliable shear connections for timber composite systems, the use of mechanical fasteners is still actual and relevant for the situations where gluing is not possible due to economic or practical reasons (prefabrication, ease of assembly, on-site assembly or renovations) (Ceccotti, 2003).

1.3 Mechanical shear connections

Mechanically jointed timber composite systems can be built with most of the traditional timber fasteners: nails, screws, bolts, and dowels. Nails are often used for the assembly of relatively thin wooden panels to timber joists (e.g. stress skinned panels). Screws can be used for thicker assemblies. The advantage of using screws is that the joint can benefit from the high withdrawal strength and stiffness of the threads. When used in an inclined position, the withdrawal contribution increases and the screws can provide high load-carrying capacity and stiffness compared to joints with vertical screws (Bejtka & Blass, 2002; Kevarinmäki, 2002).

For rapid assembly of timber members in factory, punched metal plate fasteners are a potentially interesting alternative to other traditional shear connectors. Single sided punched metal plate fasteners have been used since the 1950's to produce roof trusses and are popular in Scandinavia (Whale, 1995). Punched metal plate fasteners have been also used to produce composite timber-timber members (Fig. 4).

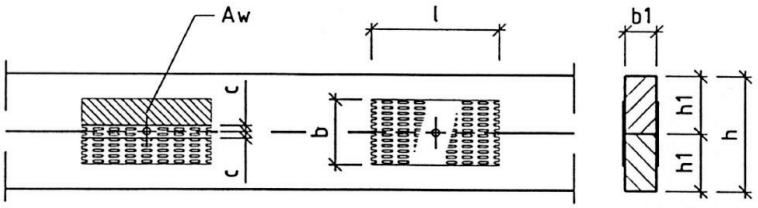

Fig. 4: Timber-timber composite beam element made with punched metal plate fasteners according to Z-9.1-210 (DIBt, 2005)

Double-sided punched metal plate fasteners (also called double-sided nail plates (DSNP) for short) (Fig. 5) have been developed in order to produce fire protected and aesthetic joints in trusses (Zhou & Guan, 2011). Their usage is in practice not common and most of these fasteners remain at the prototype level. These fasteners may however be able to provide a high level of composite action compared to other types of mechanical fasteners due to the large timber area that can be mobilised.

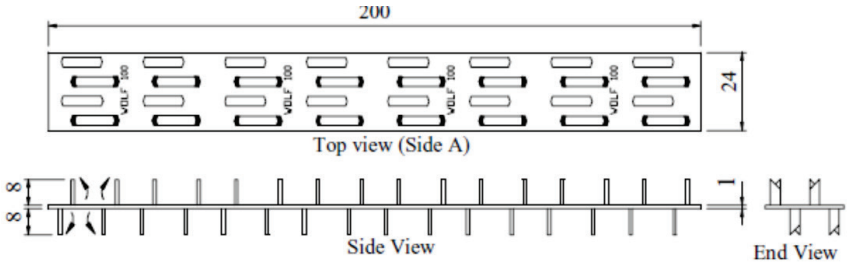

Fig. 5: Example of double-sided nail plate fastener by (Zhou, Rodd, Guan, & Pope, 2004), (dimensions in mm).

1.4 Combining different mechanical fasteners

Punched metal plate fasteners are installed by being pressed into the timber members. They have by nature a limited resistance to separation forces. Concerning the double-sided nail plates used as shear connectors in mechanically jointed T-cross-sections (i.e. CLT panel connected to a glulam beam as shown in Fig. 6), there might be a risk of separation under certain loading situations (for example during element handling or in the case of hanging loads). For this reason, a combination with another type of mechanical fastener such as screws could improve the resistance against separation forces. This could secure the shear connection and increase the level of structural safety of the system. Considering that inclined screws may provide a positive effect on the double-sided nail plate behaviour by introducing compressive forces between the timber members, the combination of double-sided nail plates and inclined screws is considered in this thesis.

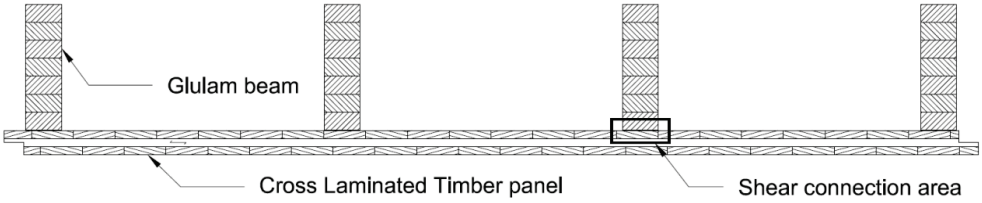

Fig. 6: Example of a CLT-glulam ribbed floor element with CLT on the bottom side. (Note that only the structural part of the floor element is shown and that this orientation with the CLT at the bottom is the actual configuration which is considered and presented in more detail in the Research Context chapter)

The combination of punched metal plate fasteners and screws forms a so-called "multiple fastener joint" with fasteners of different type. Such a combination requires the compatibility of the load-deformation behaviour of the different types of mechanical fasteners to be investigated (CEN, 2014). One aspect of the work presented in this thesis is therefore to characterise the behaviour of double-sided punched metal plate fasteners used as shear connectors and to evaluate the compatibility and relevance of a combination with inclined screws in a timber composite system.

1.5 Aims and research questions

The overall aim of the work presented in this thesis is to discuss the possibilities of using new types of shear connections for timber composite floor elements in a particular building system development context. This objective can be divided in several smaller and more specific aims. One of these is to investigate the behaviour of double-sided punched metal plate fasteners used as shear connectors in timber composite floor elements with CLT. In addition this work aims at providing a better understanding of how the combination of different types of mechanical fasteners should be treated since the combination of double-sided nail plates and screws is considered in this floor system development. The fact that screws are considered in the combination implies that this work also includes the evaluation of analytical models used to predict the load-displacement behaviour of joints with inclined screws. A specific focus is put on the serviceability limit state due to the fact that floor vibration design criteria often govern the design of timber floors.

The following research questions are formulated:

- **RQ 1**: How do double-sided punched metal plate fasteners perform as shear connectors in timber composite floor elements?
- **RQ 2**: How can the combined effect of different types of mechanical fasteners in a timber joint be considered?

- **RQ 3**: How can we model the stiffness of inclined screw joints in shear-tension in the serviceability limit state?

1.6 Limitations

The experimental work presented in this thesis is restricted to the short-term behaviour of the mechanical fasteners and structures analysed. Dynamic, cyclic and long-term effects and behaviour under fire and changing moisture conditions have not been evaluated. Also, it should be considered that the evaluations presented concern proprietary fasteners, and that further investigations are necessary in order to extend the results to other similar types of fasteners.

1.7 Appended papers and contributions

Paper I *"Tests on shear connections in prefabricated composite cross-laminated-timber and concrete elements"*, Nicolas Jacquier and Ulf-Arne Girhammar (World Conference on Timber Engineering, 2012) (Published)

> The paper presents the results of an experimental test programme on special shear connection system for connecting prefabricated concrete beams to CLT panels. The load-carrying capacities and slip modulus values for the different joint configurations test are reported. The failure modes are analysed and a partially composite timber-concrete floor design is discussed. Nicolas Jacquier has designed and carried out the tests, and reported the results. The analysis of the tests and writing of the paper were done jointly with Ulf Arne Girhammar.

Paper II "*Tests on Glulam-CLT shear connections with double-sided punched metal plate fasteners and inclined screws*", Nicolas Jacquier and Ulf Arne Girhammar (Construction and Building Materials, 2014) (Published)

> The paper presents the experimental results of shear tests performed on glulam-CLT joints made with double-sided punched metal plate fasteners, inclined screws, and joints with both fasteners types combined. The compatibility and the combination effect of the different fasteners types are discussed and a simple calculation method based on calculation models available in the literature is proposed for the design of combined joints with these types of fasteners. Nicolas Jacquier's contributions in this paper are the design of the experimental programme, the planning and run of the tests. In addition, the evaluation of the tests, the analysis and the writing of the paper was done by Nicolas Jacquier. Ulf Arne Girhammar has provided guidance along the test planning and analysis, and participated in the writing of the paper.

Paper III *"Evaluation of bending tests on composite glulam-CLT beams connected with double-sided punched metal plates and inclined screws"*, Nicolas Jacquier and Ulf-Arne Girhammar (Construction and Building Materials, 2015) (Accepted for publication – Under revision)

This paper presents experimental results of bending tests performed on composite glulam-CLT beam elements assembled with inclined screws, double-sided nail plates, or combined double-sided nail plates and inclined screws, as well as the results of a bending test on a glulam-CLT beam assembled with screw-gluing. The behaviour of double-sided nail plates as a shear connector in a bending situation is evaluated and the relevance of the combination of screws with double-sided nail plates is discussed. The serviceability design criteria of the Finnish National Annex of the Eurocode 5 are considered for the practical evaluation of the composite beams tested. Nicolas Jacquier's contributions in this paper are the design of the experimental programme, the planning and run of the tests. The evaluation of the tests, the analysis and the writing of the paper was also done by Nicolas Jacquier. Ulf Arne Girhammar has provided guidance along the test planning and analysis, and participated in the writing of the paper.

Paper IV *"Stiffness model for inclined screws in shear-tension in timber-to-timber joints – Part 1: Derivation of the model"* Ulf Arne Girhammar and Nicolas Jacquier (Draft to be submitted)

This paper is the companion paper of Paper V. The paper presents a stiffness model for timber-to-timber joints with inclined screws in shear-tension. The dowel and withdrawal action of the screw are considered as well as the friction between the timber members. The model is simplified in the way that the screw is assumed rigid and that the withdrawal stresses along the screw are assumed evenly distributed. The behaviour of the model is discussed and the contributions from the friction, the dowel and withdrawal actions are illustrated. Comparisons with other stiffness models are discussed. Nicolas Jacquier has initiated and noted the need for this study and given the background and basis for some existing stiffness models. Ulf Arne Girhammar has developed the model, but Nicolas Jacquier has derived some secondary equations and supported in this evaluation and presentation of the model.

Paper V *"Stiffness model for inclined screws in shear-tension in timber-to-timber joints – Part 2: Evaluation and parameter study"* Nicolas Jacquier (Draft to be submitted)

This paper is the companion paper of Paper IV. The model derived in the companion paper requires the specific input values for the embedding and withdrawal stiffness of the inclined screws. This paper discusses how these parameters should be determined

experimentally. Similar values available for these material parameters in the literature are gathered and used as input for the stiffness model. The sensitivity of the model around these values is discussed through a parameter study. The model also presents some comparisons with existing inclined screw joints tests results. Nicolas Jacquier's contributions in this paper are the suggestion for experimental tests, the collection of input values and test results from the literature, the parameter study and discussion.

1.8 Additional publications

Technical Report - *"Shear tests on glulam-CLT joints with double-sided punched metal plate fasteners and inclined screws"* – Luleå University of Technology - Nicolas Jacquier (2014) (Published)

Technical Report - *"Bending tests on glulam-CLT beams connected with double-sided punched metal plate fasteners and inclined screws"* - Luleå University of Technology - Nicolas Jacquier (2015) (Published)

2 Research context

This chapter presents in more details the context in which this research has been carried out and describes the motives for the different studies presented in this thesis.

2.1 Building system development and requirements

The investigations performed along this research project follow the development of a multi-storey timber building system primarily based on Cross Laminated Timber (CLT). This building system was developed by the company Stora Enso Timber essentially for Finland and Sweden. The development of this system implies the consideration of certain aspects such as structural and building physics requirements, defined prefabrication level, as well as limitations in production facilities and supply chain. Stora Enso followed a so called open building system scheme for multi-storey timber construction in Finland called RunkoPES (Finnish Wood Research, 2013), influencing their development.

The CLT based building system considered in this context can shortly be described as a flat platform frame element system (walls, floors and possibly roof elements) with a rather large degree of prefabrication. By prefabrication, it should be understood that the CLT based structural components are not only CLT panels pre-cut to the right dimensions. The CLT panels are completed in a factory with additional functional layers before delivery to the construction site for further assembly. The wall elements are usually prefabricated from the inner gypsum board to the facade including windows, and the cassette floor elements are also prefabricated to a large extent, including possible technical installations in the elements and part of the floating floor. Multi-storey buildings are understood as multi-family buildings from over 2 to 10 storeys high.

As pointed out by Smith and Frangi (2008), and by Ringhofer and Schickhofer (2014), the design of a multi-storey timber building system is an interdisciplinary task where multiple requirements have to be considered already from the conceptual design phase. In addition to the basic structural design requirements, fire safety, acoustic performance, durability and buildability should be considered. Depending on the construction details, these issues can be highly interrelated and their simultaneous consideration is essential. The work carried out and presented in this thesis specifically concerns the floor element and the solutions investigated were influenced by these interdisciplinary considerations. The aim of this research context chapter is to briefly present the additional aspects considered in this development.

From a structural point of view, the floor structure needs to have the required bending stiffness to satisfy the necessary demands in terms of span length while minimising the floor height for economic reasons. One of the demands in this context was to create a cassette floor

element where the CLT panel would be located at the bottom of the floor element, as one of the possibilities to fit into the RunkoPES open building system (Finnish Wood Research, 2013) as shown in Fig. 7 and Fig. 8.

This configuration was also suggested because it has the following advantages:

- The CLT panel placed at the bottom acts as a fire cell separation between different functional units in the building and can provide a certain fire resistance even if it is left visible for aesthetic reasons. This resistance can be further increased by the addition of gypsum boards.
- The large timber area offered by the CLT plate on the tensile side of the floor loaded in bending is beneficial from a static design point of view, making possible in a composite cassette floor element to develop a more ductile failure with compression failure in the upper timber joists.
- The structural floor is completed by a loosely connected floating floor lying on a step sound insulation substrate (e.g. Sylomer, see Fig. 8) in order to form a mass-spring-mass system, beneficial in terms of airborne and step sound insulation (Bartlomé & Liebl, 2014). There is therefore no composite action contribution from the upper part of the floor.
- With the present configuration the need for a suspended ceiling, which is considered to be costly in the Nordic countries, can be avoided. With respect to on-site completion work, placing the CLT at the bottom of the floor element was also considered as way to reduce the amount of work to be done from the storey below to obtain the finished ceiling surface. This is considered beneficial from the working environment point of view.

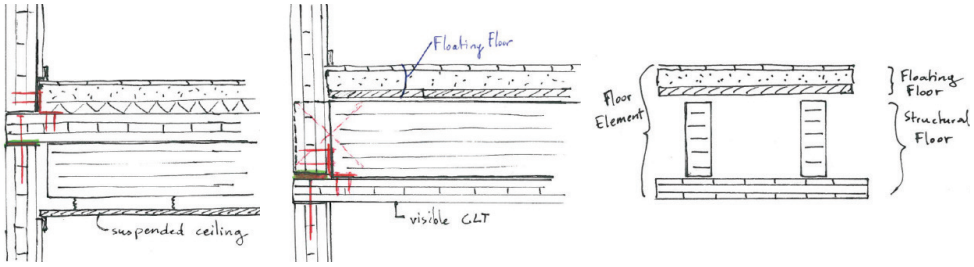

(a) (b) (c)

Fig. 7: Conceptual floor element configuration: example sketches of wall–to-floor joint early details (a) with CLT at the top requiring a suspended ceiling, (b) "upside down" configuration with CLT at the bottom and floating floor (avoiding the need for a suspended ceiling), (c) "Upside down" CLT-glulam floor element (structural floor + floating floor) floor cross-section.

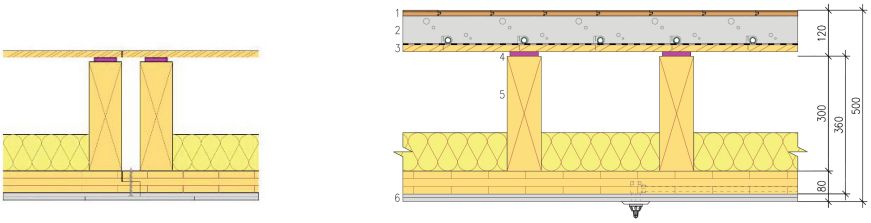

Fig. 8: Extracts of floor configurations with CLT-glulam floor elements from RunkoPES 2.0 (Finnish Wood Research, 2013) – Legend - 1: parquet flooring; 2: cement screed; 3: wood based panel; 4: Sylomer or equivalent; 5: structural floor glulam-CLT; 6: gypsum boards, (dimensions in mm).

It has to be noted that this configuration of the floor element presents also some drawbacks. One of them is related to the risk of damage due to accidental excessive moisture especially if technical installations run through the floor element (water damage) which may cause the CLT to rot in a hidden manner as was exemplified in Ringhofer and Schickhofer (2014). The authors also raised the question of the replacement of damaged CLT panels in a multi-storey building, which cannot be easily answered. These aspects have not been taken in consideration in the present development work.

In the end, the balanced consideration of the advantages and disadvantages of the system solution have to be weighted. In the present context, the balance was in favour of a system where the CLT panel is positioned at the bottom of the structural part of the floor element. The following sections present the development context regarding specific cases which were investigated for cassette floor elements made with CLT; a preliminary study on CLT combined with prefabricated concrete beams, and the main study concerning the cassette floor element with CLT and glulam beams.

2.2 CLT-concrete prefabricated floor system

Timber-concrete composite structures have been investigated as early as from the second quarter of the 20th century as reported by Van der Linden (1999). The early works focused on timber concrete bridges in the USA (McCullough, 1943). The interest for timber-concrete structures and especially timber concrete floors has further increased during the last 20-30 years for renovation and new construction purposes. Usually built as timber floor joist completed with a concrete slab and connected via mechanical fasteners, timber-concrete structures aim at taking advantage from the best of both materials, with the concrete at the top loaded mainly in compression and the timber at the bottom loaded in tension.

The fact that concrete is a wet component in a mostly dry construction process brings some issues as pointed out in Lukaszewska (2009). The main issues are the necessary concrete

curing time, the low stiffness of the floor when the concrete is wet, therefore often a need for propping on site, and the stresses induced in the composite structure due to the concrete shrinkage. Several authors have investigated solutions for prefabricated timber concrete systems in order to develop solutions for an entirely dry manufacturing and assembly process of timber concrete composite structures (Lukaszewska, 2009), (Crocetti, Sartori, & Tomasi, 2014).

For the building systems under development considered in this research context, several configurations were proposed. One of these configurations was to place prefabricated concrete beams on top of the CLT panels to form the structural part of the floor element. This configuration is somewhat unconventional and not optimal from a structural point of view since part of the concrete remains loaded in tension when the floor is loaded in bending. In other solutions which have been investigated, e.g. (L. Jorge, Habenbacher, & Dujic, 2010), where a concrete slab is casted on top of a CLT panel, the floor element can be designed so that concrete remains loaded mostly in compression and the CLT panel underneath in tension. The reason for suggesting the use of concrete beams instead of a concrete slab was the need to run technical installations within the floor element as mentioned in section 2.1. The structural part of the floor element consists of the CLT panel and concrete beams as shown in Fig. 9. The floor element is completed by a floating floor.

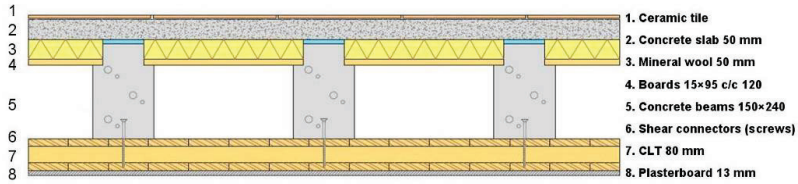

Fig. 9: Early conceptual floor element configuration of a composite floor with CLT and concrete beams (semi-prefabricated structure with beams casted on CLT) – floating floor structurally disconnected form the ribbed floor structure

One of the requirements coming from the system development context was also to produce prefabricated beam elements in order to obtain a dry assembly process, and to have the possibility to produce the beams separately in the assembly line. A shear connection system for the assembly of prefabricated concrete beams on top of CLT panels has therefore been investigated and the results of the shear tests are presented in this thesis and in Paper I.

This configuration presents nevertheless some disadvantages which can be discussed. A part of the concrete beam is loaded in tension, complicating the analysis of the structure, and therefore its design. Another disadvantage is the fact that the self-weight of the concrete beams is problematic for the vibration behaviour of the floor and therefore for the design verifications in the serviceability limit state. In addition, this mass is not distributed over the

entire floor area and therefore does not bring any advantage in terms of airborne sound insulation unlike a concrete slab. Only a preliminary study on some shear connection types was therefore performed in order to assess their strength and stiffness and to judge the technical feasibility of such a floor element. This study did not give promising enough results to justify the need for such a system. Ringhofer and Schickhofer (2013) point out that when developing timber construction systems, one should try to use existing reliable details rather than complicated in-house developments. The present timber-concrete system is presented in this thesis as a part of the development work which led to the second study, focusing on a timber-timber composite floor element made of glulam and CLT, and with the same type of configuration (CLT panel placed at the bottom of the floor).

2.3 Glulam-CLT composite floor system

In this section, some background about the glulam-CLT composite floor system is presented. Replacing the concrete beam from the system shown in Fig. 9 by glulam beams, the type of cassette floor element presented in Fig. 10 is obtained where the structural part of the floor consists of the CLT panel and glulam beams only. The upper wood based panel is loosely connected to the structural floor and does not contribute in the composite structure. This panel is installed on a step sound insulation medium and serves as the base for the cement screed. The conceptual reasons for having the CLT panel at the bottom of the floor which were described in section 2.2 are still valid for this floor element. The use of glulam beams leads to thicker floor elements than when using concrete but the design is simplified. One of the demands for the system development was to be able to rely on mechanical shear connection and to avoid using structural glue for practical reasons. The solution proposed was to connect CLT panels and glulam beams via a shear connection system made of double-sided punched metal plate fasteners, possibly combined with inclined screws.

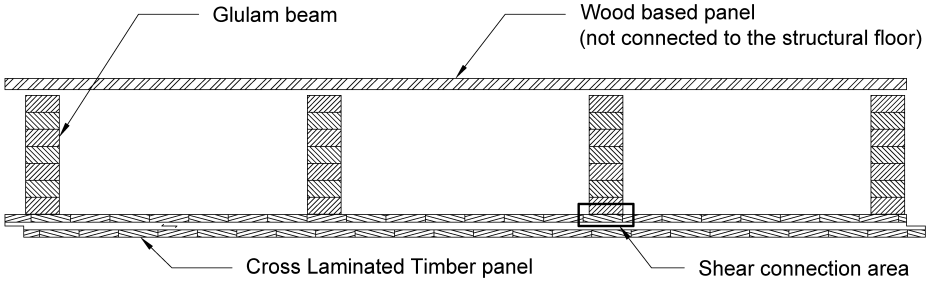

Fig. 10: Example of a glulam-CLT cassette floor element with CLT panel located at the bottom.

The Eurocode 5 (EC5) (CEN, 2014) with the Finnish National Annex (Finnish Ministry of the Environment, 2007) is the regulation that the floor element developed in this context should fulfil due to the fact that the system essentially aims at being used in Finland. These

regulations indirectly set specific requirements in terms of necessary bending stiffness due to the demands of minimum floor fundamental frequency to fulfil the vibration design criteria in the serviceability limit state. Considering the present cassette floor element where it is of interest to take advantage of all parts and therefore achieve a certain degree of composite action in order to optimise the material usage, these requirements are translated into certain demands in terms of strength and stiffness of the shear connectors.

It should be noted that the recommendations given in the EC5 and Finnish National Annex are not discussed in this thesis and that these evaluation methods are not compared with other definitions concerning the floor vibration behaviour. They have been considered because they represent the current design practice. The performance of the system studied with respect to these requirements allows therefore to evaluate the technical feasibility of the solutions proposed from a practical point of view.

As described in the introduction chapter, the focus of the study on CLT-glulam composite cassette floor elements in this context leads to the investigations on double-sided punched metal plate fasteners and their combination with inclined self-tapping screws for strengthening and system robustness reasons.

3 Theoretical background

Essential aspects concerning Cross Laminated Timber as a material and joints in Cross Laminated Timber are presented in this chapter. Theoretical models used to predict the behaviour partially composite structures are also introduced. The rest of this chapter focuses on some types of mechanical fasteners which can be utilised as shear connectors in timber composite structures. A brief background on the existing shear connection systems for timber-concrete composite systems is first presented. A more detailed background is then given for the types of timber-to-timber mechanical fasteners considered in this study, which are the punched metal plate fasteners and the self-tapping screws. Some information about the combination of different types of mechanical fasteners in a joint is also given.

3.1 Cross Laminated Timber

Cross Laminated Timber (CLT), also called X-lam, is an engineered wood product which was developed in Austria and Germany in the 1990's (Brandner, 2013). CLT is a massive timber element which can be perceived as a thick plywood panel. It is usually manufactured with dimensions of 3 m by 16 m for a thickness varying from 60 mm to 350 mm (variations exist between manufacturers). CLT is made of a number of usually odd layers of sawn timber boards which are face-glued to each other at right angles (3 to 7 layers for most of the standard panels) using a hydraulic or vacuum press. Computer Numerically Controlled (CNC) machines can be used for further cutting the panels at right dimension, creating openings for doors and windows, grooves and holes depending on the project needs. CLT is used as load bearing element in different types of structures; in single family houses and multi-storey buildings as wall, floors and roofs, but also in bridges or other types of structures such as towers for wind turbines for example.

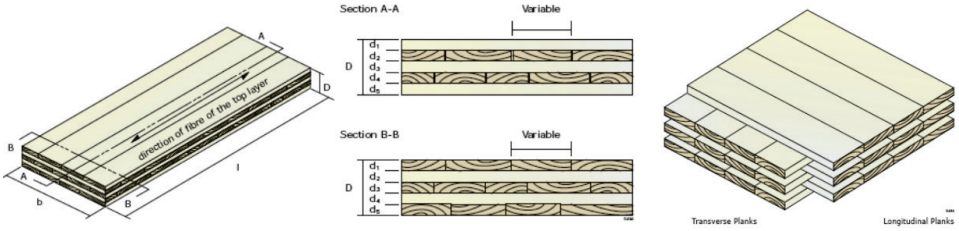

Fig. 11: Cross Laminated Timber (source: CLT Handbook FP Innovations (Gagnon & Pirvu, 2011))

3.1.1 Design of CLT panels loaded perpendicular to the plane

The grain orientation of the different layers in CLT has an effect on the behaviour of the panel. Under transverse out of the plane loading, the layers with grain direction perpendicular to the span direction will deform significantly more in shear compared to the longitudinal layers due to the low rolling shear modulus of the timber in comparison to the shear modulus in the longitudinal direction. This effect has to be taken into account. Several methods exist and can be used to consider this effect in design. CLT is therefore usually calculated as a partially composite structure.

Detailed analytical and numerical models have been derived to analyse the behaviour of CLT as orthotropic plates (Guggenberger & Moosbrugger, 2004), (Reinhard Stürzenbecher, Karin Hofstetter, & Josef Eberhardsteiner, 2010), (R. Stürzenbecher, K. Hofstetter, & J. Eberhardsteiner, 2010). However, most of the time, the design of CLT panels loaded in bending out the plane is carried out with simplified design tools as a one way spanning system. For these designs, methods such as the composite theory (also called "k-method") (H. J. Blass & Fellmoser, 2004), the gamma method (Möhler, 1956), (CEN, 2014), and the shear analogy method (Kreuzinger, 1999) are the common tools used for simplified design.

The gamma method (presented in section 3.2), or the shear analogy method, are usually used by the CLT panels manufacturers in their product approvals. These calculation methods account for the horizontal shear deformation occurring in the layers oriented perpendicular to the span direction. The shear analogy method takes also into account the vertical shear deformation in the longitudinal layers. Computer programs become necessary for the design of two ways spanning floors elements or when dealing with concentrated loadings and special floor openings, and when dealing with CLT panels made of more than five layers.

It is therefore generally accepted that the gamma method is applicable for the design of CLT members in bending considering that only the longitudinal layers are load-carrying, and that the perpendicular ones act as flexible shear connections (Gagnon & Pirvu, 2011), (Deutsches Institut für Bautechnik (DIBt), 2011). The bending stiffness of CLT panels up to 5 layers can be calculated according to the gamma method by replacing the ratio s/K in the expressions given in Eurocode 5 (CEN, 2014) by the ratio $h_{ij}/(G_R \times b)$, where s is the fastener spacing, K is the slip modulus of a single shear connector, h_{ij} is the height of the transverse layers between the longitudinal layers i and j (see Fig. 12), G_R is the rolling shear modulus and b is the width of the CLT panel. The rolling shear modulus is an important parameter as it governs the level of flexibility introduced by the CLT transverse layer. The value of G_R, which is found in most Technical Approvals, is 50 N/mm^2.

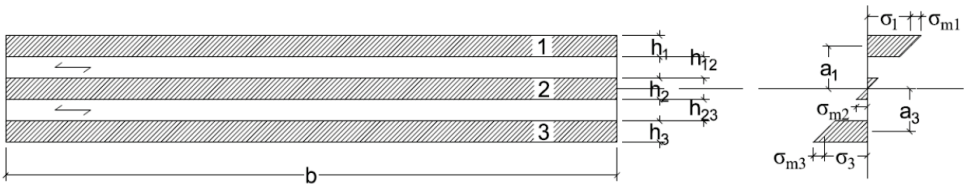

Fig. 12: Five-layers CLT cross-section and stress diagram with the notation considered in the γ-method.

The gamma method is based on the Bernoulli beam theory; therefore the shear deformations are not taken into account in the longitudinal layers. This means that is it usually considered reasonable to use the gamma method for span to depth ratios over 30. The shear analogy (Kreuzinger, 1999) is a more accurate method where the shear deformations are considered, as well as the rolling shear deformation in the transverse layers. However, the calculation requires to use a plane frame analysis program.

3.1.2 Mechanical fasteners in CLT

The crosswise orientation of the timber layers in CLT has an influence on the behaviour of mechanical fasteners in CLT. Uibel and Blass (2006) and (2007), studied the behaviour of dowel type fasteners in CLT, both on CLT face and on CLT panels edges. They derived an extension of the Johansen yield model for the strength dowel type fasteners CLT joints, taking into account different embedding strengths of the laminations depending on their orientation. It was observed that the occurrence of splitting and plug shear failure was reduced due to the natural reinforcement provided by the crosswise layer orientation in the CLT. It was also observed that joints in CLT exhibit a higher static ductility than non-reinforced and reinforced timber connections (Blaß & Schädle, 2011). Ringhofer et al. (Ringhofer, Brandner, & Schickhofer, 2013) showed that the withdrawal strength parameter of screws in orthogonal layered products (such as CLT) increases also as the number of layer increases.

3.2 Partially composite structures with CLT

This section presents in more detail the background on partially composite structures for the particular case of an assembly of CLT and glulam members. In the appendix B of the Eurocode 5 (CEN, 2014) the so-called "γ-method" gives guidelines for the design of mechanically jointed timber beams.

Since the γ-method can be used for composite cross-sections up to three layers (with two flexible layers), it can therefore be used for a glulam-CLT composite beam where the CLT element is a 3-layer CLT panel. In this work, the calculation of the effective bending stiffness according to the γ-method is presented here for the case of a composite beam element made of

a timber beam (element 1) mechanically jointed to a 3-layers CLT panel represented by the elements 2 and 3, as depicted in Fig. 13.

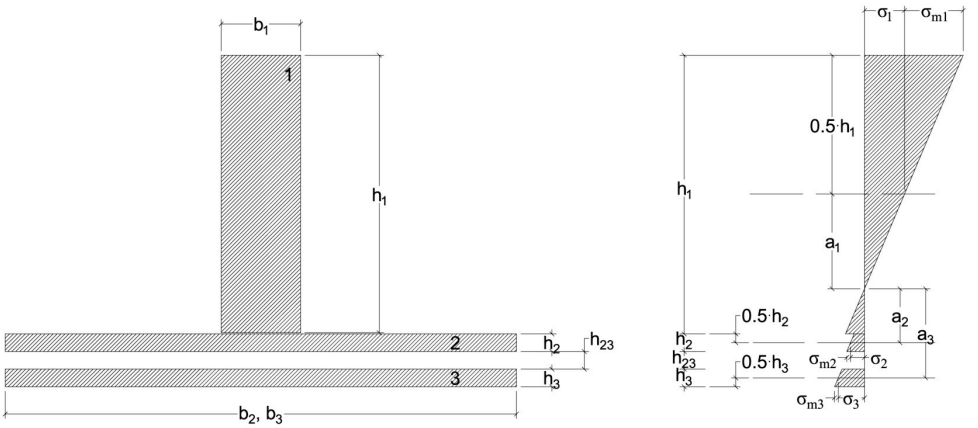

Fig. 13: Glulam-CLT cross-section and stress diagram with the notation considered in the γ-method.

The effective bending stiffness EI_{ef} of the composite glulam-CLT beam element is calculated as follows:

$$EI_{ef} = \sum_{i=1}^{3} (E_i I_i + \gamma_i E_i A_i a_i^2) \tag{1}$$

where E_i, A_i and I_i are the modulus of elasticity parallel to the grain, the area and the second moment of area of the i^{th} sub-element in Fig. 13, respectively, $\gamma_2 = 1$ and where:

$$\gamma_1 = \left(1 + \pi^2 \frac{E_1 A_1 s_1}{k_1 L^2}\right)^{-1} \tag{2}$$

$$\gamma_3 = \left(1 + \pi^2 \frac{E_3 A_3 h_{23}}{G_R b_{23} L^2}\right)^{-1} \tag{3}$$

$$a_2 = \frac{\gamma_1 E_1 A_1 \left(\frac{h_1 + h_2}{2}\right) - \gamma_3 E_3 A_3 \left(\frac{h_2 + h_3}{2} + h_{23}\right)}{\gamma_1 E_1 A_1 + \gamma_2 E_2 A_2 + \gamma_3 E_3 A_3} \tag{4}$$

$$a_1 = \frac{h_1 + h_2}{2} - a_2 \tag{5}$$

$$a_3 = \frac{h_2 + h_3}{2} + h_{23} + a_2 \tag{6}$$

The normal stress σ_i and bending stress $\sigma_{m,i}$ in each sub-element, Eq. (7) and Eq. (8), respectively, and the force F_1 in a single shear connector, Eq. (9), can be calculated according to the expressions given in the Eurocode 5:

$$\sigma_i = \frac{\gamma_i E_i a_i}{EI_{ef}} M \tag{7}$$

$$\sigma_{m,i} = \frac{0.5 E_i h_i}{EI_{ef}} M \tag{8}$$

where M is the external moment at the position of interest and h_i is the height of the sub-element evaluated;

$$F_1 = \frac{\gamma_1 E_1 A_1 a_1 s_1}{EI_{ef}} V \tag{9}$$

where V is the total shear force at the position of the fastener considered.

Conservatively, it can be assumed for the shear stress verification in the glulam that the glulam beam resists the entire shear force as suggested in (Yeoh & Fragiacomo, 2012) for the design of a LVL-concrete composite structure using Eq. (10):

$$\tau_{1,\max} = 1.5 \frac{V}{A_1} \tag{10}$$

where V is the total shear force at the position considered.

The verification which must be carried out in the CLT with respect to the shear force concerns the transverse layer with the verification of the rolling shear stresses, the rolling shear strength being much lower than the shear strength for the layers loaded parallel. The rolling shear stresses $\tau_{v,23}$ in the cross-layer can be calculated by assuming a uniform shear stress distribution over this layer equal to the shear stress level at the interface between sub-elements 2 and 3 with Eq. (11):

$$\tau_{v,23} = \frac{\gamma_3 E_3 A_3 a_3}{EI_{ef} b_3} V \tag{11}$$

A more conservative assumption is to consider that the shear stresses are distributed from the glulam beam down to the perpendicular layer with a 45° angle distribution, therefore virtually reducing the resisting width of the cross-layer. The rolling shear stress could therefore alternatively ($\tau_{v,23,\text{alt}}$) be calculated with Eq. (12):

$$\tau_{v,23,\text{alt}} = \frac{\gamma_3 E_3 A_3 a_3}{EI_{ef} (b_1 + 2h_2)} V \tag{12}$$

3.3 Timber-concrete shear connectors

Shear connections for timber-concrete composite structures have been investigated along with the development of this type of structure. Comprehensive reviews of timber-concrete shear connections systems can be found in (Van der Linden, 1999), (Dias, 2005), and (Lukaszewska, 2009). Examples of timber-concrete shear connectors are shown in Fig. 14.

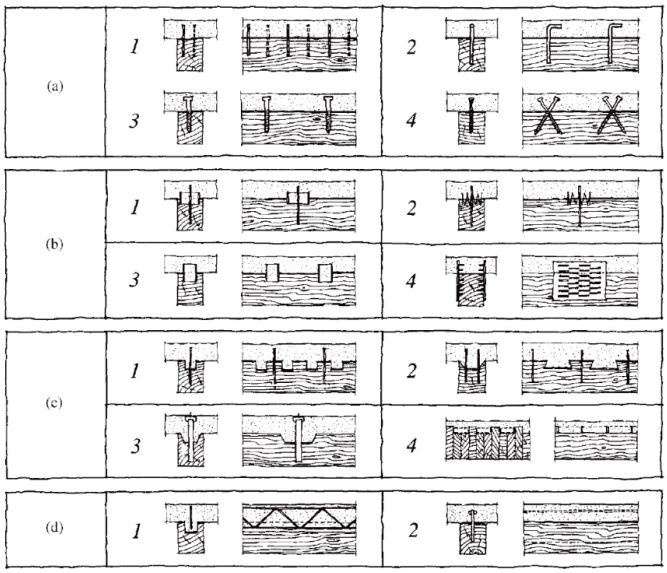

Fig. 14: Examples of timber-concrete shear connections (a1) nails; (a2) reinforced concrete steel bars, glued; (a3) screws; (a4) inclined crossed-screws; (b1) split rings; (b2) toothed plates; (b3) steel tubes; (b4) steel punched metal plates; (c1) round holes in timber and fasteners preventing uplift; (c2) square indentation and fasteners; (c3) cup indentation and prestressed steel bars; (c4) nailed timber planks deck and steel shear plates slotted through the deeper planks, (d1) steel lattice glued to timber, (d2) steel plate glued to timber – (Ceccotti, 2002)

Most of the timber-concrete shear connectors are conceived so that the assembly is made by casting concrete on top of timber members where the connectors are pre-installed. Lukaszewska (Lukaszewska, 2009) pointed out the drawbacks of the traditional assembly process for timber-concrete floors, such as the curing time, the low stiffness of the structure during curing when casting the concrete on-site, the shrinkage and moisture related issues. Prefabrication of timber-concrete structures can help to address some of these issues, either prefabricating the entire timber concrete structure off site (Lukaszewska, 2009), or by prefabricating the concrete slab before assembly to the timber members. Lukaszewska (2009) has focused on the development of timber-concrete joints with prefabricated concrete. However the solutions developed are made for connecting prefabricated concrete slabs to timber beams and cannot be reused for an assembly between CLT and prefabricated concrete beams, which is the aim of the preliminary study in this thesis (see Paper I).

3.4 Punched metal plate fasteners

3.4.1 Single-sided punched metal plates

Punched metal plate fasteners (sometimes referred to as "nail plates" for short) are traditionally used in light roof trusses structures (Fig. 15). They are used to connect the different timber members of a truss and are therefore often subjected to loadings in different directions within the same plane. They can also be used for butt joints (also called splice joints) in order to create longer members out of shorter ones (Fig. 15c).

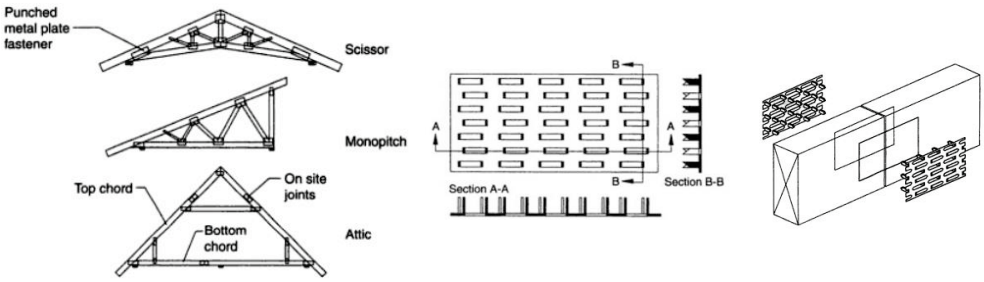

(a) (b) (c)

Fig. 15: (a) Examples of light timber roof trusses made with punched metal plate fasteners, (b) Punched metal plate fasteners, (c) Splice joints with punched metal plate fasteners (Nielsen, 2003)

The installation of punched metal plate fasteners requires the use of hydraulic pressing tools. This type of fastener is therefore suited essentially for factory production. Solutions nevertheless exist for on-site assembly using portable pressing tools or special plates designed for being hammered on site.

Punched metal plate fasteners can also be used to create composite members (stacked beams, stacked roof rafters, etc.) from timber beams stacked on each other along their narrow edge by pressing them on both sides (Fig. 16).

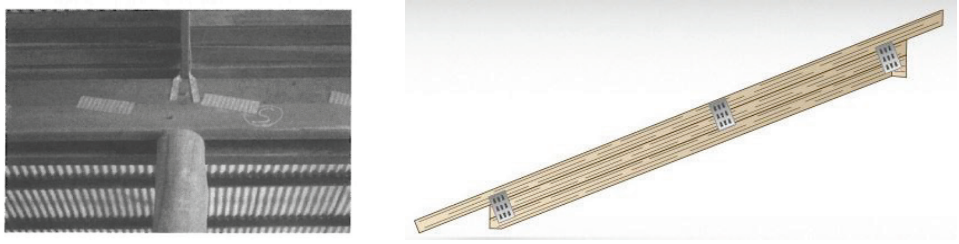

(a) (b)

Fig. 16: Examples of: (a) stacked beams (Ceccotti, 2003), and (b) stacked roof rafters (source: www.sepa.fi), made with punched metal plate fasteners.

The use of punched metal plate fasteners in horizontally mechanically laminated composite structures is limited. Folded punched metal plates were investigated in several studies on timber-concrete shear connections and floor elements (Van der Linden, 1999), (Lukaszewska, Johnsson, & Fragiacomo, 2008). In these studies the nail plates were pressed on top of glulam beams and the folded part with removed nails was sticking upwards for being casted in the concrete.

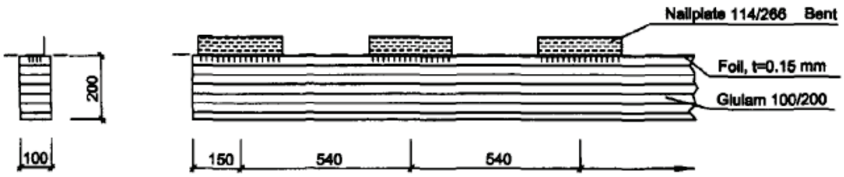

Fig. 17: Shear connection for timber concrete with folded nail plate pressed first in the glulam beam (Van der Linden, 1999), (dimensions in mm).

The same type of fastener was evaluated among other solutions for connecting prefabricated concrete slabs on top of glulam beams for floor applications (Lukaszewska, 2009). In this study on the shear connection system, the nail plate was first casted in the concrete and the cured concrete block was then pressed onto the glulam element. The results in this study show that the performance is satisfactory in terms of stiffness and strength but the assembly process is relatively complicated compared to the other solutions investigated. Bending tests have not been performed with this type of connection.

3.4.2 Double-sided punched metal plates

Double-sided punched metal plate fasteners (also called "double-sided nail plates" for short) are similar to the conventional punched metal plate fasteners but have nails punched towards both sides of the steel plate.

Studies on timber-concrete joints with double-sided nail plates were performed by Jorge (2005). It was shown that this type of connector was able to provide high slip modulus and load-carrying capacity compared to other types of mechanical fastener tested. This was, however, due to the fact that the nail plate area used in the test was relatively large. A slip modulus of 114 kN/mm and an average ultimate strength of 53 kN were obtained in a joint made of five nail plates of dimensions (200×24 mm^2).

Fig. 18: Double-sided nail plate type (plate dimensions: 200×24 mm^2) used in timber-concrete shear connections by Jorge (2005)

As an alternative to traditional mechanical fasteners and especially to nails for the assembly of mechanically laminated timber girders and posts, investigations on the behaviour of shear transfer plates (STP) (Fig. 19) have been carried out (Wolfe, Bohnhoff, & Nagel, 1993). These fasteners are relatively similar to double-sided punched metal plate fasteners, made out of a thin steel plate, but have punched projections on both faces of the plate. The essential difference between STP connectors and traditional punched metal plate fasteners is that the load is transferred across the plate in STP, while for single-sided punched metal plates the load transfer remains within the same plane.

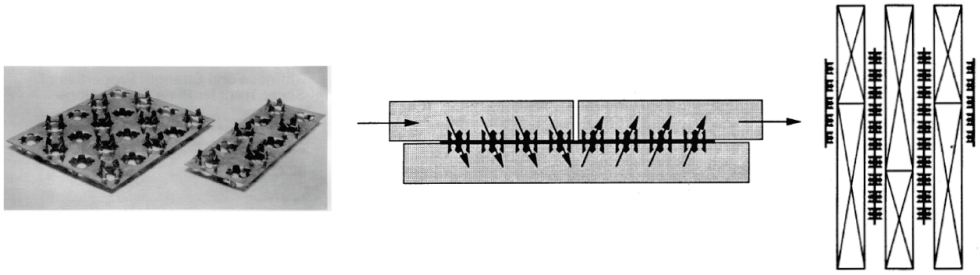

(a) (b) (c)

Fig. 19: (a) Shear transfer plates (STP), (b) butt joint with STP, (c) vertically mechanically laminated timber girder with STP (Bohnhoff, Williams, & Moody, 1998)

3.4.3 Calculation models

Punched metal plate fasteners are usually proprietary fasteners. The design verifications are often the responsibility of the nail plate or truss manufacturer. Detailed descriptions of their behaviour and design are therefore rare. In addition, their behaviour is largely related to the geometry of the plate, and therefore values can significantly vary between different nail plates producer.

The design in Eurocode 5 (CEN, 2014) specifies a set of characteristic values for different properties of the nail plate which should be determined by testing in accordance with EN 14545 (European Committe for Standardization (CEN), 2008). Eurocode 5 provides a number of general rules for the design of the joint strength using these characteristic values but does not specify any guideline regarding the joint slip. Most rules concern nail plates used in trusses and therefore subjected to simultaneous loadings in different directions. These loads are also at a certain angle with respect to the nail plate principal direction.

The load-displacement behaviour of punched metal plate fasteners is often characterised using a non-linear three parameter Foschi model (Foschi, 1977), see Fig. 20. For loadings parallel to the principal direction, the expression for the curve is given by Eq. (13):

$$P(\Delta) = \left(p_0 + k_1 \cdot \Delta\right) \cdot \left(1 - e^{\left(\frac{-k_0 \cdot \Delta}{p_0}\right)}\right) \tag{13}$$

where $P(\Delta)$ is the load for a slip Δ [m], k_0 [N/m] is the initial connector stiffness, k_1 [N/m] is the stiffness for large slip values, and p_0 [N] is the intercept of the asymptote with the slope k_1. These parameters are obtained by curve fitting from experimental test results.

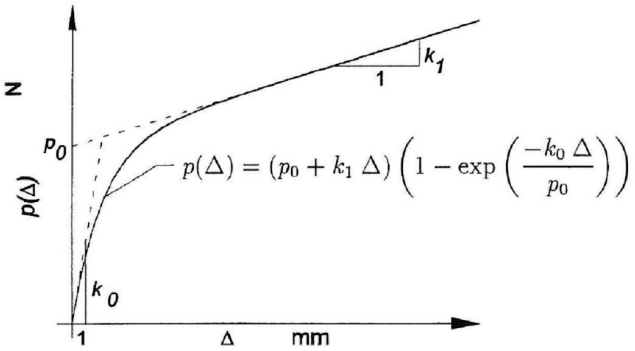

Fig. 20: Stiffness parameters of the Foschi model for the load deformation behaviour of nails (Foschi, 1977) (Figure from (Nielsen, 1996))

For nail plates used as shear connectors in the present context, the definition of the load-displacement relationship is necessary in the principal direction only, as the shear connector is not subjected to loadings in any other direction. This type of model may be used for double-sided nail plates as well.

3.5 Timber joints with inclined screws

Traditionally, screws were used to resist actions mainly in one direction: perpendicular or parallel to their axis. Recently and along the development of new screw types (self-drilling screws, very long screws, etc.), screws have been increasingly used on purpose in an inclined position with respect to the loadings in order to take advantage of the high withdrawal strength and stiffness that the screw can develop when axially loaded (Tomasi, Crosatti, & Piazza, 2010). This section presents some background about inclined screw joints in terms of strength and stiffness.

3.5.1 Joint strength

Screws are categorised as dowel types fasteners and when loaded perpendicular to their axis, their load-carrying capacity can be determined according to the Johansen's yield model (Johansen, 1949). The Johansen model takes into account the joint geometry and basic material properties such as the embedment strength of the timber members, the yield moment of the fastener, and to some extent the axial resistance through the rope effect. The design of laterally loaded screws is carried out according to this theory in Eurocode 5 (CEN, 2014). The Eurocode 5 provides also the guidelines to calculate the load-carrying capacity of axially loaded screws. For screws subjected to combined lateral and withdrawal action, the verification of the load-carrying capacity should be done considering both actions. However the recommendations given in Eurocode 5 are considered to be inadequate for inclined screws joints and too conservative (Tomasi et al., 2010).

Early works on timber joints with inclined screws were carried out by Blass and Bejkta (2000), and also Kevarinmäki (2002). Blass and Bejkta tested joints with varying angle between the screw axis and the force direction in the joint between 45° and 90°, they observed an increase of the load-carrying capacity of 53% for an inclination of 60° compared to 90°. Concerning the stiffness, the increase observed in this study was of 12 times comparing 45° and 90° angles. Bejtka and Blass (2002) proposed to determine the load-carrying capacity based on a modified Johansen yield theory model considering in addition a withdrawal parameter for the screw. A detailed presentation of the derivation and extension of the Johansen yield model for determining the load-carrying capacity of inclined screw joints was therefore presented by Bejtka and Blass (2002) for all possible failure modes. The single shear capacity of a shear connection with an inclined screw is the minimum capacity of the following six possible failure modes:

$$R_{\mathrm{a}} = R_{\mathrm{ax}} \cdot \sin\alpha + f_{\mathrm{h},1} \cdot d \cdot s_1 \cdot \cos\alpha \tag{14a}$$

$$R_{\mathrm{b}} = R_{\mathrm{ax}} \cdot \sin\alpha + f_{\mathrm{h},2} \cdot d \cdot s_2 \cdot \cos\alpha \tag{14b}$$

$$R_{c} = R_{ax} \cdot (\mu \cdot \cos\alpha + \sin\alpha) + \frac{f_{h,1} \cdot d \cdot s_1}{1+\beta} \cdot (1 - \mu \cdot \tan\alpha) \cdot \left[\sqrt{\beta + 2 \cdot \beta^2 \cdot \left(1 + \frac{s_2}{s_1} + \left(\frac{s_2}{s_1} \right)^2 \right) + \beta^3 \cdot \left(\frac{s_2}{s_1} \right)^2} - \beta \cdot \left(1 + \frac{s_2}{s_1} \right) \right] \quad (14c)$$

$$R_{d} = R_{ax} \cdot (\mu \cdot \cos\alpha + \sin\alpha) + \frac{f_{h,1} \cdot d \cdot s_1}{2+\beta} \cdot (1 - \mu \cdot \tan\alpha) \cdot \left[\sqrt{2 \cdot \beta \cdot (1+\beta) + \left(\frac{4 \cdot \beta \cdot (2+\beta) \cdot M_y}{f_{h,1} \cdot d \cdot {s_1}^2} \right)^2} - \beta \right] \quad (14d)$$

$$R_{e} = R_{ax} \cdot (\mu \cdot \cos\alpha + \sin\alpha) + \frac{f_{h,1} \cdot d \cdot s_2}{1+2 \cdot \beta} \cdot (1 - \mu \cdot \tan\alpha) \cdot \left[\sqrt{2 \cdot \beta^2 \cdot (1+\beta) + \left(\frac{4 \cdot \beta \cdot (1+2 \cdot \beta) \cdot M_y}{f_{h,1} \cdot d \cdot {s_2}^2} \right)^2} - \beta \right] \quad (14e)$$

$$R_{f} = R_{ax} \cdot (\mu \cdot \cos\alpha + \sin\alpha) + (1 - \mu \cdot \tan\alpha) \cdot \sqrt{\frac{2 \cdot \beta}{1+\beta}} \cdot \sqrt{2 \cdot M_y \cdot f_{h,1} \cdot d \cdot \cos^2\alpha} \quad (14f)$$

where $R_{ax} = \min\{R_{ax,1}; R_{ax,2}\}$, and $R_{ax,1}$, $R_{ax,2}$ are the withdrawal capacity of the screw in the first and second timber member, respectively, s_1, s_2 the anchorage depth of the screw perpendicular to the shear plane in the first and second member, respectively, $f_{h,1}$, $f_{h,2}$ the embedment strength of the first and second member, respectively, α the angle between the screw axis and the normal to the shear plane ($\alpha = 0°$ for a screw perpendicular to the shear plane, and $\alpha = 90°$ for a screw parallel to the shear plane), $\beta = f_{h,2} / f_{h,1}$ the ratio of embedment strengths, d and M_y the diameter and yield moment of the screw, respectively, and μ the friction coefficient between the timber members.

Tomasi et al. (2010) carried out push-out tests on joints with inclined screws considering different inclinations angles and different configurations (screws in shear-compression, shear-tension, crossed-screws), see Fig. 21 and Fig. 22. The angle was varied between 45° and -45°. Joints with screws in shear-compression or shear-tension correspond to the same configuration and differ by the sign of the angle. The load-slip curves clearly demonstrate the influence of the joint configuration and chosen inclination angle. The highest load-carrying capacity and stiffness based on the results of Tomasi et al. was obtained for inclined screws in shear tension with 45° inclination, (see Fig. 22).

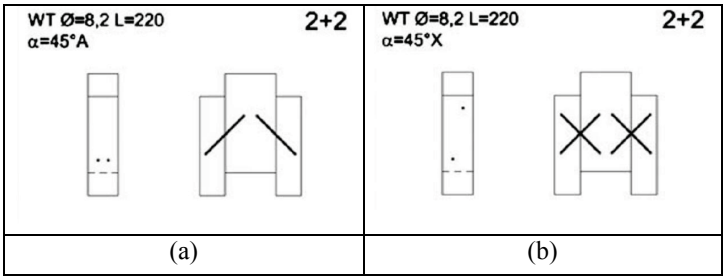

Fig. 21: Two examples of push-out tests joints configurations tested by Tomasi et al., (a) screws in shear-tension or shear-compression, (b) Cross-screw joint configuration - (Tomasi et al., 2010)

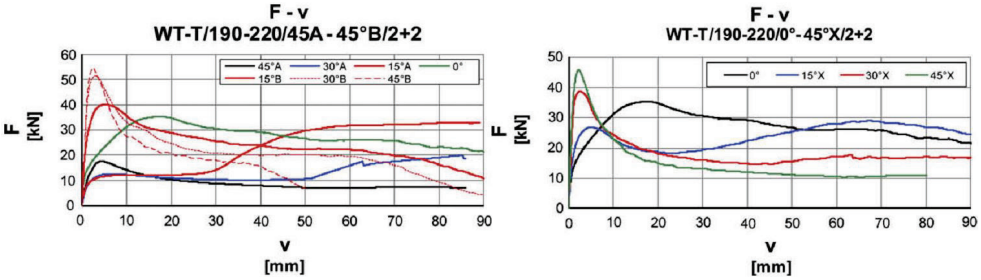

Fig. 22: Load-slip curves from push-out test for different inclination anlge correspnding to the configurations presented in Fig. 21 - (Tomasi et al., 2010)

3.5.2 Joint stiffness

In Eurocode 5 (CEN, 2014) the slip modulus K_{ser} per shear pane per fastener under service load for screwed timber-to-timber joints is calculated using Eq. (15):

$$K_{ser} = \frac{\rho_m^{1.5} \cdot d}{23} \tag{15}$$

where ρ_m is the mean density of the timber members (taken as $\rho_m = \sqrt{\rho_{m,1} \cdot \rho_{m,2}}$ when the joined timber member have different mean densities), and d is the diameter for the fastener. This expression is valid for dowels, bolts, screws and nails with pre-drilling. The expression does not take into account the fastener length, the wood grain direction or the inclination angle of the fastener with respect to the loading direction. Eq. (15) is an empirical expression which is appropriate for laterally loaded dowel type fasteners. However the stiffness of joints with inclined screws is much higher than for screw loaded perpendicular to their axis due to the withdrawal action of the screw (Bejtka & Blass, 2002) (Kevarinmäki, 2002) and this expression can for some configurations largely underestimate the slip actual slip modulus of inclined screw joints (Tomasi et al., 2010), see Fig. 22.

Kevarinmäki (2002) carried out tests on joints with inclined screws and proposed prediction models for the joint stiffness. Kevarinmäki considered different types of screws and configurations with an inclination of 45 degrees (pairs of crossed-screws and screws in shear-tension). Kevarinmäki mentioned that values for the withdrawal stiffness were missing and carried out tests to obtain values for different proprietary screws and timber materials (sawn timber and Kerto).

Kevarinmäki (2002) proposed a model based on the cosine-component of the axial withdrawal stiffness of the screw considering the friction component for joints with screws in shear tension. He pointed out the fact that the friction plays an important role in the joint stiffness for screws loaded in shear-tension, but mentioned the risk of having a gap at the interface between the timber members due to shrinkage under varying moisture conditions, or due to an untightened assembly. A small gap between the timber members may have a significant effect on the joint stiffness observed, especially on the initial stiffness. Kevarinmäki argued that in the case of crossed screw joints, there no compression force is generated at the shear plane interface since force components perpendicular to the shear plane generated by the screw loaded in shear-tension (compression) and shear-compression (separation) cancel each other. Kevarinmäki also pointed out that the slip at failure load being very small in joints with inclined screws, (1 to 2 mm for 45 degree angle), the dowel effect should not be taken into account.

Tomasi et al. (2010) proposed a calculation method for the stiffness of inclined screw joints considering both the dowel effect perpendicular to the screw axis and the withdrawal action along the screw axis. Fig. 23 shows a representation of the inclined screw joint and forces acting in the shear plane where F_{ser} is the total shearing force applied on the joint, s_1 and s_2 are the depths of the timber members measured form the shear plane, t_1 and t_2 are the screw penetration depths measured along the screw axis, H is the resulting compressive force which is developed in the shear plane due to the withdrawal resistance of the screw when loaded in shear-tension.

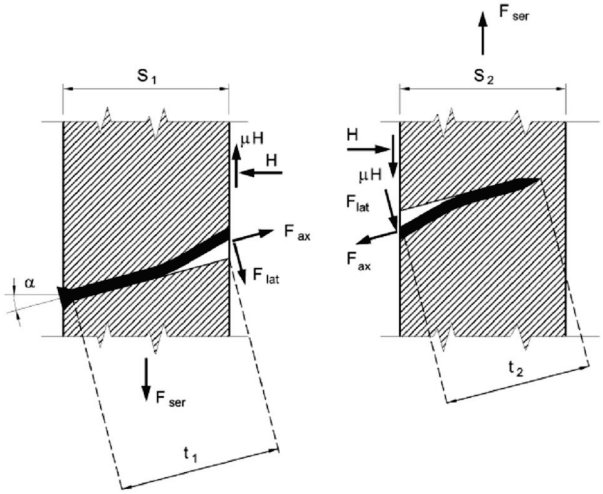

Fig. 23: Inclined screw joint representation and forces acting in the shear plane (Tomasi et al., 2010)

The slip modulus of the inclined screw joints, noted $k_{s,Tom}$, is calculated as proposed by (Tomasi et al., 2010) according to Eq. (16):

$$k_{s,Tom} = k_{\perp} \cdot \cos\alpha \cdot (\cos\alpha - \mu \cdot \sin\alpha) + k_{\parallel} \cdot \sin\alpha \cdot (\sin\alpha + \mu \cdot \cos\alpha) \quad (16)$$

where $k_{\perp}$ and $k_{//}$ [N/m] are the stiffness values of the screw with respect to forces acting perpendicular to the screw axis and along the screw axis, respectively, α is the angle between the screw axis and the normal to the shear plane, and μ is the friction coefficient between the timber members.

From Eq. (16) the authors suggest two different calculation methods depending on the interpretation made for the withdrawal stiffness parameter $k_{//}$.
The first one, which is considered to be theoretically correct, assumes that the withdrawal along the screw occurs simultaneously in each timber member. This model is referred to as the "Double Stiffness Model". The corresponding expression of the withdrawal stiffness parameter $k_{//}$ is given in Eq. (17):

$$k_{//,DSM} = \frac{1}{\frac{1}{k_{ax,1}} + \frac{1}{k_{ax,2}}} \quad (17)$$

For the second model referred to as the "Single Stiffness Model" (withdrawal stiffness parameter noted $k_{//,SSM}$ and obtained according to Eq. (18)), they argue that it can be justified to consider that the withdrawal slip occurs in one of the timber members only, referring to the

conditions in the ultimate limit state (failure observations showing that withdrawal failure occurred in one of the timber members only) and assuming the same kind of behaviour in the serviceability limit state.

$$k_{//,SSM} = \min(k_{ax,1}, k_{ax,2}) \tag{18}$$

This hypothesis can be questioned, as the assumption is equivalent to considering that the screw is totally fixed in one of the timber members and that no withdrawal displacement can occur within this member at the serviceability limit state. The authors themselves argue that the single stiffness model is the one that appears to be correct from a theoretical point of view. However they obtained the best agreement with their experimental results when using the so called "single stiffness model" together with input parameters the values for the withdrawal stiffness and lateral slip modulus available in the Eurocode 5 (CEN, 2014) and European Technical Approval for the screw used (Deutsches Institut für Bautechnik (DIBt), 2006), respectively.

The double stiffness model seems to be more appropriate from a theoretical point of view, but different values for the input parameters may be necessary in order to obtain a satisfactory agreement with experimental results.

Several other authors have developed models based on beams on elastic foundation to describe the behaviour of vertical and inclined screws in timber-concrete joints (Symons, Persaud, & Stanislaus, 2010), (Moshiri, Gerber, Valipour, Shrestha, & Crews, 2013). Symons (Symons et al., 2010) proposed a model for the slip modulus of inclined screws joints using a beam on elastic foundation model where the screw is considered as an elastic beam element, and the timber as an elastic foundation medium surrounding the screw. This model takes into account both the embedment perpendicular and parallel to the grain but not the withdrawal of the screws as it is done in the model of Tomasi et al. (2010). The model did not consider friction and the screw was considered fixed in the concrete. The comparison with experimental results indicates that the model overestimates the stiffness of the joint by about 20 %. The author considered that this was due to the assumption of the screw being fixed in the concrete.

Models based on beam on elastic foundation may be applied for timber-to-timber joints with inclined screws, considering the withdrawal action of the screw in addition to the dowel effect. It can be noted that the withdrawal action of the screw is the dominant parameter for the load-displacement response of inclined screw joints. Therefore, the determination of the basic fastener parameters such as the withdrawal stiffness parameter should be prioritised. In addition, values for the foundation modulus for different loading directions with respect to the

grain should be determined in order to be implemented in the calculations models, both for the simpler analytical model (i.e. Tomasi model) and for the more detailed models based on beam on elastic foundation.

3.6 Combination of different types of mechanical fasteners

Different fastener types have different load-displacement behaviour, see Fig. 24. As mentioned in the Eurocode 5, the combination of mechanical fasteners of different types in a joint requires the verification of the compatibility of their load deformation behaviour.

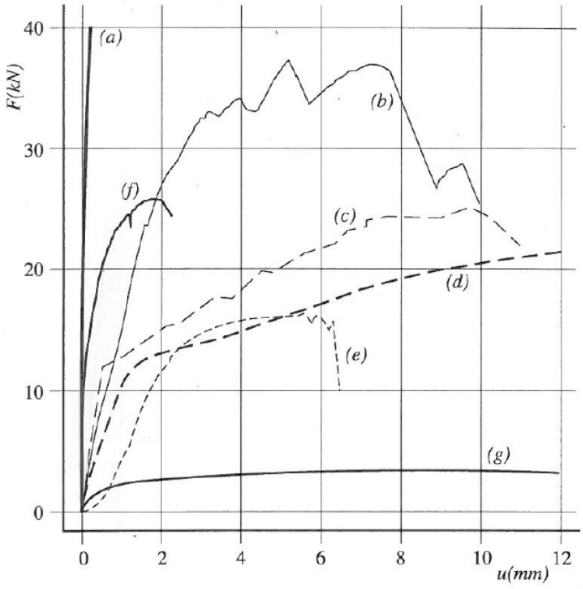

Experimental load-slip curves for joints in tension parallel to the grain: (a) glued joints (12,5 10^3 mm^2), (b) split-ring (100 mm), (c) double sided toothed-plate (62 mm) (Hirashima, 1990), (d) dowel (14 mm), (e) bolt (14 mm), (f) punched plate (10^4 mm^2), (g) nail (4,4 mm).

Fig. 24: Typical experimental load-slip curves for different connections types (Racher, 1995)

Some timber joints reinforcements are made by combining different types of fasteners as for example dowel type fastener joints reinforced with punched metal plate fasteners (Hans Joachim Blass, Schmid, Litze, & Wagner, 2000), (Kevarinmäki, 2000) or dowel reinforced with screws (Bejtka, 2005). In the first case, the punched metal plate mostly improves the embedment resistance and prevents the timber splitting. In the second situation, the screws prevent the timber splitting and also provide a resistance against embedment by contact, making a larger timber area to contribute. These examples are different from the situation where mechanical fasteners are independently loaded in parallel and share the load transfer in proportion of their respective stiffness.

The combination of mechanical fasteners (independently loaded and acting in parallel) requires a verification of the compatibility of their load deformation behaviour. Studies specifically devoted to the combination of mechanical fasteners are not common (Wanyama, Sawata, Hirai, Koizumi, & Sasaki, 2012). Recommendations for the design of joints made with different types of fasteners are given in STEP (Racher, 1995), see Fig. 25 and Eq. (19) to Eq. (21).

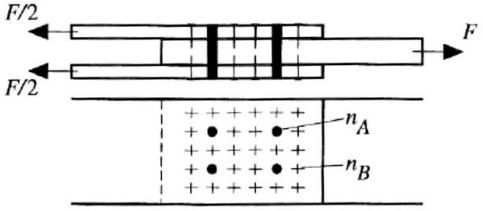

Fig. 25: Joint made with a combination of fasteners: n_A dowels and n_B nails (Racher, 1995)

$$F_{\mathrm{v,tot}} = \sum_{i=1}^{n} F_i = n_{\mathrm{A}} \cdot F_{\mathrm{A}} + n_{\mathrm{B}} \cdot F_{\mathrm{B}} \tag{19}$$

$$u = \frac{F_{\mathrm{A}}}{K_{\mathrm{u,A}}} = \frac{F_{\mathrm{B}}}{K_{\mathrm{u,B}}} \tag{20}$$

where

$$F_{\mathrm{A,d}} = \frac{K_{\mathrm{u,A}}}{n_{\mathrm{A}} \cdot K_{\mathrm{u,A}} + n_{\mathrm{B}} \cdot K_{\mathrm{u,B}}} F_{\mathrm{d}} \qquad \text{and} \qquad F_{\mathrm{B,d}} = \frac{K_{\mathrm{u,B}}}{n_{\mathrm{A}} \cdot K_{\mathrm{u,A}} + n_{\mathrm{B}} \cdot K_{\mathrm{u,B}}} F_{\mathrm{d}} \tag{21}$$

It is mentioned that the different fasteners are loaded in proportion to their stiffness and that the load on each fastener can be determined according to Eq. (21). This expression is valid under the assumption of an elastic perfectly plastic behaviour of the fasteners with the change of slope at the same applied displacement. When fasteners have different load-deformation behaviour, the response of the combined joint will be different.

4 Methods

This chapter presents the experimental programmes which were carried out, the methods of evaluation of the test results, as well as the analytical model derived for the stiffness of inclined screws joints. The experimental part of the work consists of three test programmes. The first one concerns shear test on CLT-concrete joints for a floor element made of CLT panels and prefabricated concrete beams. The second and the third test programmes belong to the study of the composite floor element made of CLT and glulam beams, for which shear tests and bending tests were carried out. The following sections give an overview of these test programmes. A detailed description of each of these test programmes can be found in the appended papers (Papers I, II and III).

4.1 Shear tests on CLT-concrete shear connections

The test programme consisted of asymmetric shear tests on CLT-concrete joints with five different shear connection configurations. The shear test specimen and the types of connectors used are shown in Fig. 26. The first part of the assembly was a prefabricated concrete block casted on a steel plate with two different types of steel-concrete shear connectors, welded headed studs Fig. 26-b, or expanded metal mesh, Fig. 26-c, respectively. The concrete block was first pre-casted on the steel plate and then assembled to the CLT element after curing via a steel-to-timber connection with coach screws. Different number of coach screws and screw lengths were used in the different test series. A summary of the test specimen configurations is presented in Table 1 for a total of twelve specimens tested. A representation and views of the test setup is shown in Fig. 28.

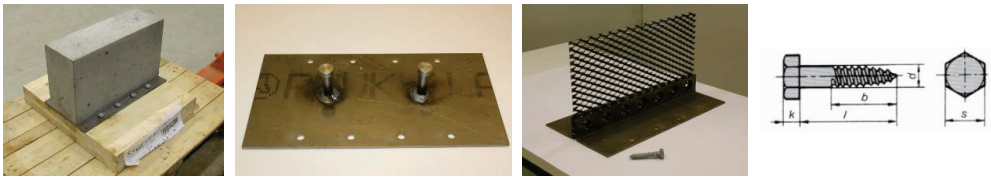

(a) (b) (c) (d)

Fig. 26: (a) CLT-concrete shear test specimen. (b) steel plat with headed studs, (c) steel plate with expanded metal mesh. (d) coach screw.

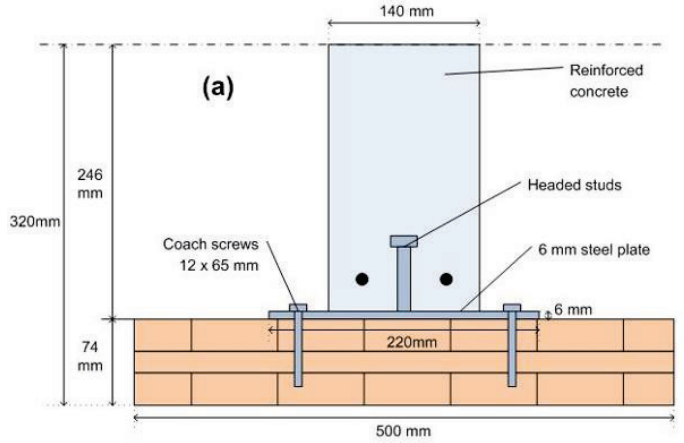

(a)

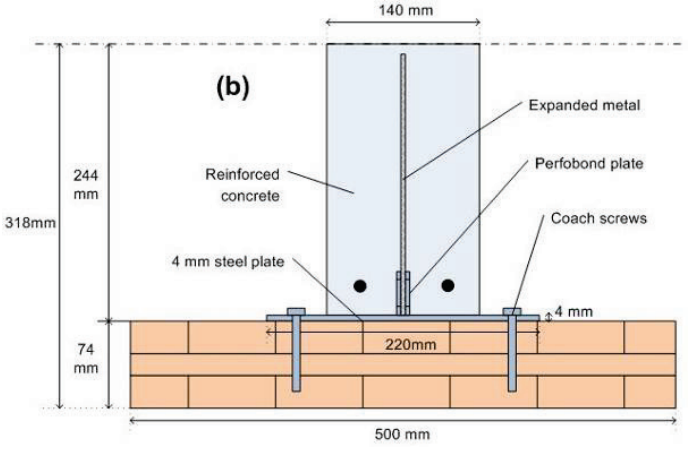

(b)

Fig. 27: Test specimens, (a) S-series, (b) M-series

The test series names in Table 1 are made so that the first letter, indicates the type of steel-to-concrete shear connection used ("S" for studs, and "M" for mesh). The following number indicates if the steel-to-CLT connection is made with 4 or 8 screws, and the last number indicates the screw length *l* according to Fig. 26-d.

Table 1: CLT-concrete shear test series configuration

Series Name	No. of tests	Shear connector type / steel plate thickness	Distance between screws in loading direction / edge distance (mm)	CLT panel thickness (mm)
S-8S-65	3	Studs / 6 mm	80 / 90	74
S-4S-65	3	Studs / 6 mm	240 / 90	74
M-8S-65	3	Mesh / 4 mm	80 / 90	74
M-4S-65	2	Mesh / 4 mm	240 / 90	74
M-8S-100	1	Mesh / 4 mm	80 / 90	103

The total slip between the CLT and the concrete was measured as well as the slip between the CLT and the steel plate. In addition the separation between the concrete below and the CLT at the top and bottom of the test specimen (see Fig. 28) was measured. A metal sheet and a low friction foil were placed between the concrete element and the test setup frame to minimise friction. The test setup allowed separation between the CLT and the concrete block at the top but not at the bottom. This configuration has some effect on the load deformation behaviour, especially for large displacements. The load application was displacement controlled and the loading procedure according to EN 26891 (European Committe for Standardization (CEN), 1991) was followed.

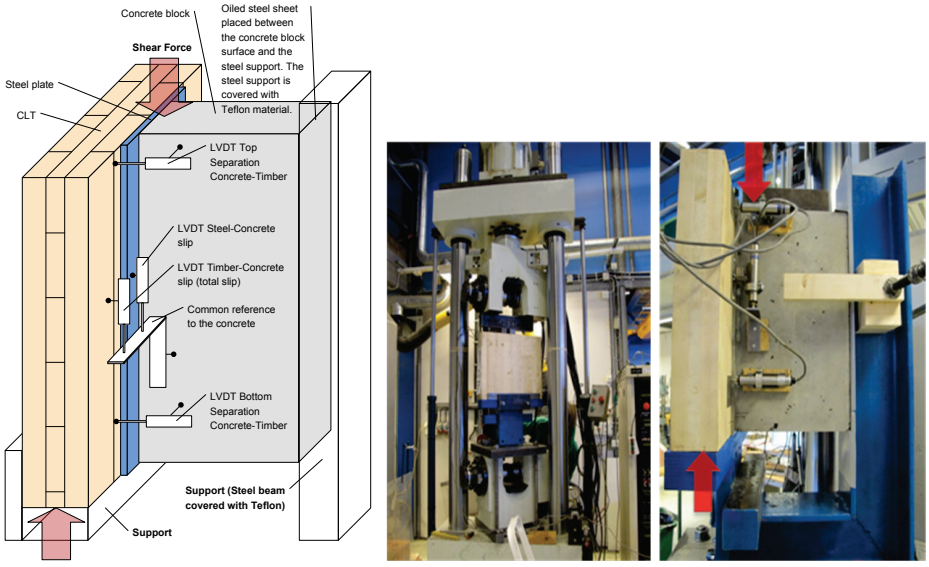

Fig. 28: CLT-concrete joint shear test setup

4.2 Shear tests on glulam-CLT shear connections

The shear connections for composite glulam-CLT members were tested at the VTT laboratories in Finland. A shear test and a bending test programmes were carried out. The shear tests aimed at investigating first the behaviour of double-sided punched metal plate fasteners. In addition and for the reasons described in Chapter 1, the combination of double-sided nail plates and inclined screws was also investigated. Bending tests were also performed on glulam to CLT members with double-sided punched metal plate fasteners and screws.

Both shear and bending tests were made on assemblies between glulam and CLT. The glulam was of strength class GL32 (also marked with the Nordic strength class L40) and the CLT was according to ETA-08/0271 (Deutsches Institut für Bautechnik (DIBt), 2011). The double-sided nail plates (Fig. 29) were Sepa-SE2P nail plates. The screws were SFS Intec WT-T screws (Fig. 30) according to ETA-12/0063 (Österreichisches Institut für Bautechnik (OIB), 2012).

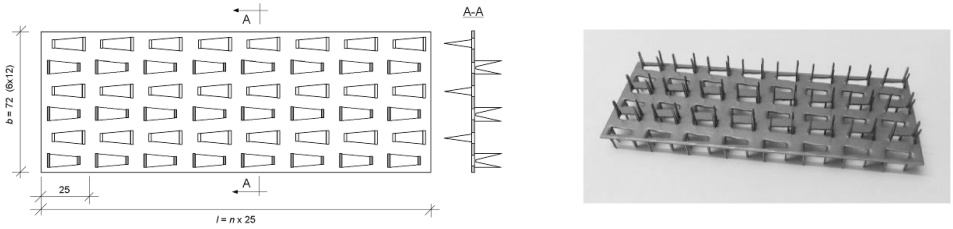

Fig. 29: Double-sided punched metal plate Sepa-SE2P, 72×200 mm^2, (dimensions in mm).

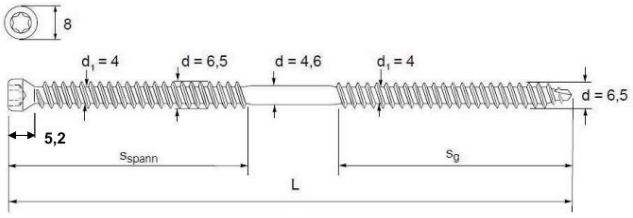

Fig. 30: SFS Intec WT-T screw geometry with diameter 6.5 mm, (dimensions in mm), (source ETA-12/0063 SFS Intec (2012))

The shear tests were performed on elements of eight 600 mm and cross-section shown in Fig. 31. A summary of the configuration of the different tests series is given in Table 2 and Fig. 32.

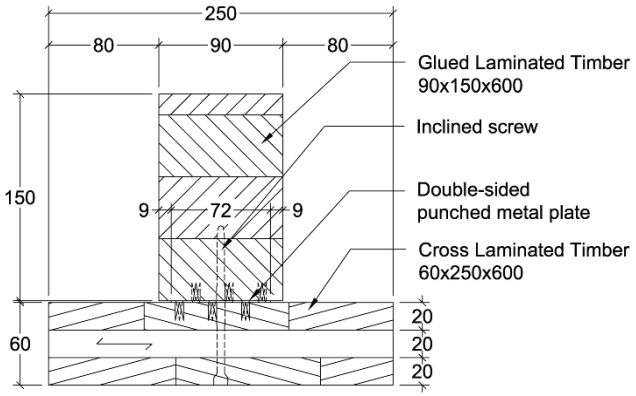

Fig. 31: Cross-section of a shear test specimen (dimensions in mm).

Table 2: Description of the test series

Test series				Screws		Double-sided nail plates (DSNP)		
Name	**Short name**	**No. of tests**	**Estimated maximum load F_{est} (kN)**	**No. of screws**	**$d \times l_S$ (mm)**	**No. of DSNP**	**$b_{NP} \times l_{NP}$ (mm)**	**Total DSNP area (mm^2)**
S1_2S-6.5	S1	4[(a)]	15	2	6.5 × 160	-	-	-
S2_2S-8.2	S2	4[(a)]	20	2	8.2 × 160	-	-	-
S3_1NP-200_2S-6.5	S3	6	50	2	6.5 × 160	1	72 × 200	14400
S4_1NP-200_2S-8.2	S4	6	55; 50[(b)]	2	8.2 × 160	1	72 × 200	14400
S5_2NP-100_1S-6.5	S5	6	40	1	6.5 × 160	2	72 × 100	14400
S6_2NP-100	S6	6	35	-	-	2	72 × 100	14400
S7_1NP-100_2S-6.5	S7	6	30	2	6.5 × 160	1	72 × 100	7200
S8_1NP-200	S8	6	35	-	-	1	72 × 200	14400

(a) Six tests were planned and performed but due to errors in manufacturing some of the test specimens, a slight gap was created between the members. Due to the influence of the gap on the test results, only the four tests for which manufacturing was correct are considered for these test series.

(b) The estimated load for series S4 was 55 kN for the 3 first tests specimens and then adjusted to 50 kN according to EN 26891 (European Committe for Standardization (CEN), 1991)

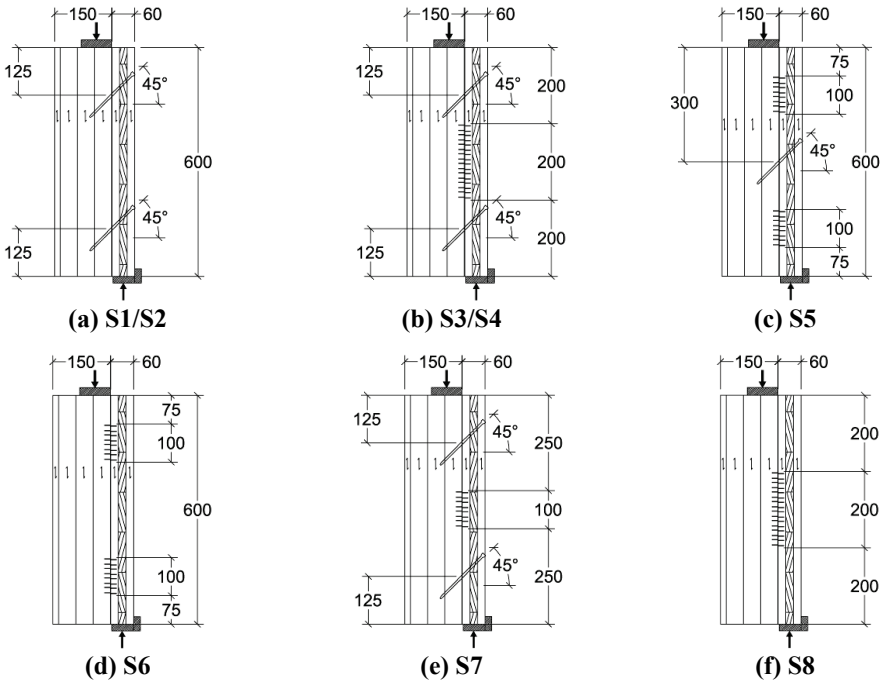

Fig. 32: Test configurations for all glulam-CLT shear test series (detailed notations of the test series according to Table 2) (dimensions in mm).

The tests were carried out with an asymmetric shear test setup which is usually used for tests on joints with punched metal plate fasteners (EN 1075 (European Committe for Standardization (CEN), 1999)). The loading procedure and measurements were done according to the EN 26891 standard (European Committe for Standardization (CEN), 1991).

(a)

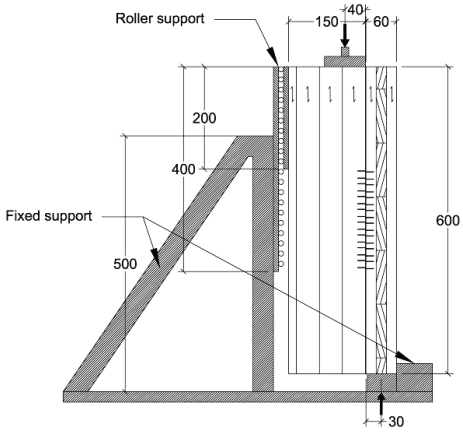

(b)

Fig. 33: Glulam-CLT shear test setup (dimensions in mm).

4.3 Bending tests on glulam-CLT beam elements

The same type of shear connectors as tested in the glulam-CLT shear test program were used for the bending tests. Nail plates of dimensions 200×72 mm^2, see Fig. 29, and SFS Intec WT-T screws (diameter 6.5mm), see Fig. 30, were used. The choice of the smaller diameter screw for the bending tests was made by considering the cost of the screws and their ease of installation. Indeed, screws with 6.5 mm diameter can be installed more easily than 8.2 mm diameter screws and have a better cost/performance ratio and 8.2 mm diameter screws. The shear connections configurations for each test series is given in Table 3. The cross-section of the beams tested is shown in Fig. 34.

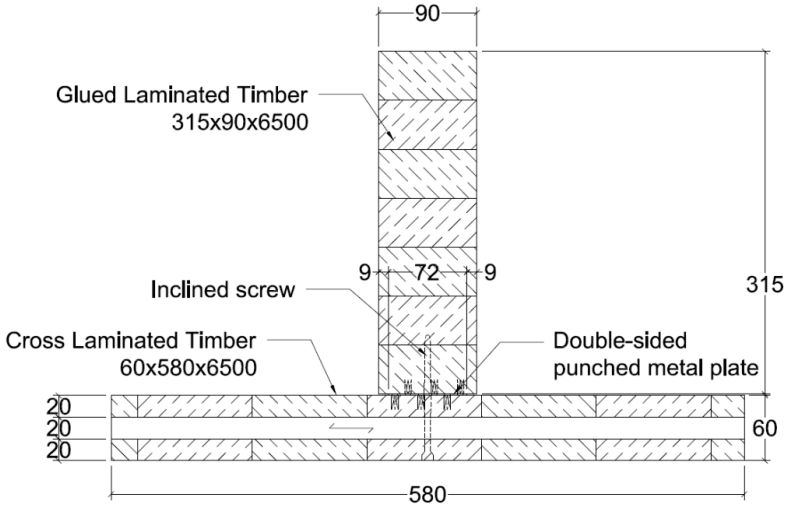

Fig. 34: Cross-section of the composite Glulam-CLT beam with double-sided nail plate and screw shear connection (dimensions in mm).

Table 3: Description of the test series with screws only (B1_S), double-sided nail plates only (B2_NP), double-sided nail plates and screws (B3_NP+S), and screw-gluing (B4_SG).

Test series			**Spacing s = 450 mm**		**Spacing s = 200 mm**
Series Name	**No. of tests**	**Estimated load F_{est} (kN)**	**Screws inclined at 45° in shear tension $d \times l_s$ (mm)**	**Double-sided nail plates $b_{NP} \times l_{NP}$ (mm)**	**Vertical screws for screw-gluing $d \times l_s$ (mm)**
B1_S	3	75	6.5 × 160	-	-
B2_NP	3	75	-	72 × 200	-
B3_NP+S	3	90	6.5 × 160	72 × 200	-
B4_SG	1	110	-	-	8 × 180

d is the nominal screw diameter, l_s is the screw length, b_{NP} and l_{NP} are the DSNP width and length, respectively.

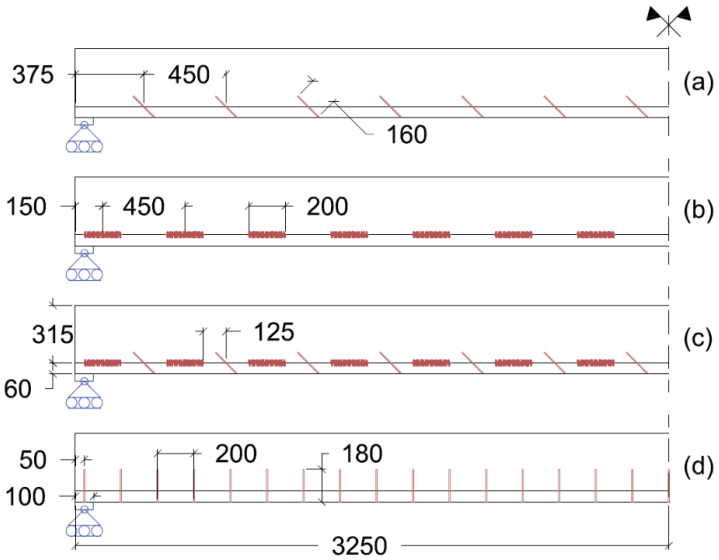

Fig. 35: Configuration of the test series: (a) screws only (B1_S), (b) double-sided nail plates only (B2_NP), (c) double-sided nail plates and screws (B3_ NP+S), (d) screw-gluing (B4_SG), (dimensions in mm).

The tests were done with a four-points bending arrangement with the load application at the third points of the beam span (Fig. 36 and Fig. 37). The supports were running along the entire CLT width and had length of 100 mm on each side (representing the actual support conditions of a floor element on a CLT wall).

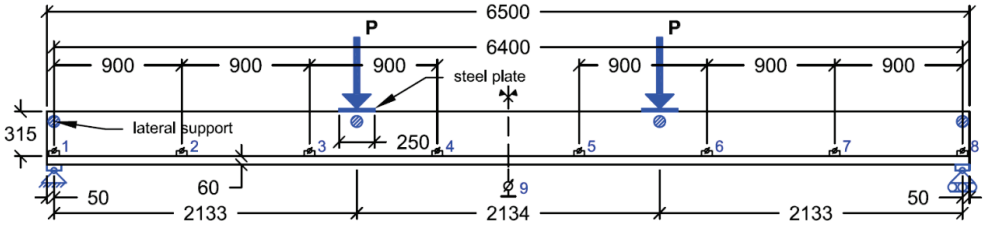

Fig. 36: Description of the loading arrangement (#1 to #8: longitudinal slip measurement; #9: mid-span deflection measurement), (dimensions in mm).

Fig. 37: View of the bending test setup and loading frame.

The practical design load case considered for the design of the floor element is based on a uniformly distributed load combination with a permanent load G_k = 1.8 kN/m^2 and a service load Q_k = 2 kN/m^2. The characteristic load combination in the serviceability limit state, noted ω_{SLS}, and the fundamental load combination in the ultimate limit state, noted ω_{ULS}, are defined in expressions (22) and (23), respectively:

$$\omega_{SLS} = G_k + Q_k \tag{22}$$

$$\omega_{ULS} = \gamma_G G_k + \gamma_Q Q_k \tag{23}$$

where γ_G and γ_Q are 1.15 and 1.5, respectively.

The corresponding load levels considered in the 4-point bending test, noted F_{SLS} and F_{ULS}, are obtained from the equivalence of the bending moment under the uniformly distributed load and 4-point load cases. When the point loads are located symmetrically at the third points of the beam span, $F = 2 \cdot P = (3 \cdot \omega \cdot L)/4$, where F is the total load applied, P is one point load, ω is the distributed load case considered and L is the span of the beam. For the cross-section considered (580 mm width), these load levels are F_{SLS} = 10.6 kN and F_{ULS} = 14.1 kN, respectively. These values are used in Chapter 6 to evaluate the flexural stiffness under the serviceability design load (design action) in order to evaluate the design of the beam and shear connections from a practical point of view.

4.4 Stiffness model for joints with inclined screws in shear-tension

An analytical model for the stiffness of inclined screw joints in shear-tension was derived. A free body diagram (see Fig. 38) depicts the forces and actions considered in the joint. The model takes into account for the screw both dowel and withdrawal actions as well as the friction in the shear plane. The screw is assumed to be rigid in bending and tension, i.e. no deformation of the screw can occur. The model is considered to be valid until the first hinge forms in the screw. This model is general and applicable for different geometries and material properties in each of the jointed timber members. This is one of the advantages of the model. The complete derivation is presented in Paper IV. Only the final expressions for the joint stiffness k and the yield slip limit δ_y (hinge forming in the screw) are presented here.

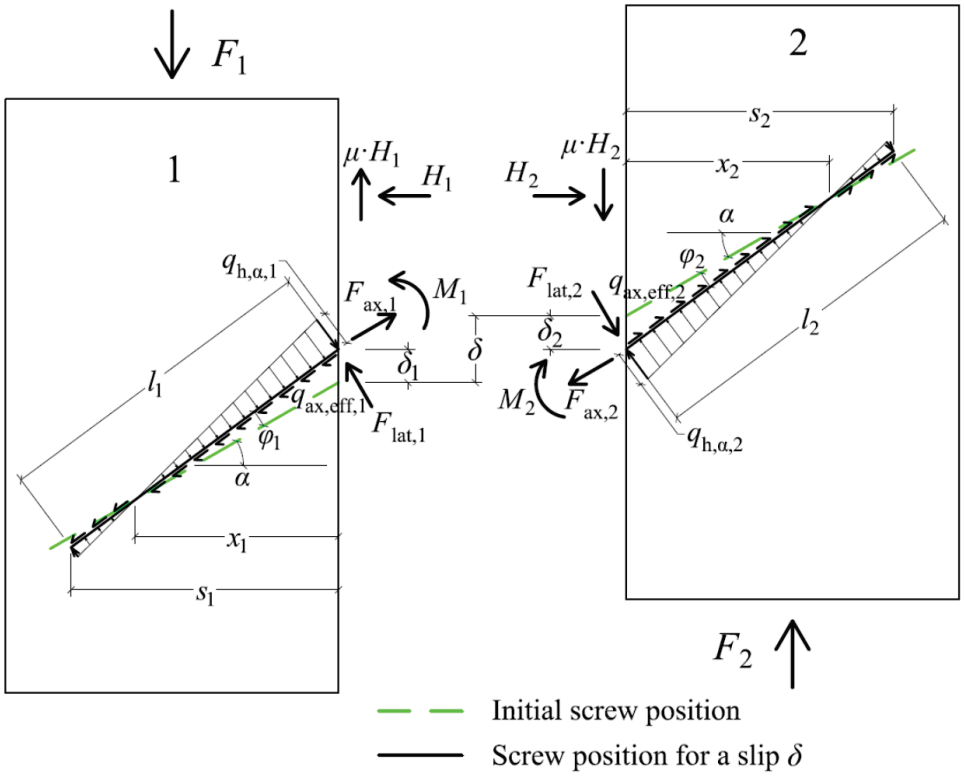

Fig. 38: Forces acting in on the screw in each timber member and forces acting on the joint slip plane

The final expression of the joint stiffness k [N/m] is given by Eq. (24)

$$k = d\, l_1 \cos\alpha \left\{ \frac{1}{2} \left(\cos\alpha - \mu \sin\alpha \right) K_{\mathrm{h},\alpha,1} \frac{2 - s_1/x_1}{1 + x_2/x_1} + \sin\alpha \left(\tan\alpha + \mu \right) K_{\mathrm{ax,eff},1} \frac{l_{\mathrm{thr},1}/l_1}{1 + 1/\beta_{\mathrm{ax}} \beta_{l,\mathrm{thr}}} \right\} \quad (24)$$

where d is the screw diameter, l_1 and $l_{\mathrm{thr},1}$ are the length of the screw and the threaded length in the timber member 1, respectively. s_i and x_i are the normal distances from the shear plane to the end of the screw and to the rotation point of the screw in the i^{th} element, respectively. β_{ax}, and $\beta_{\mathrm{l,thr}}$ are ratios reflecting the differences in geometries and material properties in both elements. They are expressed as $\beta_{l,\mathrm{thr}} = l_{\mathrm{thr},2}/l_{\mathrm{thr},1}$ and $\beta_{\mathrm{ax}} = K_{\mathrm{ax},2,\mathrm{eff}}/K_{\mathrm{ax},1,\mathrm{eff}}$. μ is the friction coefficient. $K_{\mathrm{h},\alpha,1}$ and $K_{\mathrm{ax,eff},1}$ are the embedding stiffness parameter [N/m^3] and the effective withdrawal stiffness parameter [N/mm^3] in the timber member 1, respectively.

The definition of these parameters is described in detail along the derivation presented in Paper IV. In the analysis in this thesis, a discussion will be presented concerning the essential non-geometrical parameters influencing the joint behaviour in the serviceability limit state. These parameters are the effective withdrawal stiffness parameter $K_{\mathrm{ax,eff},1}$, the embedding stiffness parameter $K_{\mathrm{h},\alpha,1}$, and the friction coefficient μ. Some of these parameters need to be obtained experimentally in a new way for the stiffness model, which will also be detailed in the analysis.

The limit of applicability of the model is when the screw cannot be assumed to be rigid anymore. This limit is obtained by calculating the slip causing the screw to yield with Eq (25) as:

$$\delta_{\mathrm{y}} = \left(\frac{m_{\mathrm{s,l,max}}}{M_{\mathrm{y}}} + \frac{f_{\mathrm{ax},1}}{F_{\mathrm{y}}} \right)^{-1} \quad (25)$$

where $m_{\mathrm{s,l,max}}$ (bending moment stiffness [Nm/m]) and $f_{\mathrm{ax},1}$ (axial force stiffness [N/m]) are convenience factors given by Eq. (26) and Eq. (27), respectively:

$$m_{\mathrm{s,l,max}} = \frac{2}{3} \frac{K_{\mathrm{h},\alpha,1} d\, l_1^2 \cos\alpha}{1 + x_2/x_1} \frac{s_1}{x_1} \left(1 - \frac{x_1}{s_1} \right)^3 \quad (26)$$

$$f_{\mathrm{ax},1} = \frac{K_{\mathrm{ax,eff},1} d\, l_{\mathrm{thr},1} \sin\alpha}{1 + 1/\beta_{\mathrm{ax}} \beta_{l,\mathrm{thr}}} \quad (27)$$

The derivation and evaluation of this model is a further development from the stiffness model presented by Tomasi et al. (2010) which considers also these essential parameters but in a simplified way. The model presented in this thesis is however restricted at the moment to

inclined screw joints in shear-tension. The approach of using a linear elastic simplified model is chosen over a model based on beam on elastic foundation because it is believed that the resulting model will be simpler and more practical for engineering calculations. It can be noted that this model is somewhat equivalent to the beam on elastic foundation model considering an infinitely rigid screw, and where the effects of the screw axial stiffness contribution and friction between the members are considered.

5 Experimental results

5.1 CLT-concrete shear tests

The shear tests are reported in detail in Paper I. The load-slip curves of all test series are presented in Fig. 39. The curves represent the total slip measured, i.e. the slip between the timber (CLT) and concrete members. It was noted in Paper I that this measurement was difficult to interpret at low load levels due to the very small displacement involved and due to a small rotation of the specimen during the test, leading the measurement of some negative slip values. The test setup allowed to obtain by deduction the slip between the CLT and the steel plate exempt of this effect. The steel-timber slip is presented up to 2 mm slip in Fig. 40. A very high initial stiffness in all tests series can be clearly noticed in both figures up to 10 or 20 kN for the joints with 4 or 8 screws, respectively.

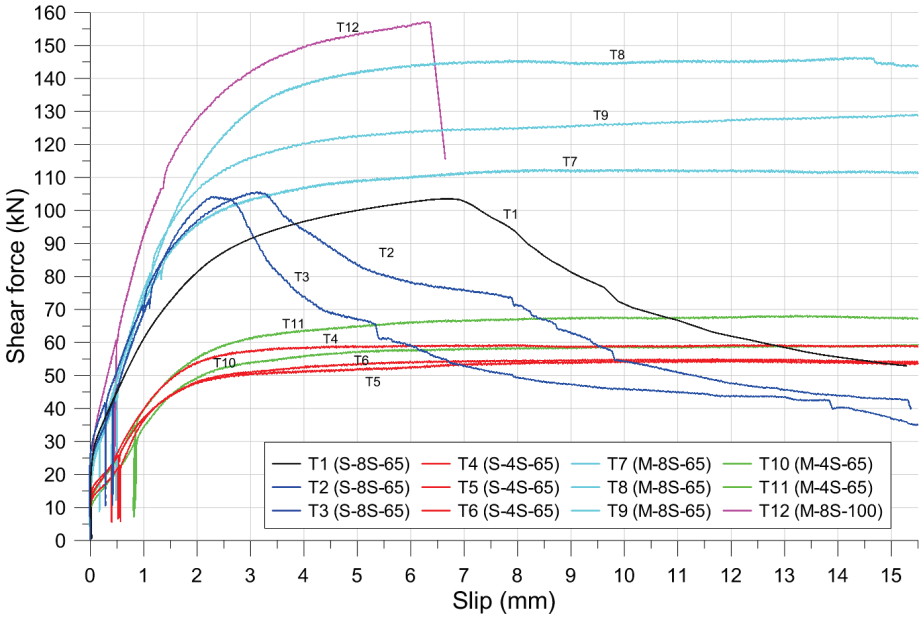

Fig. 39: Load-slip curves for all CLT-concrete shear tests - Total slip (timber-concrete)

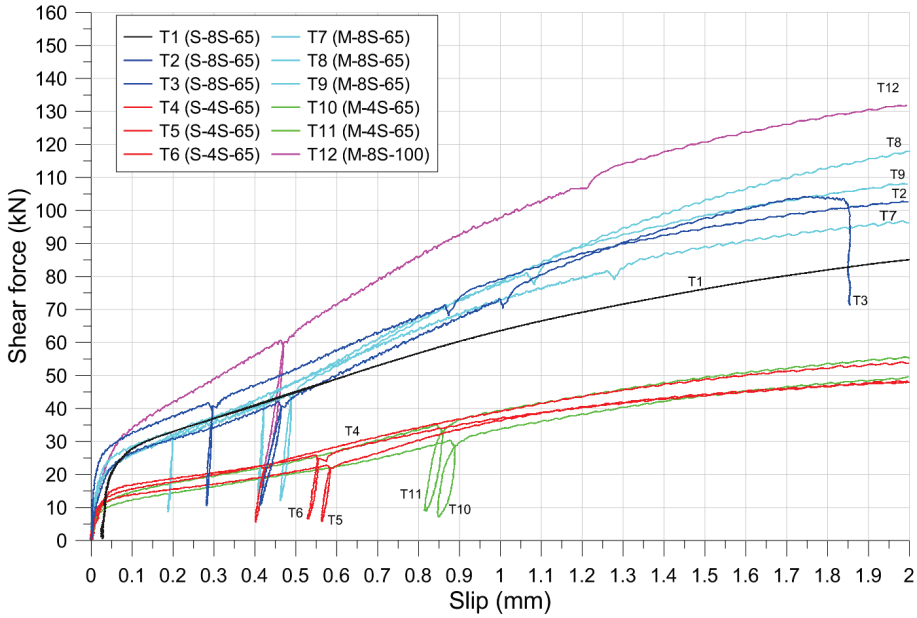

Fig. 40: Detailed load-slip curves for all CLT-concrete shear tests – Steel-timber slip up to 2 mm.

The failure occurred either in the concrete or in the timber for both types of steel-concrete shear connections. Comparing series where failure occurred in the concrete (series S-8S-65 and M-8S-100), it can be observed that the headed stud connection provides a lower load-carrying capacity than the steel mesh connections. The post peak-load behaviour is however better with a gradual reduction of the load-carrying capacity due to the yielding of the studs. A brittle failure of the concrete block was observed for the mesh connection. The steel-concrete shear connection with studs should therefore be preferred, both for its post peak-load behaviour and for the ease of manufacturing compared to the mesh connector type. It is also noted that the load-carrying capacity of the stud shear connection with 4 screws is high enough for the joint failure to be governed by the steel-timber connection.

When failure occurred in the CLT, no brittle failure was observed due to the group effect. Therefore, the load-carrying capacity per screw in the series with 4 and 8 screws are similar, Table 4. The failure mode observed was between mode I and mode II as described in the appended Paper I, with yielding of the screw in the steel plate vicinity and some rotation of the screw head, as it can be seen in Fig. 41. The screw yielded only in the head region due to the clamping effect provided by the steel plate thickness and the hexagonal screw head. At large deformations some bending (waving) in the steel plate could also be observed.

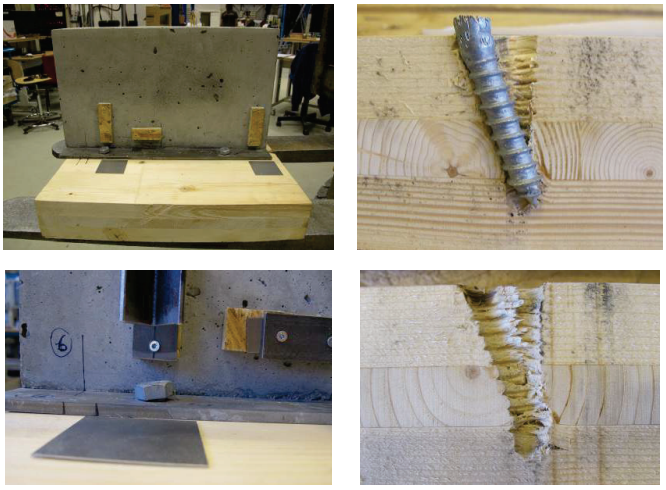

Fig. 41: Pictures from test specimens after failure (more observations can be found in Paper I)

The slip modulus (steel-timber) and the load-carrying capacity are presented in Table 4 for each test series. The evaluation of the slip modulus was not done according to EN 26891 (European Committe for Standardization (CEN), 1991). The slip modulus was obtained as the secant value at 40% of the maximum load and therefore includes the initial slip modulus. In Fig. 42 the load-slip curves for the test series with studs and 4 screws (S-4S-65) is plotted with the obtained secant value of the slip modulus. It can be observed that the evaluated slip modulus $K_{0.4,mean}$ fits well the experimental curve beyond the initial stiffness range. The secant stiffness value was therefore considered acceptable and nevertheless conservative.

Table 4: Average load-carrying capacity and slip modulus for the test series (mean values) - values for one screw are given in parentheses.

	Tests results (mean values)		
Series Name	Failure mode	$F_{v.Rmean}$ (kN)	Slip modulus (steel/timber) $K_{0.4,mean}$ (kN/mm)
S-8S-65	Semi-brittle	104.4 (13.1)	112.9 (14.1)
S-4S-65	Ductile	56.3 (14.1)	44.1 (11.0)
M-8S-65	Ductile	129.2 (16.2)	93.0 (11.6)
M-4S-65	Ductile	63.7 (15.9)	40.5 (10.1)
M-8s-100	Brittle	157.1 (19.6)	126.5 (15.8)

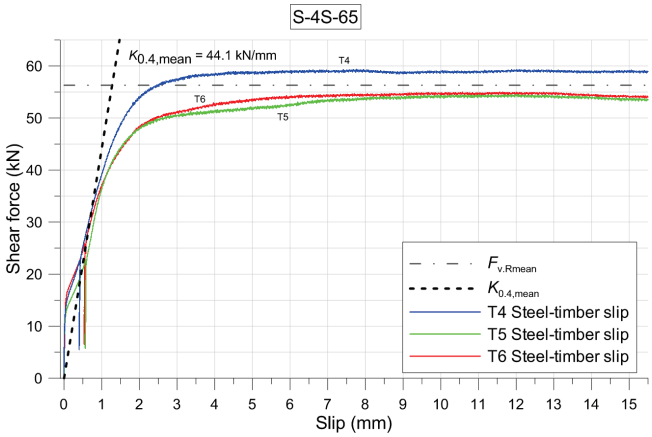

Fig. 42: Load-slip curves for the steel-timber interface – Test series S-4S-65 (T4-T6)

Some design calculations were presented in Paper I for the case of a timber concrete floor element using the shear connection types tested in series S-4S-65. With a total structural floor height of 324 mm and a span of L = 7 m and for an ordinary loading situation, it was estimated that the floor could satisfy the serviceability and ultimate limit state demands. Details about the calculation method and the input parameters used in the calculation example can be found in Paper I.

One of the outcomes of the test programme was the observation that aiming for assembling prefabricated concrete beams on top of CLT panel with these types of connectors was cumbersome from manufacturing and assembly point of view. The need of specially made fasteners is also an important aspect to consider from a cost perspective. In addition, the design calculation for such a system was considered complicated compared to the benefits brought by the floor configuration.

The concept of the floor element with CLT at the bottom using prefabricated concrete beam on the top has some advantages, especially the relatively low floor element height that can be achieved. However this solution is complicated from a practical point of view compared to a solution where timber beams would be used, both with respect to the cost and acceptance of the system.

5.2 Glulam-CLT shear tests

An overview of all the glulam-CLT shear tests results is presented in Table 5 and in Fig. 43 showing the main test results and a plot of the mean load-slip curve for each test series. A detailed description of the test results can be found in Paper II and in the technical report

concerning these tests (Jacquier, 2014). The unloading/reloading cycle between $0.1 \times F_{est}$ and $0.4 \times F_{est}$ was removed in the load-slip curves in Fig. 43. The curves are truncated at 15 mm slip or at the lowest maximum slip value recorded for any test specimen in the test series.

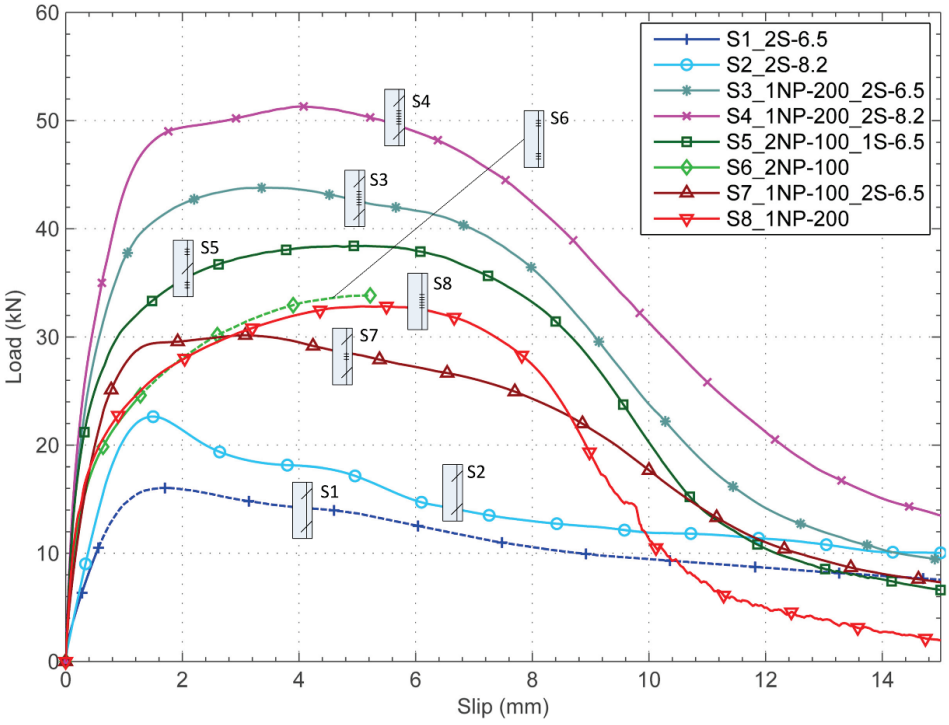

Fig. 43: Mean load-slip curves for each test series

Table 5: Shear test results, mean values for the test series[a]

Test series	No. of tests	Glulam		CLT		Estimated maximum load	Maximum load	Yield slip	Slip at maximum load	Slip at failure load	Slip modulus	Secant modulus at $0.6\times F_{max}$	Secant modulus at $0.8\times F_{max}$
		$\rho_{g,\omega}$ kg/m^3	ω_g %	$\rho_{c,\omega}$ kg/m^3	ω_c %	F_{est} kN	F_{max} (CoV) kN (%)	u_y (CoV) mm (%)	u_{max} (CoV) mm (%)	u_f (CoV) mm (%)	k_s (CoV) kN/mm (%)	$k_{0.6}$ (CoV) kN/mm (%)	k_s (CoV) kN/mm (%)
S1_ 2S-6.5	4	456	12.2	471	12.4	15	16.1 (5.3)	0.67 (16.9)	1.78 (9.4)	5.69[c] (18.9)	19.4 (7.3)	19.6 (5.5)	16.7 (5.4)
S2_ 2S-8.2	4	462	12.4	459	12.3	20	22.8 (10.3)	0.79 (11.0)	1.54 (11.0)	3.41 (28.8)	25.4 (9.3)	25.7 (7.5)	22.8 (6.0)
S3_ 1NP-200_2S-6.5	6	467	12.6	457	12.9	50	44.1 (6.2)	0.34 (7.9)	3.48 (17.5)	8.28 (6.5)	72.2 (12.4)	61.7 (7.7)	30.6 (10.0)
S4_ 1NP-200_2S-8.2	6	451	12.5	460	12.8	55; 50[b]	51.5 (7.2)	0.38 (13.1)	4.18 (11.3)	8.42 (9.9)	85.0 (10.4)	64.8 (7.9)	35.1 (9.2)
S5_ 2NP-100_1S-6.5	6	461	12.5	451	13.1	40	38.5 (3.5)	0.25 (7.3)	4.84 (11.2)	8.50 (5.1)	80.8 (7.8)	58.2 (7.1)	23.2 (6.9)
S6_ 2NP-100	6	444	12.7	450	13.8	35	33.9 (4.9)	0.33 (14.1)	5.20 (7.1)	-[d]	45.6 (21.0)	29.7 (20.5)	11.6 (14.3)
S7_ 1NP-100_2S-6.5	6	452	12.4	457	12.8	30	30.1 (2.2)	0.48 (11.0)	2.85 (17.0)	7.52 (19.4)	46.9 (7.7)	42.8 (9.0)	25.7 (8.5)
S8_ 1NP-200	6	473	13.0	446	13.7	35	32.9 (3.2)	0.27 (1.5)	5.26 (8.8)	8.47 (10.9)	53.6 (7.8)	35.54 (7.4)	12.75 (5.9)

(a) The values in parentheses represent the coefficient of variation (CoV) in %. The density ρ is given for the moisture content ω measured at the time of testing. The subscripts c and g denote the CLT and glulam members, respectively.

(b) The estimated load for series S4 was 55 kN for the 3 first tests specimens and then adjusted to 50 kN according to EN 26891 (European Committe for Standardization (CEN), 1991)

(c) This result should be considered as indicative only (tests conducted under load control).

(d) No value is given due to the collapse of test specimens after maximum load (tests conducted under load control).

In all test series, the failure of the fasteners has occurred either in the CLT or in the glulam member or sometimes in both timber members. The failure had, however, a tendency to occur more often in the glulam member, both for the double-sided nail plates and the inclined screws. Concerning screws, this may be due to the fact that the head of the screw was located in the CLT member and, maybe also, because of the cross-wise make-up of the layers. Concerning the double-sided nail plate, this may be due to the fact that the plate is first fastened to the CLT member with better penetration of the nails of the plate as a result.

(a) (b) (c) (d) (e)

Fig. 44: Double-sided nail plate of length 100 mm after failure – (a) upper double-sided nail plate (series S6) – (b) lower double-sided nail plate (series S6); (c) Specimen with screws only (series S2); (d) and (e) Specimens with inclined screws and double-sided nail plate, (series S4 and S7, respectively). In all three figures (c) – (e), the gaps are such that both of the screws are visible.

Specific slip values presented in Table 5 (yield slip u_y, slip at maximum load u_{max} and failure slip u_f) are defined according to the principle load-deformation curve shown in Fig. 45. The yield slip is determined according to EN 12512 (European Committe for Standardization (CEN), 2001). More information about different methods to determine the yield slip for these tests can be found in (Jacquier, 2014).

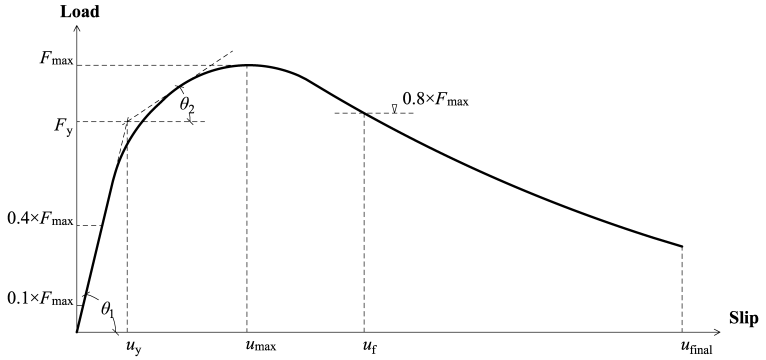

Fig. 45: Load-slip curve and specific slip values (Jorissen & Fragiacomo, 2011)

It can be noted that for joints with inclined screws only (S1, S2), the slip at maximum load u_{max} and the slip at "failure" load u_f are lower than for joints with double-sided nail plate fasteners only (S6, S8). The yield slip u_y of inclined screw joints is however at least two times higher than the one of double-sided nail plates, indicating that the inclined screws behave linearly up to a higher proportion of their capacity compared to the double-sided nail plates.

5.3 Glulam-CLT bending tests

The main results from the bending tests are presented in this section. A more detailed presentation of the results can be found in Paper III and in the technical report about the tests (Jacquier, 2015).

5.3.1 Load-deflection behaviour

The curves of load-deflection at mid-span are presented in Fig. 46 to Fig. 49 for each test series with a closer view up to about 50 % of the estimated failure load F_{est}.

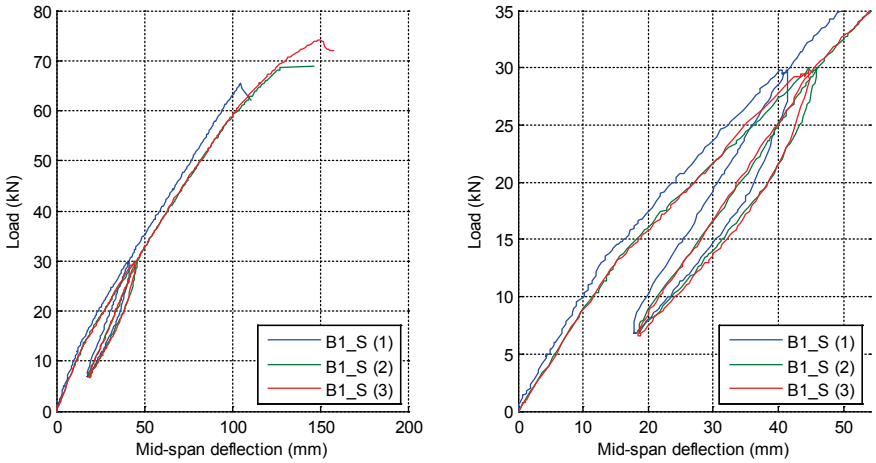

Fig. 46: Load-deflection curves at mid-span (full curves and curves up to 50% of F_{est}) - Series B1_S

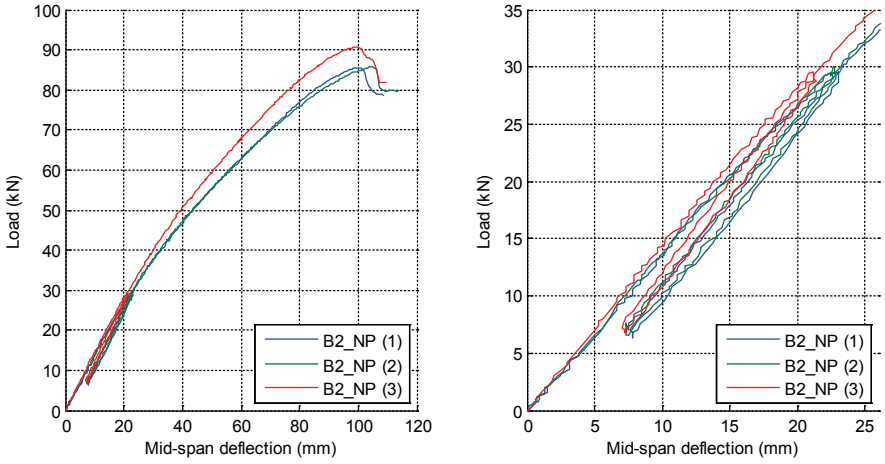

Fig. 47: Load-deflection curves at mid-span (full curves and curves up to 50% of F_{est}) - Series B2_NP

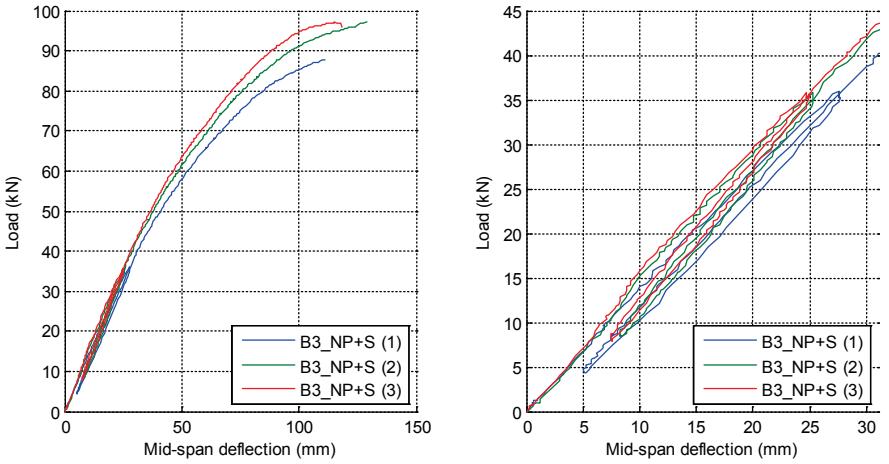

Fig. 48: Load-deflection curves at mid-span (full curves and curves up to 50% of F_{est}) - Series B3_NP+S

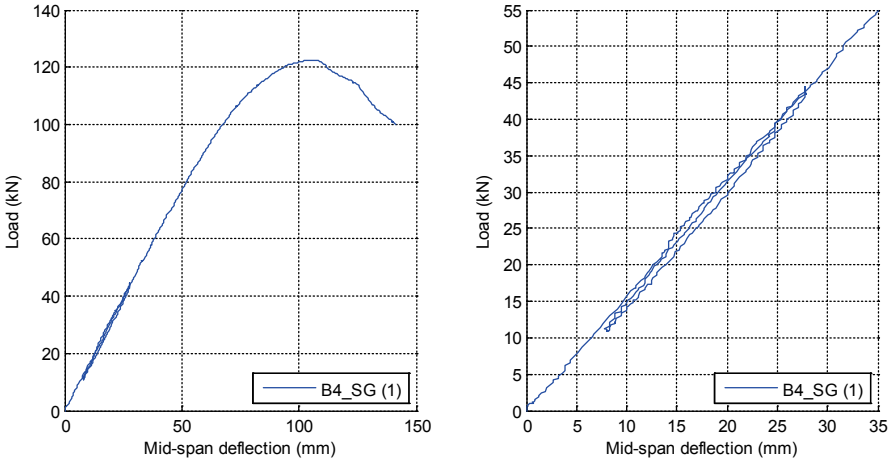

Fig. 49: Load-deflection curves at mid-span (full curves and curves up to 50% of F_{est}) - Series B4_SG

Table 6 presents the mean values of the main test results for each test series. The density of the timber at the moisture content ω was measured just after the bending tests and is noted $\rho_{g,\omega}$ and $\rho_{c,\omega}$, for the glulam and CLT members respectively.

Table 6: Summary of the bending test results for the series with screws only (B1_S), double-sided nail plates only (B2_NP), double-sided nail plates and screws combined (B3_NP+S), and screw gluing (B4_SG) – Mean values.

Test series	No. of tests	Glulam		CLT		Maximum load	Failure load	Mid-span deflection at $0.4 \cdot F_{max}$
		D	MC	D	MC			
		$\rho_{g,\omega}$ kg/m^3	ω_g (%)	$\rho_{c,\omega}$ kg/m^3	ω_c (%)	F_{max} (CoV) kN (%)	F_f (CoV) kN (%)	$\delta_{04 \cdot Fmax}$ (CoV) mm (%)
B1_S	3	474	13.7	455	12.9	69.4 (6.2)	67.7 (7.4)	39.9 (12.8)
B2_NP	3	438	13.9	461	13.0	87.4 (3.4)	80.1 (2.0)	26.8 (0.7)
B3_NP+S	3	454	14.0	463	12.9	94.0 (5.9)	93.9 (5.8)	27.2 (2.2)
B4_SG	1	489	14.2	467	12.7	122	99.8	30.9

In the test series with mechanical fasteners (B1_S, B2_NP and B3_NP+S) the glulam beam exhibited a bending failure in tension with failure located in the finger joints (Fig. 50a-c) and the CLT members remained undamaged. Compression failure could be observed on the upper side of the glulam member between the points of load application for all test series.

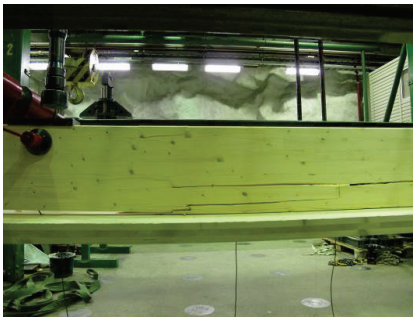

(a)

(b)

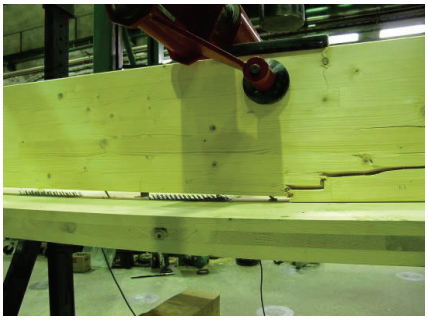

(c)

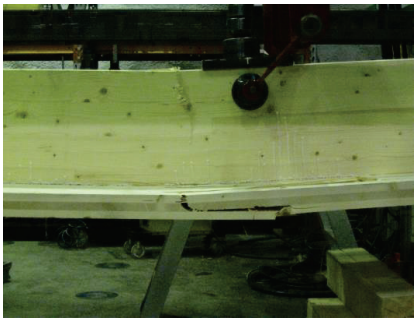

(d)

Fig. 50: Failure observations (a) series B1_S, (b) Series B2_NP, (c) series B3_NP+S, (d) series B4_SG.

For the specimen B4_SG (Fig. 50d), a bending failure with a tension failure in the CLT panel and a very large compression failure at the top of the glulam beam were observed. The compression failure, located near the load application point, extended down to half the height of the glulam beam, and could be observed already before the collapse of the beam. The glue line at the glulam-CLT interface did not fail and no separation of the members was observed.

5.3.2 Slip between the glulam beam and CLT panel

The measured slip v at the glulam-CLT interface is plotted in Fig. 51 to Fig. 53 along the beam length for the test series B1_S, B2_NP and B3_NP+S at certain load values F_{01}, F_{04}, F_{06}, F_{08}, F_{max}, and $F_{failure,}$ ($F_{failure}$ being the last load level recorded before a drop of load of more than 20 % from the maximum load). For the series B4_SG the slip was only measured at both beam ends.

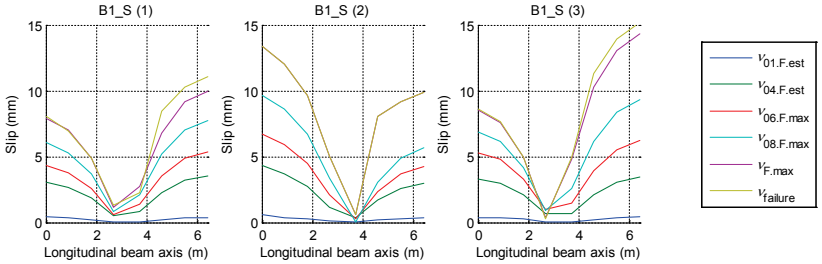

Fig. 51: Slip measurements along the beam length at the load levels F_{01}, F_{04}, F_{06}, F_{08}, F_{max}, and $F_{failure}$ – Series B1_S

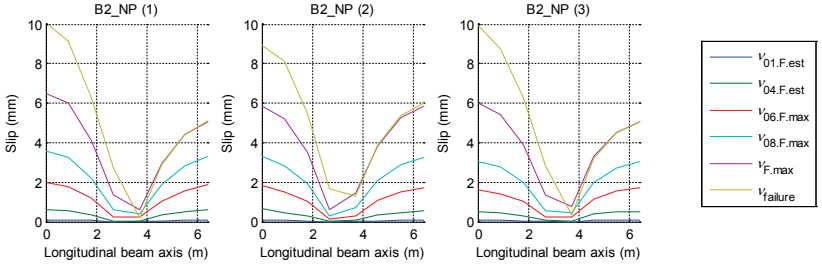

Fig. 52: Slip measurements along the beam length at the load levels F_{01}, F_{04}, F_{06}, F_{08}, F_{max}, and $F_{failure}$ – Series B2_NP

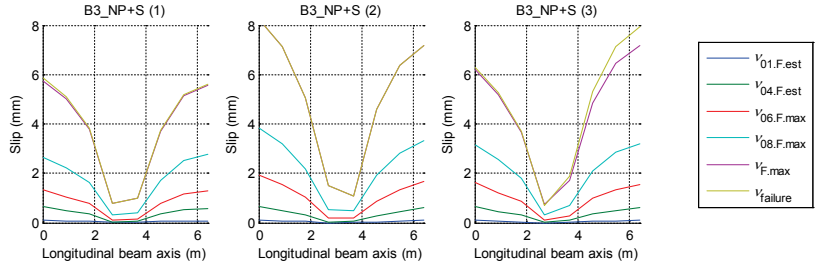

Fig. 53: Slip measurements along the beam length at the load levels F_{01}, F_{04}, F_{06}, F_{08}, F_{max}, and $F_{failure}$ – Series B3_NP+S

5.3.3 Estimated material properties

The modulus of elasticity of the glulam beams and that of the CLT longitudinal layers was estimated from some non-destructive bending tests on individual members. The global modulus of elasticity (MOE) according to EN 408 (European Committe for Standardization (CEN), 2012) was measured on three glulam beams and three CLT panels under a 4-point bending loading up to $0.4 \times F_{max,est}$, with $F_{max,est}$ taken as 18 kN and 3 kN for the glulam beams and the CLT panels, respectively.

The global MOE obtained for the glulam was $E_{global,glulam} = 11\ 898$ N/mm^2 when neglecting the shear deformation. When considering the deflection due to shear deformation and assuming a shear modulus of 850 N/mm^2 according to the GL32h strength class, the estimated MOE was $E_{global,glulam,shear} = 12\ 290$ N/mm^2. The vertical shear deformation is however neglected for the CLT as the span is very large in comparison to the CLT layers thicknesses. The global MOE of the longitudinal layers was estimated using the "γ -method" (cf. section 3.1.1), considering a rolling shear modulus $G_R = 50$ N/mm^2 (Deutsches Institut für Bautechnik (DIBt), 2011) for the transverse layer, giving $E_{global,CLT} = 11\ 445$ N/mm^2 for the longitudinal CLT layers.

In this thesis the MOE values $E_{global,glulam} = 11\ 898$ N/mm^2 and $E_{global,CLT} = 11\ 445$ N/mm^2 are the values considered in the analysis for the glulam and CLT members, respectively.

6 Analysis and discussion

In this chapter, a discussion on the compatibility of different types of mechanical fasteners and on the application range for the glulam CLT floor element with punched metal plate fasteners are presented. As part of the study on shear connections a discussion around the stiffness model for inclined screw joints is presented.

6.1 Combination of different types of mechanical fasteners

The combination of different types of fasteners in a joint is discussed for the particular case of double-sided punched metal plate fasteners and inclined screws based on the experimental results from shear and bending tests (Paper II and Paper III).

In Paper II, it is shown that the load-slip behaviour of joints with combined double-sided nail plates and screws corresponds to the superimposition of the load-slip curves obtained for each mechanical fastener individually. This is illustrated in Fig. 54, for the test series S4_1NP-200_2S-8.2 combining a double-sided punched metal plate and two inclined screws. The curve labelled "S2+S8", obtained as the summation of the mean curves from series with single fastener types (series S2_2S-8.2 and S8_1NP-200), fits well the curve of series S4. This shows that there is globally no strengthening or weakening effect when combining these two types of fasteners in these proportions.

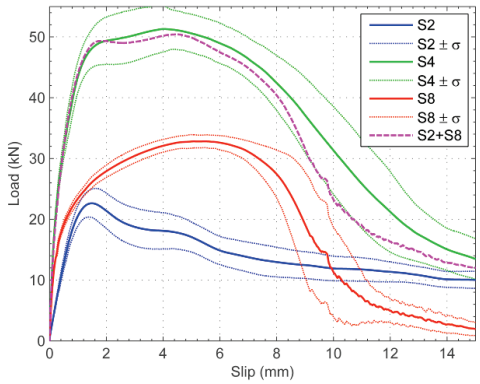

Fig. 54: Mean load-slip curve for the combined joint (series S4_1NP-200_2S-8.5) compared to superposition of the corresponding single fastener mean load-slip curves (series S2_2S-8.5 and S8_1NP-200, respectively). The mean curves are shown with +/- one standard deviation noted σ.

A possible strengthening effect for the double-sided nail plate could have been expected from the screw loaded in shear-tension, generating a compressive force in the shear plane and therefore on the nail plate. On the other hand, a possible weakening effect for the inclined screws could have been expected from the small gap between the glulam and CLT members

due to the presence of the nail plate. Based on the tests results it is assumed that these effects had a minor influence or have compensated each other.

It should also be noted that the asymmetric shear test setup used provides a compression force on the shear plane due to the eccentricity in the load application and therefore a compressive force between the timber members that is not present in the bending test situation. This effect from the shear test setup generally leads to an overestimation of the load-carrying capacity and stiffness of the mechanical fasteners. For the inclined screw joints this contribution was estimated in Paper III to be between 4 to 8 % depending on the value considered for the friction coefficient.

In Paper II, the load-carrying capacity and slip modulus of the joints with combined fasteners were compared with the sum of the load-carrying capacities and slip modulus of the individual fasteners. For the considered combinations of double-sided nail plates and inclined screws, the slip modulus values obtained according to EN 26891 (European Committe for Standardization (CEN), 1991) for each of the fasteners could be conservatively added to estimate the slip modulus of the combined joint. Even though the slip at maximum load is much lower for screws than for DSNP, the initial part of the load-deformation curve for both types of fastener is rather compatible. The inclined screw joint actually behaves linearly up to larger slip values than the DSNP, the DSNP having a more pronounced non-linear behaviour from the beginning of the test.

For estimating the load-carrying capacity of the combined joint, a lower value than the sum of the capacity of each fastener needs to be considered due to the fact that the load-deformation behaviours of the inclined screws and nail plates are different near to the failure load. In Paper II a reduction factor of $k_r = 0.9$ was suggested for the calculation of the load-carrying capacity of the combined joint according to Eq. (28)

$$F_{v,tot} = k_r \cdot \left(n_{NP} \cdot F_{v,NP} + n_s \cdot F_{v,S} \right) \tag{28}$$

where $F_{v,NP}$ and $F_{v,S}$ are the individual load-carrying capacities for double-sided nail plate and screw, respectively, and n_{NP} and n_s are the number of nail plates and screws in the joint, respectively. This recommendation is however only valid for the joint configurations tested in this paper.

A more general prediction of the load-carrying capacity of the combined joint than in Paper II is proposed hereafter. The combined joint behaviour can be evaluated based on the summation of the non-linear models obtained for each of the fastener types and Eq. (29):

$$F_{\mathrm{v,reg}}(\Delta) = n_{\mathrm{NP}} \cdot F_{\mathrm{v,NP,reg}}(\Delta) + n_{\mathrm{s}} \cdot F_{\mathrm{v,S,reg}}(\Delta) \tag{29}$$

where $F_{\mathrm{v,S,reg}}(\Delta)$ and $F_{\mathrm{v,NP,reg}}(\Delta)$ are non-linear regression models, functions of the joint slip Δ, for the inclined screws and double-sided punched metal plate fasteners, respectively. Eq. (29) is similar to Eq. (19) that was reported from STEP 1 (Racher, 1995) in section 3.6. However the STEP 1 expression is only valid for estimating the load-carrying capacity of multiple fastener joints with fasteners having the same kind of load-deformation and an idealised perfectly plastic behaviour after maximum load. Eq. (29) can be used to predict the load-deformation response of multiple fastener joints with fasteners having different types of behaviour, before and after the maximum load.

The non-linear regression for the double-sided punched metal plate fastener proposed is based on a 5-parameters exponential regression model derived by Bovim (Bovim, 2015), see Eq. (30):

$$F_{\mathrm{v,NP,reg}}(\Delta) = \left(p_0 + K_1 \cdot \Delta\right) \cdot \left(1 - \exp\left(-\frac{K_0 \cdot \Delta}{p_0}\right)\right) \cdot \exp\left(-\frac{\Delta^{\alpha}}{\beta}\right) \tag{30}$$

where the parameters p_0, K_0, and K_1 are the Foschi parameters (Foschi, 1977) as defined in section 3.4.3 obtained by curve fitting on the load-deformation curve up to the slip at maximum load $\delta_{\max}$. The parameters α and β are obtained by iteration using Eq. (31) and Eq. (32):

$$\alpha = \frac{\ln\left[\beta \cdot \left(\ln\left(p_0 + K_1 \cdot \delta_0\right)\right) - \ln\left(0.01\right)\right]}{\ln(\delta_0)} \tag{31}$$

$$\beta = \frac{\alpha \cdot \left(p_0 + K_1 \cdot \delta_{\max}\right) \cdot \delta_{\max}^{\alpha-1}}{K_1 + \left(K_0 - K_1 + \frac{K_0 \cdot K_1}{p_0} \cdot \delta_{\max}\right) \cdot \exp\left(-\frac{K_0 \cdot \delta_{\max}}{p_0}\right)} \cdot \left(1 - \exp\left(-\frac{K_0 \cdot \delta_{\max}}{p_0}\right)\right) \tag{32}$$

where δ_0 is the chosen post-peak-load slip value for which the fastener is considered to have no remaining load-carrying capacity. For the DSNP, δ_0 is taken as δ_0 = 15 mm. The fit of the model with the experimental results is shown in Fig. 55 for the series S8-1NP-200, and the values of the parameters obtained is given in Table 7.

Table 7: Parameters for the non-linear regression model for double-sided nail plates (series S8-1NP-200)

	Series S8-1NP-200	Unit
p_0	23.63	kN
K_0	74.13	kN/mm
K_1	2.03	kN/mm
α	4.63	-
β	32436.1	-
δ_{max}	5.26	mm
δ_0	15	mm

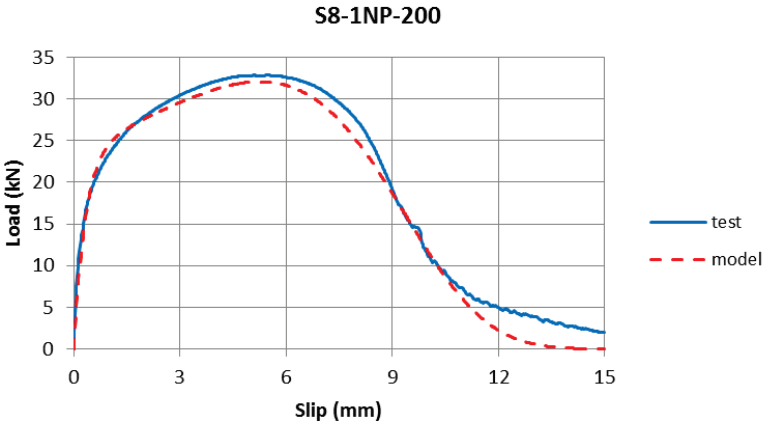

Fig. 55: Experimental results (average curve) for the series S8_1NP-200 and model approximation.

The load-deformation curve of the inclined screw joints at 45 degrees, (series S2) is modelled using Eq. (33):

$$F_{v,S,reg}(\Delta) = \frac{a + b \cdot \Delta}{1 + c \cdot \Delta + d \cdot \Delta^2} \tag{33}$$

where the parameters a, b, c, and d are determined through curve-fitting on the load-displacement curve. The obtained parameters for the fit with the test series S2_2S-8.2 are given in Table 8. The fit is considered acceptable according to the observation of Fig. 56.

Table 8: Parameters for the non-linear regression model for screws inclined at 45° in shear tension (series S2-2S-8.2)

	Series S2-2S-8.2	Unit
a	-3.288	kN
b	64.97	kN/mm
c	1.872	mm^{-1}
d	3.442	mm^{-2}

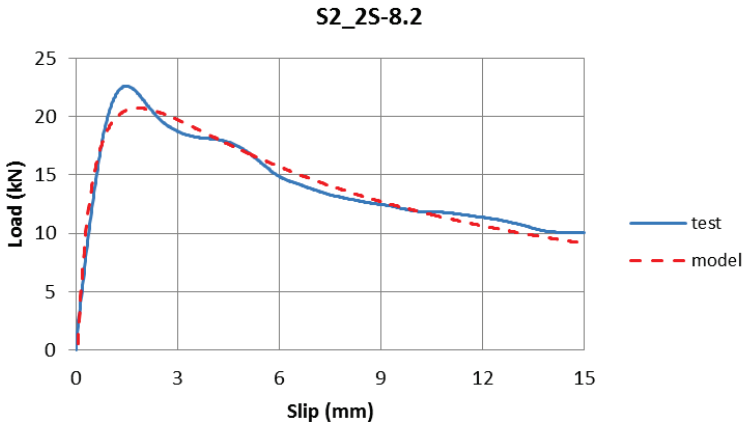

Fig. 56: Experimental results (average curve) for the series S2_2S-8.2 and model approximation.

The maximum load-carrying capacity and slip at maximum load for the combined joint can be estimated by combining the analytical models. Fig. 57 shows the predicted load-slip curve according to Eq. (29) for the series S4_1NP-200_2S-8.5 compared to the experimental results and summation of experimental results (S2-2S-8.2 + S8-1NP-200).

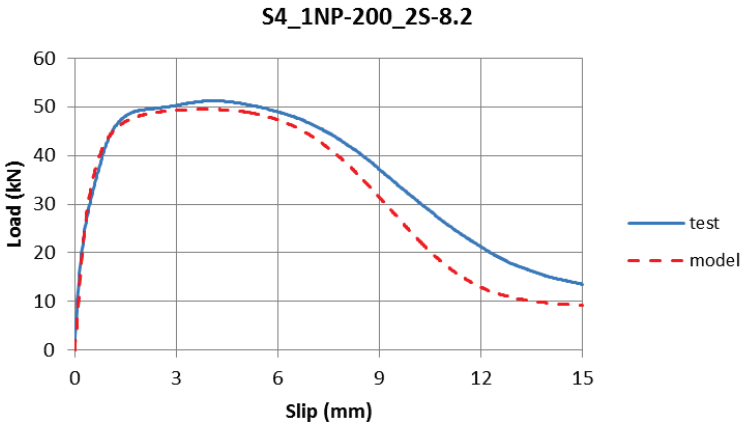

Fig. 57: Experimental results (average curve) for the series S4_1NP-200_2S-8.2 and model approximation.

The values of maximum load-carrying capacity and slip at maximum load from experimental results and the regression models are given in Table 9. The agreement between experimental results and values obtained from the regression model is good. This approach for estimating the load-carrying capacity is more general than the one in Paper II and could be used to estimate combinations with any proportions of these fasteners types in the joint.

Table 9: Combination of double-sided nail plates and inclined screws - Comparison between load-carrying capacity from experimental results and regression model

		Experimental results Series S4	Regression models S4 = S2 + S8
F_{max}	kN	51.5	49.5
δ_{max}	mm	4.18	3.82

As stated earlier in the results section, the present combination of double-sided nail plates and screws maximises the stiffness contribution form the screws, and improves the shape of the overall load deformation curve. However, the combination with a screw inclined at 45° is not ideal from a design point of view as both fastener types have different maximum slip values, leading therefore to a non-maximal load-carrying capacity. A higher load-carrying capacity could be obtained if both fasteners would reach their maximum load for the same applied displacement.

The behaviour of joints with inclined screws depends on the inclination angle of the screw, as shown by Tomasi et al. (Tomasi et al., 2010). In order to tune or optimise the behaviour of

combined joint including inclined screws, one possibility is therefore to use inclination angle as a lever to adjust the screw load-deformation behaviour. The following section will discuss aspects related to the stiffness of inclined screw joints.

6.2 Stiffness model for inclined screw joints in shear tension

The new analytical model presented in Paper IV for estimating the stiffness of inclined screw joints in shear-tension is discussed in this section. The stiffness model derived in Paper IV was presented in the Methods chapter (cf. section 4.4).

Different test setups were suggested in Paper V in order to determine experimentally the withdrawal stiffness parameter and embedment stiffness parameters needed for the model derived in Paper IV. The test setups proposed intend to take into account, besides the inclination angle, the effect of the screw length, and diameter and thread length. The effect of having simultaneous embedment and withdrawal will be evaluated with the test setups proposed. The proposed tests could not be carried out. Therefore approximate values were considered based on available results in the literature. The tests results found in the literature do not match exactly with the test setups proposed in Paper V. However the values that can be found from standard embedment tests and withdrawal tests allow to obtain some input values for the model and to carry out some comparison with existing experimental results of joints with inclined screws. Comparison between tests results from Tomasi et al. (2010) and from Paper II with the new stiffness model and the stiffness models from Tomasi et al. (2010) are presented in Table 11.

Table 10: Input values considered for the calculation of $k_{UAG,NJ}$ (from Paper V)

Friction coefficient	μ	0.3	-
Effective withdrawal stiffness parameter	$K_{ax,eff}$	40	N/mm^3
Embedment stiffness parameter parallel to the grain	$K_{h,0}$	60	N/mm^3
Embedment stiffness parameter perpendicular to the grain	$K_{h,90}$	30	N/mm^3

The input values considered to estimate the slip modulus $k_{UAG,NJ}$ for the stiffness model from Paper IV are given in Table 10. The stiffness k_{DSM} and k_{SSM} , for the double stiffness model (DSM) and single stiffness model (SSM), respectively, according to Tomasi et al. are calculated using the input values considered in their original publication (Tomasi et al., 2010), i.e. using the empirical value from the Eurocode 5 for the stiffness of dowel type fasteners for

the dowel action and the withdrawal stiffness value given in the technical approval for SFS Intec WT-T screws (Deutsches Institut für Bautechnik (DIBt), 2006).

Table 11: Comparison between experimental slip modulus ($k_{s,test}$) and calculated slip modulus based on the model from Paper IV ($k_{UAG,NJ}$), and based on (Tomasi et al., 2010) (k_{DSM} and k_{SSM})

		Tomasi et al. (2010)				(Jacquier & Girhammar, 2014)	
d	[mm]	8.2	8.2	8.2	8.2	6.5	8.2
l_{tot}	[mm]	190	190	220	220	160	160
α	[°]	0	15	30	45	45	45
$k_{UAG,NJ}$	[kN/mm]	5.84	6.44	9.09	11.62	6.36	8.02
k_{DSM}	[kN/mm]	2.27	3.25	5.64	8.15	4.68	5.95
k_{SSM}	[kN/mm]	2.27	4.53	9.83	15.46	8.64	10.95
$k_{s,test}$	[kN/mm]	2.08	6.18	9.14	16.84	9.70	12.71
$k_{UAG,NJ}$ / $k_{s,test}$		2.80	1.04	0.99	0.69	0.66	0.63
k_{DSM} / $k_{s,test}$		1.09	0.53	0.62	0.48	0.48	0.47
k_{SSM} / $k_{s,test}$		1.09	0.73	1.08	0.92	0.89	0.86

The best agreement between the new model ($k_{UAG,NJ}$) and experimental results is obtained for inclination angles between 15° and 30°. At 0° degree, the new model overestimates the slip modulus using the stiffness parameters from Table 10. This is due to the fact that when the screw is perpendicular to the shear plane, the dowel action governs and the assumption of a rigid screw is questionable for the screw length considered here. It can be mentioned that the values obtained with the new model lie in between the values obtained from the single stiffness and the double stiffness models. With the input parameters considered the new model is still not able to predict well the stiffness of joints with inclined screws at 45°. The calculated values are then about 30-35% below the experimental results. For inclinations of 15° and higher the prediction is better than the one obtained with Tomasi's double stiffness model.

The new model does not predict very well the stiffness of inclined screw joints given the current values taken for the stiffness parameter. However the model is consistent, general and represents a reasonable base to be improved considering different input values. If the model can improve the prediction of the stiffness at different angles, it could be a practical tool for the optimisation of combined joints but also for the joints with inclined screws only.

At the moment and with the underlying assumptions, the model works best for short screws with rather larger diameters, and when the inclinations angle is in the range 30° to 60°. For

low inclinations, the embedment response needs to be improved and the influence of the penetration depth considered. An important assumption is that the screw is assumed to be rigid. This is not true; the screw will bend and cause the embedding stiffness to be different from the triangular distribution assumed here. This development of the model is left to future research. It was mentioned that with the tests proposed could improve the calculation model or a different model considering beam on elastic foundation, especially important for vertical screws.

6.3 Evaluation of the tests results on glulam-CLT composite beams

The tests on glulam-CLT composite beams were evaluated in Paper III with a practical focus. It was mentioned in the Methods chapter that the design of the beam was carried out to fulfil the serviceability vibration criteria of the Eurocode 5 and Finnish National Annex. Given an ordinary load case for residential floor, the requirement in terms of flexural rigidity was governing the design. With the cross-section considered, the stiffness of the shear connection was the lever used to fulfil the design requirements. In that respect, it was therefore the shear connection stiffness that was the governing design parameter.

In the ULS, depending on the test series, the shear connection strength or the beam bending strength was governing the design. The failure load observed for the series B2 and B3 was about three times the estimated design load-carrying capacity (beam design resistance $F_{R.uls}$) in the ULS calculated as in (Ceccotti, Fragiacomo, & Giordano, 2007). This means that when evaluating the beam deflection at 40 % of the beam load-carrying capacity, the fasteners are loaded at a load close to or exceeding their design capacity. The beam flexural stiffness at this load levels is therefore lower than when the fasteners are within their expected working load range, say near F_{SLS}. For that reason, the composite beam flexural stiffness (or bending stiffness) in the serviceability limit state was evaluated not only at $0.4 \cdot F_{max}$ but also at the design load F_{SLS} derived from the characteristic load combination in Eurocode (CEN, 2014).
It is emphasised that F_{SLS} and F_{ULS} are about the design actions, and should not be misinterpreted with estimated load for reaching the beam design resistance, noted $F_{R.sls}$ and $F_{R.uls}$. It should also be noted that F_{SLS} corresponds to a reasonable load case for a residential floor in practice. It is noted that doing so, some bias in the evaluation is introduced as it can be argued that different load cases may be chosen. It is nevertheless considered that this is a way to estimate the relevance of this connection system from a practical point of view.

Table 12 presents the bending stiffness values, noted EI, for the different test series. $EI_{04 \cdot Fmax}$ is estimated from the load-deflection curves between the load levels $0.1 \cdot F_{max}$ and $0.4 \cdot F_{max}$, while $EI_{F.sls}$ is obtained between the load levels $F_{SLS}/4$ and F_{SLS}. The predicted values calculated according to the gamma method $EI_{ef,sls,calc}$ are obtained using the modulus of

elasticity reported in section 5.3.3, $E_{global,glulam}$ = 11 898 N/mm^2 and $E_{global,CLT}$ = 11 445 N/mm^2, for the glulam and CLT member, respectively, the slip modulus k_s from the shear tests, see Table 5 (values from series S1 and S8). The degree of composite action (DCA), see Eq. (34), is also presented in Table 12 for each test series:

$$\text{DCA} = \frac{EI_{ef} - EI_0}{EI_\infty - EI_0} \times 100 \tag{34}$$

where EI_{ef}, EI_0 and EI_∞ are the effective bending stiffness of the partially composite section, the bending stiffness of the non-composite section, and the bending stiffness of the fully composite section, respectively. The predicted bending stiffness is represented by dotted curves in Fig. 58.

Table 12: Bending stiffness and degree of composite action (DCA) of the composite beam – values from load-deflection curves and predicted values

Test series	Bending stiffness between $0.1 \cdot F_{max}$ and $0.4 \cdot F_{max}$		Bending stiffness between $F_{SLS}/4$ and F_{SLS}		Predicted bending stiffness	
	$EI_{04 \cdot Fmax}$ MN·m^2	DCA (%)	$EI_{F.sls}$ MN·m^2	DCA (%)	$EI_{ef,sls,calc}$ MN·m^2	DCA (%)
NCA* (EI0)	-	-	-	-	2.90	0
B1_S	3.00	1.9	4.13	23.7	4.86	37.7
B2_NP	5.99	59.7	6.57	70.9	6.89	77.0
B3_NP+S	6.35	66.6	6.96	78.3	7.04	79.9
B4_SG	7.40	86.9	7.63	91.3	8.08	100
FCA** (EI_∞)	-	-	-	-	8.08	100

*NCA = No composite action ($EI_{ef,sls,calc} = EI_0$ calculated as the sum of the bending stiffness of the glulam beam and the CLT panel)

**FCA = Full composite action ($EI_{ef,sls,calc} = EI_\infty$ is calculated assuming that no slip can occur between the glulam and the CLT)

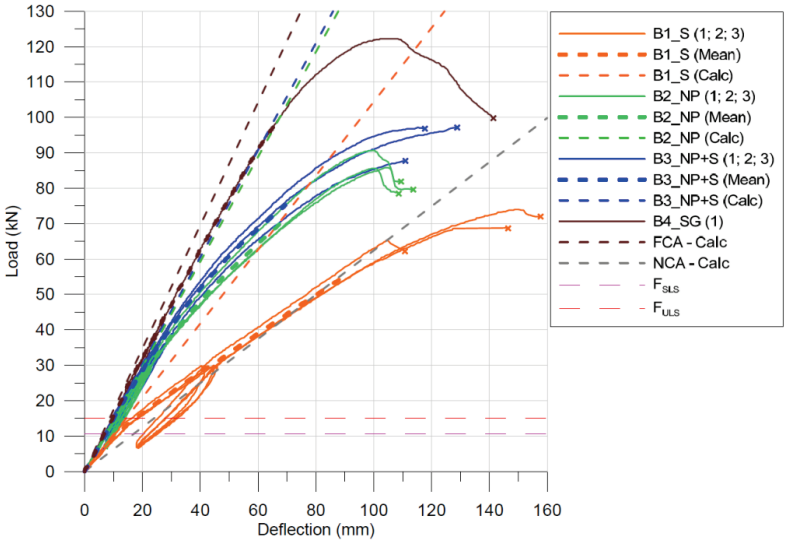

(a)

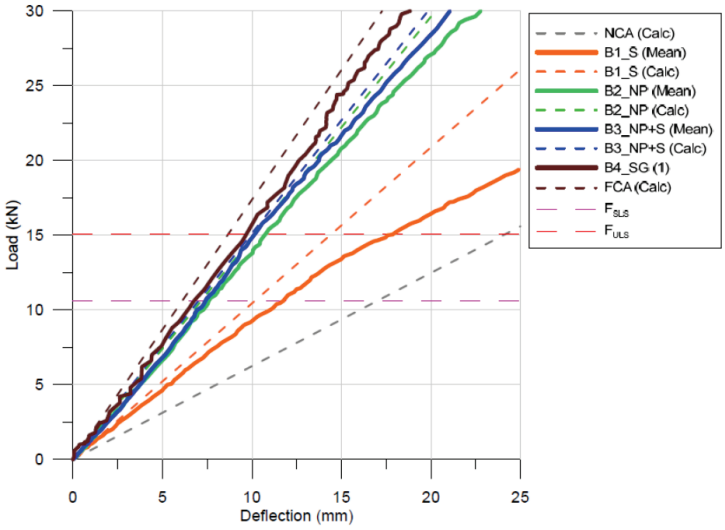

(b)

Fig. 58: Mid-span load-deflection curves for the four-point bending tests and calculated load-deflections curves with the *γ*-method: (a) entire curves; (b) curves up to 25 mm deflection.

The measured longitudinal slip along the beam at the loads F_{SLS}, F_{ULS} and $F_{04.Fmax}$ is shown in Fig. 59 for each test specimen and compared to the yield slip of each fastener type estimated from shear tests (cf. Table 5). The end slip values $s_{sls,2P,calc}$ and $s_{uls,2P,calc}$ calculated according to expressions (35) and (36) are presented with markers on the figure for the load F_{SLS} and F_{ULS}, respectively.

$$s_{\mathrm{sls,2P,calc}} = \frac{\gamma_{1,\mathrm{s}} E_1 A_1 a_{1,\mathrm{s}} s_1}{k_{1,\mathrm{s}} EI_{\mathrm{eff,sls,calc}}} V_{SLS} \tag{35}$$

$$s_{\mathrm{uls,2P,calc}} = \frac{\gamma_{1,\mathrm{u}} E_1 A_1 a_{1,\mathrm{u}} s_1}{k_{1,\mathrm{u}} EI_{\mathrm{eff,uls,calc}}} V_{ULS} \tag{36}$$

where the parameters are described in expressions (1) to (6) with the subscripts "s" and "u" denoting the SLS and ULS values, and V the shear force at the end of the beam. The slip modulus of the fasteners at the ULS is taken as $(2/3)\cdot k_{\mathrm{s}}$.

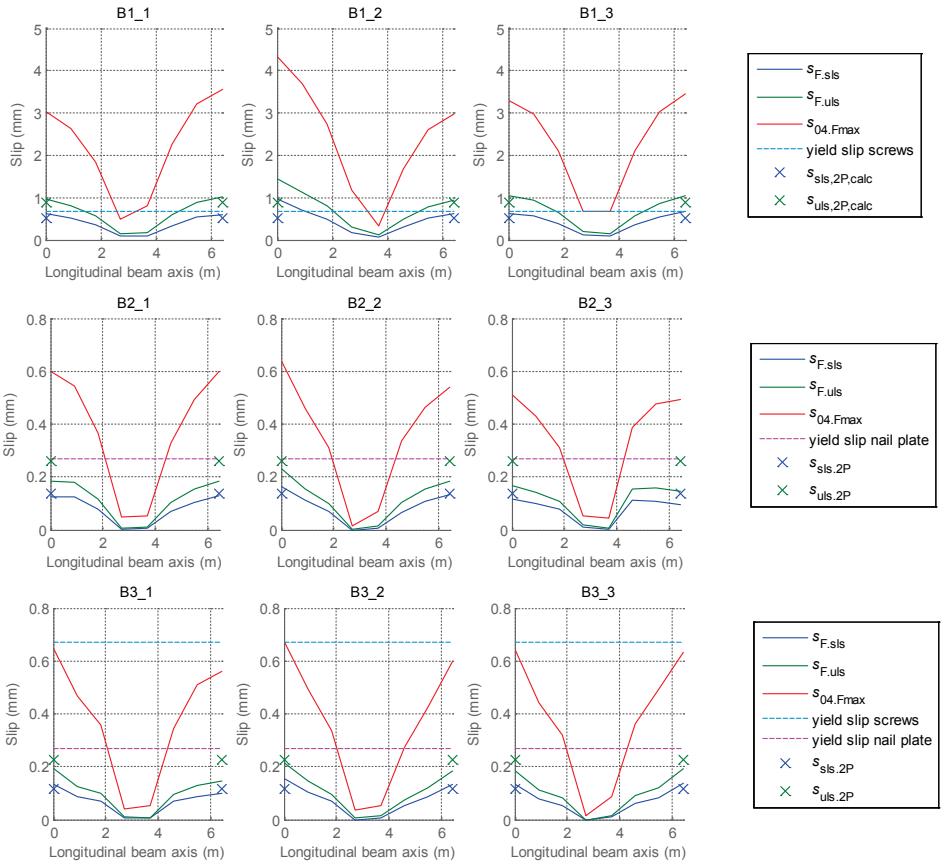

Fig. 59: Glulam-CLT slip along the beam length at loads F_{SLS}, F_{ULS}, $F_{04\cdot\mathrm{Fmax}}$, and yield slip values for the inclined screws and DSNP. The markers show the calculated slip values (γ-method) SLS and ULS design loads considering the 4-point loading case ($s_{\mathrm{sls,2P,calc}}$ and $s_{\mathrm{uls,2P,calc}}$).

Table 13: Comparison between predicted bending stiffness values and test results at different load levels: 0.4·F_{max} and F_{SLS}

Test series	$EI_{ef,sls,calc}$ / $EI_{04\cdot Fmax}$	$EI_{ef,sls,calc}$ / $EI_{F.sls}$
B1_S	1.63	1.17
B2_NP	1.15	1.05
B3_NP+S	1.10	1.01
B4_SG	1.09	1.06

The calculated values according to the Eurocode 5 in Table 13 are not conservative. The flexural stiffness is overestimated. In the serviceability designed load range, analytical values are between 1% and 17 % higher than the measured values.

In general it was observed that the deflection measured was larger than the one predicted according to the gamma method. There are several possible reasons which may explain the difference: overestimation of the shear connector stiffness, shear deformation in the beam, possible shear lag, or the stiffness of the CLT material. One should also note that some variation can be attributed to the method used to interpret the MOE in the CLT, since it is a plate rather than a beam.

6.4 Parameter evaluation and practical implications for partially composite glulam-CLT floor elements

In this section, the practical implications for the composite glulam-CLT floor structure are discussed. The aim is to estimate the practical range of utilisation of the shear connections system made with double-sided nail plates and inclined screws. The gamma method is used to evaluate the efficiency of the floor element type presented in (fig. 10). Figs 60-61 show the influence of the geometrical configuration on the efficiency of the composite section considering a reference CLT panel of 2400 mm width and 60 mm thickness (three 20 mm lamellas) with 3 to 6 glulam beams of width 90 mm. The degree of composite action within the CLT panel is unchanged and depends on the thickness of the cross layer and the value of rolling shear modulus. In Figs 60-61, full composite action (bending stiffness EI_{max}) refers to the connection between the glulam and the CLT. It can be noted that the maximum level of composite action for this particular case is between 3.6 and 3.7 depending on the number of beams while for a two layer composite, the optimum is 4 (Van der Linden, 1999).

Table 14 indicates the minimum bending stiffness required in order to fulfil different serviceability design criteria for single floor spans between 6 to 7 meters. The vibration requirements are usually more demanding than the static deflection requirements. The order of magnitude of the floor bending stiffness needed according to the 9 Hz fundamental frequency criteria for vibration (Finnish National Annex) is between 9 and 17 MN·m^2 for floors spans between 6 and 7 meters. In figs 60-61, the order of magnitude of the bending stiffness per meter width which is necessary to fulfil the serviceability vibration design criteria (9 Hz) is represented by the two horizontal dotted lines for the floor spans of 6 and 7 meters, respectively. Note that the given limit is indicative and represents an order of magnitude. The exact limit for a particular design depends on the floor details affecting the calculation of the mass of the finished floor, which is needed for the fundamental frequency calculation.

Table 14: Minimum bending stiffness value per meter width to fulfill different serviceability design criteria(values in MN·m^2)

Design criteria	Floor span	
	6 m	**7 m**
***L*/400**[(a)]	4.50	7.15
***L*/600**[(a)]	6.75	10.72
0.5 mm 1kN [(b)]	9.00	14.3
8 Hz [(c)]	7.23	13.49
9 Hz [(c)]	9.15	16.94

(a) Static deflection criteria
(b) Static deflection for vibration according to EC5 Finnish National Annex
(c) Fundamental frequency for vibration

Several parameters can be adjusted in order to optimise the floor configuration. The changes to be done depend on the aim of the optimisation (minimising material usage or amount of fasteners, total floor height, etc.). The plots only indicate in which way the modification of some of the parameters affect the main output, the bending stiffness of the floor.

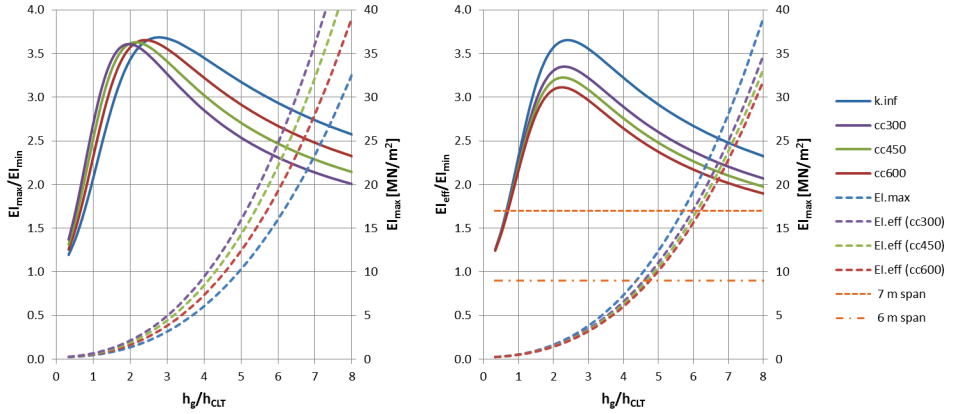

Fig. 60: Influence of the geometry (a) and of the shear connectors (b) on the bending stiffness and efficiency of the connection – Fixed CLT thickness h_{CLT} = 60mm (20/20/20) and varying glulam height h_g, cc300 etc is the distance between the shear connectors

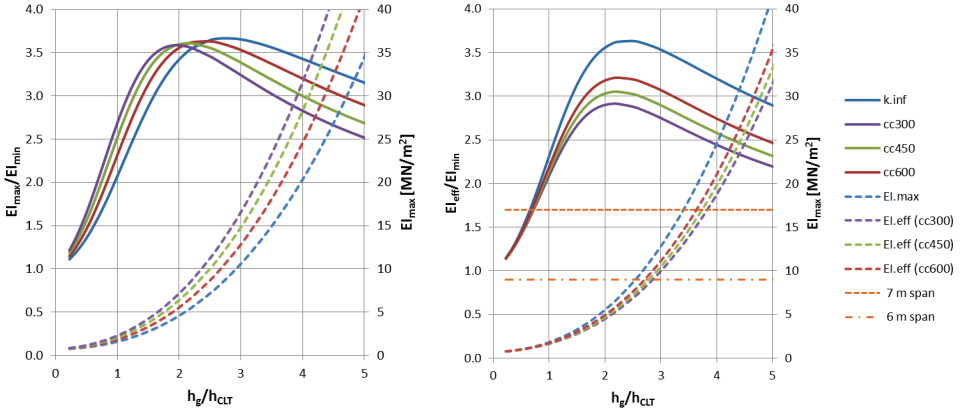

Fig. 61: Influence of the geometry (a) and of the shear connectors (b) on the bending stiffness and efficiency of the connection – Fixed CLT thickness h_{CLT} = 90mm (30/30/30) and varying glulam height h_g, cc300 etc is the distance between the shear connectors

The maximum ratio EI_{max}/EI_{min}, noted λ_{EI} in Figs 60-61 is about 3.6 for both CLT panels thicknesses. The ratio λ_{EI} is presented up to 8 and 5, respectively, and corresponds to the same total floor height ($h_g + h_{CLT} = 8 \cdot 60 + 60 = 5 \cdot 90 + 90 = 540$mm). The optimal ratio is obtained for h_g/h_{CLT} between 2 and 3.

For the same floor height, λ_h = 5 and 3, respectively, the material usage increases by 24 % while the fully composite structure bending stiffness remain similar. The ratio λ_{EI} is higher when the CLT is thicker, indicating that the level of composite action achieved by the shear connection has a larger influence on the bending stiffness when the CLT panel thickness increases. The calculations are presented for a 6 meter beam span.

7 Conclusions

Different types of mechanical shear connection systems were investigated with the aim of creating timber composite floor elements with CLT panels as a base element. A preliminary study concerning the assembly of prefabricated concrete beams elements to CLT panels was carried out. Further investigations were performed on glulam-CLT structural members assembled with double-sided punched metal plate fasteners and inclined screws.

- **RQ1**: How do double-sided punched metal plate fasteners perform as shear connectors in timber composite floor elements?

The use of double-sided punched metal plate fasteners in timber composite structural systems can be relevant for the production of certain types of timber building components. Double-sided punched metal plate fasteners used as shear connectors have a non-linear behaviour. The slip modulus and load-carrying capacity of the 200×72 mm^2 plates tested are sufficiently high to efficiently connect timber members in floor applications at least up to 7 m span. It is considered that double-sided nail plate joints should be secured against separation forces until further research is done due to the post peak-load behaviour of this fastener. The nail plates can be secured using screws.

- **RQ2**: How can the combined effect of different types of mechanical fasteners in a timber joint be considered?

The load-deformation behaviour of mechanical fasteners needs to be known in detail in order to be able to predict the behaviour of joints where different types of mechanical fasteners are combined. The fasteners should have a load-carrying capacity and stiffness with a similar order of magnitude for the combined effect to be relevant. Up to an applied displacement (slip) which is below the yield point of both fastener types, the slip moduli of the fasteners may conservatively be summated. For the estimation of the load-carrying capacity of combined fasteners joints, information about the post peak behaviour of the fasteners, and slip at failure is necessary. An optimal combination will be obtained when both fastener types yield and reach their maximum load for the same applied displacement.
For the particular case of the assembly of double-sided nail plates and inclined screws, it was shown that the stiffness of both fastener types could reasonably be added. Inclined screws have a linear behaviour up to 60-70 % of their ultimate load capacity. The double-sided nail plates have a more non-linear behaviour from the start. The fasteners reach their maximum load-carrying capacity at different slip values and have very different post peak behaviours,

the load-carrying capacity of the combined joint was less than the sum of the capacity of each fastener type and a reduction factor of 0.9 is suggested for the summation of the capacity.

- **RQ 3**: How can we model the stiffness of inclined screw joints in shear-tension in the serviceability limit state?

Joint with inclined screws have varying load-deformation behaviour depending on the inclination of the screw. Strength, stiffness and ductility depend on the chosen inclination of the screws. The inclination angle can be used as a lever to obtain a better compatibility between different types of fasteners used in a multiple fastener joint. The theoretical model presented in this thesis can be used to predict the load-deformation behaviour of inclined screw joints acting in shear tension depending on the inclination angle. The limitation is that the model is valid for the linear elastic range and therefore up to the first yielding point of the screw, giving also an indication in terms of compatibility of displacements for the combined joint.

8 Future research

The long-term behaviour of double-sided punched metal plate fasteners used as shear connectors should be evaluated, considering the effects of moisture variation and transverse loading (compression and separation forces). From a production point of view, the assembly of elements with double-sided punched metal plate fasteners should also be further investigated.

Along with the derivation of the stiffness model for inclined screw joints in shear tension, new test configurations were proposed to determine experimentally the values of some of the required input parameters in the model. These tests may be carried out to validate the model. Additionally, a beam on elastic foundation approach could be used to refine the model with respect to the embedment of the screw, and still considering the effects of withdrawal action and friction.

References

Bartlomé, Olin, & Liebl, Andreas. (2014). *Acoustic solutions for wooden intermediate floors.* Paper presented at the 43rd International Congress on Noise Control Engineering, Inter.noise 2014, Melbourne.

Bejtka, Ireneusz. (2005). *Verstärkung von Bauteilen aus Holz mit Vollgewindeschrauben.* (Doctoral), Universitätsverlag Karlsruhe, Karlsruhe Karlsruher Berichte zum Ingenieurholzbau.

Bejtka, Ireneusz, & Blass, Hans Joachim. (2002). *Joints With Inclined Screws*. Paper presented at the CIB W18, Japan.

Blass, H. J., & Fellmoser, Peter. (2004). *Design of solid wood panels with cross layers.* Paper presented at the WCTE, Lahti, Finland.

Blaß, H. J., & Schädle, P. (2011). Ductility aspects of reinforced and non-reinforced timber joints. *Engineering Structures, 33*(11), 3018-3026.

Blass, Hans Joachim, & Bejtka, Ireneusz. (2000). *Screws with continuous threads in timber connections*. Paper presented at the Joints in Timber Structures, Rilem Proceedings PRO 22.

Blass, Hans Joachim, Schmid, Martin, Litze, Harald, & Wagner, Barbara. (2000). *Nail plate reinforced joints with dowel-type fasteners*. Paper presented at the WCTE.

Bohnhoff, D. R., Williams, G.D., & Moody, Russell C. (1998). *Bending Properties of STP-Laminated Wood Girders*. Paper presented at the An ASAE Meeting Presentation, Orlando, Florida.

Bovim, Nils Ivar (2015). [Personal communication, Unpublished work].

Brandner, Reinhard. (2013). *Production and Technology of Cross Laminated Timber (CLT): A state-of-the-art Report.* Paper presented at the Focus Solid Timber Solutions - European Conference on Cross Laminated Timber (CLT), Graz.

Ceccotti, Ario. (2002). Composite concrete-timber structures. *Progress in structural engineering and materials, 4*(3), 264-275.

Ceccotti, Ario. (2003). Composite Structures. In S. Thelandersson & H. J. Larsen (Eds.), *Timber Engineering* (pp. 409-427). West Sussex, England: John Wiley and Sons Ltd.

Ceccotti, Ario, Fragiacomo, Massimo, & Giordano, Saverio. (2007). Long-term and collapse tests on a timber-concrete composite beam with glued-in connection. *Materials and Structures, 40*(1), 15-25. doi: 10.1617/s11527-006-9094-z

CEN. (2014). EN 1995-1-1:2004/A2:2014 *Eurocode 5 - Design of timber structures - Part 1-1: General - Common rules and rules for buildings*. Brussels, Belgium: European Committe for Standardization.

Crocetti, Roberto, Sartori, T., & Tomasi, R. (2014). Innovative Timber-Concrete Composite Structures with Prefabricated FRC Slabs. *Journal of Structural Engineering, 0*(0), 04014224. doi: doi:10.1061/(ASCE)ST.1943-541X.0001203

Zulassung Z-9.1-472 - SFS Befestiger WT-T-6,5, WT-T-8,2 und WR-T-8,9 als Holzverbindungsmittel (2006).

Deutsches Institut für Bautechnik (DIBt). (2011). European Technical Approval ETA-08/0271 - CLT - Cross Laminated Timber. In European Organisation for Technical Approvals (EOTA) (Ed.), *ETA-08/0271* (pp. 17).

Dias, A. M. P. G. (2005). Mechanical Behaviour of timber-concrete joints.

DIBt, Deutsches Institut für Bautechnik. (2005). Zulassung Z-9.1-210 vom: 19.09.2005 Wolf-Nagelplatten Typ 15 N, 15 NE, 15 Z und 15 ZE als Holzverbindungsmittel.

European Committe for Standardization (CEN). (1991). EN 26891:1991 - Timber structures - Joints made with mechanical fasteners - General principles for the determination of strength and deformation characteristics.

European Committe for Standardization (CEN). (1999). EN 1075:1999 - Timber Structures - Test methods – Joints made with punched metal plate fasteners. Brussels.

European Committe for Standardization (CEN). (2001). EN 12512:20014 - Timber strucutres - Test methods - Cyclic testing of joints made with mechanical fasteners. Brussels.

European Committe for Standardization (CEN). (2008). EN 14545:2008 - Timber structures - Connectors - Requirements. Brussels.

European Committe for Standardization (CEN). (2012). SS-EN 408:2010+A1:2012 Timber structures - Structural timber and glued laminated timber - Determination of some physical and mechanical properties: Swedish Institute for Standards (SIS).

National Annex To Standard SFS-EN 1995-1-1 EUROCODE 5: Design of Timber Structures Part 1-1: Common rules and rules for buildings (Unofficial translation) (2007).

Finnish Wood Research. (2013). RunkoPES 2.0.

Foschi, Ricardo O. (1977). Analysis of wood diaphragms and trusses. Part I: Diaphragms. *Canadian Journal of Civil Engineering, 4*(3), 345-352. doi: 10.1139/l77-043

Gagnon, Sylvain, & Pirvu, Ciprian. (2011). *CLT Handbook Cross-Laminated Timber - Canadian Edition*. Québec: FP Innovations.

Guggenberger, Werner, & Moosbrugger, Thomas. (2004). *Mechanics of Cross-Laminated Timber Plates under Uniaxial Bending*. Paper presented at the WCTE 2004.

Jacquier, N. (2014). Shear tests on glulam-CLT joints with double-sided punched metal plate fasteners and inclined screws (D. o. S. a. C. Engineering, Trans.). Luleå Univeristy of Technology.

Jacquier, N. (2015). Bending tests on glulam-CLT composite beams with double-sided punched metal plate fasteners and inclined screws (D. o. S. a. C. Engineering, Trans.). Luleå Univeristy of Technology.

Jacquier, N., & Girhammar, U. A. (2014). Tests on glulam-CLT shear connections with double-sided punched metal plate fasteners and inclined screws. *Construction and Building Materials, 72*, 444-457.

Johansen, K. W. (1949). Theory of Timber Connections. *International Association of Bidge and Structural Engineering, 9*, 249-262.

Jorge, Louis, Habenbacher, Johannes, & Dujic, Bruno. (2010). *Timber-concrete composite systems with Cross Laminated Timber*. Paper presented at the WCTE.

Jorge, Luís Filipe de Carvalho. (2005). *Estruturas mistas madeira-betão com a utilização de betões de agregados leves [Timber-concrete composite structures using lightweight concrete]*. (Doctoral).

Jorissen, André, & Fragiacomo, Massimo. (2011). General notes on ductility in timber structures. *Engineering Structures, 33*(11), 2987-2997. doi: 10.1016/j.engstruct.2011.07.024

Kevarinmäki, Ari. (2000). *Nail plate reinforced metal plate-to-timber joints made with nail screw or pop rivet fasteners*. Paper presented at the WCTE.

Kevarinmäki, Ari. (2002). *Joints with Inclined Screws*. Paper presented at the CIB W18, Japan.

Kolb, Josef. (2008). *Systems in Timber Engineering* (L.-H. Schweiz Ed. 1 ed.): Birkhäuser Architecture.

Kreuzinger, Heinrich. (1999). Platten, Scheiben und Schalen. Ein Berechnungsmodell für gängige Statikprogramme. *Bauen mit Holz*(Jg.101, Nr.1), S.34-39.

Lukaszewska, E. (2009). *Development of Prefabricated Timber-Concrete Composite Floors.* (Doctoral), Luleå University of Technology, Luleå.

Lukaszewska, E., Johnsson, H., & Fragiacomo, M. (2008). Performance of connections for prefabricated timber-concrete composite floors. *Materials and Structures/Materiaux et Constructions, 41*(9), 1533-1550.

McCullough, Conde B. . (1943). Oregon Tests on Composite (Timber-Concrete) Beams. *Journal of the American Concrete Institute, 39*. doi: 10.14359/8637

Möhler, Karl. (1956). *Uber das Tragverhalten von Biegeträgern und Druckstäben mit zusammengesetzten Querschnitten und nachgiebigen Verbindungsmitteln.* Karlsruhe. Available from http://worldcat.org /z-wcorg/ database.

Moshiri, F., Gerber, C., Valipour, H. R., Shrestha, R., & Crews, K. I. (2013). *The predictive model for strength of inclined screws as shear connection in timber-concrete composite floor.* Paper presented at the From Materials to Structures: Advancement Through Innovation - Proceedings of the 22nd Australasian Conference on the Mechanics of Structures and Materials, ACMSM 2012.

Nielsen, Jacob. (1996). *Stiffness Analysis of Nail-Plate Joints Subjected to Short-Term Loads.* Aalborg University. Department of Mechanical Engineering, Aalborg.

Nielsen, Jacob. (2003). Trusses and Joints with Punched Metal Plate Fasteners. In S. Thelandersson & H. J. Larsen (Eds.), *Timber Engineering* (pp. 365-382). West Sussex, England: John Wiley and Sons Ltd.

Österreichisches Institut für Bautechnik (OIB), Member of EOTA. (2012). European technical approval ETA-12/0063 - SFS self-tapping screws WT.

Racher, P. (1995). Mechanical timber joints - General *Timber Engineering STEP 1*. The Netherlands: Centrum Hout.

Ringhofer, Andreas, Brandner, Reinhard, & Schickhofer, Gerhard. (2013). Withdrawal resistance of self-tapping screws in unidirectional and orthogonal layered timber products. *Materials and Structures*, 1-13. doi: 10.1617/s11527-013-0244-9

Ringhofer, Andreas, & Schickhofer, Gerhard. (2013). *Timber in Town - Current examples for residential buildings in CLT and tasks for the future.* Paper presented at the Focus Solid Timber Solutions -European Conference on Cross Laminated Timber (CLT), Graz.

Ringhofer, Andreas, & Schickhofer, Gerhard. (2014). *Multi-storey residential buildings in CLT - Interdisciplinary principles of design and construction*. Paper presented at the World Conference on Timber Engineering, Quebec City, Canada.

Smith, I., & Frangi, A. (2008). Overview of design issues for tall timber buildings. *Structural Engineering International: Journal of the International Association for Bridge and Structural Engineering (IABSE), 18*(2), 141-147.

Stürzenbecher, R., Hofstetter, K., & Eberhardsteiner, J. (2010). Structural design of Cross Laminated Timber (CLT) by advanced plate theories. *Composites Science and Technology, 70*(9), 1368-1379. doi: DOI: 10.1016/j.compscitech.2010.04.016

Stürzenbecher, Reinhard, Hofstetter, Karin, & Eberhardsteiner, Josef. (2010). *Cross Laminated Timber: a multi-layer, shear compliant plate and its mechanical behavior*.

Symons, D., Persaud, R., & Stanislaus, H. (2010). Slip modulus of inclined screws in timber-concrete floors. *Proceedings of the Institution of Civil Engineers: Structures and Buildings, 163*(4), 245-255.

Tomasi, Roberto, Crosatti, Alessandro, & Piazza, Maurizio. (2010). Theoretical and experimental analysis of timber-to-timber joints connected with inclined screws. *Construction and Building Materials, 24*(9), 1560-1571. doi: 10.1016/j.conbuildmat.2010.03.007

Uibel, T., & Blass, H. J. (2006). *Load carrying capacity of joints with dowel type fasteners in solid wood panels*. Paper presented at the CIB W18, Italy.

Uibel, T., & Blass, H. J. (2007). *Edge joints with dowel type fasteners in Cross Laminated Timber*. Paper presented at the CIB W18, Slovenia.

Van der Linden, Mario. (1999). *Timber-concrete composite floor systems.* (Doctoral).

Wanyama, O. G., Sawata, K., Hirai, T., Koizumi, A., & Sasaki, Y. (2012). Effective lateral resistance of combined timber joints with nails and bolts. *Journal of Wood Science, 58*(1), 9-19.

Whale, L.R.J. (1995). Punched metal plate fastener joints *Timber Engineering STEP 1*: Centrum Hout.

Wolfe, Ronald, Bohnhoff, David, & Nagel, Robert. (1993). Stiffness and Strenghth Properties of Shear Transfer Plate Connections. United States Deprtment of Agriculture: Forest Product Laboratory.

Yeoh, D., & Fragiacomo, M. (2012). The design of a semi-prefabricated LVL-concrete composite floor. *Advances in Civil Engineering, 2012*.

Zhou, T., & Guan, Z. (2011). Numerical modelling for sensitivity analysis of wood joints made with double-sided punched metal plate fasteners. *Advances in Structural Engineering, 14*(2), 163-177.

Zhou, T., Rodd, Peter D., Guan, Zhongwei, & Pope, David J. (2004). *Deformation Behaviour of Double-Sided Metal Nail Plate Timber Joints*. Paper presented at the WCTE.

Doctoral and licentiate theses

Timber Structures

Luleå University of Technology

Doctoral theses

2001 Nils Olsson: Glulam Timber Arches – Strength of Splices and Reliability-Based Optimisation. 2001:12D.

2004 Helena Johnsson: Plug Shear Failures in Nailed Timber Connections – Avoiding Brittle and Promoting Ductile Failures. 2004:03D.

2004 Max Bergström: Industrialized Timber Frame Housing – Managing Customization, Change and Information. 2004:45D.

2005 Andreas Falk: Architectural Aspects of Massive Timber – Structural Form and Systems. 2005:41D.

2005 Ylva Sardén: Complexity and Learning in Timber Frame Housing – The Case of a Solid Wood Pilot Project. 2005:43D.

2006 Anders Björnfot: An Exploration of Lean thinking for Multi-Storey Timber Housing Construction – Contemporary Swedish Practices and Future Opportunities. 2006:51D.

2008 Matilda Höök: Lean Culture in Industrialized housing – A study of Timber Volume Element Prefabrication, 2008:21D.

2008 Tomas Nord: Prefabrication strategies in the timber housing industry - A comparison of Swedish and Austrian markets, 2008:51D.

2009 Elzbieta Lukaszewska: Development of prefabricated timber-concrete composite floors, ISBN 978-91-86233-85-3.

2010 John Meiling: Continous improvement and experience feedback in off-site construction – Timber-framed module prefabrication, ISBN 978-91-7439-180-0.

2011 Gabriela Tlustochowicsz: Stabilising system for multi-storey beam and post timber buildings, ISBN 978-91-7439-339-2.

2012 Susanne Engström: Managing information to unblock supplier-led innovation in construction – Barriers to client decision-making on industrialized building in Sweden, ISBN 978-91-7439-407-8.

2012 Martin Lennartsson: The transition of industrialised house-building towards improved production control, ISBN 978-91-7439-458-0.

2013 Erika Hedgren: Overcoming organizational lock-in in decision making – Construction clients facing innovation, ISBN 978-91-7439-572-3.

2013 Gustav Jansson: Platforms in industrialised house-building, ISBN 978-91-7439-758-1.

2014 Jarkko Erikshammar: Supply chain integration for small sawmills in industrialized house-building, ISBN 978-91-7439-934-9.

2014 Martin Haller: Design Iteration Control Framework for Offsite Building Projects, ISBN 978-91-7583-124-4

2014 Giuseppe Caprolu: Evaluation of Splitting Capacity of Bottom Rails in Partially Anchored Timber Frame Shear Walls, ISBN 978-91-7586-150-3

2015 Nicolas Jacquier: Development and Evaluation of Mechanical Joints for Composite Floor Elements with Cross Laminated Timber, ISBN 978-91-7583-307-1

Licentiate theses

2001 Helena Johansson: Systematic Design of Glulam Trusses. 2001:07L.

2003 Ylva Fredriksson: Samverkan mellan träkomponenttillverkare och stora byggföretag – en studie av massivträbyggandet. 2003:14L.

2003 Sunna Cigén: Materialleverantören i byggprocessen – en studie av kommunikationen mellan träkomponentleverantören och byggprocessens övriga aktörer. 2003:69L.

2004 Anders Björnfot: Modular Long-Span Timber Structures – a Systematic Framework for Buildable Construction. 2004:34L.

2005 Henrik Janols: Communicating Long-Span Timber Structures with 3D Computer Visualisation. 2005:30L.

2005 Tomas Nord: Structure and Development in the Solid Wood Value Chain – Dominant Saw Milling Strategies and Industrialized Housing. 2005:57L.

2005 Matilda Höök: Timber Volume Element Prefabrication – Production and Market Aspects. 2005:65L.

2008 Annicka Cettner: Kvinna i byggbranschen – Civilingenjörers erfarenheter ur genusperspektiv. 2008:05L.

2008 John Meiling: Product Quality through experience feedback in industrialised housing, 2008:36L

2009 Martin Lennartsson: Modularity in Industrial Timber Housing – A Lean approach to develop building service systems, ISBN 978-91-7439-047-6.

2010 Erik Söderholm: Applicability of Continuous Improvements in Industrialised Construction Design Process, ISBN 978-91-7439-086-5.

2010 Erika Levander: Addressing Client Uncertainty – A Swedish property owners´ perspective on industrial timber framed housing and property, ISBN 978-91-7439-109-1.

2010 Gustav Jansson: Industrialised Housing Design Efficiency, ISBN 978-91-7439-138-1.

2011 Jarkko Erikshammar: Collaborative product development – a purchasing method in small industrialized house-building companies, ISBN 978-91-7439-329-3.

2012 Martin Haller: Critical design activities in house-building projects – an industrial process perspective, ISBN 978-91-7439-383-5.

2014 Gustav Nordström: Use of energy-signature method to estimate energy performance in single-family buildings, ISBN 978-91-7583-023-0

2014 Alex Kaiser: Architecturally Innovative Multi-Storey Timber Buildings: Methodology and Design, ISBN 978-91-7583-139-8

2014 Magnus Larsson: Conflict and Compromise: An Evolutionary Framework for the Design of Multi-Storey Timber Buildings, ISBN 978-91-7583-142-8

Part II - Appended papers

Paper I

Tests on shear connections in prefabricated composite cross-laminated-timber and concrete elements

by Nicolas Jacquier and Ulf-Arne Girhammar

Presented at the 12th World Conference on Timber Engineering,

Auckland, New Zealand, 2012

WCTE Auckland 2012
16 - 19 July
World Conference on Timber Engineering

TESTS ON SHEAR CONNECTIONS IN PREFABRICATED COMPOSITE CROSS-LAMINATED-TIMBER AND CONCRETE ELEMENTS

Nicolas Jacquier[1], Ulf Arne Girhammar[2]

ABSTRACT: The authors report on an experimental test program on different shear connectors to be used in floor elements where prefabricated concrete beams are to be connected on top of cross-laminated timber (CLT) panels. The objective is to evaluate the level of composite action that can be achieved and the increase of strength and stiffness when combining effectively these structural components in a floor element. Shear tests were performed on 12 specimens in total. The shear connector consists of a steel plate as the common part to connect to both the concrete beam and the CLT panel. To the steel plate, studs or a metal mesh were welded and casted in the concrete beam to form a prefabricated unit. The CLT panel was then attached to the steel plate by screws. The main slip occurred between the CLT panel and the steel plate. The test results show a high ultimate load capacity for all types of shear connectors and a ductile type of behaviour for most of them. The test results for the shear connectors were compared with the capacity obtained from analytical models. Also, the strength and stiffness of partially composite floor elements with these shear connectors were analysed. It was found that from a structural point of view these shear connections are suitable to be used to form floor elements with a high level of composite action.

KEYWORDS: CLT, prefabricated concrete, shear test, shear connectors, slip modulus, coach screws

1 INTRODUCTION

The company Stora Enso is developing a new building system based on composite structures with prefabricated elements, including the use of cross-laminated timber (CLT) panels. In that process, the company wanted to evaluate the contribution of a CLT panel added underneath to the main load-carrying concrete beams with respect to strength and stiffness of the total composite floor structure. This floor element is not a conventional composite concrete-timber structure, but rather a combined structure for the purpose of making use of and benefitting from the materials and components present in the total floor structure by connecting them together. In addition, by connecting several concrete beams on a CLT panel, a prefabricated floor element ready for assembly on site is obtained. One focus then is the development of an efficient shear connection between the prefabricated concrete beams and the CLT panel. Luleå University of Technology (LTU) was given the assignment to evaluate the above mentioned composite system and to study different shear connection systems designed for connecting together components prefabricated separately. The aim of the paper is to present the outcomes of the test program that has been performed at LTU, consisting in shear tests on two different types of connectors for prefabricated concrete-CLT elements.

[1] Nicolas Jacquier, PhD student, Timber Structures, Division of Structural and Construction Engineering, Luleå University of Technology, SE-971 87 Luleå, Sweden.
Email: nicolas.jacquier@ltu.se
[2] Ulf Arne Girhammar, Professor, Timber Structures, Division of Structural and Construction Engineering, Luleå University of Technology, SE-971 87 Luleå, Sweden.
Email: ulf.arne.girhammar@ltu.se

2 TIMBER-CONCRETE COMPOSITE STRUCUTRES

2.1 BACKGROUND

Extensive research has been carried for several decades for assessing the behavior of timber concrete composite structures, with a strong focus on shear connectors since it is a key parameter governing the overall behavior and efficiency of composite structures. However, most of the systems used today work with “wet connections” where concrete is poured on timber elements preinstalled with shear connectors. The drawbacks of the traditional timber-concrete structures are well known, such as the time needed for concrete to cure, the low stiffness of the structure and the shrinkage that takes place during the curing time, as well as the problems related to the introduction of wet components in the timber construction process [1]. The interests for developing prefabricated timber concrete structures are growing since an off-site production of elements could reduce the influence of the above mentioned shortcomings [1], [2]. Some work has been done on prefabricated timber-concrete composite floors elements in the last years [1], [3]. However, the solutions developed are not applicable for the present floor configuration where concrete beams are to be connected on top of a CLT panel. New types of shear connectors were thus developed for this floor structure.

2.2 REQUIREMENTS FOR THE FLOOR ELEMENTS PRESENTED

The floor system for which the connectors are developed is not conventional since concrete is not used in form of a plate but in form of beams elements. Concrete beams, attached on top of the CLT panel allow for some technical installations to be placed between the beams. In this floor configuration, the CLT panel forms a platform for mounting and connecting the installations from above during the prefabrication process at the factory. An objective for the floor elements is to allow for a high level of prefabrication in order to ensure a quick assembly on site. For manufacturing these floor elements the concrete beams should be prefabricated due to the following aspects:

- Avoid a wet assembly process and avoid deflections induced by concrete shrinkage.
- Reduce the space required for storage of the elements during curing time compared with concrete beams casted on CLT.
- Be able to produce the CLT and the concrete at different locations and assemble them at the last possible moment in the prefabrication process.
- Be able to reduce the production time both on site and at the factory.
- Bring about a demountable system.

The requirements for the design of the shear connectors were to enable a dry assembly process, and to be able to mount the connectors from the top side of the CLT panel in order to have them protected in case of fire.

3 EXPERIMENTS - SHEAR TESTS

The test program consisted of asymmetric shear tests on CLT-steel-concrete blocks (see Figure 1) with five different connection configurations (with different number of screws and screw lengths) for two series differing by the steel-concrete shear connector used, series S (studs) and series M (expanded metal mesh). For each series, the connection was tested with 4 and 8 screws. Totally, twelve specimens were tested.

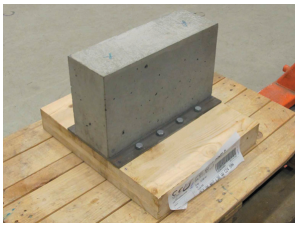

Figure 1: *Picture of a test specimen*

3.1 MATERIALS

3.1.1 CLT

The CLT panels, provided by Stora Enso, were made with 3 layers of timber of strength class C24 according to EN 338 [4]. The grain direction of the outer layers is oriented in the direction of the concrete beams. All the tests were performed with panel of nominal thickness 74 mm (lamella structure in mm: 27.5/19/27.5), except one in which the CLT had a nominal thickness of 103 mm (lamella structure in mm: 42/19/42). Density and moisture content were measured on all CLT specimens from timber located near the failure region, giving ρ_m = ***448 kg/m^3*** and ρ_k = ***396 kg/m^3***, and average moisture content of **11.6 %** at testing.

3.1.2 Steel shear connectors

Two different types of connectors were chosen for the tests, see Figure 2. The first type of connector, named *Studs* in this paper, consisted of a 6 mm thick steel plate with two welded headed studs. The second type, noted *Mesh* in this paper, was made using an expanded metal mesh welded in between two folded steel plates of 4 mm thickness with large holes, similar to the so-called "perfobond" shear connector. Both steel shear connectors were made out of mild steel S355. Pre-drilling of the steel plates for the screws can be made vertically only, unless some specific drilling tools are used. Thus, vertical holes of 12.0 mm diameter were made in the steel plates for the screwed connection to the CLT with 80 mm spacing. Geometrical details for the shear connectors are presented in Figure 4.

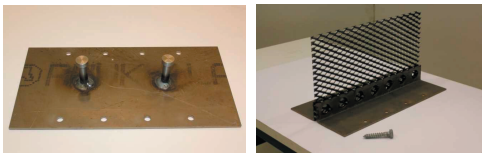

(a) (b)

Figure 2: *Pictures of the shear connectors (a) Studs, (b) Mesh*

3.1.3 Concrete

Concrete was casted onto the steel shear connectors in a factory to form the concrete-steel prefabricated units. The same batch of concrete was used for all the test specimens and the nominal strength class was C25/30. 15 cubic samples were made for strength testing, giving a compressive strength $f_{cm,cube}$ = 40,81 N/mm^2, at 28 days, in accordance with the strength class C25/30. Two rebars of 8 mm of diameter were placed in each prefabricated unit as the minimum bottom reinforcements in all concrete blocks.

3.1.4 Mechanical fasteners

Due to the limited depth of the CLT panel, coach screws with rather large diameter were chosen in order to provide the connection with sufficient strength and stiffness. The coach screws used to connect the concrete beam blocks to the CLT panels for tests specimens 1 to 11 were timber screws DIN 571 - 4.6/FZV - 12x65 with dimensions according to Figure 3.

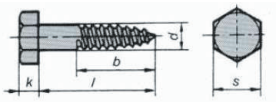

k = 8 mm, l = 65 mm, d = 12 mm, s = 19 mm, b = 50 mm

Figure 3: *Geometrical description of the screws*

For the test specimen 12, longer screws were used, with geometrical parameters k = 8 mm, l = 100 mm, d = 12 mm, s = 19 mm, b = 60 mm, according to Figure 3.

3.2 TEST SPECIMENS

CLT elements, 500 mm wide and 420 mm long, were all predrilled with 8 holes according to EC5 recommendations. The lead hole for the threaded portion of the screws had a diameter of 8.5mm and the lead hole for the shank of the screw had a diameter of 11.5mm since it was the diameter actually measured on the shank of the screws used. The steel-concrete blocks were mounted with 40 kN·m torque applied on each screw. Geometrical details for the S-series, with studs, and M-series, with mesh shear connectors are presented in Figure 4. Complementary specifications for the test specimens are given in Table 1.

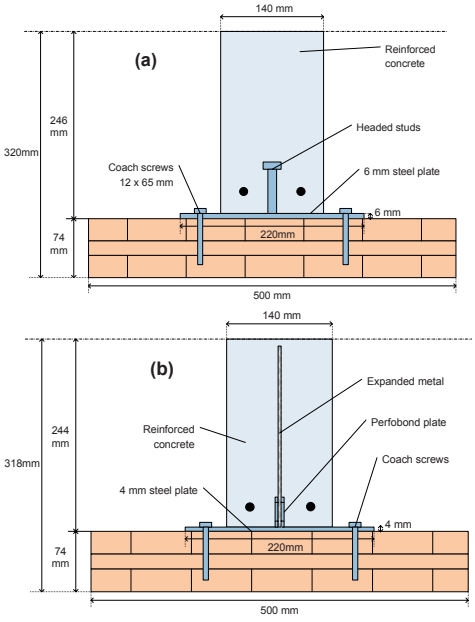

Figure 4: *Test specimens, (a) S-series, (b) M-series*

Table 1: *Description of the test series*

Test series	Tests	Shear connector / steel plate thickness	Screw spacing in loading direction / edge distance (mm)	CLT panel thickness (mm)
S-8S-65	T1, T2, T3	Studs /6mm	80 / 90	74
S-4S-65	T4, T5, T6	Studs /6mm	240 / 90	74
M-8S-65	T7, T8, T9	Mesh /4mm	80 / 90	74
M-4S-65	T10, T11	Mesh /4mm	240 / 90	74
M-8S-100	T12	Mesh /4mm	80 / 90	103

3.3 DESIGN OF THE SHEAR CONNECTIONS

The load carrying capacity and the slip modulus of the steel-timber connection were calculated according to Eurocode 5 [5] and the European technical approval for CLT from the manufacturer [6] and are given in Table 2.

3.4 TEST SETUP

The shear tests were performed on asymmetric elements in a hydraulic press, Dartek Server hydraulic load frame of capacity ± 600 kN, with two data acquisition systems HPM 8 Channels Spider 8. Height LVDTs (Linear Variable Differential Transformer) were used for each test. The specimens were supported on the end face of the CLT panel, with the concrete block hanging by the side of the CLT panel by the shear connection (Figure 5). Due to size limitations of the test setup, it was not possible to install a roller support at the top of the concrete to prevent the rotation of the test specimen. Instead, Teflon material was taped onto the vertical steel frame support and an oiled steel plate was placed between the concrete block and the steel frame to minimise friction. The top surface of the concrete block was grinded, in order to provide an even surface for the contact with this steel plate.

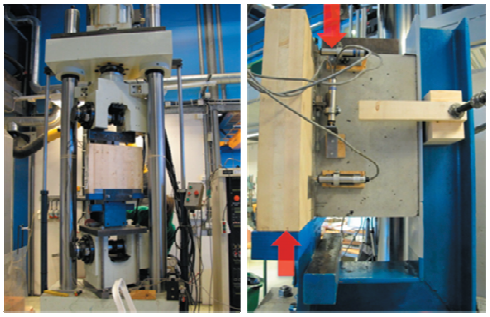

Figure 5: *Pictures of the test setup for the shear test*

3.5 SLIP MEASUREMENTS

Slip measurements were made symmetrically on both sides of the specimen. The results presented are average values from both sides. The longitudinal slip was measured between the CLT and the concrete block and between the steel plate and the concrete in order to verify that the steel-concrete slip is negligible compared to the slip at the steel-timber interface as it is assumed in the calculation model. The separation between the concrete block and the CLT panel (Figure 6) was measured as a control of the test setup and are not presented explicitly in this paper.

Displacement-controlled tests were performed with loading conditions according to ISO Standard 6891 [7], except for specimen T1, which was a load-controlled test. Only the ultimate load for this latter test is used as the test results. The rate of the different tests was adjusted for each test according to the estimated load and the results from previous tests. The tests were stopped if 15 mm slip was reached at the steel-timber interface. The

ultimate load capacity is evaluated as the absolute maximum value occurring during the test within 15 mm of slip.

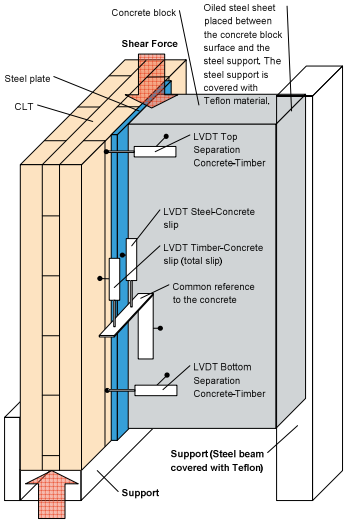

Figure 6: *Location of the LVDTs on the test specimens*

The adjustment of the estimated maximum capacity F_{est} between the different tests in accordance with ISO 6891, affects the estimation of the slip modulus as pointed out in [8]. In this paper, the slip modulus is evaluated based on the observed maximum value for each test and not on the estimated value. The slip modulus for the serviceability limit state is evaluated as the slope of the curve up to the level of 40 % of the maximum load. Due to the unusual character of the curve in the beginning of the load-slip relationship, the suggested lower level of 10 % of the maximum load usually used for the evaluation is disregarded in this paper, see below.

4 RESULTS

Three different values for the slip between the different components of the specimen are used:
- The **total slip** between the concrete and the CLT panel (2 LVDTs).
- The **steel-concrete slip** between the steel plate and the concrete beam (2 LVDTs).
- The **steel-timber slip** between the steel plate and the CLT panel (obtained as the difference between the two former values).

4.1 TEST RESULTS FOR ALL SPECIMENS

The load-displacement curves for the total slip are presented in Figure 7 for all five test series according to Table 1.

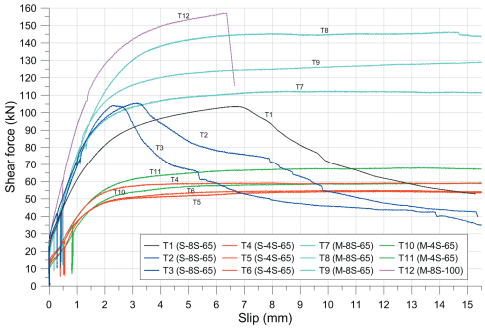

Figure 7: *Load slip curves for all shear tests - Total slip (timber-concrete)*

The first group of tests (S-8S-65: T1-T3) with studs in the concrete and 8 screws in the panel, showed semi-brittle behaviour; the failures occurred in the concrete after yielding of the studs in the concrete at an applied load of about 105 kN (Figure 8). After the peak load, the curves were gradually softening due to increased cracking of the concrete.

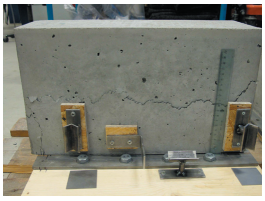

Figure 8: *Picture of the failure in the concrete (Test series S-8S-65)*

Test specimens T4-T6 (S-4S-65), with 4 screws in the panel, exhibited a very ductile type of behaviour, an almost perfect plastic behaviour with an extended yield plateau. The failure occurred by combined embedment failure in the CLT panel and yielding of the screws (Figure 9). The average ultimate load of 56.3 kN was about half of that of the first series with twice as many screws.

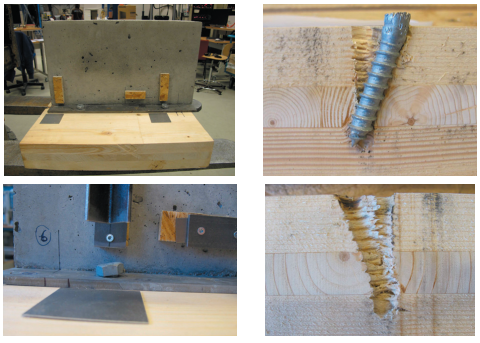

Figure 9: *Pictures of the failure in the timber (Test series S-4S-65)*

The third series (M-8S-65: T7–T9) with a mesh in the concrete and 8 screws in the panel, behaved almost the same as the second series, however, with an average ultimate load of 129.2 kN, about twice as high (Figure 10).

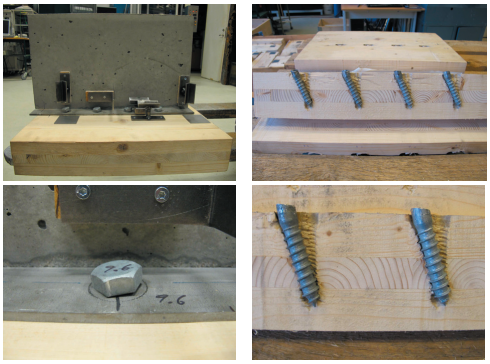

Figure 10: *Pictures of the failure in the timber (Test series M-8S-65)*

Tests T10 and T11 (M-4S-65) with a mesh in the concrete and 4 screws in the panel, had both the same characteristics and level of yielding as the second series with an average ultimate load of 63.7 kN (Figure 11).

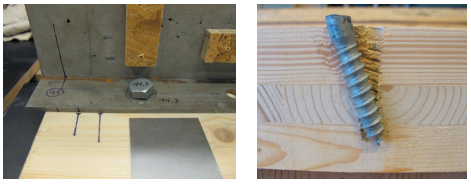

Figure 11: *Pictures of the failure in the timber (Test series M-4S-65)*

The final series (M-8S-100: T12) with a mesh in the concrete and 8 screws in the panel, but with thicker panel and longer screws compared to other series, had a brittle failure after some yielding; the concrete block was split apart in line with the expanded metal mesh at 157 kN applied shear force (Figure 12).

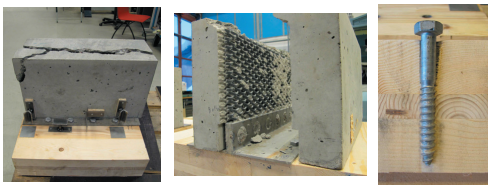

Figure 12: *Pictures of the failure in the concrete (Test series M-8S-100)*

As is evident from Figure 7, the initial stiffness is very high, probably due to friction between the steel plate and the CLT-panel (the screws were tightened rather hard).

A close look at the measured data shows that even some negative slip occurred. The LVDTs measuring the separation at the top and bottom of the test specimen (Figure 6) actually showed that the concrete block was slightly rotating during the test, due to some imperfections in the test setup. This affected the measurements of the total and the steel-concrete slips. The negative slip measured at the steel-concrete interface never exceeded -0.05 mm for all tests and reached a maximum for applied shear forces between 20 kN and 50 kN. It was therefore not possible to evaluate quantitatively the steel-concrete slip modulus.

However, for the steel-timber slip values, which are obtained as the difference between the total and the steel-concrete slips, this negative absolute rotation is eliminated in the subtraction. Detailed load-slip curves for this steel-timber interface are shown in Figure 13. The high initial stiffness is observable up to 10 kN and 20 kN of applied shear force for connections with 4 and 8 screws, respectively. These load values are near or below the serviceability load levels. It means that it is reasonable to exclude this high initial stiffness branch when evaluating the slip modulus. In this paper, the slip modulus will be evaluated using the 40 % level of the maximum shear force as the upper limit and the origin as the lower limit.

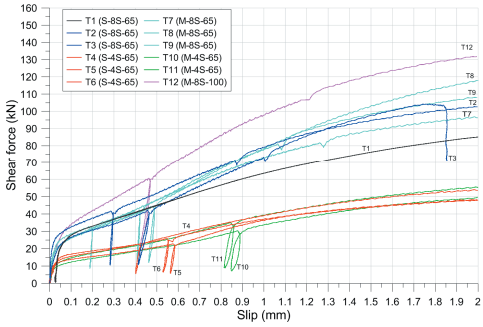

Figure 13: *Detailed load-slip curves for all shear tests – slip at the steel-timber interface up to 2 mm.*

After the initial stiffness area, there is a drastic change in the stiffness according to Figure 13. At a later stage and, especially, after un- and reloading, a slight increase in the stiffness can be observed. When the deformations become larger the screw head will be more and more clamped and, at the same time, press the steel plate against the CLT panel. Also, the deformation rate was changed during the course of the test. The small drops in the shear force observed for shear forces above 70 kN in Figure 13 is due to this change of rate.

The measured mean values of the ultimate load capacity, $F_{v,R,mean}$, and the mean slip modulus for serviceability limit state, $K_{0.4,mean}$, are presented in Table 2 for each type of shear connection tested. Just for the comparison, the corresponding characteristic values obtained from the Eurocode 5 are also given in the table (the CLT panel

measured mean density and characteristic density were used in the calculation for the slip modulus and the ultimate strength, respectively)

Table 2: *Load-carrying capacity and slip modulus of the shear connections. Ultimate load and slip modulus per screw is given in parentheses) – EC5 estimated values and test results (mean values)*

	Estimated values according to EC5		Tests results (mean values)		
Name	$F_{v,Rk}$ (kN)	Slip modulus (steel/timber) K_{ser} (kN/mm)	Failure mode	$F_{v,Rmean}$ (kN)	Slip modulus (steel/timber) $K_{0.4,mean}$ (kN/mm)
S-8S-65	38.0 (4.7)	79.2 (9.9)	Semi-brittle	104.4 (13.1)	112.9 (14.1)
S-4S-65	25.8 (6.4)	39.6 (9.9)	Ductile	56.3 (14.1)	44.1 (11.0)
M-8S-65	39.3 (4.9)	79.2 (9.9)	Ductile	129.2 (16.2)	93.0 (11.6)
M-4S-65	26.6 (6.7)	39.6 (9.9)	Ductile	63.7 (15.9)	40.5 (10.1)
M-8s-100	61.8 (7.7)	79.2 (9.9)	Brittle	157.1 (19.6)	126.5 (15.8)

(Estimations according to EC5 are made by using d_{eff} to estimate the embedment strength and d for K_{ser})

The limited number of tests does not allow us to estimate the characteristic load-carrying capacity based on the test results and to compare it with the predicted ones. However, it can be observed that the mean values for the maximum load exceeded 2.2 to 3.3 times the characteristic values provided by EC5 for the steel-timber connection. An evaluation of the capacity according to an analytical model is proposed in section 5.2.

It is important to note that when a brittle failure occurred in the concrete (related to the concrete-steel connection), the failure load should not be compared with the predicted failure load given by EC5, which is based on a failure mode for the steel-timber connection. In addition, the slip moduli for the steel-timber connection of connections S-8S-65 and M-8S-100, where brittle failure occurred in the concrete, are not fully relevant because the 40 % level is based on an ultimate load for a different failure mode (the slip moduli for these connectors are about 50 % higher than that predicted by the EC 5). For test series S-4S-65, M-4S-65 and M-8S-65, where ductile failure due the steel-timber connection occurred, the test results for the slip modulus were between 2 – 18 % higher than those predicted by EC 5.

There was no effect observed with respect to multiple fastener in a row, in the tests for the comparable series M-4S-65 and M-8S-65 (2+2 screws with a spacing of 240 mm and 4+4 screws with a spacing of 80 mm, respectively). The EC 5 predicts a reduction of ultimate strength of 26 %.

The test results showed that the slip between concrete and steel can be neglected compared to that between steel and timber. The contribution from the concrete-steel slip to the total slip was about 2 % for connections with 4 screws and at maximum 12 % for connections with 8 screws.

It is obvious from Figure 7 that the design of the shear connections according to test series S-4S-65, M-8S-65 and M-4S-65 are appropriate and have the desired load-slip characteristics. They all behave as predicted by the analytical models discussed below. Therfore, these designs are evaluated in more detail.

4.2 DETAILED RESULTS FOR SHEAR CONNECTORS WITH DUCTILE CHARACTERISTICS

In this section, detailed tests results are given for the connection types S-4S-65, M-4S-65 and M-8S-65. These test series all have ductile characteristics and, therefore, are suitable for practical applications and adaptable for evaluation with respect to the analytical models for the shear connectors according to section 5.2 and for the partially composite beam with these shear connectors according to section 6.1.
The load-slip curves for the steel-timber interface for the 3 test specimens T4–T6 (S-4S-65) are presented in Figure 14.

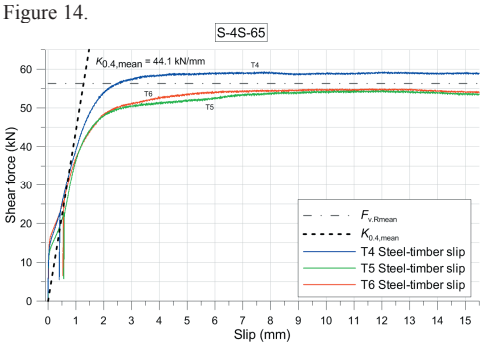

Figure 14: *Load-slip curves for the steel-timber interface – Test series S-4S-65 (T4-T6)*

As given by Figure 14 and Table 2, the average maximum load-carrying capacity for this type of connection is 56.3 kN or 14.1 kN per screw. The average value for the slip modulus is 44.1 kN/mm or 11.0 kN/mm per screw. The test results show that the steel-timber slip governs the overall behaviour of the connection. The contribution from the steel-concrete slip did no exceed 2.5 % of the total slip.

The load-slip curves for the steel-timber interface for the test specimens T10–T11 (M-4S-65) are presented in Figure 15. According to Table 2 and Figure 15, the average load carrying capacity for this type of connection is 63.7 kN (15.9 kN per screw) and the slip modulus is 40.5 kN/mm (10.1 kN/mm per screw). In this test series, the contribution of steel concrete slip did not exceed 1.5 % of the total slip. These results are similar to those of the S-4S-65 series.

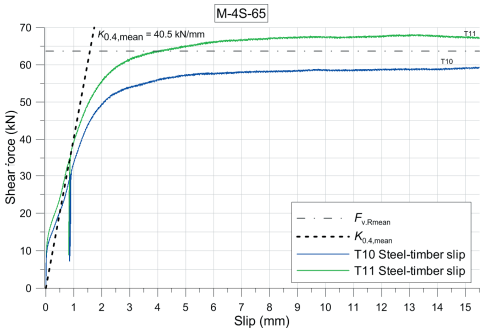

Figure 15: *Load-slip curves for the steel-timber interface – Test series M-4S-65 (T10-T11)*

The load-slip curves for the steel-timber interface for the test specimens T7–T9 (M-8S-65) are presented in Figure 16. According to Table 2 and Figure 16, the average load carrying capacity for this type of connection is 129.2 kN (16.2 kN per screw) and the slip modulus is 93.0 kN/mm (11.6 kN/mm per screw). In this test series, the contribution of steel-concrete slip was larger than in the test series with 4 screws. For tests T7 – T9, the contribution was 6.5 %, 11.5 % and 4 % of the total slip, respectively, at 75 % of the ultimate load. In this paper, only the connections with 4 screws will therefore be considered in a numerical application.

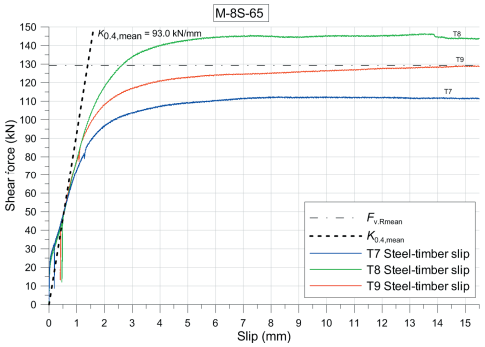

Figure 16: *Load-slip curves for the steel-timber interface – Test series M-8S-65 (T7-T9)*

The slip modulus per screw as well as the steel-timber ultimate load capacity for the connection types S-4S-65, M-4S-65 and M-8S-65 are similar and the difference between the results from the test series with mesh and studs connectors is marginal.

5 ANALYSIS AND EVALUATION

5.1 EVALUATION OF THE SLIP MODULUS

As mentioned above, the slip modulus will be evaluated as the slope of the load-slip curve between the origin of the curve and the point on the curve corresponding to 40 % of the measured ultimate load. It means that the initial high stiffness observed in the load-slip curves will not be taken into account. This will give a conservative secant modulus.

5.2 LOAD-CARRYING CAPACITY OF SHEAR CONNECTION

For the shear connections with a failure in the CLT panel, the load-carrying capacity can be derived using the K. W. Johansen´s plastic model (European Yield Model) [9]. It is based on the assumption that both fasteners and the timber are ideal rigid-plastic materials. The embedment strength of the different layers of the CLT-panel is here assumed to be the same parallel and perpendicular to grain. A distinction is made between the yielding moment in the threaded part of the screw and in the smooth shank of the screw due to their different diameters. Four failure modes are derived according to Figure 17.

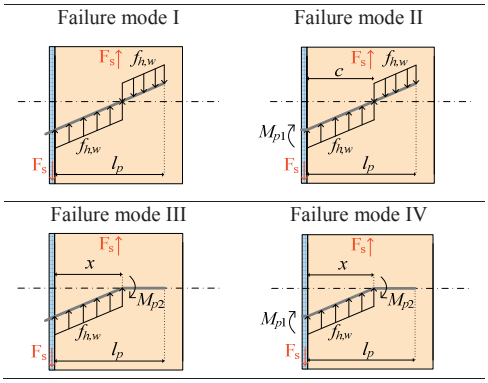

Figure 17: *Failure modes I, II, III and IV*

5.2.1 Failure mode I

According to [9], we have

$$F_s = \left(\sqrt{2}-1\right) f_{h,w} d \cdot l_p \qquad (1)$$

where $f_{h,w}$ is the embedment strength of the wood, d the nominal diameter of the screw and l_p the penetration length of the screw.

5.2.2 Failure mode II

Fore equilibrium and moment equilibrium at the steel-timber interface, respectively, give

$$F_s = f_{h,w} d \cdot c - f_{h,w} d \left(l_p - c\right) = 0 \qquad (2)$$

$$M_{p1} - f_{h,w} d \frac{c^2}{2} + f_{h,w} d \left(l_p - c\right) \frac{l_p + c}{2} = 0 \qquad (3)$$

Solving for c gives

$$c = \frac{l_p}{\sqrt{2}} \sqrt{1 + \frac{2 M_{p1}}{f_{h,w} d \cdot {l_p}^2}} \qquad (4)$$

Substituting (5) in (3) gives

$$F_s = f_{h,w} d \cdot l_p \left[\sqrt{2} \sqrt{1 + \frac{2 M_{p1}}{f_{h,w} d \cdot {l_p}^2}} - 1 \right] \qquad (5)$$

5.2.3 Failure mode III

According to [9], we have

$$F_s = \sqrt{2M_{p2}f_{h,w}d} \quad (6)$$

$$x = \frac{F_s}{f_{h,w}d} \quad (7)$$

5.2.4 Failure mode IV

Moment equilibrium at the distance x from the steel-timber interface gives

$$M_{p1} - F_s x + f_{h,w}d\frac{x^2}{2} + M_{p2} = 0 \quad (8)$$

M_{p2} is maximum where the shear force is zero, i.e.

$$x = \frac{F_s}{f_{h,w}d} \quad (9)$$

Which then gives

$$F_s = \sqrt{2(M_{p1} + M_{p2})f_{h,w}d} \quad (10)$$

5.2.5 Evaluation of the capacity of the shear connectors

The evaluation of the ultimate capacity of the ductile shear connectors according to the 4 failure modes presented above is made according to the geometrical data of the tests specimens. The steel plate thickness differs in the connectors with studs and with mesh. Therefore the penetration length l_p , is 59 mm and 61 mm, for connectors with studs and mesh, respectively. f_u = 400 MPa, d = 12 mm, and d_t = 8.7 mm. According to Eurocode 5, due to the small length of the smooth shank of the 65 mm long screws, an effective diameter d_{ef} is assumed for estimating the screw load carrying capacity with d_{ef} = 1.1d_t. The values estimated for the embedment strength and the yield moment are as follows:

$f_{h,w}$ = 41.73 N/mm^2

M_{p1} = 76750 N·mm

M_{p2} = 33260 N·mm

The estimated capacity according to failure modes I, II, III, and IV is given by $F_{s,I}$, $F_{s,II}$, $F_{s,III}$ and $F_{s,IV}$, respectively in Table 3.

Table 3: *Evaluation of the ultimate capacity per screw according to failure modes I, II, III and IV*

	Capacity in kN per screw	
	Connectors with studs	Connectors with mesh
$F_{s,I}$	9.8	10.1
$F_{s,II}$	11.2	11.5
$F_{s,III}$	5.0	
$F_{s,IV}$	9.2	

The observations of the failure from the test series S-4S-65, M-4S-65 and M-8S-65 show that the failure mode was between mode I and mode II with a yielding of the screws in the region of the screw head followed in a later stage by a yielding of the threaded part of the screw just below the smooth shank. This observation was made by comparing the screws of specimens loaded up to 15 mm slip and of some specimens where larger displacements at the steel-timber interface occurred. Considering that the effective number of screw is equal to the actual number of screws, the estimated load carrying capacity according to mode I and mode II obtained for studs connectors with 4 screws and mesh connectors with 4 and 8 screws is given in Table 4.

Table 4: *Comparison between test results and estimated load carrying capacity for the shear connectors according to failure modes I and II*

	Ultimate load capacity (kN)		
	S-4S-65	M-4S-65	M-8S-65
Failure mode I	39.0	40.4	80.7
Failure mode II	44.8	45.9	91.8
Test results (mean values)	56.3	63.7	129.2

The difference between the test results and the estimated capacity according to failure mode I and II might be explained by the fact that the friction between the steel and the CLT as well as the withdrawal contribution was neglected in the equations.

6 APPLICATION – COMPOSITE CLT-CONCRETE FLOOR

6.1 ANALYSIS OF COMPOSITE FLOORS WITH STUDS SHEAR CONNECTORS

Composite CLT-concrete floors with shear connectors as discussed above are analysed in this section. The partial interaction introduced by the mechanical shear connectors is taken into account. The purpose is to evaluate the increased performance (strength and stiffness) that is achieved by connecting the prefabricated concrete beam to the CLT-panel.

Here the analysis will be based on the simplified analysis method for composite beams with interlayer slip [10]. In this somewhat unusual composite structure, the concrete beam will be cracked and the stiffness reduced. The concrete will be assumed to be in stage II, i.e. a linear elastic stress distribution is assumed in the compressed zone. Long-term behaviour of the concrete is not included. The concrete is assumed to have no tensile strength.

Two elements are considered in the analysis. Element 1 is the cracked reinforced concrete beam and Element 2 is the CLT panel. The CLT panel has a symmetrical layup and is considered as fully composite section where the contribution of the core layer is neglected. The area of uncracked concrete in the analysis is determined based on the analysis of the non composite section (NCS), see Figure 18. The position of the centroid of element 1 (equal to the depth of uncracked concrete) and of element 2, respectively, is given by

$$z_{cg,1} = \frac{E_s A_s}{E_c b_1}\left(\sqrt{1 + 2d\frac{E_c b_1}{E_s A_s}} - 1\right) \quad (11)$$

$$z_{cg,2} = h_1 + \frac{h_2}{2} \quad (12)$$

The axial stiffness for each element is obtained as

$$EA_1 = E_c b_1 z_{cg,1} + E_s A_s \quad (13)$$

$$EA_2 = E_t b_2 (h_{21} + h_{23}) \quad (14)$$

The sum and product of the axial stiffness of sub-elements, respectively, are given by

$$EA_0 = EA_1 + EA_2 \quad (15)$$

$$EA_p = EA_1 \cdot EA_2 \quad (16)$$

The bending stiffness of elements 1 and 2 is given by

$$EI_1 = E_c \frac{b_1 z_{cg,1}^3}{3} + E_s A_s (d - z_{cg,1})^2 \quad (17)$$

$$EI_2 = \frac{E_t b_2}{12}\left(h_2^3 - h_{22}^3\right) \quad (18)$$

The bending stiffness for the non-composite and fully composite section, respectively, can be expressed as [10]

$$EI_0 = EI_1 + EI_2 \quad (19)$$

$$EI_\infty = EI_0 + \frac{EA_p r^2}{EA_0} \quad (20)$$

where

$$r = r_1 + r_2 = z_{cg,2} - z_{cg,1} \quad (21)$$

Considering the cross section shown in Figure 18, equilibrium requires

$$V = V_1 + V_2 \quad (22)$$

$$M = M_1 + M_2 + N_1 r \quad (23)$$

According to the simplified method for composite beams with interlayer slip [10], the internal actions are given by

$$N_{1,eff} = \left(1 - \frac{EI_0}{EI_{eff}}\right)\frac{M}{r} = N_{2,eff} \quad (24)$$

$$M_{1,eff} = \frac{EI_1}{EI_{eff}} M \quad (25)$$

$$M_{2,eff} = \frac{EI_2}{EI_{eff}} M \quad (26)$$

$$V_{s,eff} = \left(1 - \frac{EI_0}{EI_{eff}}\right)\frac{V}{r} \quad (27)$$

where EI_{eff} denotes the effective bending stiffness for the partially composite section and $V_{s,eff}$ is the interlayer shear force per unit length.

The effective bending stiffness EI_{eff} of the cross section is according to [10] given by

$$EI_{eff} \approx \left[1 + \frac{EI_\infty / EI_0 - 1}{1 + (\mu/\pi)^2 (\alpha L)^2}\right]^{-1} EI_\infty \quad (28)$$

where

$$\alpha L = \sqrt{\frac{Kr^2}{EI_0 (1 - EI_0 / EI_\infty)}} L \quad (29)$$

K [N/m/m] is the smeared slip modulus of the partial shear connection per unit length, and L the span of the beam element.

Knowing the interlayer slip force, the load on each connector is given by $F_{s,eff} = V_{s,eff} \cdot s$, where s is the spacing between the shear connectors along the composite beam.

Here we use the simplifying assumption that the neutral axis coincides with the centroid of the cross section, i.e. we are neglecting the shift downwards of the neutral axis and, hence, the centroid that is caused by the internal axial force N_1 (Figure 18). This assumption is conservative with respect to the maximum concrete compression stresses, but not with respect to the tensile stresses in the reinforcement. It is a conservative assumption with respect to the stiffness of the concrete beam and, therefore, also for the composite beam.

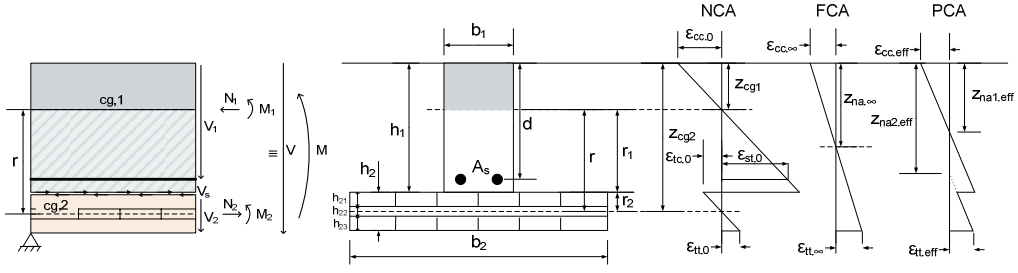

***Figure 18**: Cross section geometry and strain diagrams for non composite action (NCA), full composite action (FCA) and partial composite action (PCA)*

The maximum normal stresses at the top of the concrete beam, in the steel reinforcement and at the bottom of the CLT-panel, respectively, are given by

$$\sigma_{cc,eff} = -\frac{N_{1,eff} E_c}{EA_1} - \frac{M_{1,eff} E_c}{EI_1} z_{cg,1} \quad (30)$$

$$\sigma_{st,eff} = -\frac{N_{1,eff} E_s}{EA_1} + \frac{M_{1,eff} E_s}{EI_1} \left(d - z_{cg,1}\right) \quad (31)$$

$$\sigma_{tt,eff} = \frac{N_{2,eff} E_t}{EA_1} + \frac{M_{2,eff} E_t}{EI_2} r_2 \quad (32)$$

6.2 COMPUTATION

Consider the following geometric and material properties according to the cross section presented in Figure 18.

Element 1:

h_1	250	mm
b_1	140	mm
E_c	31	GPa
A_s	402	mm^2 (2Φ16)
E_s	210	GPa

Element 2:

E_t	11	GPa
h_2	74	mm (layup 27.5/19/27.5)
b_2	500	mm

CLT-concrete shear connection: S-4S-65

$K_{0.4}$	44.1	kN/mm
s	600	mm
$K = K_{0.4}/s$ =	73.5	MN/m^2

For a simply supported composite beam element (μ = 1), of span L = 7 m, and uniformly distributed loads at serviceability and ultimate limit state $q_{0,SLS}$ = 2.8 kN/m, and $q_{0,ULS}$ = 3.9 kN/m, respectively, corresponding to a 2 kN/m^2 live load and to the self-weight of the finished floor structure, the following results are obtained.

EI_0	2.69	MN.m^2	
EI_∞	10.47	MN.m^2	
EI_{eff}	7.95	MN.m^2	
EI_{eff} / EI_0	2.95		
$F_{s,eff,SLS}$	18.2	kN	
$F_{s,eff,ULS}$	25.6	kN	
$\sigma_{cc,eff,ULS}$	12.6	MPa	(< f_{cd} = 16.67 MPa)
$\sigma_{st,eff,ULS}$	55.8	MPa	(< f_y = 355 MPa)
$\sigma_{tt,eff,ULS}$	3.9	MPa	(< $f_{t,0,d}$ = 8.96 MPa)

The normal compression stresses estimated in the concrete are brought to an acceptable level in the partially composite beam, while in the non composite section (i.e. when $EI_{eff} = EI_0$), the design strength of the concrete would be exceeded.

$\sigma_{cc,0,ULS}$	20.84	MPa	(> f_{cd} = 16.67 MPa)
$\sigma_{st,0,ULS}$	276.38	MPa	(< f_y = 355 MPa)
$\sigma_{tt,0,ULS}$	3.60	MPa	(< $f_{t,0,d}$ = 8.96 MPa)

The partially composite section has a bending stiffness about 3 times greater than the non-composite section. The mid-span deflection at the serviceability limit state is given by $\delta_{eff,max,SLS} = (5q_{0,SLS} \cdot L^4)/(384EI_{eff})$ = 10.9 mm for the instantaneous deflection. This is well below the criteria demanded in the Eurocode.

7 CONCLUSIONS

Five types of shear connections have been tested and three of them (S-4S-65, M-4S-65 and M-8S-65 series) showed desired ductile characteristics and can be recommended for use in composite floor elements. The main slip occurred at the steel-timber interface. The slip modulus and ultimate capacity were satisfactorily high, providing a high degree of composite action.

The test results compared reasonably well with the shear capacity obtained analytically. For a typical design of a partially composite floor structure with these types of shear connectors the bending stiffness was increased almost three times.

The behaviour of the shear connections could probably be improved by using inclined self tapping screws.

ACKNOWLEDGEMENT

The authors would like acknowledge Stora Enso, Vinnova and the EU Structural Fund – Regional Fund for funding this research, as well as the laboratory team for their help during the tests.

REFERENCES

[1] E. Lukaszewska: "Development of Prefabricated Timber-Concrete Composite Floors," Doctoral Thesis, Luleå University of Technology, 2009.

[2] D. Yeoh, M. Fragiacomo, M. De Franceschi, K. Heng Boon: "State of the art on timber-concrete composite structures: Literature review," Journal of Structural Engineering, vol. 137, pp. 1085-1095, 2011.

[3] L. A. Bathon, O. Bletz, J Schmidt: "Hurricane proof buildings – An innovative solution using prefabricated modular wood-concrete-composite elements," presented at the WCTE, 2006.

[4] CEN, "EN 338: Structural Timber - Strenght classes," ed. Brussels: European Committee for Standardization, 2009.

[5] CEN, "EN 1995-1-1:2004 (E)," Eurocode 5 Design of timber structures, ed: CEN, 2004.

[6] DIBT, "European Technical Approval ETA-08/0271," ed: Deutsches Institut für Bautechnik, 2009.

[7] I. O. f. Standardization, "Timber structures - Joints made with mechanical fasteners - General principles for the determination of stength and deformation characteristics," ed, 1983.

[8] A. M. P. G. Dias, H. M. P. Cruz, S. M. R. Lopes, J. W. van de Kuilen: "Stiffness of dowel-type fasteners in timber-concrete joints," Proceedings of the Institution of Civil Engineers: Structures and Buildings, vol. 163, pp. 257-266, 2010.

[9] K. W. Johansen: "Theory of Timber Connections," International Association of Bidge and Structural Engineering, vol. 9, pp. 249-262, 1949.

[10] U. A. Girhammar: "A simplified analysis method for composite beams with interlayer slip," International Journal of Mechanical Sciences, vol. 51, pp. 515-530, 2009.

Paper II

Tests on Glulam-CLT shear connections with double-sided punched metal plate fasteners and inclined screws

by Nicolas Jacquier and Ulf-Arne Girhammar

Published in *Construction and Building Materials*, 2014,

Construction and Building Materials 72 (2014) 444–457

Contents lists available at ScienceDirect

Construction and Building Materials

journal homepage: www.elsevier.com/locate/conbuildmat

Tests on glulam–CLT shear connections with double-sided punched metal plate fasteners and inclined screws

Nicolas Jacquier *, Ulf Arne Girhammar

Division of Structural and Construction Engineering – Timber Structures, Luleå University of Technology, SE-971 87 Luleå, Sweden

HIGHLIGHTS

- Shear tests on glulam–CLT shear connections were performed.
- Double-sided nail plate (DSNP) fasteners combined with inclined screws were tested.
- The compatibility of DSNP fasteners and screws inclined at 45° is discussed.
- The slip modulus of each fastener can be added in the combined joint.
- The estimation of the load-carrying capacity requires a reduction factor.

ARTICLE INFO

Article history:
Received 25 April 2014
Received in revised form 26 August 2014
Accepted 27 August 2014

Keywords:
Timber joint
Shear test
Glulam
CLT
Double-sided punched metal plate fasteners
Inclined screws

ABSTRACT

A new shear connection system was tested in order to be used in off-site manufactured cassette floor elements made with glulam beams and cross laminated timber (CLT) panels. This type of floor element can present advantages from weight, structural and assembly point of view in multi-storey timber construction. The shear connection proposed is made of double-sided punched metal plate fasteners, connecting CLT and glulam members to form a T-cross-section. Inclined screws are used in combination with the double-sided nail plates to secure the shear connection. Shear test results are presented and compared with a simple calculation model for estimating the mean load-carrying capacity and stiffness of the combined joint according to methods available in the literature.

1. Introduction

Floor elements in modern multi-storey timber buildings often need to reach relatively long spans (over 6 m) and need to fulfil requirements for the ultimate and serviceability limit states, such as structural and fire safety, as well as comfort for occupants. Vibration in the serviceability limit state is one of the requirements which is often governing the design of timber floors [1,2]. Timber floors therefore often need to have a high stiffness to mass ratio to achieve acceptable performance [2]. Cross Laminated Timber (CLT), also called X-Lam, has been used increasingly since this type of engineered wood product was introduced, more than 15 years ago. The use of standard CLT panels for floor spans over 6 m leads to relatively thick and material intensive floor structures as is exemplified in [3] concerning floor designs with respect to vibration, where a 240 mm CLT panel is recommended for floor spans of 6.1 m. In addition, floor elements are often used as one-way spanning elements. Therefore, the combination of CLT panels with other linear engineered wood products can be beneficial in order to increase the bending stiffness and reduce the self-weight of CLT-based floor structures.

The focus of the study presented in this paper is the evaluation of a connection system for prefabricated floor elements made with CLT panels and glulam beams. An example of glulam–CLT floor structure, where the CLT panel is located at the bottom, is shown in Fig. 1. The load-bearing structure of the floor consists of the CLT panel and glulam beams only. The glulam beams are structurally connected to the CLT panel by a shear connection which is shown in Fig. 4. In this configuration, the CLT panel serves also as fire cell separation between different functional units in the building. The CLT can also be used as the main fire protection and be left visible or provide an additional fire resistance when cladded with gypsum boards for example. In addition, the floor element is completed with an acoustically separated wood based panel on top of the floor serving as a support for the rest of the floor structure (for example a non-structural cement-based layer and finish flooring).

* Corresponding author. Tel.: +46 920 49 28 89.
E-mail address: nicolas.jacquier@ltu.se (N. Jacquier).

http://dx.doi.org/10.1016/j.conbuildmat.2014.08.095
0950-0618/

In order to obtain a high bending stiffness of the floor element, the connection system between the timber members must transfer shear forces effectively and must therefore have a high slip modulus and sufficient load-carrying capacity. Today, the common way of connecting such ribbed panels or hollow-box floor structures is to use structural glue or screw-gluing techniques (the screws being used to apply the required pressure on the glue joint and, in case of failure of the glue, to provide an additional safety) [4]. Structural glue provides full composite action between the members and is, therefore, a very effective solution from a structural point of view. However, the gluing process can be demanding in terms of equipment, preparation and quality controls [4]. Self-tapping screws can also be used as shear connectors for this type of timber composite structure as presented by Chen and Lam [5] and can provide relatively high stiffness and capacity, especially when they are used in an inclined position [6]. For relatively long spans (from 6 m and over), the amount of screws necessary to reach a high level of composite action can become large and alternative connection systems or combinations of different connectors can be interesting in order to minimize the amount of screws needed and the installation time.

In this study, an alternative connection system made with punched metal plate fasteners is evaluated for the shear connection of CLT and glulam members. Punched metal plate fasteners are mechanical fasteners that are commonly used in manufacturing prefabricated trusses since their development in the 1950's [7]. These fasteners are made of a thin steel plate (1–2 mm thick) with teeth punched perpendicular to the plate. Punched metal plates fasteners need to be installed with dedicated pressing equipment and are, therefore, used almost exclusively for prefabricated elements. Less common, double-sided punched metal plate fasteners, also called double-sided nail plates (DSNP) for short, have been developed more recently and used to create fire protected and aesthetic joints in light timber trusses [8]. The double-sided nail plates can be pressed in-between the timber members, for example in order to join two light timber trusses side by side. An example of double-sided nail plate is shown in Fig. 2.

Despite the fact that it is not their intended original use, double-sided nail plates represent an alternative solution for shear load transfer when pressed horizontally between two layered timber members. Due to the possibly large timber area mobilised by the fastener, high values of load-carrying capacity and slip modulus can be reached. The manufacturing process requires the use of specific pressing equipment but with this type of fasteners the assembly time of glulam–CLT floor elements can be reduced compared with a gluing technique as there is no need for curing. As a first step in this development, this study presents an evaluation of the performance of double-sided punched metal plate fasteners as shear connectors for built-up glulam–CLT floor elements.

The use of double-sided nail plates as the main shear connector in a composite floor element can be problematic due to separation forces and to the small withdrawal capacity of punched metal plate fasteners. In service, separation forces between the CLT panel and glulam beams can be of some significance especially in the case of hanging loads on the CLT panel. Therefore, the shear connection made with double-sided punched metal plates should be secured against separation forces.

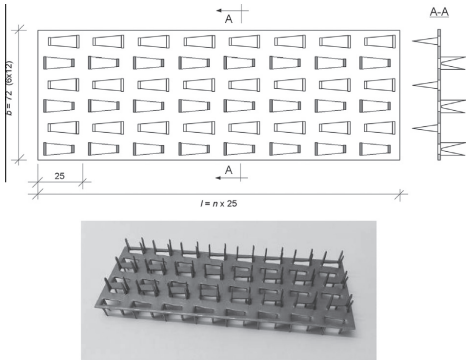

Fig. 2. Double-sided punched metal plate Sepa-SE2P, 72 × 200 mm^2.

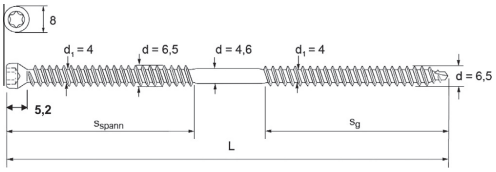

Fig. 3. SFS Intec WT-T screw geometry with diameter 6.5 mm (source SFS Intec [12]).

Self-tapping screws have a high withdrawal capacity and when used in an inclined position in a direction parallel to the forces in the shear plane, compressive forces between the timber members are generated, and can counteract the separation forces. The screws added in the joint with double-sided nail plates may also limit the pull-out of the nails of the nail plates, which are very weak in that respect. This limitation of the possible withdrawal of the nails is especially important in case of repeated loading [9] and, therefore, is essential for the long term behaviour of the joint. It is proposed in this study to evaluate the use of self-tapping inclined screws in order to secure a shear connection made with double-sided nail plates and take the combined effect into account.

The authors present results of shear tests on different combinations of the shear connector types discussed above between glulam and CLT members:

- Double-sided nail plates only;
- inclined self-tapping screws only;
- double-sided nail plates combined with inclined self-tapping screws.

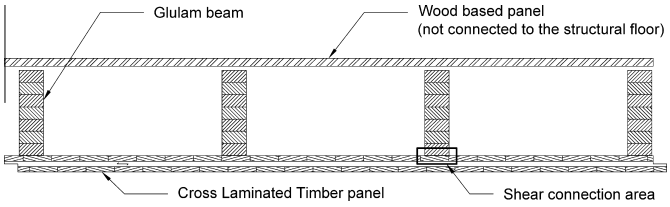

Fig. 1. Example of glulam–CLT floor structure with the shear connection between the glulam beams and the CLT panel on the lower side.

The aim of the study is twofold: to evaluate if a connection made with double-sided nail plates secured with self-tapping screws is a suitable shear connection system for composite timber floors in terms of load-carrying capacity and stiffness, and to evaluate the compatibility of the two types of mechanical fasteners having different individual load-deformation characteristics for combined use in a joint.

2. Methods

The experimental shear test program presented in this paper was carried out at the laboratories of VTT Expert Services Ltd in Finland. Totally, 48 shear tests in 8 different series were performed.

2.1. Materials

2.1.1. Glulam

The glulam used was made of Norway Spruce (Picea abies) and labelled GL32 (SS-EN 1194 [10]) and L40 (Nordic glulam strength class). Glulam members of cross section 90 × 150 mm^2 were made out of beams of cross section 90 × 315 mm^2 by a longitudinal cut. The thickness of the glulam lamellas was 45 mm.

2.1.2. CLT

The CLT was manufactured from solid wood lamellas of strength class C24 according to European Technical Approval ETA-08/0271 [11], and was composed of three 20 mm thick layers with the outer ply grain direction oriented in the longitudinal direction.

2.1.3. Double-sided punched metal plate fasteners

The double-sided punched metal plate fasteners Sepa-SE2P, made of zinc coated steel, had dimensions ($b_{NP} \times l_{NP}$) 72 × 100 mm^2 and 72 × 200 mm^2, see Fig. 2. The steel plate thickness was 1.3 mm and the teeth length 15.6 mm. Mechanical properties (mean values) according to the manufacturing's inspection certificate were: tensile yield strength f_y = 410 N/mm^2, ultimate tensile strength f_u = 485 N/mm^2, elongation ε_u = 28.0% and weight of zinc coating 293 g/m^2.

2.1.4. Screws

Two different SFS Intec WT-T screws were used and were according to European Technical Approval ETA-12/0063 [12] with dimensions ($d \times L$ in mm) 6.5 × 160 and 8.2 × 160, respectively. The geometry of one screw with outer thread diameter 6.5 mm is shown in Fig. 3 and some mechanical properties from [12] are reported in Table 1.

2.2. Test specimens

The details for all test series are shown in Table 2, Figs. 4 and 5.

Table 1
Mechanical properties of SFS WT-T self-tapping screws according to ETA-12/0063 [12].

		WT-T-6.5 × L	WT-T-8.2 × L
Characteristic yield moment	$M_{y,k}$ (Nm)	12.7	19.5
Characteristic tensile capacity	$f_{tens,k}$ (kN)	14.4	28.6
Characteristic yield strength	$f_{y,k}$ (N/mm^2)	990	870

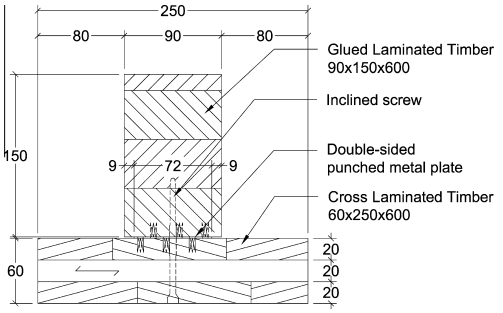

Fig. 4. Cross-section of a shear test specimen (dimensions in mm).

With the test configurations presented in this paper, the aim is to be able to compare the behaviour of joints where different fastener types are combined, Fig. 5b, c, and e, with the one of joints with individual fastener types, Fig. 5a, d and f. The configuration of Fig. 5c represents a situation with a low number of screws per nail plate area corresponding to one screw inserted between each double-sided nail plate of length 200 mm in a floor application where the amount of screws should be minimised. Configurations shown in Fig. 5b and e aim at evaluating the combined effect of double-sided nail plates and inclined screws, where there is a larger share of screws in the connection.

For the preparation of the test specimens, 600 mm long glulam members were cut out from different glulam beams so that the lamella of the connection side came from different original lamella for each test specimens of a test series. CLT members of width 250 mm were sawn out of master panels of dimensions 60 × 250 × 2500 mm^3 with the same principle to the length of 600 mm.

The timber materials were first stored in climate room with 85% relative humidity (RH) and temperature (T) 20 °C for five weeks according to EN 1075 [14]. The grain direction of the CLT outer lamellas was parallel to the long side of the member. The double-sided nail plates and screws were assembled to the middle line of timber members (see Fig. 4). The connection was always on the outer lamella side of the original glulam beam (90 × 315 mm^2). After the test specimens with double-sided punched metal plate fasteners were assembled, they were stored with the unassembled timber members to be used in the test specimens with only screws for about three weeks in a climate room with RH 65% and T 20 °C before the loading tests.

For the fabrication of the test specimens the double-sided nail plates were first pressed into the CLT members using a steel comb for double-sided nail plate so that the non-pressed teeth on the upper side of the plate remained untouched, Fig. 6a and b. The double-sided nail plates were fastened by a MTS testing machine by a deformation guided compression (5 mm/s) with a maximum load limitation of 55 kN so that the nail plates came to full contact with the timber member. No teeth were bent during the process, Fig. 6c. Then the glulam members were pressed onto the double-sided nail plates with the same procedure, Fig. 6d.

For the test series where screws were used, the screws were installed some hours before the tests. The screwing angle was 45° for all tests (see Fig. 5). The screws were tightened so that no gap was left between the timber members. How-

Table 2
Description of the test series.

Test series				Screws		Double-sided nail plates (DSNP)		
Name	Short name	No. of tests	Estimated maximum load F_{est} (kN)	No. of screws	$d \times l_S$ (mm)	No. of DSNP	$b_{NP} \times l_{NP}$ (mm)	Total DSNP area (mm^2)
S1_2S-6.5	S1	4[a]	15	2	6.5 × 160	–	–	–
S2_2S-8.2	S2	4[a]	20	2	8.2 × 160	–	–	–
S3_1NP-200_2S-6.5	S3	6	50	2	6.5 × 160	1	72 × 200	14,400
S4_1NP-200_2S-8.2	S4	6	55; 50[b]	2	8.2 × 160	1	72 × 200	14,400
S5_2NP-100_1S-6.5	S5	6	40	1	6.5 × 160	2	72 × 100	14,400
S6_2NP-100	S6	6	35	–	–	2	72 × 100	14,400
S7_1NP-100_2S-6.5	S7	6	30	2	6.5 × 160	1	72 × 100	7200
S8_1NP-200	S8	6	35	–	–	1	72 × 200	14,400

[a] Six tests were planned and performed but due to errors in manufacturing some of the test specimens, a slight gap was created between the members. Due to the influence of the gap on the test results, only the four tests for which manufacturing was correct are considered for these test series.
[b] The estimated load for series S4 was 55 kN for the 3 first tests specimens and then adjusted to 50 kN according to EN 26891 [13].

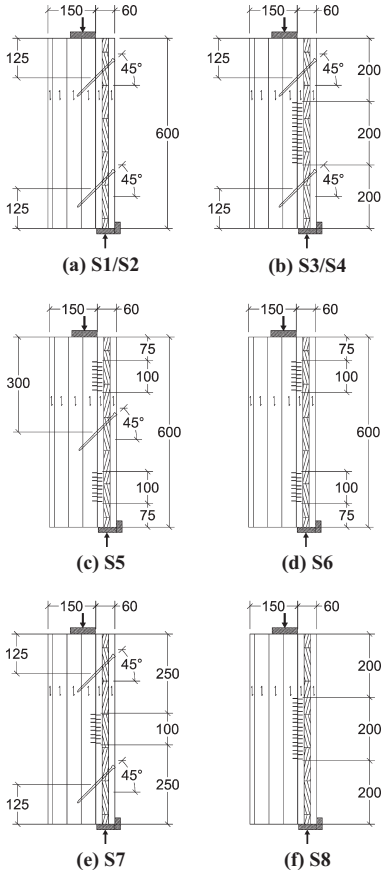

Fig. 5. Test configurations for all glulam–CLT joint shear test series (detailed notations for the test series and specifications are given in Table 2) (dimensions in mm).

ever, in test series with screws and double-sided nail plates combined, the gap of 1–2 mm between the members existing due to the presence of the double-sided nail plate was not closed by the application of the screws.

2.3. Loading arrangement

The test setup was made following the standard EN 1075 [14]. A general view of the test setup is shown in Fig. 7.

Test specimens were loaded by a MTS testing machine with the calibrated compression capacity of 250 kN. The deformation was measured by two HBM displacement transducers W10 (±10 mm) on both sides of the test specimen. The loading procedure according to EN 26891 [13] was followed, where the loading rate was $0.2 \times F_{est}$/min, with F_{est} the estimated maximum load (cf. Table 2), up to $0.7 \times F_{est}$ when a constant rate of slip was used (deformation controlled) up to failure. However, by mistakes the change to deformation control was not done for series S1 and S6 where the tests were run under load control until failure. Tests were intentionally stopped after 15 mm slip.

It should be noted that the upper right part of the specimen was free to move and, thus, allowed separation of the two members (Fig. 7b), while the separation was essentially prevented on the lower side by both the roller support on the left side and the fixed support on the lower right side. This difference with respect to the separation of the members will have an influence on the test results depending on the location of the double-sided nail plates.

The moisture content ω at the time of testing was measured immediately after loading tests for each test specimens on the outer lamellas on the joint side. The density $\rho_\omega = m_\omega/V_\omega$ at moisture content ω, where m_ω and V_ω are the wood sample mass and the volume of the wood sample, respectively, at the time of testing, was determined according to ISO 3130 [15] and ISO 3131 [16].

2.4. Specific slip values and slip modulus evaluation

In order to compare the behaviour of double-sided nail plates and inclined screws and assess the compatibility of their load–slip curves for a combined use, existing methods used to evaluate the ductility of timber joints based on load–slip curves were used. For the evaluation of the ductility of a timber joint the yield slip, noted u_y, needs to be estimated, see Fig. 8. In this paper, the method according to EN 12512 [17] is considered to determine the yield slip. Different methods are available in the literature [18], but the EN 12512 method is the one that captures the behaviour of the studied joints in the most appropriate way, especially for inclined screws [19]. In addition, the slip u_{max} (slip at maximum load) and the slip u_f at the chosen "failure" load (load value of $0.8 \times F_{max}$ on the descending part of the load–slip curve after the maximum load according to [17]) are determined for each test series for comparison reasons between the series. These specific slip values are shown on the load–slip curve example in Fig. 8, where u_{final} denotes the slip at collapse of the connection or termination of the test.

The slip modulus for the shear connection, k_s, is calculated according to EN 26891 based on the slope of the curve between 10% and 40% of F_{est}. The alternative method for estimating the slip modulus (also called the secant slip modulus method) which consists in evaluating the slip modulus value up to 40% of F_{max} (test result value), is not considered here. This is because the $0.4 \times F_{max}$ load level will sometimes be attained before and sometimes after the unloading cycle prescribed in EN 26891 (depending on the difference between F_{max} and F_{est}), and, therefore, the different slip moduli would not be comparable due to creep deformations occurring during the unloading and reloading cycle.

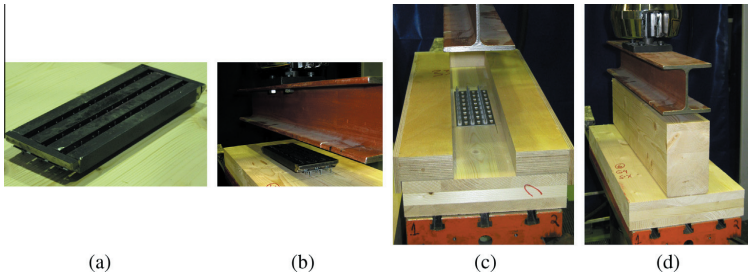

Fig. 6. Fabrication of the test specimens with double-sided punched metal plate: (a) steel comb for double-sided nail plate; (b) pressing of the first side of the nail plate; (c) half-pressed nail plate; (d) pressing of the glulam on the nail plate.

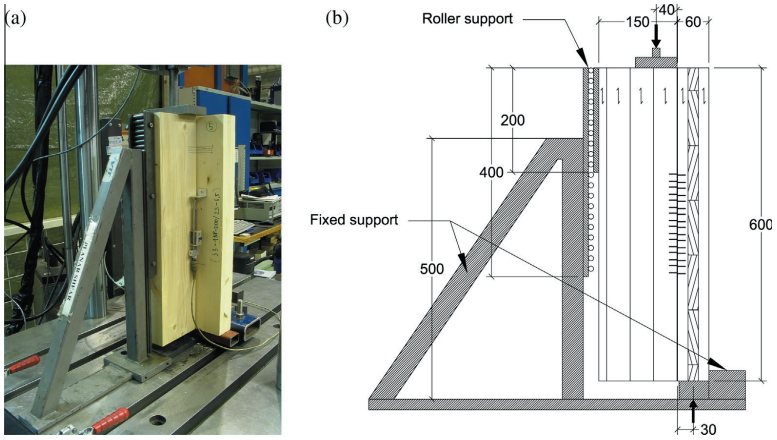

Fig. 7. Test setup and loading arrangement for shear tests (dimensions in mm).

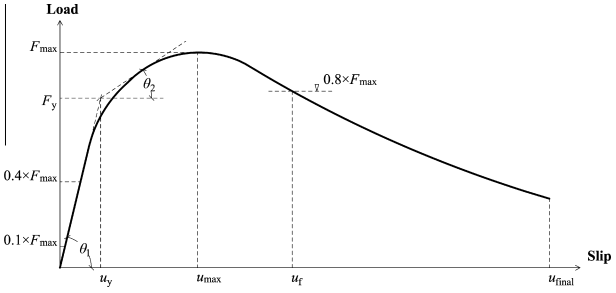

Fig. 8. Load–slip curve and specific slip values [18].

3. Results

3.1. Overview

An overview of all the test results is presented in Table 3 and in Fig. 9 with a plot of the mean load–slip curve for each test series. The individual test curves are shown in Appendix A and more details can be found in a technical report published at Luleå University of Technology [19]. The mean curve for a test series was obtained by removing the unloading cycle between $0.1 \times F_{est}$ and $0.4 \times F_{est}$ of each load–slip curve and by averaging the load observed at slip intervals of 0.02 mm. The mean load–slip curve is truncated at 15 mm slip or at the lowest maximum slip value recorded for any test specimen in the test series. For series *S*1 and *S*6, the curves are represented with a dashed line from the instant when the loading protocol differed from the one followed for the other series, i.e. load control instead of deformation control. One curve of the series *S*7 was removed when creating the mean load–slip curve due to a strange post-peak behaviour (cf. Appendix A), but the data up to the maximum load is considered in the test

Table 3
Shear test results, mean values for the test series.[a].

Test series	No. of tests	Glulam		CLT		Estimated maximum load	Maximum load	Slip at maximum load	Slip modulus
		$\rho_{g,\omega}$ (kg/m^3)	ω_g (%)	$\rho_{c,\omega}$ (kg/m^3)	ω (%)	F_{est} (kN)	F_{max} (CoV) kN (%)	u_{max} (CoV) mm (%)	k_s (CoV) kN/mm (%)
S1_2S-6.5	4	456	12.2	471	12.4	15	16.1 (5.3)	1.78 (9.4)	19.4 (7.3)
S2_2S-8.2	4	462	12.4	459	12.3	20	22.8 (10.3)	1.54 (11.0)	25.4 (9.3)
S3_1NP-200_2S-6.5	6	467	12.6	457	12.9	50	44.1 (6.2)	3.48 (17.5)	72.2 (12.4)
S4_1NP-200_2S-8.2	6	451	12.5	460	12.8	55; 50[b]	51.5 (7.2)	4.18 (11.3)	85.0 (10.4)
S5_2NP-100_1S-6.5	6	461	12.5	451	13.1	40	38.5 (3.5)	4.84 (11.2)	80.8 (7.8)
S6_2NP-100	6	444	12.7	450	13.8	35	33.9 (4.9)	5.20 (7.1)	45.6 (21.0)
S7_1NP-100_2S-6.5	6	452	12.4	457	12.8	30	30.1 (2.2)	2.85 (17.0)	46.9 (7.7)
S8_1NP-200	6	473	13.0	446	13.7	35	32.9 (3.2)	5.26 (8.8)	53.6 (7.8)

[a] The values in parentheses represent the coefficient of variation (CoV) in%. The density ρ is given for the moisture content ω measured at the time of testing. The subscripts *c* and *g* denote the CLT and glulam members, respectively.
[b] The estimated load for series S4 was 55 kN for the 3 first tests specimens and then adjusted to 50 kN according to EN 26891 [13].

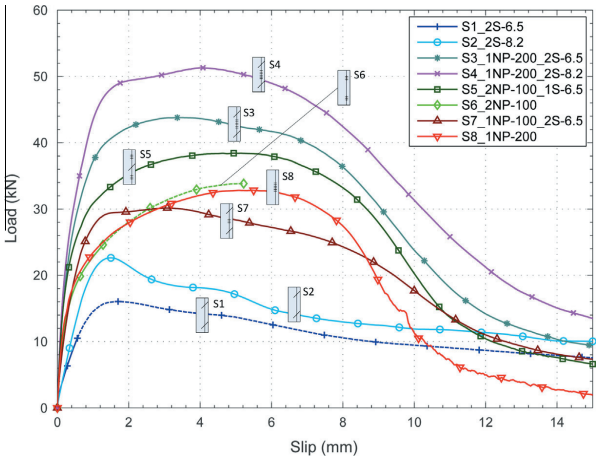

Fig. 9. Mean load–slip curves for each test series.

results for this series. Mean values presented in Table 3 are calculated based on the individual load–slip curve for each test specimen in the test series (and not on the mean load–slip curve in Fig. 9).

The measured average density of the glulam for all test series was 458 kg/m^3. This value is only slightly above the characteristic density of 430 kg/m^3 for glulam GL32 according to [10]. The average density measured for the CLT was 456 kg/m^3. This value is high compared with the 350 kg/m^3 expected characteristic density for sawn timber C24 according to [20], but it is common for cross laminated timber [4].

In all test series, the failure of the fasteners has occurred either in the CLT or in the glulam member or sometimes in both timber members. The failure had, however, a tendency to occur more often in the glulam member, both for the double-sided nail plates and the inclined screws. Concerning screws, this may be due to the fact that the head of the screw was located in the CLT member and, maybe also, because of the cross-wise make-up of the layers. Concerning the double-sided nail plate, this may be due to the fact that the plate is first fastened to the CLT member with better penetration of the nails of the plate as a result.

3.2. Test series with inclined screws only (S1, S2)

The joints with only inclined screws present load–slip curves with a relatively long linear part with respect to their capacity and a low slip value at maximum load (1.78 mm and 1.54 mm, respectively). As observed in [6], where push-out tests with similar inclined self-tapping screws were performed, self-tapping screws inclined at 45° angle exhibit a rather short ascending part of the curve before maximum load, but keep an important load-carrying capacity for large displacement due to the dowel effect [21]. The post-peak behaviour is characterised by a slight gradual reduction of the load-carrying capacity until the end of the test. The failure was initiated by withdrawal of the screw, followed by crushing of the timber perpendicular to the screw axis at larger slip values. The withdrawal of the screw occurred in one of the timber members and seldom in both members at the same time. Due to the inclination of the screws, the dowel effect of the screw is deemed limited in the early stage of the test. Small plastic hinges were visible on the screws after the tests, often located in the head-side threaded part of the screw close to the shear plane. However, it is not possible to determine precisely at which instant the hinges developed, but it is likely that they have formed after the maximum load was reached.

3.3. Test series with double-sided nail plates only (S6, S8)

The joints with double-sided nail plates are characterised by a more non-linear behaviour before maximum load than the screw joints. The slip at maximum load is large compared with the one of joints with inclined screws (5.2–5.26 mm). The post-peak behaviour for series S6 (2NP-100) cannot be evaluated due to the sudden collapse of the test specimen, because of the load-controlled loading procedure, but it is available for *S*8 (1NP-200) and is characterised by a rapid decrease of the load-carrying capacity. At 15 mm slip, the double-sided nail plate joints have almost no remaining load-carrying capacity. The failure is caused by the simultaneous bending of the teeth of the double-sided nail plate in both timber members and the crushing of the wood in front of the teeth, cf. Fig. 10a and b. As the slip increases, the teeth bend and are withdrawn, and a gap opens between the timber members. The load-carrying capacity significantly decreases as the gap between the timber members opens. The significant influence of the gap on the characteristics of nailed connections has been demonstrated by Antonides et al. [22]. Concerning the creation of gaps, note, however, the possible difference between the test set-up in Fig. 7b and the situation in a real floor structure. From the observations of the specimens after the tests, it is visible that the teeth of the nail plate are bent in both members. For specimens of series S8, the teeth were bent to about 30° from their original position, while for specimens of series S6, the angle was about 30° for the top nail plate and 45° for the bottom nail plate, see Fig. 10a and b.

The slip modulus observed in series S6 is low with 45.8 kN/mm (CoV 21%) compared to that of series S8, 53.6 kN/mm (CoV 7.8%). The difference in stiffness likely comes from the positioning of the nail plates in series S6 (located at the top and bottom, whereas in the middle in test series S8). The effect of the test setup is discussed in more detail in Section 3.5.

Fig. 10. Double-sided nail plate 100 mm after failure – (a) upper double-sided nail plate S6 – (b) lower double-sided nail plate S6; (c) specimen with screws only S2; (d) and (e) Specimens with inclined screws and double-sided nail plate, S4 and S7, respectively. In all three figures (c) – (e), the gaps are such that both of the screws are visible.

3.4. Test series with double-sided nail plates and inclined screws (S3, S4, S5, S7)

In all test series combining different fastener types the contribution of each fastener type was significant with respect to the load-carrying capacity and slip modulus. The slip u_{max} for the combined situation was in-between the values observed for the joints with screws only and with double-sided nail plates only (*S3* = 3.5 mm, *S4* = 4.2 mm, *S5* = 4.84 and *S7* = 2.8 mm). At the end of the test, the members were not totally separated due to the presence of the screws, but a gap of 10–20 mm between the members had opened and the double-sided nail plate was completely withdrawn, see Fig. 10d and e. Test series with inclined screws and double-sided nail plates present load–slip curves which are a mix of the load–slip curves observed in the tests with single fastener types. The higher the proportion of screws relative to the double-sided nail plate area, the more visible the contribution of the screws, giving a more bi-linear behaviour to the joint with a rather linear part up to 1 mm slip and a kind of plateau between 2 and 6 mm slip.

In terms of stiffness, the results of series *S5* (2NP-100_1S-6.5) significantly exceeded the value which could be expected based on the results of series *S6* (2NP-100), *S8* (1NP-200) and *S1* (2S-6.5). The slip modulus of series *S5* is higher than the slip modulus value obtained by the summation of results from series *S1* (50%) and *S6* (or even S1 (50%) and *S8*) corresponding to the configuration of *S5* (see also Table 5), while in terms of load-carrying capacity, the results were in accordance with these test series. It should also be noted that the slip modulus of series *S5* is higher than the slip modulus observed for series *S3*, with mean values 80.8 kN/mm and 72.2 kN/mm, respectively, despite the fact that *S5* contains one screw, that *S3* contains two screws and that the nail plate area in these two series is equal. These unexpected observations are discussed in more details in Section 3.5.

3.5. Effect of the fasteners position and calculation method on the slip modulus of series S5

This section details how the high stiffness observed in series *S5* can be attributed to the test configuration (position of the fasteners in the specimen and the test setup) and to some extent to the calculation method for the slip modulus according to EN 26891.

The influence of the position of the fasteners and test setup on the slip modulus results is detailed in the following, starting with additional comments on series *S6* (2NP-100) and *S8* (1NP-200). In *S8* the force distribution over the nail plate area is more even than in *S6* where the test setup gives rise to different loading situations on the two nail plates (shear combined with compressive forces at the bottom and separation force at the top), cf. Fig 7b, and Fig. 10a and b. In terms of load-carrying capacity, the effect of the test setup seems to be rather balanced and similar results are observed for *S6* and *S8*. However, comparing the slip modulus of *S6* with *S8* (45.6 kN/mm and 53.6 kN/mm, respectively), it is evident that the test setup boundary conditions have a significant influence. On the contrary, in the case of *S5*, it seems that the screw counteracts the separation of the timber members, increasing the contribution of the upper nail plate, and leading to the high slip modulus observed compared to other configurations. This phenomenon was not observed for series with nail plates located in the centre as described in Section 4.1.

The shear test results from series where the nail plates had different positions (at the centre of the joint or on either sides of the centre of the joint) should therefore not be compared directly with each other as there is an obvious effect of the nail plate position on the results, especially concerning the slip modulus. Test results from series where the nail plate was located at the centre seem more accurate (*S3*, *S4*, *S7*, *S8*) as there was a more even force distribution over the nail plate area. It should be noted that the differences observed here are relevant with respect to these test configurations and the choice of which value to prefer depends on the real situation where these connectors are used.

The second reason for the high slip modulus observed in *S5* compared to *S3* is the method chosen to estimate the slip modulus. The mean maximum load observed was 44.1 kN and 38.5 kN for series *S3* and *S5*, respectively. The chosen estimated load F_{est}, which affects how the slip modulus is calculated according to EN 26891 [13], was 50 kN (i.e. $1.13 \times F_{max}$) and 40 kN (i.e. $1.04 \times F_{max}$) for series *S3* and *S5*, respectively. The slip modulus is therefore calculated for *S5* at a lower load level than in *S3* with respect to the actual maximum load, which can explain part of the high stiffness observed since the double-sided nail plate have a non-linear behaviour.

3.6. Specific slip values

Specific slip values obtained as described in Section 2.4 were determined on each load–slip curve. Mean values are presented for each test series in Table 4. For series *S1*, u_f should be considered with care since the tests for this series were run under load-control and the part of the curve after the maximum load is therefore not totally reliable.

For joints with inclined screws only (*S1*, *S2*), the slip at maximum load u_{max} and the slip at "failure" load u_f are lower than for

Table 4
Mean specific slip values for all test series.

Test series	Yield slip (mm) u_y	Slip at maximum load (mm) u_{max}	Slip at failure load (mm) u_f
S1_2S-6.5	0.67	1.78	5.69[a]
S2_2S-8.2	0.79	1.54	3.41
S3_1NP-200_2S-6.5	0.34	3.48	8.28
S4_1NP-200_2S-8.2	0.38	4.18	8.42
S5_2NP-100_1S-6.5	0.25	4.84	8.50
S6_2NP-100	0.33	5.19	–[b]
S7_1NP-100_2S-6.5	0.48	2.85	7.52
S8_1NP-200	0.27	5.26	8.47

[a] This result should be considered as indicative only (tests conducted under load control).
[b] No value is given due to the collapse of test specimens after maximum load (tests conducted under load control).

Table 5
Comparison of test results for the load-carrying capacity and slip modulus of the combined joints with values obtained by summing results from tests on single fasteners joints.[a].

		Composition	$F_{v,test}$ (kN)	$k_{s,test}$ (kN/mm)	Combination of single fasteners	$F_{v,sum}$ (kN)	$k_{s,sum}$ (kN/mm)	$\frac{F_{v,sum}}{F_{v,test}}$ (–)	$\frac{k_{s,sum}}{k_{s,test}}$ (–)
Joints with single fastener type	S1	2 S-6.5	16.1	19.4	–	–	–	–	–
	S2	2 S-8.2	22.8	25.4	–	–	–	–	–
	S6	2 NP-100	33.9	45.6	–	–	–	–	–
	S8	1 NP-200	32.9	53.6	–	–	–	–	–
Joints with combined fasteners	S3	1 NP-200 + 2 S-6.5	44.1	72.2	S8 + S1	49.0	73.0	1.11	1.01
	S4	1 NP-200 + 2 S-8.2	51.5	85.0	S8 + S2	55.7	79.0	1.08	0.93
	S5	2 NP-100 + 1 S-6.5	38.5	80.8	S6 + $\frac{1}{2}$ S1	42.0	55.3	1.09	0.68
	$S5_{(S8)}$[b]	2 NP-100 + 1 S-6.5	38.5	80.8	S8 + $\frac{1}{2}$ S1	41.0	63.3	1.06	0.78
	S7	1 NP-100 + 2 S-6.5	30.1	46.9	$\frac{1}{2}$ S8 + S1	32.5	46.2	1.08	0.98

[a] Subscripts "sum" and "test" denote values obtained by summation and from test results, respectively. Note that values for test series S1 and S6 were obtained from a load controlled test.
[b] $S5_{(S8)}$ denotes the comparison of the test results of series S5 considering the results of series S8 instead of S6.

joints with double-sided nail plate fasteners only (*S6*, *S8*). The yield slip u_y of inclined screw joints is however at least two times higher than the one of double-sided nail plates.

The fact that the maximum load occurs at different u_{max}-values for the different types of fasteners implies that the maximum loads for the two individual fasteners cannot, in principle, be added together totally to obtain an estimation of the maximum load-carrying capacity for the combined connection in the ultimate limit state. However, regarding the slip modulus of combined joints in the serviceability limit state, it is on the safe side to consider that the slip modulus of the inclined screws can be added to the slip modulus of the double-sided nail plate since the screw joints are yielding later, and despite the fact that the inclined screws and double-sided nail plate are not ideally compatible at the ultimate limit state.

4. Analysis

4.1. Comparisons between test series – maximum load and slip modulus

In this section, the different mean load-carrying capacities and slip modulus values from test series with single fastener type are added together according to the superposition principle in order to match and be compared with the combined joint configurations tested.

Table 5 presents values for the maximum load $F_{v,sum}$ and slip modulus $k_{s,sum}$ of combined joints obtained by summation. These values are calculated using the mean values for the load-carrying capacity $F_{v,test}$ and slip modulus $k_{s,test}$ of test series with single fastener type (*S1*, *S2*, *S6*, *S8*). They are compared with the mean values of the test results for the combined joints (*S3*, *S4*, *S5* and *S7*). The comparative values in the last two columns in Table 5 are conservative if they are less than one (<1).

It is observed that the slip modulus can conservatively be estimated by using the superposition principle i.e. by summing the values from the tests with single fastener type. As introduced in Section 3.5 it can be noted that the slip moduli in test series *S3* and *S7*, compared with values obtained by summation, indicate that the presence of screws do not influence the stiffness of the nail plate when the nail plate is located in the middle. While in the case of *S5*, the stiffness is of the joint is much higher than predicted by summation, using either values from series *S6* or *S8*.

The load-carrying capacity is, as expected, over-estimated by up to 11% using this method. Depending on the difference in the load–slip characteristics of the two types of fasteners, especially concerning the difference in u_{max}-values, a lower value than the sum of the two individual maximum values needs to be used for estimating the load-carrying capacity of the combined joints. According to these test results, a reduction factor of 0.9 (= 1/1.11) seems reasonable to apply for the estimation of load carrying-capacity of joints with combined fasteners using single fasteners joints test results.

4.2. Comparisons between test series – load–slip curve superposition

Fig. 11 is made on the same principle as Table 5. The load–slip curves for the combined joints *S3*, *S4*, *S5* and *S7* are compared with curves made by the superposition of the load–slip curves for single shear connector types (*S1*, *S2* and *S8*) matching the combined joint configuration. Mean curves are presented with ± one standard deviation (noted σ) for each data point of the mean curves. For *S5*, the load–slip curve from series *S8* was used instead of *S6* in order to have data up to 15 mm slip.

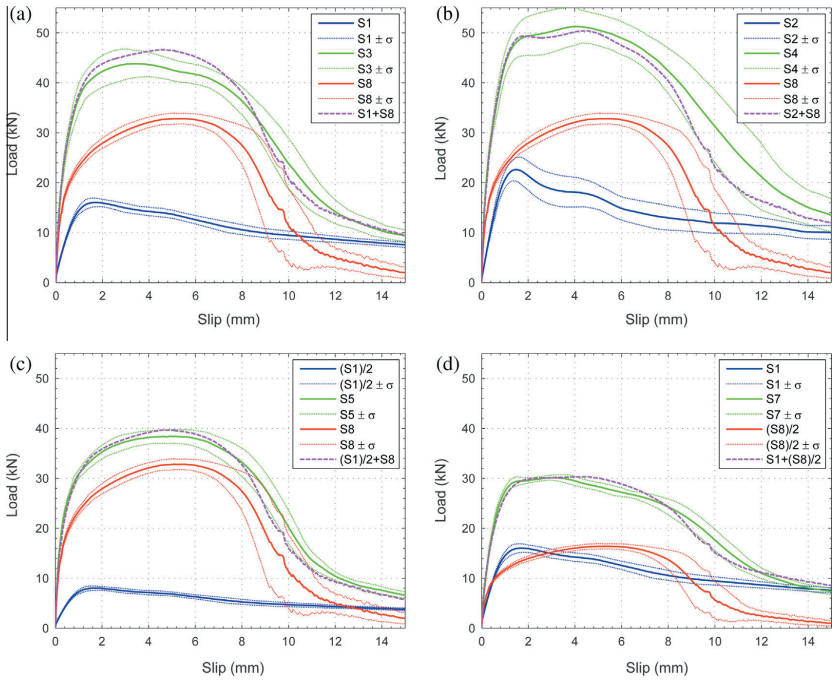

Fig. 11. Mean load–slip curves for combined joints compared to superposition of the corresponding single fastener mean load–slip curves: (a) S3_1NP-200_2S-6.5, (b) S4_1NP-200_2S-8.5, (c) S5_2NP-100_1S-6.5 and (d) S7_1NP-100_2S-6.5.

Some difference can be observed between the summation plot *S*1 + *S*8 (Fig. 11a) and the tests results of series *S*3, between 1 mm and 8 mm slip. Test series *S*1 was run under load control until failure, leading to a rapid increase of the loading rate after the maximum load was reached. It can be argued that the load observed in this case is higher due to the faster loading rate than if the test would have been carried out under displacement control and, therefore, at a lower speed.

Fig. 11b presents a comparison between *S*4 and the corresponding summation plot *S*2 + *S*8. The summation plot fits well with the tests results of the combined joint up to 8 mm slip. From 8 mm up to about 13 mm slip the summation plots exhibit a lower load-carrying capacity than the test results for the combined joints. This may be due to the fact that in the combined joint, the separation of the CLT and glulam members is prevented by the screw which limits the withdrawal of the teeth of the double-sided nail plate and improves its load-carrying capacity. This plot is the most accurate comparison presented in Fig. 11, since all load–slip curves used here were obtained from displacement controlled tests.

Fig. 11c and d present the summation plots of the individual fasteners compared with the load–slip curves of test series *S*5 and *S*7, respectively. The two curves are rather close; the summation curve is, in the most interesting slip range, a little above that of the combined joint, but essentially within the limits of one standard deviation from the mean test curve. However, as for series *S*4, the tests results of series *S*5 and *S*7 tend to show a slightly higher load-carrying capacity than what the summation plot indicates between 8 and 12 mm slip.

4.3. Analytical evaluation of the load-carrying capacity and slip modulus for joints with double-sided nail plates and/or inclined screws

4.3.1. Double-sided punched metal plate fasteners

4.3.1.1. Load-carrying capacity. It is proposed to estimate the load-carrying capacity of double-sided punched metal plate fasteners parallel to the shear plane, $F_{v,NP}$, with the following empirical expression:

$$F_{v,NP} = k_\rho \cdot f_{a,\alpha_{NP},\beta_{NP}} b_{NP}\, l_{NP} \tag{1}$$

where k_ρ is the correction factor for the timber density (see below), $f_{a,\alpha_{NP},\beta_{NP}}$ [N/m^2] the anchorage strength (where α_{NP} is the angle between the major axis of the nail plate and the direction of the applied force in the joint, and β_{NP} is the angle between the applied force in the joint and the direction of the outer lamella in the CLT), and b_{NP}, l_{NP} the width and length of the nail plate, respectively. The anchorage strength $f_{a,\alpha_{NP},\beta_{NP}}$ of the double-sided punched metal plate is taken from the mean load-carrying capacity per plate area of series *S*8, where $\alpha_{NP} = 0°$ and $\beta_{NP} = 0°$, as

$$f_{a,0,0,mean} = \frac{F_{max}}{b_{NP}\, l_{NP}} = 2.29\ \frac{N}{mm^2} \tag{2}$$

When the mean density of the glulam and of the CLT is $\rho_{g,mean} = 473$ kg/m^3 and $\rho_{c,mean} = 446$ kg/m^3, respectively, as in series S8, the correction factor is $k_\rho = 1.0$, otherwise it is proposed that the correction factor is calculated according to EN 14545 [23] considering the mean density values:

$$k_\rho = \min \begin{cases} \sqrt{\frac{\rho_{g,mean}}{473}} \\ \sqrt{\frac{\rho_{c,mean}}{446}} \end{cases} \quad (3)$$

4.3.1.2. Slip modulus. For the estimation of the slip modulus, $k_{s,NP}$ [N/m], the following empirical expression is proposed in the serviceability limit state:

$$k_{s,NP} = K_{NP,\alpha_{NP},\beta_{NP}} b_{NP}\, l_{NP} \quad (4)$$

where $K_{NP,\alpha_{NP},\beta_{NP}}$ [N/m^3] is the slip modulus per unit area of the nail plate. The mean value of this slip modulus is according to the test results of series S8, where $\alpha_{NP} = 0°$ and $\beta_{NP} = 0°$, as follows:

$$K_{NP,0,0,mean} = \frac{k_{s,test}}{b_{NP} l_{NP}} = 3.72 \ \frac{N}{mm^3} \quad (5)$$

4.3.2. Inclined screws

4.3.2.1. Load-carrying capacity. For the calculation of the load-carrying capacity of screws in CLT with screw axis perpendicular to the shear plane, an extended model based on Johansen's yield model [24] was presented by Uibel and Blass [25] to account for the different embedment strengths of the crosswise CLT layers. The model is rather laborious and due to the fact that the dowel effect is limited in the case of inclined screws as discussed in this paper, the different properties of the cross-wise layer will not be taken into account. In this study, therefore, the CLT member will be considered homogenous with a grain direction equal to that of the outer layer.

Bejtka and Blass [26] derived the extended expressions of Johansen's yield model for the load-carrying capacity of timber-to-timber connections with inclined screws. This single shear capacity $F_{v,S}$ for a shear connection with an inclined screw is the minimum capacity of the following six possible failure modes:

$$R_a = R_{ax} \cdot \sin\alpha + f_{h,1} \cdot d \cdot s_1 \cdot \cos\alpha \quad (6a)$$

$$R_b = R_{ax} \cdot \sin\alpha + f_{h,2} \cdot d \cdot s_2 \cdot \cos\alpha \quad (6b)$$

$$R_c = R_{ax} \cdot (\mu \cdot \cos\alpha + \sin\alpha) + \frac{f_{h,1} \cdot d \cdot s_1}{1+\beta} \cdot (1 - \mu \cdot \tan\alpha) \cdot \left[\sqrt{\beta + 2 \cdot \beta^2 \cdot (1 + \frac{s_2}{s_1} + (\frac{s_2}{s_1})^2) + \beta^3 \cdot (\frac{s_2}{s_1})^2} - \beta \cdot (1 + \frac{s_2}{s_1})\right] \quad (6c)$$

$$R_d = R_{ax} \cdot (\mu \cdot \cos\alpha + \sin\alpha) + \frac{f_{h,1} \cdot d \cdot s_1}{2+\beta} \cdot (1 - \mu \cdot \tan\alpha) \cdot \left[\sqrt{2 \cdot \beta \cdot (1+\beta) + (\frac{4 \cdot \beta \cdot (2+\beta) \cdot M_y}{f_{h,1} \cdot d \cdot s_1^2})^2} - \beta\right] \quad (6d)$$

$$R_e = R_{ax} \cdot (\mu \cdot \cos\alpha + \sin\alpha) + \frac{f_{h,1} \cdot d \cdot s_2}{1+2 \cdot \beta} \cdot (1 - \mu \cdot \tan\alpha) \cdot \left[\sqrt{2 \cdot \beta^2 \cdot (1+\beta) + (\frac{4 \cdot \beta \cdot (1+2 \cdot \beta) \cdot M_y}{f_{h,1} \cdot d \cdot s_2^2})^2} - \beta\right] \quad (6e)$$

$$R_f = R_{ax} \cdot (\mu \cdot \cos\alpha + \sin\alpha) + (1 - \mu \cdot \tan\alpha) \cdot \sqrt{\frac{2 \cdot \beta}{1+\beta}} \cdot \sqrt{2 \cdot M_y \cdot f_{h,1} \cdot d \cdot \cos^2\alpha} \quad (6f)$$

where $R_{ax} = \min\{R_{ax,1}; R_{ax,2}\}$, where $R_{ax,1}$, $R_{ax,2}$ are the withdrawal capacity of the screw in the first and second timber member, respectively, s_1, s_2 the anchorage depth of the screw perpendicular to the shear plane in the first and second member, respectively, $f_{h,1}$, $f_{h,2}$, the embedment strength of the first and second member, respectively, α the angle between the screw axis and the line which is perpendicular to the shear plane ($\alpha = 0°$ for a screw perpendicular to the shear plane, and $\alpha = 90°$ for a screw parallel to the shear plane), $\beta = f_{h,2}/f_{h,1}$ the ratio of embedment strengths, d and M_y the diameter and yield moment of the screw, respectively, and μ the friction coefficient between the timber members.

The embedment and withdrawal strength of self-tapping screws in timber-to-timber joints for different inclination angles α have been determined experimentally by Blass et al. [27]. For angles $\alpha = 0°$ to $\alpha = 90°$ they are respectively expressed as:

$$f_{h,\alpha,mean} = \frac{0.022 \cdot \rho_{mean}^{1.24} \cdot d^{-0.3}}{2.5 \cdot \sin^2\alpha + \cos^2\alpha} \quad [N/mm^2] \quad (7)$$

$$R_{ax,mean} = \frac{0.6 \cdot \sqrt{d} \cdot l_{ef}^{0.9} \cdot \rho_{mean}^{0.8}}{1.2 \cdot \sin^2\alpha + \cos^2\alpha} \quad [N] \quad (8)$$

where ρ_{mean} [kg/m^3] is the mean density of the timber member considered, and d and l_{ef} [mm] the outer thread diameter and threaded length of the screw in the timber member considered, respectively.

The mean value for the yield moment of the screw M_y is estimated based on the characteristic values given in the ETA-12/0063 [12] and Table 1. Assuming a normal distribution, a confidence level of 75%, a coefficient of variation of 10% and a large test series (a statistical coefficient of 1.65), the mean value of the yield moment is given by $M_{y,mean} = M_{y,k}/(1 - 1.65 \cdot 0.1) \approx 1.20 \cdot M_{y,k}$.

4.3.2.2. Slip modulus. In Eurocode 5 [28] the values for the slip modulus that are given include the dowel effect but not the rope effect or withdrawal stiffness for nails or screws perpendicular to the shear plane. Tomasi et al. [6] have proposed an expression for the slip modulus for inclined screws that considers both the embedment of the screw with respect to the dowel action and the withdrawal of the screw. The slip modulus $k_{s,S}$ [N/m] for inclined screws in shear tension is calculated according to Tomasi et al. [6] as:

$$k_{s,S} = k_\perp \cdot \cos\alpha \cdot (\cos\alpha - \mu \cdot \sin\alpha) + k_\parallel \cdot \sin\alpha \cdot (\sin\alpha + \mu \cdot \cos\alpha) \quad (9)$$

where $k_\perp$ and $k_\parallel$ [N/m] are the connector stiffnesses for lateral and withdrawal loading, respectively, and μ is the friction coefficient between the timber members ($k_\perp$ and $k_\parallel$ correspond to the slip modulus in the directions perpendicular to the screw axis and along the screw axis, respectively, and projected to the shear plane).

Deformation due to the withdrawal action is generally assumed to take place simultaneously in both timber members in the serviceability limit state [21]. Such assumption is referred to as the "double stiffness model" in Tomasi et al. [6]. The withdrawal stiffnesses of each threaded screw part in each timber member are summed as springs in series (cf. Eq. (12)).

Empirical formulas available in the Eurocode 5 [28] and in the European technical Approval for WT-T screws [12] are used for the stiffness parameters $k_\perp$ and $k_\parallel$ since more specific values are not available, and are therefore taken as follows:

$$k_\perp = \frac{\rho_m^{1.5} \cdot d}{23} \quad [N/mm] \quad (10)$$

where ρ_m is the mean density in the timber members in kg/m^3 and d the outer diameter of the screw thread in mm (another interpretation is to consider the effective diameter as $1.1 \times d_{core}$.). When the mean densities of the timber members are different, the mean density ρ_m is calculated according to the Eurocode 5 expression [28] as $\rho_m = \sqrt{\rho_{m,1} \cdot \rho_{m,2}}$;

$$k_{\parallel} = \frac{1}{\frac{1}{k_{ax,1}} + \frac{1}{k_{ax,2}}} \quad (11)$$

where $k_{ax,i}$ is the screw withdrawal stiffness in the ith timber member and is for any angle between the screw axis and the grain direction given in [12] by:

$$k_{ax} = 25 \cdot l_{ef} \cdot d \quad [\mathrm{N/mm}] \quad (12)$$

where d is the outer thread diameter in mm of the screw and l_{ef} is the penetration length of the threaded part of the screw in the timber member in mm. In the older technical approval for SFS WT-T screws [29], this formula is given as $k_{ax} = 30 \cdot l_{ef} \cdot d$.

Tomasi et al. [6] argued that it can be justified to consider withdrawal only in one of the members ("single stiffness model"); then they refer to the conditions in the ultimate limit state and assume the same kind of behaviour in the serviceability limit state, which is highly questionable, as the assumption is equivalent to considering that the screw is fixed in one of the timber members and that no withdrawal displacement can occur within this member at the serviceability limit state. We note however that this assumption was made in Tomasi et al. [6] as a comparison with the "double stiffness model" and provided the best agreement with their test results when using values given in the EC5 and values given in the technical approval of the screws for $k_{\perp}$ and $k_{\parallel}$, respectively. It might also be that the values for $k_{\perp}$ and $k_{\parallel}$ taken in the EC5 and in the European technical Approval for inclined screws, respectively, are too conservative and that more accurate parameters are necessary to estimate the slip modulus of inclined screws in the SLS when using Eq. (9). Both the single stiffness model (SSM) and the double stiffness model (DSM) are considered for comparison with the test results in this paper.

4.3.3. Combined joint with double-sided punched metal plate fasteners and inclined screws

4.3.3.1. Load-carrying capacity. The total load carried by a joint made with multiple fasteners equals the sum of the load on each single fastener for any applied displacement [30]. Therefore, the shape of the total load–slip curve of a joint made of multiple fasteners is the superposition of the load–slip curve of each single fastener. When different types of fasteners with different types of load–slip curves are combined in a joint the resulting load-carrying capacity is usually less than the sum of the load-carrying capacity of each single fastener [30].

In Table 5 the summation of the load-carrying capacity of the individual fasteners gives values that exceed by up to 11% the actual capacity observed in the tests. In this study, a reduction factor $k_r = 1/1.11 = 0.9$ is therefore proposed to estimate the total load-carrying capacity of joints with combined double-sided nail plates and screws inclined at 45°. The total capacity is given by:

$$F_{v,tot} = k_r \cdot (n_s \cdot F_{v,S} + n_{NP} \cdot F_{v,NP}) \quad (13)$$

where n_s, and n_{NP} are the number of screws and double-sided nail plates in the joint, respectively.

4.3.3.2. Slip modulus. As is evident from the discussion in Section 3.6, the slip modulus of the inclined screw can be added to the slip modulus of the double-sided nail plates to give the combined value. Thus, the total slip modulus of the combined joint can be expressed as:

$$k_{s,tot} = k_{s,S} + k_{s,NP} \quad (14)$$

4.3.4. Comparison between calculated values and test results

For each test series, the load-carrying capacity is calculated according to the calculation methods described in this paper. The estimated mean values for the load-carrying capacity and the slip modulus are presented in Table 6 for the individual fastener joints and for the combined joint, and they are compared with the test results. The ratios presented for comparison show that the calculated values are conservative when the ratio is less than one (<1). Calculations are made considering the mean density measured for each member in each test series. The angles α_{NP} and β_{NP} are both equal to 0°. The angle α between the screw axis and the applied force direction in the plane perpendicular to the shear plane is equal to 45° for all series with screws. The effective thread length on each part of the screw is in all cases l_{ef} = 65 mm and the diameter d is taken as the outer thread diameter. The friction coefficient μ for the timber-to-timber interlayer is considered equal to 0.25.

Adding the individual capacities according to expression (13) gives estimated values ranging from 80% to 100% of the load-carrying capacity observed in the shear test, the lowest estimates being obtained for joints with inclined screws of diameter 8.2 mm. Concerning the slip modulus, the analytical expressions give significantly more underestimated values for the joints with screws only, corresponding to 43% and 45% of the slip modulus measured in the tests with the double stiffness model, and 76% and 79% with the single stiffness model, respectively. This fact is of course affecting the estimation of the stiffness of the combined joints which is therefore conservative with values ranging from 72% to 95% of the stiffness measured in the test. The slip modulus of series S6 is

Table 6
Calculated load-carrying capacity and slip modulus compared with test results.

Test series		Test results		Calculated values												
				Double-sided nail plates		Screws			Joints with single and combined connectors							
							DSM[a]	SSM[b]				DSM[a]		SSM[b]		
		$F_{v,test}$ (kN)	$k_{s,test}$ (kN/mm)	$F_{v,NP}$ (kN)	$k_{s,NP}$ (kN/mm)	$F_{v,S}$ (kN)	$k_{s,S}$ (kN/mm)	$k_{s,S}$ (kN/mm)	k_r (-)	$F_{v,tot}$ (kN)	$\frac{F_{v,tot}}{F_{v,test}}$ (-)	$k_{s,tot}$ (kN/mm)	$\frac{k_{s,tot}}{k_{s,test}}$ (-)	$k_{s,tot}$ (kN/mm)	$\frac{k_{s,tot}}{k_{s,test}}$ (-)
S1	2 S-6.5	16.1	19.4			15.9	8.7	15.3			0.99		0.45		0.79
S2	2 S-8.2	22.8	25.4			18.3	11.0	19.3			0.80		0.43		0.76
S6	2 NP-100	33.9	45.6	31.9	53.6						0.94		1.18		1.18
S8	1 NP-200	32.9	53.6	32.9	53.6						1.00		1.00		1.00
S3	1 NP-200 2 S-6.5	44.1	72.2	32.7	53.6	15.9	8.7	15.3	0.9	43.8	0.99	62.3	0.86	68.9	0.95
S4	1 NP-200 2 S-8.2	51.5	85.0	32.2	53.6	18.1	10.9	19.3	0.9	45.2	0.88	64.5	0.76	72.9	0.86
S5	2 NP-100 1 S-6.5	38.5	80.8	32.5	53.6	7.9	4.3	7.6	0.9	36.4	0.94	57.9	0.72	61.2	0.76
S7	1 NP-100 2 S-6.5	30.1	46.9	16.1	26.8	15.8	8.7	15.3	0.9	28.7	0.95	35.5	0.76	42.1	0.90

[a] DSM denotes the Double Stiffness Model according to Tomasi et al. [6].
[b] SSM denotes the Single Stiffness Model according to Tomasi et al. [6].

overestimated by about 18%. As mentioned, the reason for this result is attributed to the location of the double-sided nail plates in the test specimen (Fig. 7b).

5. Discussion and comments

The results show that the double-sided punched metal plate fasteners tested have a high load-carrying capacity and stiffness compared to inclined screws. A $72 \times 200\ mm^2$ double-sided nail plate has about 3.6 times the load-carrying capacity and 4.2 times the stiffness of a self-tapping screw ($d \times L = 8.2 \times 160$ mm) inclined at 45° and loaded in shear-tension. Therefore, in a composite floor application a shear connection made with double-sided nail plates ($72 \times 200\ mm^2$) with a spacing of 420 mm may provide the same level of composite action than inclined self-tapping screws (diameter 8.2 mm) with a spacing of 100 mm.

For the combination of double-sided nail plates and inclined screws, and for the combination of different types of mechanical fasteners in general, the compatibility of the load–slip curves should be considered. Concerning the combined joint load-carrying capacity the value of the slip at maximum load of each type of fastener should be known. When these values are similar, the capacity of the combined joints will be maximised and be close to the sum of the capacity of each fastener type, otherwise it will of course be lower. Regarding the stiffness of the combined joint, the yield point of each fastener type on the load–slip curve can be a good indicator for the verification of the compatibility of the fasteners for combined use.

Based on the test results on inclined screw joints with different angles presented by Tomasi et al. [6], it would be possible to propose a configuration of the joint where the slip at maximum load would be the same for the screws and the double-sided nail plates. An angle of 15° to 30° between the screw axis and the normal to the shear plane would make the slip at maximum load for the screw close to 5 mm and therefore more compatible with the one of the double-sided nail plates. This configuration could be more predictable in terms of load-carrying capacity since the fasteners would reach their respective maximum load for similar applied displacements. However, at this inclination angle, the slip modulus of the inclined screws will be significantly lower than with an angle of 45°.

6. Conclusions

Double-sided punched metal plate fasteners may effectively be used as shear connectors for glulam–CLT composite floor elements. Securing this type of shear connection with inclined screws can significantly increase the slip modulus and the load-carrying capacity despite the different nature of the shear connectors. This is interesting from the point of view of minimising the amounts of connectors used for the manufacturing of glulam–CLT floor elements. The use of this type of fasteners may be advantageous in an automated production process and represent an alternative to glued or screwed shear connections for composite floor elements as described in the introduction.

From the tests, it was noted that the failures were initiated more often in the glulam member than in the CLT for both fastener types and that the dowel effect of the screws seemed limited in the early stage of the test due to their inclination. The test setup boundaries and the location of the double-sided nail plates in the different tests had an influence on the results, especially for nail plates combined with inclined screws and with regards to the joint stiffness. It was shown in Section 3.5 that for these reasons, the different tests where the nail plates had different locations should not be compared directly with each other. The double-sided nail plates have a more pronounced non-linear behaviour than inclined screws in the early stage of the shear test. They exhibit a ductile behaviour to a certain degree, but their capacity after the maximum load is very limited. Inclined screws have a less ductile behaviour but keep nevertheless an important load-carrying capacity after maximum load.

Regarding the compatibility of the fasteners, the double-sided nail plates reach their maximum load-carrying capacity at a higher slip value than the inclined screws, but they yield at a lower slip value (cf. Section 3.6.). The combined joints behaved as the superposition of the individual load–slip curve of the single fasteners (cf. Section 4.1). In terms of load-carrying capacity, the combined joint exhibit a total capacity which is lower than the sum of the capacity of each fastener taken individually due to the fact that the double-sided nail plates and the inclined screws reach their respective maximum load at different slip values. The overall shape of the load–slip curve of the double-sided nail plate joints is improved by the addition of the inclined screws. Inclined screws are increasing the slip modulus of the shear connection at low load levels. They are also increasing the reserve load-carrying capacity after failure, preventing a rapid separation of the specimens after the maximum load.

The paper presents a simple calculation model in Section 4.3 for combined joints made with double-sided punched metal plate fasteners and inclined screws according to exiting guidelines given in relevant standards and literature. For the combined joint, the load-carrying capacities of the different fastener types may be added together using a reduction factor (0.9 is suggested) while the slip modulus of each fastener may be summed without reduction factor. This method gives a reasonable agreement between calculated values and test results. However, regarding the calculation method for stiffness of inclined screw joints, the comparison between the test results in this paper and the model from Tomasi et al. [6] did not give acceptable agreement, not even for the single stiffness model. Whether this discrepancy is due to the analytical assumptions or the applicability of the different empirical values for the parameters in the model, needs further study.

Acknowledgements

The centre for Lean Wood Engineering, the Swedish governmental agency for innovation systems (VINNOVA), Stora Enso Timber, the County Administrative Board in Norrbotten under Grant Number 303-2602-13 (174311); the Regional Council of Västerbotten under Grant Number REGAC-2013-000133 (00179026); and the European Union's Structural Funds – The Regional Fund under Grant Number 2013-000828 (174106) are acknowledged for their financial support to this research.

Ari Kevarinmäki is acknowledged for his comments and assistance for carrying out the tests at VTT Expert Services laboratories in Finland.

Appendix A. Load–slip curves of all shear test series

The load–slip curves of all test series are presented including the discarded load–slip curves, which were: Test 1 and Test 2 in series *S*1 (Fig. A1a), Test 1 and Test 5 in series *S*2 (Fig. A1b), due to a gap between the timber members leading to a low slip modulus; and Test 2 in series *S*7 due to an unexpected post-peak behaviour (Fig. A1g). The load–slip curves and the measured values for all test series are presented in detail in the test report [19].

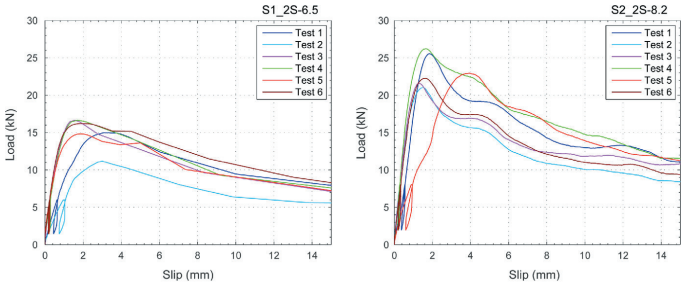

(a) Series S1_2S-6.5 (b) Series S2_2S-8.2

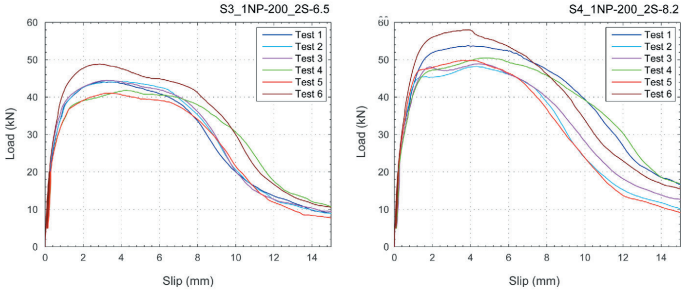

(c) Series S3_1NP-200_2S-6.5 (d) Series S4_1NP-200_2S-8.2

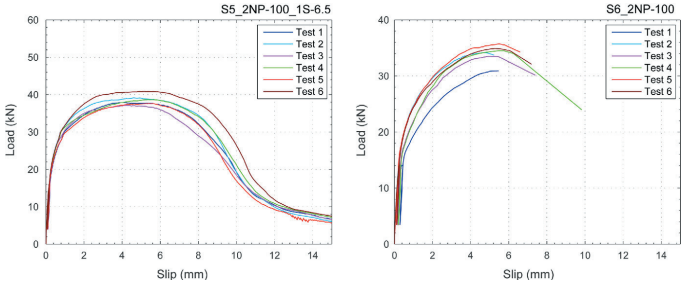

(e) Series S5_2NP-100_1S-6.5 (f) Series S6_2NP-100

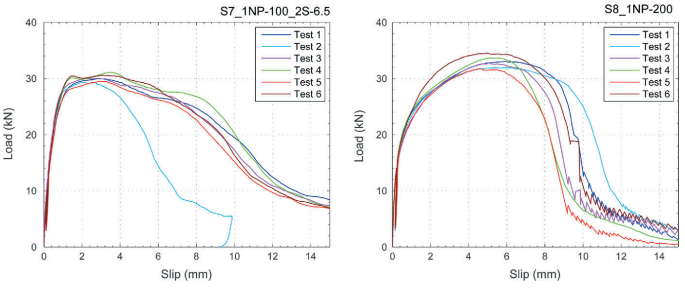

(g) Series S7_1NP-100_2S-6.5 (h) Series S8_1NP-200

Fig. A1. Load–slip curves of all test series (including discarded curves).

References

[1] Jorissen A. The design of timber floors, presented at the World Conference on Timber Engineering (WCTE), Portland, Oregon, USA; 2006.
[2] Smith I. Vibrations of timber floors: serviceability aspects. In: Thelandersson S, Larsen HJ, editors. Timber Engineering. Wiley; 2003. pp. 241–266.
[3] Gagnon S, Pirvu C. CLT Handbook Cross-Laminated Timber – Canadian Edition. Québec: FP Innovations; 2011.
[4] Kolb J. Systems in Timber Engineering, 1 ed.: Birkhäuser Architecture; 2008.
[5] Chen Y, Lam F. bending performance of box-based cross-laminated timber systems. J Struct Eng 2013;139:04013006.
[6] Tomasi R, Crosatti A, Piazza M. Theoretical and experimental analysis of timber-to-timber joints connected with inclined screws. Constr Build Mater 2010;24:1560–71.
[7] Whale LRJ. Punched metal plate fastener joints. in Timber Engineering STEP. 1 ed: Centrum Hout; 1995.
[8] Zhou T, Guan Z. Numerical modelling for sensitivity analysis of wood joints made with double-sided punched metal plate fasteners. Adv Struct Eng 2011;14:163–77.
[9] Karadelis JN, Brown P. Punched metal plate timber fasteners under fatigue loading. Constr Build Mater 2000;14:99–108. 3/30/2000.
[10] European Committe for Standardization (CEN). SS-EN 1194:1999 – Glued laminated timber – Strength classes and determination of characteristic values, vol. SS-EN 1194:1999 Sv. Swedish Institute for Standards (SIS); 1999.
[11] Deutsches Institut für Bautechnik (DIBt). European Technical Approval ETA-08/0271 – CLT – Cross Laminated Timber. in ETA-08/0271, European Organisation for Technical Approvals (EOTA), Ed., ed; 2011, p. 17.
[12] M.o.E. Österreichisches Institut für Bautechnik (OIB). European technical approval ETA-12/0063 – SFS self-tapping screws WT, ed; 2012.
[13] European Committe for Standardization (CEN). EN 26891:1991 – timber structures – joints made with mechanical fasteners – general principles for the determination of strength and deformation characteristics, ed; 1991.
[14] European Committe for Standardization (CEN). EN 1075:1999 – timber structures – test methods – joints made with punched metal plate fasteners, ed. Brussels; 1999.
[15] International Organization for Standardization. ISO 3130 – wood – determination of moisture content for physical and mechanical tests, ed; 1975.
[16] International Organization for Standardization. ISO 3131 – wood – determination of density for physical and mechanical tests. vol. ISO-3131, ed; 1975.
[17] European Committe for Standardization (CEN). EN 12512:20014 – timber strucutres – test methods – cyclic testing of joints made with mechanical fasteners. ed. Brussels; 2001.
[18] Jorissen A, Fragiacomo M. General notes on ductility in timber structures. Eng Struct 2011;33:2987–97.
[19] Jacquier N. Shear tests on glulam–CLT joints with double-sided punched metal plate fasteners and inclined screws. Luleå Univeristy of Technology, Technical Report; 2014.
[20] European Committe for Standardization (CEN). EN 338: structural timber – strenght classes. ed. Brussels; 2009.
[21] Kevarinmäki A. Joints with Inclined Screws, presented at the CIB W18, Japan; 2002.
[22] Antonides CE, Vanderbilt MD, Goodman JR. Interlayer gap effect on nailed joint stiffness. Wood Sci 1980;13:41–6.
[23] European Committe for Standardization (CEN). EN 14545:2008 – timber structures – connectors – requirements, ed. Brussels; 2008.
[24] Johansen KW. Theory of timber connections. Int Assoc Bidge Struct Eng 1949;9:249–62.
[25] Uibel T, Blass HJ. Load carrying capacity of joints with dowel type fasteners in solid wood panels, presented at the CIB W18, Italy; 2006.
[26] Bejtka I, Blass HJ. Joints with inclined screws, presented at the CIB W18, Japan; 2002.
[27] Blaß HJ, Bejtka I, Uibel T. Trägfähigkeit von Verbindung mit selbst bohrenden Holzschrauben mit Vollgewinde. Lehrstuhl für Ingenieurholzbau und Baukonstruktionen; 2006.
[28] European Committe for Standardization (CEN). EN 1995-1-1:2004 (E), in Eurocode 5 Design of timber structures, ed: CEN; 2004.
[29] Zulassung Z-9.1-472 – SFS Befestiger WT-T-6,5, WT-T-8,2 und WR-T-8,9 als Holzverbindungsmittel; 2006.
[30] Blaß HJ. Multiple fastener joints, in Timber Engineering STEP 1, ed: Centrum Hout; 1995.

Paper III

Evaluation of bending tests on composite glulam-CLT beams connected with double-sided punched metal plates and inclined screws

by Nicolas Jacquier and Ulf-Arne Girhammar

Accepted for publication in *Construction and Building Materials*, (Under Revision)

Evaluation of bending tests on composite glulam-CLT beams connected with double-sided punched metal plates and inclined screws

Nicolas Jacquier[a,1], Ulf Arne Girhammar[a]

[a] *Division of Structural and Construction Engineering – Timber Structures, Luleå University of Technology, SE-971 87 Luleå, Sweden*

Abstract

Composite beam elements made of glulam beams and cross laminated timber (CLT) panels, and connected with a new shear connection system were tested under four point bending. The beams tested represent a section of a cassette floor element to be used in a multi-storey CLT construction system. The shear connection is primarily made of double-sided punched metal plate fasteners, connecting the CLT and glulam members to form a T-cross-section. Due to the uncertainty about the capacity of the double-sided nail plates to resist possible separation forces between the timber members, the shear connection may be secured with screws. Bending tests were performed with three shear connector configurations: double-sided punched metal plate fasteners only, inclined screws only, and double-sided punched metal plate fasteners combined with inclined screws. An additional test with a screw glued connection was made for comparison. The results show that a shear connection with double-sided nail plates can be designed to provide a sufficiently high level of composite action and load-carrying capacity and represents an alternative shear connection system for glulam-CLT composite floors.

Key words: bending tests; composite beam; double-sided punched metal plate fasteners; inclined screws; Cross Laminated Timber; CLT; glulam

[1] Corresponding author. Tel.: +46 920 49 28 89; E-mail: nicolas.jacquier@ltu.se (N. Jacquier)

1. Introduction

This article presents the evaluation of a connection system for build-up floor elements made with cross laminated timber (CLT) panels and glulam beams. Fig. 1 shows an example of glulam-CLT floor element where the CLT panel is located under the glulam beam. The load-bearing part of the floor element consists of the CLT panel and glulam beams only, which are assembled with a shear connection. In this study, the connection system which is evaluated is made of double-sided punched metal plate fasteners and inclined screws.

Double-sided punched metal plate fasteners (Fig. 3), also called double-sided nail plates for short (DSNP), are proprietary fasteners which have been developed for fire protected and aesthetic joints in light timber trusses [1]. DSNP are usually pressed in-between two timber members and are supposed to transfer forces between the members in the same manner as traditional punched metal plate fasteners. Despite the fact that it is not their intended original function, double-sided nail plates can be used for shear load transfer when pressed between two timber members subjected to relative sliding, i.e. in a layered composite structure. The large timber area mobilised by this type of fastener compared to nails or screws can provide high values of load-carrying capacity and slip modulus and can be beneficial in timber composite structures.

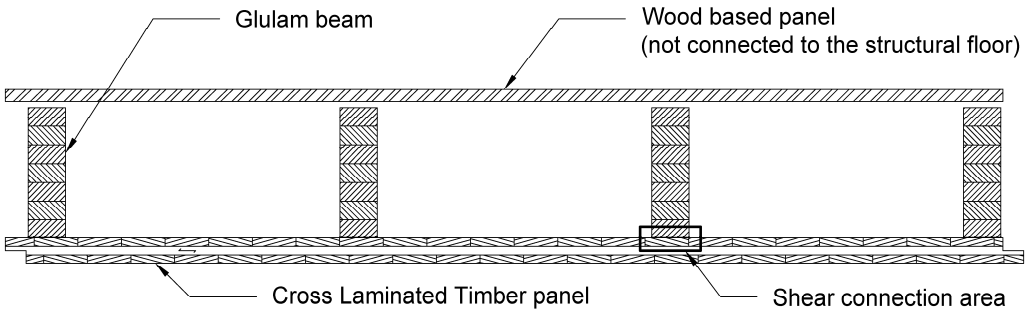

Fig. 1: Example of a glulam-CLT cassette floor element with CLT panel located at the bottom.

The shear behaviour of joints with double-sided nail plates has been evaluated in a previous study [2] individually and in combination with self-tapping screws in order to compensate the low withdrawal capacity of double-sided nail plates. The combination of these different fastener types improves the overall joint strength and stiffness and was suggested to make a robust design of the composite member. A more detailed background about the motivation for combining inclined screws and double-sided nail plates is presented in the background section and in [2]. The combination of double-sided nail plates and screws is also evaluated in this article which presents the results of three different series of bending tests performed on glulam-CLT beam elements connected with either:

- double-sided punched metal plate fasteners;

- inclined self-tapping screws;
- double-sided punched metal plate fasteners combined with inclined self-tapping screws.

In addition, a single test on a glulam-CLT beam specimen assembled with screw gluing is also presented for comparison reasons.

The aim of the study is to evaluate the performance (strength, stiffness, behaviour) of composite beam elements with double-sided nail plates used as shear connectors and to evaluate the influence of inclined screws added to this type of shear connection on the overall beam performance. The study intends to evaluate the technical feasibility of a particular design of a glulam-CLT composite floor element of 6.4 m span made with such shear connectors.

2. Background

Vibration in the serviceability limit state is one of the requirements which often governs the design of timber floors [3], [4], especially in modern multi-storey buildings where spans of 6 meters or more can be seen. The Eurocode 5 [5] recommends to carry out special investigations with respect to vibrations for residential floors having a fundamental frequency below 8 Hz. In Finland, the country where the floor element presented in this study is intended to be used, the National Annex [6] sets this limit at 9 Hz. These requirements therefore means that the floor structure needs to have a bending stiffness to mass ratio as high as necessary to achieve an acceptable vibration performance [4].

Long spans CLT floors can be considered as material intensive structures. The CLT Handbook [7] shows examples of CLT floor designs with respect to vibration with a recommended thickness of 240 mm for a floor span of 6.1 m. In order to increase the bending stiffness and reduce the self-weight of CLT-based floor structures, CLT can be combined with other linear engineered wood products. In this study, a so-called “ribbed floor” element, or cassette floor element, made with glulam beams connected to a CLT panel is investigated.

Ribbed floor elements present some advantages such as a reduced self-weight and the possibility to use the voids between beams for technical installation and airborne sound insulation. In the configuration shown in Fig. 1, the CLT contributes to the fire resistance between apartments and may be left visible for aesthetic reasons. This floor element is completed with an acoustically separated wood based panel serving as a support for the complementing layers (e.g. a non-structural cement-based layer and floor finishes).

The bending stiffness of the built-up floor element is to a large extent governed by the performance of the shear connection between the timber members. The slip modulus and the load-carrying capacity of the shear connection determine the level of composite action of the composite beam as well as the

stress distribution in the different timber members. Screwing, gluing, or screw-gluing (the screws being used to apply the required pressure on the glue joint) [8], are some of the solutions which can be used for ribbed floors or hollow-box floor structures, as described in more details in the parallel shear tests study [2]. Press-gluing techniques are very effective from a structural point of view but can be considered as demanding in terms of equipment, preparation and quality controls [8]. Alternatively, the screw gluing technique is also demanding in terms of quality control, amount of screws and manual work needed. The shear connection can also be made of self-tapping screws only as shown in [9] or for refurbishment of old timber structures [10]. When used in inclined position, screws can provide high stiffness and load-carrying capacity [11], [12]. However, for long span composite floors, the amount of screws needed to reach a high level of composite action can become large and alternative connection systems or combination of different connectors can be interesting in order to minimize the amount of fasteners needed and installation time in an industrialised production process.

The new shear connection system with double-sided punched metal plate fasteners evaluated in this study needs to be installed with dedicated pressing equipment and can therefore be used for prefabricated structures only, but the assembly time of glulam-CLT elements may be reduced compared with a gluing technique as there is no need for curing. In addition, the production controls might also be less demanding than for a glued connection. This type of fasteners is therefore particularly suited for production lines of floor elements where there is a need for rapid assembly time.

The uncertainty about the use of double-sided nail plate fasteners used as the sole shear connection for the glulam-CLT floors is due to their low capacity to resist the possible separation forces which may occur (e.g. during handling and erection, and also because of possible hanging loads). The double-sided nail plates can be combined with inclined self-tapping screws in order to reduce or eliminate the possibility of a separation between the timber members for safety and robustness of the composite element, see [2]. Self-tapping screws have a high withdrawal capacity. When used in an inclined position in “shear-tension” [13], compressive forces between the timber members are generated, and can counteract the separation forces. The screws added in the joint with double-sided nail plates may therefore limit the possible withdrawal of the nail plates. This is also important in case of repeated loading and, therefore, is essential for the long-term behaviour of the connection.

3. Methods

The experimental test program on glulam-CLT beams connected with double-sided nail plates and inclined screws was carried out at the laboratories of VTT Expert Services Ltd in Finland. Three different series of composite beams with different types of shear connectors were tested under 4-point bending. Each series consisted of three specimens. An additional specimen with a screw-glued connection was tested in order to compare the results with a beam with full composite action. All

beams were 6.5 meter long and had the same cross-section as shown in Fig. 2 for a specimen with double-sided nail plates and screws.

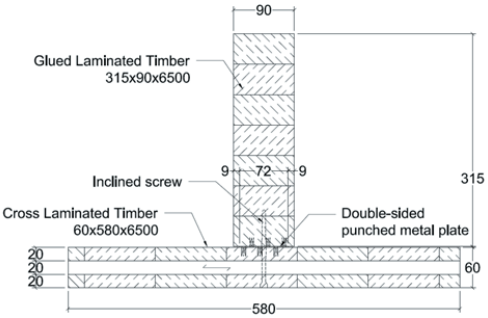

Fig. 2: Cross-section of the composite Glulam-CLT beam with double-sided nail plate and screw shear connection.

3.1. Shear connectors

The shear connection is made with double-sided punched metal plate fasteners and self-tapping screws used either individually or combined. The configurations of the shear connectors in the different test series are presented in section 3.4.

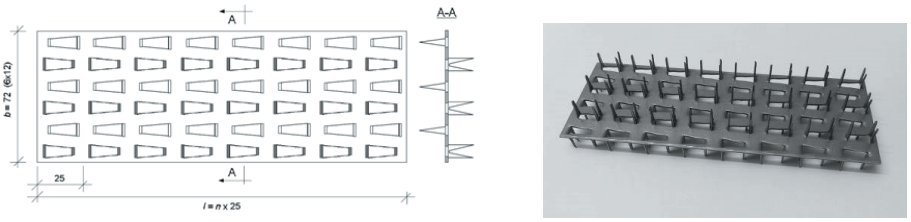

Fig. 3: Double-sided punched metal plate Sepa-SE2P, 72×200 mm^2.

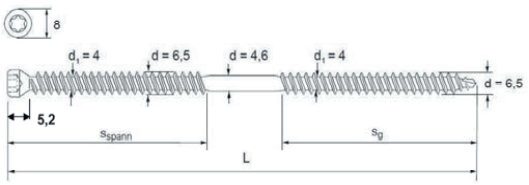

Fig. 4: SFS-Intec WT-T screw geometry with diameter 6.5 mm (source SFS Intec [14]).

The double-sided punched metal plate fasteners Sepa-SE2P (see Fig. 3), made of zinc coated steel, had dimensions (b_{NP}×l_{NP}) 72×200 mm^2, with a steel plate thickness of 1.3 mm and teeth length of 15.6 mm. Mechanical properties (mean values) according to the manufacturing's inspection certificate were: tensile yield strength f_y = 410 N/mm^2, ultimate tensile strength f_u = 485 N/mm^2, elongation ε_u = 28.0 % and weight of zinc coating 293 g/m^2.

SFS Intec WT-T self-drilling screws (see Fig. 4) were used in series with inclined screws, with dimensions ($d \times L$ in mm) 6.5×160 and properties according to European Technical Approval ETA-12/0063 [14].

Shear tests on glulam-CLT joints made with these connectors were presented in [2]. Some of the results from this study are reported in Table 1 for clarity. It can be noted that these values might be slightly overestimating the actual capacity and slip modulus of the connectors due to the compressive force generated by the shear test setup (load application eccentricity and restraints). Effects of the compressive force on the joint behaviour were discussed in [2] but not quantified. It may be argued that for the shear tests with screws only, the measured slip modulus value should be further reduced by 4-8 % to remove the contribution due to the friction resistance generated by the test setup. Considering this effect should have a positive effect on the agreement between the calculated and measured load-deflection curves in the bending tests presented in this load-deflection. However, since the exact contribution due to the friction and test setup cannot be evaluated with certainty, the unmodified values given in Table 1 are the ones used in this article. Concerning the DSNP, the influence of the shear test setup is more difficult to evaluate as there was no timber-to-timber friction component due the gap which remains between the timber members by the presence of the nail plate. It may be assumed that the stiffness and load-carrying capacity of the DSNP is not affected by the compressive force.

Table 1: Load-carrying capacity, slip modulus and specific slip values for single shear connectors [2].

Shear connector type (Test series name in [2])	Load-carrying capacity	Slip modulus	Yield slip	Slip at maximum load
	F_{max} (CoV) kN (%)	k_s (CoV) kN/mm (%)	u_y (CoV) mm (%)	u_{max} (CoV) mm (%)
Screw SFS-WT-T 6.5×160 in shear-tension (α = 45°) (S1_2S-6.5)	8.0 (5.3)	9.7 (7.3)	0.67 (19.9)	1.78 (9.4)
Double-sided nail plate Sepa-SE2P (S8_1NP-200)	32.9 (2.9)	53.6 (7.8)	0.27 (1.4)	5.26 (8.8)

For the test specimen made with screw-gluing, the glue was the one-component polyurethane glue Purbond HB110 (250 gr/m2). To apply the necessary pressure in the glue joint, vertical SFS Intec screws WFD-T-H12-8×180 were used with 28 mm diameter washers. The screws were inserted from the CLT to the glulam and had a smooth shank part of 72 mm (larger than the CLT thickness) so that the threaded part of the screw could tighten the glulam and CLT members together.

3.2. Timber members

The glulam beams of cross-section 90×315 mm^2 were made of Norway Spruce (Picea Abies) and labelled L40 (Nordic glulam strength class) and GL32 [15]. The thickness of the glulam lamellas was 45 mm. The CLT panels of cross-section 60×580 mm^2 were manufactured from solid wood lamellas of strength class C24 according to European Technical Approval ETA-08/0271 [16]. The CTL was composed of three 20 mm thick layers with the outer ply grain direction oriented in the longitudinal direction.

The global modulus of elasticity according to EN 408 [17] was measured for three glulam beams and three CLT panels from the same production batch under a 4-point bending test, up to $0.4 \times F_{max,est}$, where $F_{max,est}$ was18 kN and 3 kN for the glulam beams and the CLT panels, respectively. When neglecting the shear deformation, the mean global modulus of elasticity obtained for the glulam was $E_{global,glulam}$ = 11 898 N/mm^2. Considering deflection due to shear deformation and assuming a shear modulus of G_{mean} = 850 N/mm^2 the mean global modulus of elasticity was $E_{global,glulam,shear}$ = 12 290 N/mm^2. The former value $E_{global,glulam}$ = 11 898 N/mm^2 is used in this load-deflection since the calculation method for the deflection does not account for the shear deformation. For the CLT, the global modulus of elasticity observed was $E_{global,CLT}$ = 11 445 N/mm^2. This value corresponds to the stiffness of the outer CLT layers with grain oriented parallel to the span direction and was calculated using the so called γ-method [EC5] described in section 0 and assuming a rolling shear modulus G_R = 50 N/mm^2. The influence of shear deformation in the longitudinal layers was not considered for the evaluation of the modulus of elasticity in the CLT.

3.3. Design method

The design of the composite glulam-CLT beam element with mechanical fasteners was carried out using preliminary test results for the shear connectors. Presented in [18], the complete design of this composite floor element according to the Eurocode 5 [5] and Finnish National Annex [6] shows that the minimum fundamental frequency f_1 of at least 9 Hz specified by the National Annex for the vibration in service is the governing design criteria. This requirement is far more demanding than the other short-term and long-term strength and deformation criteria and that it can be fulfilled if the floor element has a sufficiently high bending stiffness. Therefore, the stiffness of the shear connection in the composite structure is a crucial parameters for the design when other variables are fixed (i.e. floor height, glulam beam width, etc.), which is often the case in multi-storey residential construction. This section presents the calculation method for the effective bending stiffness of the partially composite glulam-CLT beam according to the γ-method.

3.3.1. Bending stiffness of glulam-CLT composite beam using the γ-method

The design of mechanically jointed timber beams can be carried out with the γ-method which is presented in the Annex B of the Eurocode 5, and which was first developed by Möhler [19]. The Eurocode 5 does not describe how to design CLT structures but it is generally accepted that the design of CLT panels in bending can be treated as a mechanically jointed structure and calculated with the γ-method by considering that only the layers with grain oriented parallel to the span direction are load-carrying, and that the other layers oriented perpendicularly act as a flexible shear connection [7], [16]. This assumption is applied in the γ-method by replacing the ratio s/K by the ratio $h/(G_R \times b)$ in the expression of the γ factor given in the Eurocode 5, where s is the spacing of the individual mechanical fasteners, K is the slip modulus of the mechanical fastener [N/mm], h is the thickness of the layer oriented perpendicular to the span direction, G_R is the rolling shear modulus and b is the width of the CLT panel. The γ-method can be used for composite cross-sections up to three layers as in the present glulam-CLT composite section (Fig. 5). To consider shear deformations or for the design of composite sections with more than two flexible interlayers, other methods need to be used.

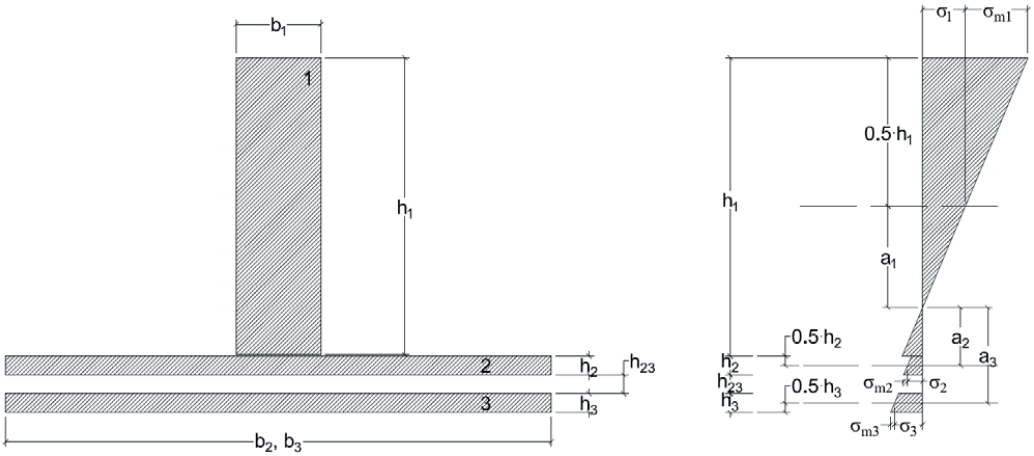

Fig. 5: Glulam-CLT cross-section and notation considered in the γ-method and stress diagram.

The effective bending stiffness EI_{ef} of the present composite glulam-CLT beam element is calculated according to the γ-method as follows:

$$EI_{ef} = \sum_{i=1}^{3} (E_i I_i + \gamma_i E_i A_i a_i^2) \tag{1}$$

where E_i, A_i and I_i are the modulus of elasticity, the area and the second moment of area of the i^{th} element in Fig. 5, respectively, $\gamma_2 = 1$ and where:

$$\gamma_1 = \left(1 + \pi^2 \frac{E_1 A_1 s_1}{k_1 L^2} \right)^{-1} \tag{2}$$

with s_1 and k_1 the spacing and slip modulus of the discrete shear connectors between element 1 and element 2, respectively,

$$\gamma_3 = \left(1 + \pi^2 \frac{E_3 A_3 h_{23}}{G_R b_3 L^2}\right)^{-1} \tag{3}$$

with h_{23} the height of the cross layer,

$$a_2 = \frac{\gamma_1 E_1 A_1 \left(\frac{h_1 + h_2}{2}\right) - \gamma_3 E_3 A_3 \left(\frac{h_2 + h_3}{2} + h_{23}\right)}{\gamma_1 E_1 A_1 + \gamma_2 E_2 A_2 + \gamma_3 E_3 A_3} \tag{4}$$

$$a_1 = \frac{h_1 + h_2}{2} - a_2 \tag{5}$$

$$a_3 = \frac{h_2 + h_3}{2} + h_{23} + a_2 \tag{6}$$

It can be noted that considering the transverse CLT layer has a small influence on the bending stiffness and similar results would be obtained if no slip was considered between the top and bottom CLT longitudinal layers. However the influence of the cross layer can become more important in the case of a thicker layer or for shorter spans. For comparison with the test results, the effective bending stiffness of the composite beam is calculated according to expressions (1) to (6) with the average modulus of elasticity measured on individual timber members (cf. section 3.2) and with the fastener slip modulus values from Table 1. For the composite beams with combined double-sided nail plates and inclined screws, the slip moduli of the different fastener types are added according to the superposition principle as suggested in [2]. For the screw-glued shear connections, full composite action between glulam and CLT is assumed.

3.3.2. Fundamental frequency design criteria

The fundamental frequency f_1 of simply supported one-span floors is calculated according the Finnish National Annex of the EC5 with expression (7):

$$f_1 = \frac{\pi}{2L^2}\sqrt{\frac{(EI)_l}{m}} \tag{7}$$

where L is the floor span, $(EI)_l$ is the equivalent bending stiffness of the floor about an axis perpendicular to the span direction, and m is the mass of the floor. The mass m is calculated according to [20] as $m = m_G + 30$ kg/m^2 where m_G is the self-weight of the finished floor element and where the term 30 kg/m^2 accounts for the permanent part of the service load. This recommendation for the

calculation of the floor mass replaces the former recommendation of the Finnish National Annex which previously specified to calculate this mass as $m = m_G + \psi_2 q_k$, where ψ_2 is the partial coefficient for the quasi-permanent load combination and q_k is the characteristic service load for the floor.

3.4. Test series

The description of the test specimens is given in Table 2 and Fig. 6. The series B1_S (screws only), B2_NP (double-sided nail plates only) and B3_NP+S (double-sided nail plates and screws combined) are designed with a constant spacing of the connectors s = 450 mm. This spacing was chosen in order for the series B2_NP and B3_NP+S to meet the 9 Hz fundamental frequency criteria considering the load case made of a uniformly distributed dead load G_k = 1.8 kN/m^2 and a service load Q_k = 2 kN/m^2. The design of series B1_S does not satisfies the vibration criteria but it was made to observe the behaviour of the composite beam with screws only with the same spacing as in the other test series. For the single specimen tested with a screw-glued connection B4_SG, the spacing of the vertical screws was 200 mm.

Table 2: Description of the test series with screws only (B1_S), double-sided nail plates only (B2_NP), double-sided nail plates and screws (B3_NP+S), and screw-gluing (B4_SG).

Test series			Spacing s = 450 mm		Spacing s = 200 mm
Series Name	No. of tests	Estimated load F_{est} (kN)	Screws inclined at 45° in shear tension $d \times l_s$ (mm)	Double-sided nail plates $b_{NP} \times l_{NP}$ (mm)	Vertical screws for screw-gluing $d \times l_s$ (mm)
B1_S	3	75	6.5 × 160	-	-
B2_NP	3	75	-	72 × 200	-
B3_NP+S	3	90	6.5 × 160	72 × 200	-
B4_SG	1	110	-	-	8 × 180

d is the nominal screw diameter, l_s is the screw length, b_{NP} and l_{NP} are the DSNP width and length, respectively.

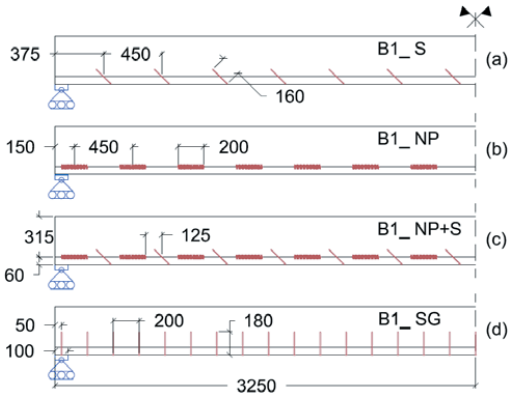

Fig. 6: Test series configurations: (a) screws only (B1_S), (b) double-sided nail plates only (B2_NP), (c) double-sided nail plates and screws (B3_ NP+S), (d) screw-gluing (B4_SG).

3.5. Test specimens conditioning and assembly

The CLT panels and glulam beams were stored in a climate chamber with 65 % relative humidity (RH) and temperature (T) 20 °C for 8 weeks before assembly of the specimens with double-sided nail plates. After the test specimens with nail plates were assembled, they were stored again in the climate chamber for 4 weeks before the loading tests.

The assembly of the beam elements with double-sided nail plates was done in the laboratory in two steps. First, each fastener was pressed individually on the CLT panel using a steel comb for double-sided nail plate (Fig. 7a and b) and a hydraulic jack with load-controlled force application and a maximum load limitation of 55 kN per fastener. Once all the double-sided nail plates were pressed into the CLT panel, the glulam beam was pressed onto the CLT using a two-point press and two steel beams in order to distribute the pressing load over the entire glulam beam length (Fig. 7c and d). The total load applied on the beam was 770 kN in order to press the 14 double-sided nail plates simultaneously. It was noticed that some nail plates were not fully pressed at certain locations, especially towards the ends. An additional pressing load was applied towards each end of the beam until full contact was achieved. The penetration depth of the nail plate teeth was satisfactory with less than 2 mm gap between the members in average (the minimum gap being 1.3 mm due to the steel plate thickness). The teeth of the nail plates become visible when the gap between the glulam and CLT elements exceeds 2.5 mm (Fig. 8a and b). A 3 mm gap nevertheless remained for most of the specimens on the glulam beam side and was observed usually for the second and third double-sided nail plate from the beam ends, and for the two ones in the centre. Stiffer distributing beams for the load application should improve the assembly. In an industrial production process, a more uniform pressing load could be also achieved using multiple hydraulic presses along the beam length.
The inclined screws of the test specimens B1 and B3 were installed some hours before running the test using a dedicated equipment to control the 45° insertion angle.

The assembly of the specimen with screw-gluing was done in a climate chamber under 65% relative humidity and 20°C temperature. The glue opening time was 18 minutes, and the specimen cured for 24 hours before testing.

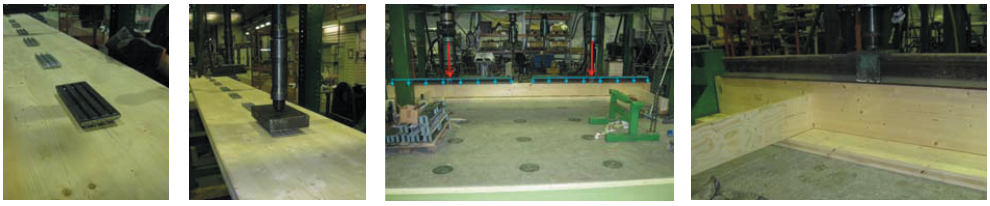

(a) (b) (c) (d)

Fig. 7: Fabrication process of the bending tests specimens with double-sided nail plates.

(a) (b)

Fig. 8: (a) Double-sided nail plate fully pressed (gap < 2.5 mm); (b) Double-sided nail plate with a gap on the glulam side (gap ≥ 2.5 mm).

3.6. Loading arrangement

The tests were done with a four-points bending arrangement (Fig. 9 and Fig. 10). The support length was 100 mm on each side (representing the actual support conditions of a floor element on a CLT wall) and the points of load application were located at the third points of the beam span.

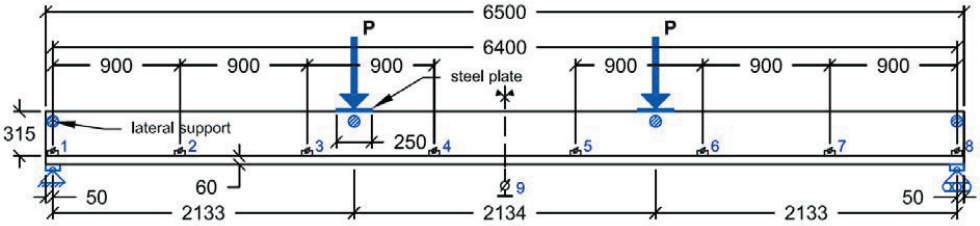

Fig. 9: Description of the loading arrangement (#1 to #8: longitudinal slip measurement; #9: mid-span deflection measurement).

Fig. 10: View of the bending test setup and loading frame.

The global deflection at mid-span was measured from the bottom of the CLT panel with a Tokyo Sokki DP-500E inductive sensor. The longitudinal slip at the CLT-glulam interface was measured with linear displacement transducers (HBM-W10-TK) at each second shear connector positions along the beam (Fig. 9) starting 50 mm from the beam end. The load was applied under load-control for the entire test with two VEB hydraulic jacks and measured by Instron UPM load cells and following the loading procedure given in EN 26891[21]. The tests were stopped at the collapse of the beam.

3.7. SLS and ULS design load

The design load for the floor element is based on uniformly distributed load cases with a permanent load G_k = 1.8 kN/m^2 and a service load Q_k = 2 kN/m^2. The characteristic load combination in the serviceability limit state, noted ω_{SLS}, and the fundamental load combination in the ultimate limit state, noted ω_{ULS}, are defined in expressions (8) and (9), respectively:

$$\omega_{SLS} = G_k + Q_k \tag{8}$$

$$\omega_{ULS} = \gamma_G G_k + \gamma_Q Q_k \tag{9}$$

where γ_G and γ_Q are 1.15 and 1.5, respectively.

The corresponding load levels considered in the 4-point bending test, noted F_{SLS} and F_{ULS}, are obtained from the equivalence of the bending moment under the uniformly distributed load and 4-point load cases. When the point loads are located symmetrically at the third points of the beam span, $F = 2 \cdot P = (3 \cdot \omega \cdot L)/4$, where F is the total load applied, P is one point load, ω is the distributed load case considered and L is the span of the beam. For the reduced cross-section of 580 mm width, the load levels considered for the SLS and ULS are therefore F_{SLS} = 10.6 kN and F_{ULS} = 14.1 kN, respectively. These values are used in section 4 for the evaluation of the shear connections performance in the beam designs tested from a practical point of view.

4. Experimental results and analysis

The load-slip curves of all tests specimens are presented in Fig. 11. The marker at the end of each curve represents the collapse of the specimen caused by the brittle bending failure in tension of one of the timber members, and, therefore, the end of the test. The dashed lines represent the calculated load-deflection curves at mid-span according to expression (10):

$$\delta = \frac{Fa\left(3L^2 - 4a^2\right)}{48EI} \tag{10}$$

where δ the mid-span deflection, F is the total applied load ($F = 2P$), L is the beam span, a is the distance from the support to the point of load application, and EI is the bending stiffness of the composite section for each test series estimated according to the γ-method (cf. section 3.3.1) using the measured global modulus of elasticity for each timber member (cf. section 3.2) and the slip modulus values from Table 1. In addition, the calculated lower and upper bound theoretical load-deflection curves for this cross-section are shown Fig. 11 and labelled NCA (no composite action) and FCA (full composite action). F_{SLS} and F_{ULS} indicate the load levels corresponding to the considered SLS and ULS design loads.

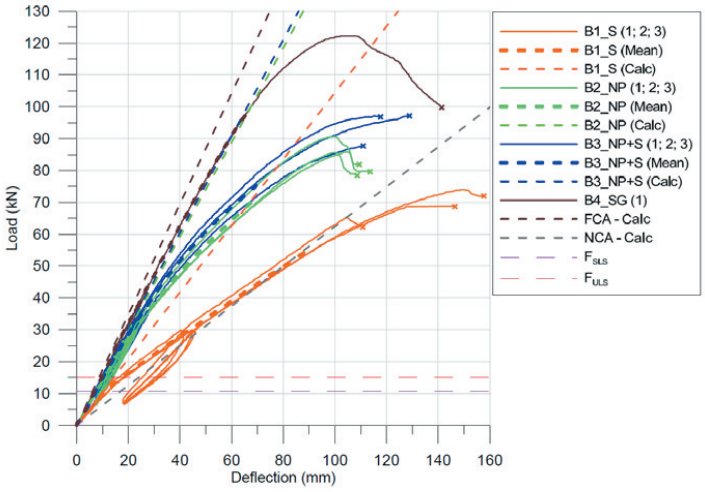

(a)

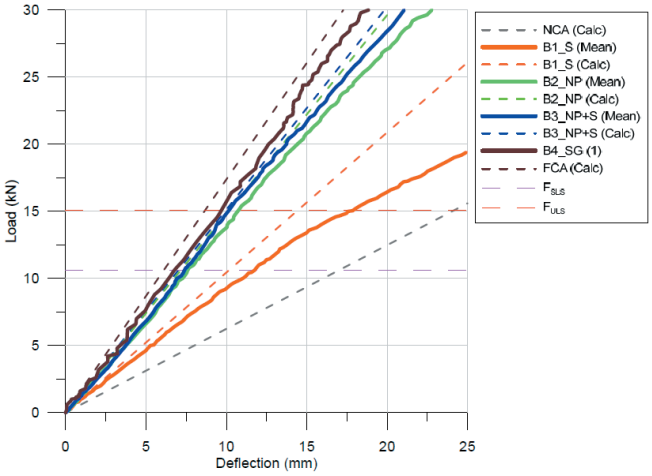

(b)

Fig. 11: Load-deflection curves for the four-point bending tests and calculated load-deflections curves with the γ-method: (a) full curves; (b) curves up to 25 mm deflection.

Table 3 presents for each test series the mean values for the measured density $\rho_{g,\omega}$ and $\rho_{c,\omega}$ of the glulam and CLT members, respectively, at the moisture content ω measured just after the bending tests, the mean maximum load F_{max}, the failure load F_f, the deflection at mid-span $\delta_{04\cdot Fmax}$ and δ_{SLS} at the loads $0.4\cdot F_{max}$ and F_{SLS}, respectively, as well as the ratios L/δ_{SLS} and $L/\delta_{0.4\cdot F,max}$ where L is the span of the beam element.

Table 3: Summary of the bending test results for the series with screws only (B1_S), nail plates only (B2_NP), nail plates and screws combined (B3_NP+S), and screw gluing (B4_SG) – Mean values.

Test series	No. of tests	Glulam		CLT		Maximum load	Failure load	Mid-span deflection at $0.4 \cdot F_{max}$	Span to deflection ratio at $0.4 \cdot F_{max}$	Mid-span deflection at F_{SLS}	Span to deflection ratio at F_{SLS}
		D	MC	D	MC						
		$\rho_{g,\omega}$ kg/m^3	ω_g (%)	$\rho_{c,\omega}$ kg/m^3	ω_c (%)	F_{max} (CoV) kN (%)	F_f (CoV) kN (%)	$\delta_{04 \cdot Fmax}$ (CoV) mm (%)	$L/\delta_{04 \cdot Fmax}$	δ_{SLS} (CoV) mm (%)	L/δ_{SLS}
B1_S	3	474	13.7	455	12.9	69.4 (6.2)	67.7 (7.4)	39.9 (12.8)	160	11.7 (7.4)	545
B2_NP	3	438	13.9	461	13.0	87.4 (3.4)	80.1 (2.0)	26.8 (0.7)	239	7.58 (3.5)	844
B3_NP+S	3	454	14.0	463	12.9	94.0 (5.9)	93.9 (5.8)	27.2 (2.2)	235	7.39 (4.0)	866
B4_SG	1	489	14.2	467	12.7	122	99.8	30.9	207	6.75	948

4.1. Failure observations

Test series with mechanical fasteners, B1_S, B2_NP and B3_NP+S, exhibited a bending failure in tension of the glulam beams with failure located in the finger joints (see Fig. 12). The CLT members remained undamaged. Compression failure could be observed on the upper side of the glulam member between the points of load application for all test series.

In series B1_S (Fig. 12a), at the collapse of the glulam beam the screws were suddenly withdrawn at some locations due to the brittle failure of the beam. Before the collapse, the withdrawal of the screws had already started, as indicated by the interlayer slip (Fig. 13), but the timber members remained tightly connected up to the point of failure. In series B2_NP (Fig. 12b), a separation between the CLT and glulam members started to occur before the ultimate collapse of the glulam beam. A gradual withdrawal of the double-sided nail plates was observed after the maximum load leading to a small strength reduction followed by the glulam beam failure. In series B3_NP+S (Fig. 12c), the inclined screws seem to prevent the separation before the failure of the glulam beam, providing a slightly higher maximum load for the composite beam. However, it is not clear whether the screw provided sufficient resistance to prevent the separation or if they provided an additional strength to the shear connection to reach the beam failure before any separation between the members could be observed.

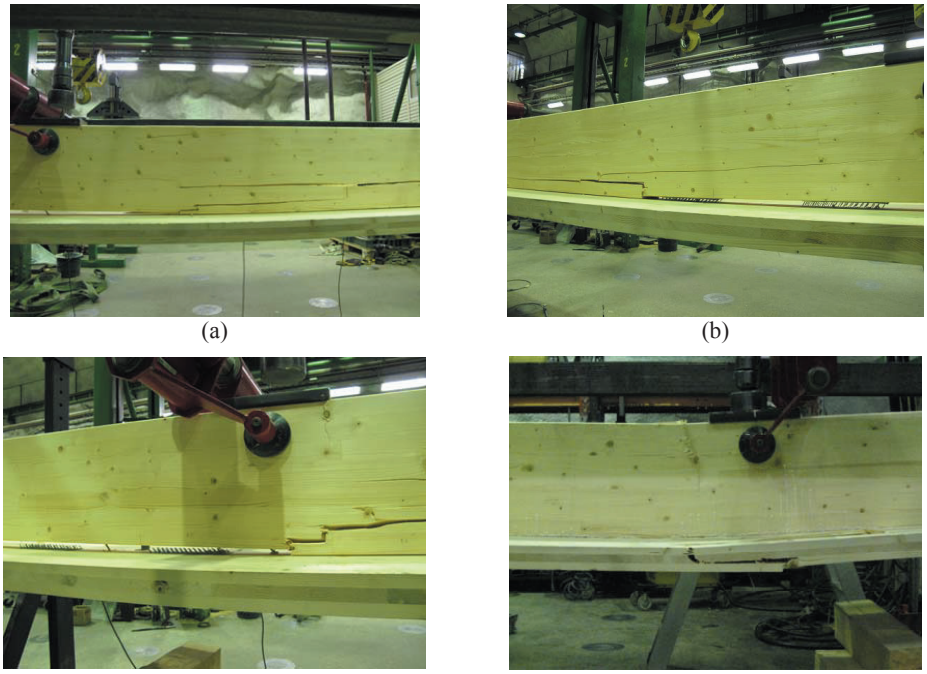

(a) (b) (c) (d)

Fig. 12: Failure observations (a) series B1_S, (b) Series B2_NP, (c) series B3_NP+S, (d) series B4_SG.

For the specimen B4_SG (Fig. 12d), a bending failure with a tension failure in the CLT panel and a very large compression failure at the top of the glulam beam were observed. The compression failure, located near the load application point, extended down to half the height of the glulam beam, and could be observed already before the collapse of the beam. The glue line at the glulam-CLT interface did not fail and no separation of the members was observed.

4.2. Bending stiffness and load-carrying capacity

The bending stiffness estimated from the deflection measured during the test is presented at different load levels in Table 4. The estimation of the bending stiffness $EI_{04.Fmax}$ between the loads of 10 % to 40 % of the observed maximum load F_{max} gives a relative mean of comparison between the test series. An absolute comparison of the performance of the beam designs with respect to the design load case in the serviceability limit state is obtained with the estimation of the bending stiffness $EI_{F.SLS}$ between the load levels $F_{SLS}/4$ and F_{SLS}, with F_{SLS} being a fixed value common for all series. The predicted bending stiffness by calculation based on the measured modulus of elasticity of the timber members and connectors shear test results is also presented in Table 4 for each test series. These calculated values are the ones used for the calculated load-deflection curves in Fig. 11.

The degree of composite action (DCA) is also presented in Table 4 for each test series as $\mathrm{DCA} = \frac{EI_{\mathrm{ef}} - EI_0}{EI_\infty - EI_0} \times 100$, where EI_{ef}, EI_0 and EI_∞ are the effective bending stiffness of the partially composite section, the bending stiffness of the non-composite section, and the bending stiffness of the fully composite section, respectively.

As expected, the bending stiffness observed in series B1_S is low due to low degree of composite action provided by the shear connection and spacing used. A clear bi-linear behaviour can be observed with a change in slope occurring close to the applied load of 13 kN (Fig. 11). At this load level, the slip measured toward the beam ends corresponds to the yield point of inclined screws in shear tension, which explains the change of slope of the load-deflection curve from this point. More details are given in section 4.3. The bending stiffness of the specimens of series B1_S after this point is similar to the one of a non-composite beam. In Table 4, the estimated bending stiffness $EI_{04\cdot\mathrm{Fmax}}$ is therefore very low compared to the calculated value $EI_{\mathrm{ef,sls,calc}}$, while a better agreement is obtained when comparing $EI_{\mathrm{F.SLS}}$ and $EI_{\mathrm{ef,sls,calc}}$ since $EI_{\mathrm{F.SLS}}$ is estimated earlier on the load-deflection curve.

Table 4: Bending stiffness and degree of composite action of the composite beam elements.

Test series	Bending stiffness between $0.1\cdot F_{max}$ and $0.4\cdot F_{max}$	Bending stiffness estimated between $F_{SLS}/4$ and F_{SLS}		Bending stiffness calculated based on measured MOE and connectors serviceability slip modulus	
	$EI_{04\cdot\mathrm{Fmax}}$ MN·m^2	$EI_{\mathrm{F.sls}}$ MN·m^2	DCA with $EI_{\mathrm{F.sls}}$ (%)	$EI_{\mathrm{ef,sls,calc}}$ MN·m^2	DCA with $EI_{\mathrm{ef,sls,calc}}$ (%)
*NCA (EI_0)				2.90	0
B1_S	3.00	4.13	23.7	4.86	37.7
B2_NP	5.99	6.57	70.9	6.89	77.0
B3_NP+S	6.35	6.96	78.3	7.04	79.9
B4_SG	7.40	7.63	91.3	8.08	100
**FCA (EI_∞)				8.08	100

*NCA = No composite action ($EI_{\mathrm{ef,sls,calc}} = EI_0$ is the sum of the bending stiffness of the glulam beam and the CLT panel)
**FCA = Full composite action ($EI_{\mathrm{ef,sls,calc}} = EI_\infty$ is calculated assuming that no slip can occur between the glulam and the CLT)

Series B2_NP and B3_NP+S showed a significantly higher strength and stiffness due to the high slip modulus of the double-sided nail plate shear connectors. The behaviour of the series with double-sided nail plates with and without screws is very similar, except near the failure load. The specimens with nail plates have the tendency to leave the linear regime after about 40-50 % of the estimated load. The addition of the inclined screws slightly increases the bending stiffness (+ 6% for B3 compared to B2) at both load levels considered in Table 4. In general, it can be noted that the values of $EI_{04.\mathrm{Fmax}}$ are

lower than the ones for $EI_{F.SLS}$ due to the non-linear behaviour of the double-sided nail plate shear connections, with a slightly less pronounced effect in series B3_NP+S.
The load-carrying capacity and the bending stiffness of the specimen B4_SG was the highest of all series. The pronounced compression failure at the top of the glulam beam gives a rather ductile behaviour before failure for a bending test, the width of the CLT flange allowing to resist high tensile forces at the bottom of the beam. The behaviour of the beam is also linear over a larger load range than in series B2_NP and B3_NP+S, as indicated by the load-deflection curves and the similar bending stiffness values observed at both load levels considered in Table 4. The agreement with the predicted value $EI_{ef.sls,calc}$ is nevertheless slightly worse than for series B2_NP and B3_NP+S due to the assumption of full composite action in the calculation while a screw-glued shear connection does exhibit a slight slip in reality.

4.3. Measured longitudinal slip between glulam and CLT

The measured longitudinal slip along the beam at the loads F_{SLS}, F_{ULS} and $F_{04.Fmax}$ is shown in Fig. 13 for each test specimen and compared to the yield slip of each fastener type estimated from shear tests [2]. The end slip values $s_{sls,2P,calc}$ and $s_{uls,2P,calc}$ calculated according to expressions (11) and (12) are presented with markers on the figure for the load F_{SLS} and F_{ULS}, respectively.

$$s_{sls,2P,calc} = \frac{\gamma_{1,s} E_1 A_1 a_{1,s} s_1}{k_{1,s} EI_{eff,sls,calc}} V_{SLS} \tag{11}$$

$$s_{uls,2P,calc} = \frac{\gamma_{1,u} E_1 A_1 a_{1,u} s_1}{k_{1,u} EI_{eff,uls,calc}} V_{ULS} \tag{12}$$

where the parameters are described in expressions (1) to (6) with the subscripts “s” and “u” denoting the SLS and ULS values, and V the shear force at the end of the beam. The slip modulus of the fasteners at the ULS is taken as $(2/3)\cdot k_s$.

In Fig. 13, the slip at $0.4\times F_{max}$ exceeds for all series the yield slip of the double-sided nail plates since the design of the beams is governed by the strength and stiffness of the shear connection and that the failure load largely exceeds the design load. The observations of the slip are, therefore, made at the design load levels F_{SLS} and F_{ULS}. It should be noted that the following observations are mainly practical observations in order to assess the relevance of the shear connections with double-sided nail plate fasteners for the design case considered. The conclusions may vary under other loading situations.

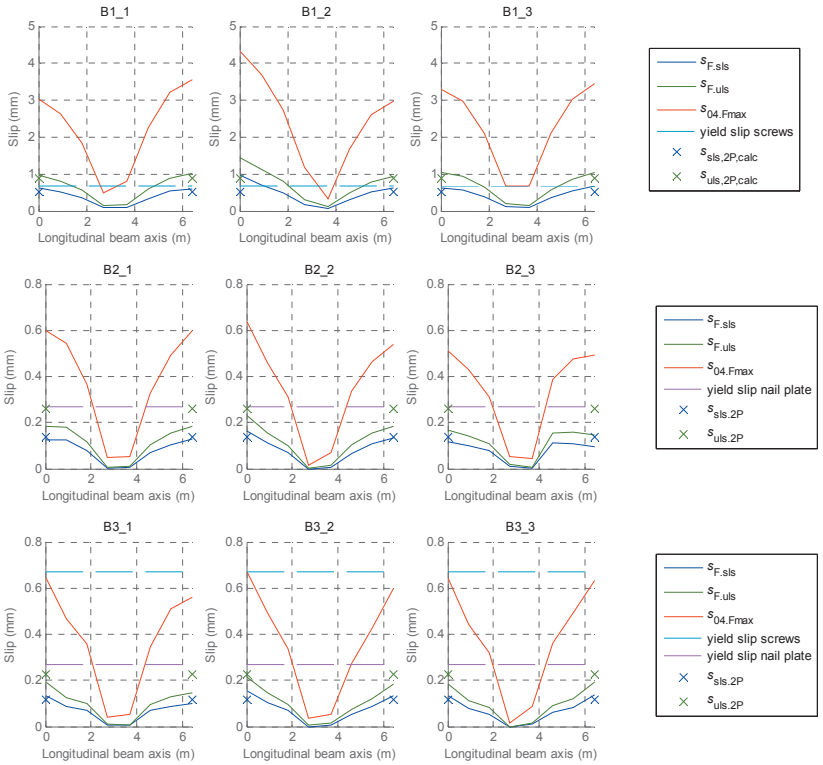

Fig. 13: Glulam-CLT slip along the beam length at loads F_{SLS}, F_{ULS}, $F_{04\text{-}Fmax}$, and yield slip values for the inclined screws and DSNP. The markers show the calculated slip values (γ-method) SLS and ULS design loads considering the 4-point loading case ($s_{sls,2P,calc}$ and $s_{uls,2P,calc}$).

In series B1, for which the shear connection is under-designed, the yield slip value of the screws is reached or slightly exceeded at the SLS load level. At the ULS load level, the yield slip value is exceeded for most of the screws between the point loads and the supports. Due to the spacing used, the shear connection is rather weak in this design both from a strength and stiffness point of view. It was noted in Fig. 11 and in Table 4 that the bending stiffness of the beam above the SLS load level was close to the one of a non-composite beam.

In series B2 and B3, the slip observed at the SLS and ULS load level remains below the yield slip of both the screws and double-sided nail plates, therefore showing that the shear connection design is satisfactory for these two series. It should be noted that this observation nevertheless depends on the chosen design loads. However, it can be seen in Fig. 13 that this conclusion could be made also with a slightly more demanding design load as the double-sided nail plate yield slip is far from being reached also at the ULS load level.

For the specimen B4_SG, the longitudinal slip was measured at both beam ends only. At the load F_{SLS}, the end slip measurements were 0.031 mm and 0.006 mm on each side, and at the load F_{ULS} the measurements were 0.045 mm and 0.016 mm, respectively, showing that almost full composite action was achieved. The larger value of 0.045 mm slip indicates a possible defect in the screw-glued connection on the side which was actually screw-glued the last during the assembly, and also explain part of the misfit observed in Table 4 between the measured and calculated bending stiffness considering full composite action. The screw-glued composite beam tested here therefore presented a very high degree of composite action but not full composite action.

5. Practical implications

5.1. Floor element geometry and failure mode

The geometry of the floor element as presented in Fig. 2 with the CLT panel located at the bottom of the composite beam is advantageous with respect to the types of failure that can occur in the composite floor. The large CLT bottom flange limits the tensile stresses in the glulam beam and provides the possibility for a more ductile failure with the development of a compression failure at the top of the beam prior to the tensile bending failure. A ductile failure can also be obtained from the choice and design of the shear connection.

5.2. The effect of screws combined with double-sided nail plates

The presence of the screws contributes to the increase in bending stiffness of the beam. The test specimen with only double-sided nail plates (series B2_NP) had a satisfactory behaviour. No major difference in behaviour was observed between series B2_NP and B3_NP+S, suggesting that the compressive force generated by the screw has nevertheless a limited effect on the overall joint behaviour, except as observed near failure. It was noted in [2] that the angle of inclination of the screw was not optimal for a combination with double-sided nail plates due to the different load-slip characteristics of the fasteners. The use of vertical screws to only secure the connection for handling purpose (floor element manufacturing and on-site assembly) and safety in case of major damage of the floor element could also be considered as an alternative. Note that a lower angle between the screw axis and the normal to the shear plane would reduce the contribution of the screw to the slip modulus compared to the present 45° angle.

5.3. Estimated floor performance

The design of this type of CLT-glulam floor is for the cross-section considered governed by the shear connection behaviour. Primarily, the stiffness of the shear connection governs the level of composite action achieved, which is decisive to reach the desired bending stiffness and fundamental frequency. When using DSNP, the second governing criteria is the strength of the shear connection, which should

be sufficient to ensure that the connectors are not subjected to excessive loadings in both the serviceability and ultimate limit state.

Estimations of the fundamental frequency of the finished floor structure for the present design case (G_k = 1.8 kN/m^2) and calculated according to the Eurocode 5 and Finnish National Annex are given in Table 5 for each test series. The corresponding maximum spans fulfilling the 9 Hz fundamental frequency are also given. The values $f_{1,F.sls}$ are calculated with expression (7) using the estimated bending stiffness values $EI_{F.sls}$, while the values $f_{1,ef,calc}$ are calculated using the calculated bending stiffness $EI_{ef,sls,calc}$ (cf. Table 4). Note that the low modulus of elasticity of the glulam beams is responsible for the relatively low fundamental frequency calculated compared to the values obtained in the design example [18] using the modulus of elasticity according to the timber strength class.

According to the estimations $f_{1,F.sls}$ based on the bending tests, only the series B3_NP+S and B4_SG satisfy the 9 Hz limit criteria. Considering the calculated values $f_{1,ef,calc}$, series B2_NP may also fulfil the vibration criteria for a 6.4 m floor span. I should be noted that these estimations of the fundamental frequency depend to a large extent on the precision of the input variables, such as the slip modulus and the modulus of elasticity of the timber members, and on the accuracy of the calculation method used for this evaluation, here, the γ-method.

Table 5: Calculated fundamental frequency of the finished floor (6.4 m span) based on the bending stiffness estimated from tests and predicted by calculation, $f_{1,F.sls}$ and $f_{1,ef,calc}$ respectively, and maximum span fulfilling the 9 Hz limit criteria.

Test series	$f_{1,F.sls}$ (using $EI_{F.sls}$)	Max. span for $f_{1,F.sls} \geq 9$ Hz	$f_{1,ef,calc}$ (using $EI_{ef,sls,calc}$)	Max. span for $f_{1,ef,calc} \geq 9$ Hz
	(Hz)	(m)	(Hz)	(m)
NCA (EI_0)			5.87	5.17
B1_S	7.00	5.64	7.60	5.88
B2_NP	8.83	6.34	9.05	6.42
B3_NP+S	9.09	6.43	9.14	6.45
B4_SG	9.52	6.58	9.80	6.68
FCA (EI_∞)			9.80	6.68

5.4. Manufacturing possibilities

The relevance (viability, cost efficiency) of a glulam-CLT floor solution with double-sided nail plates depends on the manufacturing possibilities. The assembly of the beam elements performed in the laboratory shows that it is technically feasible to connect long timber members together by pressing simultaneously a certain amount of double-sided nail plates. With equipment specifically designed for

the assembly of such elements, it should be possible to create a cost efficient solution for glulam-CLT composite floors connected with double-sided nail plates, with possibly a high level of automation.

6. Conclusions

One of the aims of this study was to assess the technical feasibility of a composite glulam-CLT beams connected with double-sided punched metal plate fasteners. It was considered necessary to compare the behaviour of the beams with double-sided nail plates used as the only shear connector type and in combination with inclined screws in order to evaluate the possible effects with respect to separation of the timber members in the composite element.

The behaviour of double-sided nail plates used as shear connectors in a timber-timber composite beam in bending (series B2_NP) was evaluated and is satisfactory with the design tested. The failure of the composite glulam-CLT beams with double-sided nail plates only is triggered by the withdrawal of the fastener when their maximum capacity is reached. The combination of double-sided nail plates with screws (series B3_NP+S) indicates that the overall behaviour is improved to a certain extent by the addition of inclined screws. In the beams tested with combined fasteners, a small increase of the composite beam strength and bending stiffness could be observed with a slightly different behaviour near failure load, the screws seeming to prevent the withdrawal of the nail plates before the collapse of the beams, compared to the series with double-sided nail plates only.

Analytical results for the bending stiffness and the load-deflection curve using the γ-method agree reasonably well with the test results when considering practical design load levels for such type of composite floor structure. This experimental programs shows that the level of composite action achieved between the glulam beam and the CLT panel can be relatively high when using double-sided nail plate shear connectors (in combinations with screws or not), and that this type of fastener is suitable for relatively long composite timber floor elements.

The long-term behaviour and the capacity of the double-sided nail plates to resist separation forces (due to hanging loads on the floor for example) has not been evaluated in this study. The addition of screws to the shear connection made with double-sided nail plate is considered needed in order to provide additional safety to the connection with respect to possible separation, repeated and long-term loadings, until further experimental work can evaluate these particular issues.

Acknowledgements

The centre for Lean Wood Engineering, the Swedish governmental agency for innovation systems (VINNOVA), Stora Enso Timber, the County Administrative Board in Norrbotten under Grant number 303-2602-13 (174311); the Regional Council of Västerbotten under Grant number REGAC-

2013-000133 (00179026); and the European Union's Structural Funds - The Regional Fund under Grant number 2013-000828 (174106) are acknowledged for their financial support to this research. Ari Kevarinmäki is acknowledged for his comments and assistance for the testing carried out at VTT Expert Services laboratories in Finland.

References

[1] Zhou T, Guan Z. Numerical modelling for sensitivity analysis of wood joints made with double-sided punched metal plate fasteners. Advances in Structural Engineering. 2011;14(2):163-77.
[2] Jacquier N, Girhammar UA. Tests on glulam-CLT shear connections with double-sided punched metal plate fasteners and inclined screws. Construction and Building Materials. 2014;72:444-57.
[3] Jorissen A. The design of timber floors. World Conference on Timber Engineering (WCTE). Portland, Oregon, USA2006.
[4] Smith I. Vibrations of Timber Floors: Serviceability Aspects. In: Thelandersson S, Larsen HJ, editors. Timber Engineering: Wiley; 2003. p. 241-66.
[5] European Committe for Standardization (CEN). EN 1995-1-1:2004 (E). Eurocode 5 Design of timber structures: CEN; 2004.
[6] Finnish Ministry of the Environment. National Annex To Standard SFS-EN 1995-1-1 EUROCODE 5: Design of Timber Structures Part 1-1: Common rules and rules for buildings (Unofficial translation). 2007.
[7] Gagnon S, Pirvu C. CLT Handbook Cross-Laminated Timber - Canadian Edition. Québec: FP Innovations; 2011.
[8] Kolb J. Systems in Timber Engineering. 1 ed: Birkhäuser Architecture; 2008.
[9] Chen Y, Lam F. Bending Performance of Box-Based Cross-Laminated Timber Systems. Journal of Structural Engineering. 2013;139(12):04013006.
[10] Giongo I, Piazza M, Tomasi R. Out of plane refurbishment techniques of existing timber floors by means of timber to timber composite structures. WCTE 2012. Auckland2012.
[11] Bejtka I, Blass HJ. Joints With Inclined Screws. CIB W18. Japan2002.
[12] Kevarinmäki A. Joints with Inclined Screws. CIB W18. Japan2002.
[13] Tomasi R, Crosatti A, Piazza M. Theoretical and experimental analysis of timber-to-timber joints connected with inclined screws. Construction and Building Materials. 2010;24(9):1560-71.
[14] Österreichisches Institut für Bautechnik (OIB) MoE. European technical approval ETA-12/0063 - SFS self-tapping screws WT. 2012.
[15] European Committe for Standardization (CEN). SS-EN 1194:1999 - Glued laminated timber - Strength classes and determination of characteristic values. Swedish Institute for Standards (SIS); 1999.
[16] Deutsches Institut für Bautechnik (DIBt). European Technical Approval ETA-08/0271 - CLT - Cross Laminated Timber. In: European Organisation for Technical Approvals (EOTA), editor. ETA-08/02712011. p. 17.
[17] European Committe for Standardization (CEN). SS-EN 408:2010+A1:2012 Timber structures - Structural timber and glued laminated timber - Determination of some physical and mechanical properties. Swedish Institute for Standards (SIS); 2012.
[18] Jacquier N. Bending tests on glulam-CLT composite beams with double-sided punched metal plate fasteners and inclined screws. Luleå Univeristy of Technology2015.
[19] Möhler K. Uber das Tragverhalten von Biegeträgern und Druckstäben mit zusammengesetzten Querschnitten und nachgiebigen Verbindungsmitteln. Karlsruhe1956.
[20] RIL 205-1-2009 korjaukset 30.1.2012. 2012. (http://www.ril.fi/)
[21] European Committe for Standardization (CEN). EN 26891:1991 - Timber structures - Joints made with mechanical fasteners - General principles for the determination of strength and deformation characteristics. 1991.

Paper IV

Stiffness model for inclined screws in shear-tension in timber-to-timber joints – Part 1: Derivation of the model

by Ulf-Arne Girhammar and Nicolas Jacquier

Draft to be Submitted

Stiffness model for inclined screws in shear-tension in timber-to-timber joints – Part 1: Derivation of the model

Ulf Arne Girhammar and Nicolas Jacquier

Division of Structural and Construction Engineering – Timber Structures, Luleå University of Technology, SE-971 87 Luleå, Sweden

Abstract

A stiffness model for inclined screws in timber joints, or as shear connectors in composite timber-timber members, is presented. Elastic conditions applicable to the initial or linearized part of the load-deformation response in the serviceability limit state are assumed. The model for the stiffness or slip modulus is general in nature; it includes both the dowel action and withdrawal action of the screw, the friction between the members and it takes into account possible dissimilar properties and geometries of the different parts of the joint configuration. The model is simplified in that the screw is assumed rigid and the withdrawal stresses along the length of the screw are assumed evenly distributed. The proposed model is illustrated showing the total stiffness versus the inclination, as well as the relative contributing effect from the shearing and withdrawal stiffnesses, respectively, the influence of the friction coefficient and the effect of the ratio between the axial and embedment stiffnesses. Also, the effect of dissimilar properties is illustrated. Comparisons with other stiffness models are also discussed.

Keywords: Timber-to-timber connections, stiffness, slip modulus, dowel action, withdrawal action.

1 Introduction

While the load-carrying capacity of laterally loaded screws is mostly governed by the embedment behaviour of the timber and by the rope effect for large deformations, joints with inclined screw have a more complex behaviour due to the combined lateral and withdrawal action on the screw already at small displacements. The load-deformation behaviour of screws under these two types of actions is different. Laterally loaded screws have a ductile behaviour at larger deformations and low stiffness compared to axially loaded screws.

The design of inclined screw joints is addressed to some extent in the Eurocode 5 [1] for screws subjected to combined lateral and axial loading. Concerning the load deformation behaviour, no specific recommendation is given for inclined screw joints and the general rules for dowel type fasteners apply, without considering the effect of the screw inclination.

The load-carrying capacity of inclined screws has been addressed by Bejkta and Blass [2], who extended the Johansen yield model [3] for dowel type fasteners considering in addition the axial contribution of the inclined screw to the load-carrying capacity. This model is more detailed than the recommendations given in the Eurocode 5.

The evaluation of the slip modulus of screws should generally include both the dowel and withdrawal actions. The influence of those actions will depend on the inclination of the screws. The stiffness of inclined screws has been addressed by several authors [4], [5], [6], [7], but contributions on this subject are rare.

Blass et al. [5] presented an analytical expression for the slip modulus for inclined screws based on their withdrawal stiffness and where the dowel action was neglected, since its effect is limited for inclined screws with marked inclination. Tomasi et al. [6] have proposed an expression for the slip modulus of inclined screw joints that considers both the contribution from the embedment of the screw in a simplified way with respect to the dowel action and the contribution from the withdrawal of the screw. It is observed that the Blass et al. [5] model gives decreasing slip modulus for increasing inclination angles, while the Tomasi et al. [6] model gives the opposite result. Blass et al. seem to have mixed up the terms in the expression for the single axial deformation as a function of the slip of the joint. Also, both Blass et al. and Tomasi et al. are using a not fully correct or general relationship between the total axial displacements of the screw as a function of the total slip of the joint when the two parts of the connection have different properties and geometries. Their relationship is only valid when the two parts have similar conditions.

Symons et al. [7] developed a stiffness model for timber-concrete inclined screw joints based on the beam on elastic foundation theory. In this model, both the screw and the timber are assumed to be linear elastic bodies. The model separates the embedment stiffness perpendicular and parallel to the grain, respectively. The withdrawal of the screw is not explicitly modelled by using stiffness values for the withdrawal of or shearing along the screw within the timber, but implicitly a corresponding effect will occur through the foundation stiffness values parallel and perpendicular to the grain. This seems questionable, since these values are based on compression tests. Friction between the two components can also be accounted for in their model. The screw was considered fixed in the concrete. To solve the equations they used some simplifying assumptions. The comparison with experimental results indicates that the model overestimates the stiffness of the joint by about 20 % (and that even without including the effect of friction in their evaluation). The authors consider that this result is due to the approximation in the assumption that the screw is fixed in the concrete.

In this paper, a detailed calculation model for the slip modulus of timber-to-timber joints with inclined screws in shear-tension is proposed considering both the dowel and withdrawal actions of the screw and the friction in the shear plane. The model presented is consistent and general for screws and timber members of different material properties and geometries. Comparisons between the present model and the models of Tomasi et al. [6] and Symons et al [7] are discussed.

2 Stiffness model for inclined partially threaded rigid screws

2.1 Derivation of the model

Consider the free-body diagram of an inclined screw in a timber-to-timber joint (Fig. 1). The joint is assumed to be in the serviceability limit state under approximate linear elastic conditions (using a secant slip modulus). The screw is assumed rigid both in bending and tension. This implies that the model is more applicable to joints with screws of shorter lengths and larger diameters. The equilibrium of the system refers to the undeformed state and the

expressions for the deformations are assumed to be of the first order. The timber components can be of dissimilar properties, denoted i = 1 and 2, respectively. The force in the screw is divided into a parallel or axial (ax) force and a perpendicular or lateral (lat) shear force. The initial angle between the screw axis and the normal to the slip plane is α.

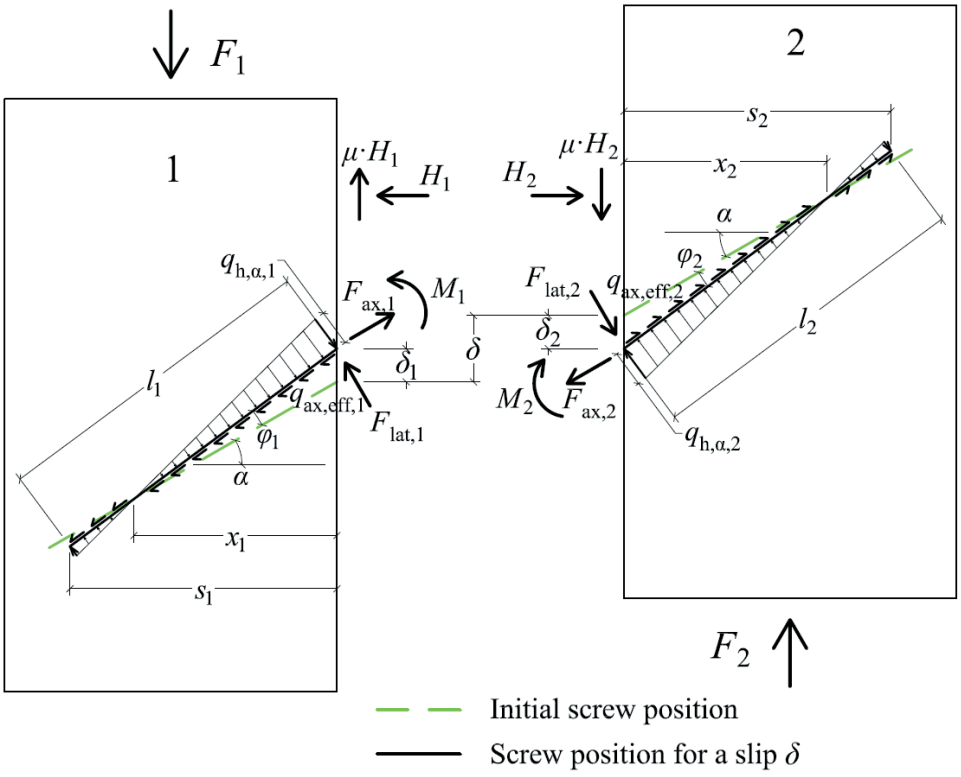

Fig. 1: Forces and moments acting in the screw in each timber member and forces acting on the slip plane of the joint.

Moment equilibrium of e.g. screw part no. 1 at the intersection (Fig. 1) gives

$$M_1 + q_{h,\alpha,1}\frac{1}{2}\frac{x_1}{\cos\alpha}\cdot\frac{1}{3}\frac{x_1}{\cos\alpha} - \frac{1}{2}q_{h,\alpha,1}\frac{s_1-x_1}{x_1}\frac{s_1-x_1}{\cos\alpha}\left[\frac{2}{3}\frac{s_1-x_1}{\cos\alpha}+\frac{x_1}{\cos\alpha}\right]=0 \qquad (1)$$

where M_1 is the moment in the screw at the interlayer, $q_{h,\alpha,1}$ [N/m] is the embedment force depending on α, s_1 is the distance perpendicular to the slip plane to the screw tip, and x_1 is the perpendicular distance perpendicular from the slip plane to the rotational point of the screw. For reference, the relationship between the perpendicular distance and the corresponding length along the screw is simply

$$s_i = l_i \cos\alpha; \quad i = 1,\ 2 \qquad (2)$$

The two corresponding moments can then be written as

$$M_i = \pm\frac{1}{6} q_{\mathrm{h},\alpha,i} \frac{s_i^2}{\cos^2\alpha}\left(2\frac{s_i}{x_i} - 3\right); \quad i = 1(+) \text{ and } 2(-), \text{ respectively} \tag{3}$$

The embedment force per unit length can be written as

$$q_{\mathrm{h},\alpha,i} = k_{\mathrm{h},\alpha,i}\delta_{\mathrm{lat},i} = K_{\mathrm{h},\alpha,i} d\, \delta_{\mathrm{lat},i}; \quad i = 1,\ 2 \tag{4}$$

where $k_{\mathrm{h},\alpha,i}$ [N/m^2] is the embedment stiffness of the timber per unit length, $\delta_{\mathrm{lat},i}$ the displacement of the screw perpendicular to its axis, $K_{\mathrm{h},\alpha,i}$ [N/m^3] the corresponding embedment stiffness per unit area, and d the diameter (here no distinction is made of the type of diameter of the screw that should be used). The stiffness parameter $K_{\mathrm{h},\alpha,i}$ is thus assumed proportional to the diameter d, which is not self-evident. Experimental evaluation of the parameters $k_{\mathrm{h},\alpha,i}$ and $K_{\mathrm{h},\alpha,i}$ is discussed in section 3 and in the second companion paper [11].

The fact that $M_1 = M_2$ gives the following relationship for the distances to the rotational points

$$\left(2\frac{s_1}{x_1} - 3\right) + \beta_{\mathrm{h}}\beta_{s,l}^2 \frac{\delta_{\mathrm{lat},2}}{\delta_{\mathrm{lat},1}}\left(2\frac{s_2}{x_2} - 3\right) = 0 \tag{5}$$

where

$$\begin{aligned} \beta_{\mathrm{h}} &= \frac{K_{\mathrm{h},\alpha,2}}{K_{\mathrm{h},\alpha,1}} = \frac{k_{\mathrm{h},\alpha,2}}{k_{\mathrm{h},\alpha,1}} \\ \beta_{s,l} &= \frac{s_2}{s_1} = \frac{l_2}{l_1} \end{aligned} \tag{6}$$

The relationship between the embedment load per unit length is then given by $q_{\mathrm{h},\alpha,2}/q_{\mathrm{h},\alpha,1} = (k_{\mathrm{h},\alpha,2}/k_{\mathrm{h},\alpha,1})(\delta_{\mathrm{lat},2}/\delta_{\mathrm{lat},1}) = \beta_{\mathrm{h}}(\delta_{\mathrm{lat},2}/\delta_{\mathrm{lat},1})$. Force equilibrium perpendicular to the screw gives

$$F_{\mathrm{lat},i} = \frac{1}{2} q_{\mathrm{h},\alpha,i} \frac{x_i}{\cos\alpha}\left[1 - \left(\frac{s_i - x_i}{x_i}\right)^2\right] = \frac{1}{2} K_{\mathrm{h},\alpha,i} d \frac{s_i}{\cos\alpha}\left(2 - \frac{s_i}{x_i}\right)\delta_{\mathrm{lat},i}; \quad i = 1,\ 2 \tag{7}$$

The fact that $F_{\mathrm{lat},1} = F_{\mathrm{lat},2}$ gives

$$\frac{\delta_{\mathrm{lat},2}}{\delta_{\mathrm{lat},1}} = \frac{1}{\beta_{\mathrm{h}}\beta_{s,l}} \frac{x_2}{x_1} \frac{(2x_1 - s_1)}{(2x_2 - s_2)} = \frac{1}{\beta_{\mathrm{h}}\beta_{s,l}^2} \frac{x_2}{x_1} \frac{(2x_1/s_1 - 1)}{(2x_2/s_2 - 1)} \tag{8}$$

Force equilibrium parallel to the inextensional screw gives

$$F_{\mathrm{ax},i} = q_{\mathrm{ax,eff},i} l_{\mathrm{thr},i} = k_{\mathrm{ax,eff},i} l_{\mathrm{thr},i} \delta_{\mathrm{ax},i} = K_{\mathrm{ax,eff},i} d\, l_{\mathrm{thr},i} \delta_{\mathrm{ax},i}; \quad i = 1,\ 2 \tag{9}$$

where $q_{\mathrm{ax,eff},i}$ [N/m] is the effective distributed axial withdrawal force of the screw per unit length, $k_{\mathrm{ax,eff},i}$ [N/m^2] is the effective axial withdrawal stiffness of the screw, $\delta_{\mathrm{ax},i}$ the displacement of the screw parallel to its axis, $K_{\mathrm{ax,eff},i}$ [N/m^3] the corresponding effective axial withdrawal stiffness parameter of the screw per unit area (screw length or threaded length × screw diameter), $l_{\mathrm{thr},i}$ the threaded length of the i^{th} screw part and d the diameter (here no distinction is made of the type of diameter of the screw that should be used). The stiffness parameter $K_{\mathrm{ax,eff},i}$ is thus assumed proportional to the diameter d, which is not self-evident. Experimental evaluation of the parameter $k_{\mathrm{ax,eff},i}$ or $K_{\mathrm{ax,eff},i}$ is discussed in section 3 and in the second companion paper [11] together with the meaning of the notation 'effective'.

The fact that $F_{\mathrm{ax},1} = F_{\mathrm{ax},2}$ gives

$$\frac{\delta_{\mathrm{ax},2}}{\delta_{\mathrm{ax},1}} = \frac{K_{\mathrm{ax,eff},1}}{K_{\mathrm{ax,eff},2}} \frac{l_{\mathrm{thr},1}}{l_{\mathrm{thr},2}} = \frac{1}{\beta_{\mathrm{ax}} \beta_{l,\mathrm{thr}}} \tag{10}$$

where

$$\begin{aligned} \beta_{\mathrm{ax}} &= \frac{K_{\mathrm{ax,eff},2}}{K_{\mathrm{ax,eff},1}} \\ \beta_{l,\mathrm{thr}} &= \frac{l_{\mathrm{thr},2}}{l_{\mathrm{thr},1}} \end{aligned} \tag{11}$$

If the screw is fully threaded or the threaded part is proportional to the respective length of each screw, we have, $\beta_{l,\mathrm{thr}} = \beta_{s,l}$. Eq. (10) implies that the relationship between the axial displacements is fixed as soon as the materials and lengths are chosen. The tensile force in component No. 1 is equal to the tensile force in component No. 2 and the fastener with the lower withdrawal stiffness will be withdrawn into the other timber member.

In Fig. 2 the details of the displacement components in the timber members are shown. In the general case when the two components differ with respect to material properties and geometry, the axial displacements will move the fastener across the interface between the two components. It is assumed that the distances (x_i) to the rotational points are not changed during the deformation process.

The relationship between the lateral displacement and the slip in each component is, according to Fig. 2, given by

$$\delta_{\mathrm{lat},i} = \delta_i \cos\alpha\,; \quad i = 1,\ 2 \tag{12}$$

It could be mentioned that the screw goes through a circular movement ($\delta_{\mathrm{arc},i}$) in the deformation process rather than a straight path perpendicular to the screw axis at the end of the deformation ($\delta_{\mathrm{lat},i}$), the corresponding arc length is closer to the slip (δ_i) between the timber pieces than the cosine of that slip. Eq. (12) gives

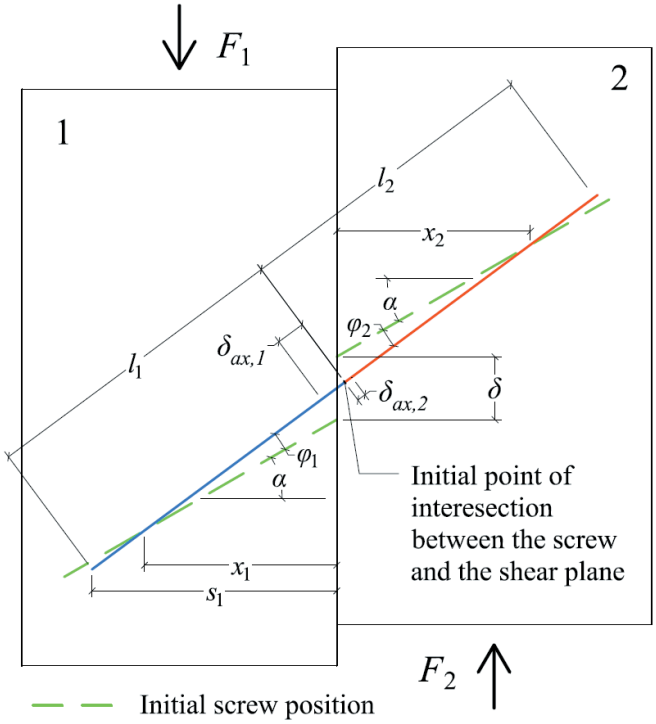

Fig. 2: Details of the displacement components in the timber members. In the general case when the two components differ with respect to material properties and geometry, the axial displacements may move the fastener across the interface between the two components.

$$\frac{\delta_{\text{lat},2}}{\delta_{\text{lat},1}} = \frac{\delta_2}{\delta_1} \tag{13}$$

The fact that $\varphi_1 = \varphi_2$ in Fig. 2 gives

$$\frac{\delta_2}{\delta_1} = \frac{x_2}{x_1} \tag{14}$$

Using Eqs (8), (13), (14) and (5), the distances to the rotational points are given by

$$\frac{x_1}{s_1} = \frac{(4+3\beta_{s,l})+\beta_{\text{h}}\beta_{s,l}^3}{6(1+\beta_{s,l})}; \qquad \frac{x_1}{l_1} = \frac{(4+3\beta_{s,l})+\beta_{\text{h}}\beta_{s,l}^3}{6(1+\beta_{s,l})}\cos\alpha \tag{15}$$

$$\frac{x_2}{s_1} = \frac{1+\beta_{\text{h}}\beta_{s,l}^2(3+4\beta_{s,l})}{6\beta_{\text{h}}\beta_{s,l}(1+\beta_{s,l})}; \qquad \frac{x_2}{l_1} = \frac{1+\beta_{\text{h}}\beta_{s,l}^2(3+4\beta_{s,l})}{6\beta_{\text{h}}\beta_{s,l}(1+\beta_{s,l})}\cos\alpha \tag{16}$$

It can be noted that for identical conditions in both timber members, $x_1 = 2s_1/3$ and $x_2 = 2s_2/3$. Eq. (15) and Eq. (16) are valid only if $x_1 \le l_1 \cos\alpha$ and $x_2 \le l_2 \cos\alpha$, respectively. If these conditions are not met, the stress distributions according to Fig. 1 are not applicable. Choosing to evaluate the condition $x_1 \le l_1 \cos\alpha$ in terms of the length, l_2, i.e. to find the limit of the ratio $\beta_{s,l} = l_2/l_1$ as a function of the ratio $\beta_h = K_{h,\alpha,2}/K_{h,\alpha,1}$, leads to a cubic equation with the following solution

$$\beta_{s,l,\text{limit}} = \sqrt[3]{\frac{1}{\beta_h} + \sqrt{\frac{1}{\beta_h^2}\left(1-\frac{1}{\beta_h}\right)}} + \sqrt[3]{\frac{1}{\beta_h} - \sqrt{\frac{1}{\beta_h^2}\left(1-\frac{1}{\beta_h}\right)}} \tag{17}$$

This relationship between the parameters $\beta_{s,l}$ and β_h can be interpreted as the degree of dissimilarity between the conditions of the two parts of the joint that is possible in order for the stiffness equation (24) below to be valid. Eq. (17) is illustrated in Fig. 3.

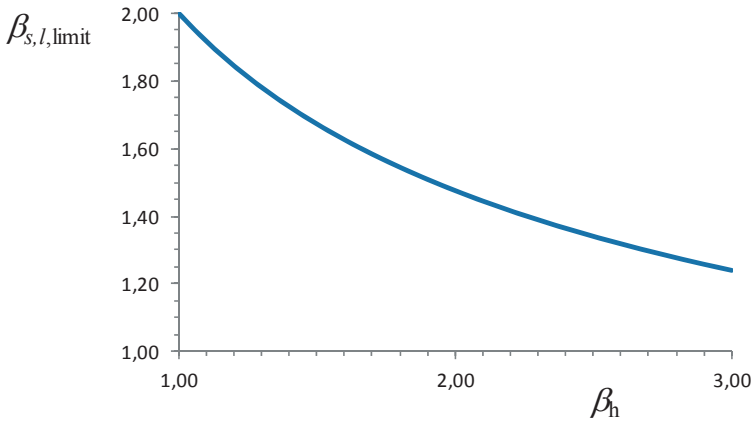

Fig. 3: The limit of length ratio, $\beta_{s,l,\text{limit}}$, versus the embedment ratio, β_h, in order for the joint stiffness according to Eq. (24) to be valid.

As mentioned above, when there are different properties and geometries in the screw parts and timber members, the axial displacements will cause the screw to move across the shear plane. This implies that the axial displacement of the screw cannot be expressed for each timber member separately, but the total axial displacement needs to be considered. A separate expression for each member is only possible to formulate if there are similar properties and geometries for the two parts of the connection. The relationship between the total axial displacement of the screw and the total slip of the joint (Fig. 2) is given by

$$\delta_{\text{ax},1} + \delta_{\text{ax},2} = (\delta_1 + \delta_2)\sin\alpha = (\delta_{\text{lat},1} + \delta_{\text{lat},2})\tan\alpha \tag{18}$$

Considering the second order effects, this relationship is discussed in Appendix A. Together with Eqs (10), (13) and (14), Eq. (18) gives

$$\delta_{\mathrm{ax},1} = \delta_{\mathrm{lat},1}\left(1+\frac{1}{\beta_{\mathrm{ax}}\beta_{l,\mathrm{thr}}}\right)^{-1}\left(1+\frac{x_2}{x_1}\right)\tan\alpha \tag{19}$$

Force equilibrium at the interface between the two components gives

$$F_i = F_{\mathrm{lat},i}\cos\alpha + F_{\mathrm{ax},i}\sin\alpha + \mu H_i\,; \quad i=1,\ 2 \tag{20}$$

$$H_i = F_{\mathrm{ax},i}\cos\alpha - F_{\mathrm{lat},i}\sin\alpha\,; \quad i=1,\ 2 \tag{21}$$

which combined gives

$$F_i = F_{\mathrm{lat},i}(\cos\alpha - \mu\sin\alpha) + F_{\mathrm{ax},i}(\sin\alpha + \mu\cos\alpha)\,; \quad i=1,\ 2 \tag{22}$$

Using the expressions above, it can be verified that, $F_1 = F_2 = F$.

The stiffness of the timber-to-timber joint can be expressed as

$$k = \frac{F}{\delta} = \frac{F_1}{(\delta_1+\delta_2)} = \frac{F_1}{\delta_1(1+\delta_2/\delta_1)} = \frac{F_1}{\delta_1(1+x_2/x_1)} = \frac{k_1}{(1+x_2/x_1)} \tag{23}$$

Introducing Eqs (22), (7), (9), (19) and (12) into Eq. (23) and using Eq. (2), we finally arrive at

$$k = d\,l_1\cos\alpha\left\{\frac{1}{2}\left(\cos\alpha-\mu\sin\alpha\right)K_{\mathrm{h},\alpha,1}\frac{2-s_1/x_1}{1+x_2/x_1} + \sin\alpha\left(\tan\alpha+\mu\right)K_{\mathrm{ax,eff},1}\frac{l_{\mathrm{thr},1}/l_1}{1+1/\beta_{\mathrm{ax}}\beta_{l,\mathrm{thr}}}\right\} \tag{24}$$

The first part of the equation represents the shearing and the second part the withdrawal of the screw. For identical conditions for the two parts of the joint, the stiffness is reduced to

$$k_{\mathrm{ident}} = \frac{1}{2}d\,l_1\cos\alpha\left\{\frac{1}{4}\left(\cos\alpha-\mu\sin\alpha\right)K_{\mathrm{h},\alpha,1} + \sin\alpha\left(\tan\alpha+\mu\right)K_{\mathrm{ax,eff},1}\frac{l_{\mathrm{thr},1}}{l_1}\right\} \tag{25}$$

In non-dimensional form, these equations can be expressed as

$$\overline{k} = \cos\alpha\left\{\frac{1}{2}\left(\cos\alpha-\mu\sin\alpha\right)\frac{2-s_1/x_1}{1+x_2/x_1} + \sin\alpha\left(\tan\alpha+\mu\right)\psi_K\frac{l_{\mathrm{thr},1}/l_1}{1+1/\beta_{\mathrm{ax}}\beta_{l,\mathrm{thr}}}\right\} \tag{26}$$

$$\overline{k}_{\mathrm{ident}} = \frac{1}{2}\cos\alpha\left\{\frac{1}{4}\left(\cos\alpha-\mu\sin\alpha\right) + \sin\alpha\left(\tan\alpha+\mu\right)\psi_K\frac{l_{\mathrm{thr},1}}{l_1}\right\} \tag{27}$$

where

$$\overline{k} = \frac{k}{K_{\mathrm{h},\alpha,1}d\,l_1}; \quad \overline{k}_{\mathrm{ident}} = \frac{k_{\mathrm{ident}}}{K_{\mathrm{h},\alpha,1}d\,l_1} \tag{28}$$

$$\psi_K = \frac{K_{\mathrm{ax,eff},1}}{K_{\mathrm{h},\alpha,1}} \tag{29}$$

The slip modulus according to Eq. (27) is illustrated in Fig. 4 (blue curve) for an ordinary joint with, $\psi_K = 1$, $l_{\mathrm{thr},1}/l_1 = 1$ and $\mu = 0.5$ (cf. section 3 and the second companion paper [11]). The shearing (red curve) and withdrawal (green curve) parts are also illustrated in the figure. As expected, it is noted that the contribution from the withdrawal action is the dominant one and that the shearing action is only contributing at lower angles. For higher angles, the shearing effect even has a negative contribution. However, the theoretical results at larger angles are not practically realistic for both the shearing and withdrawal effects. Eurocode 5 requires a maximum inclination of $\alpha \le 60°$. This requirement is probably introduced in order to avoid parallel to grain cracks, moisture induced cracks and shear stresses induced when inserting the screw itself according to Ellingsbo and Malo [8].

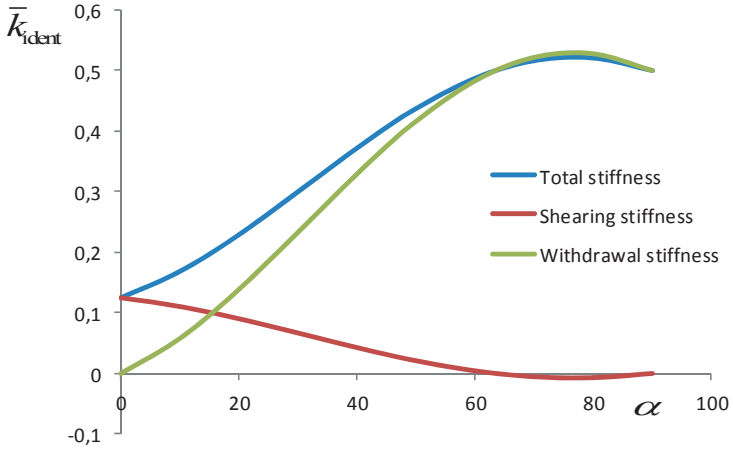

Fig. 4: The total joint stiffness $\overline{k}_{\mathrm{ident}}$ versus the inclination angle α for the case where the length of the screw is kept constant (for parameters $\psi_K = 1$, $l_{\mathrm{thr},1}/l_1 = 1$ and $\mu = 0.5$). The corresponding shearing and withdrawal parts are also shown.

Corresponding curves for the total stiffness is shown in Fig. 5, where the ratio between the withdrawal and shearing stiffnesses (Eq. (29) is varied. Theoretically, the optimum angle for maximum slip modulus of the joint is given by

$$\alpha = 90° - \frac{1}{2}\arctan\mu \tag{30}$$

Depending on the friction coefficient, $0 \le \mu \le 1$, this inclination varies between $90° - 67.5°$, which is beyond the practical range for inclined screws.

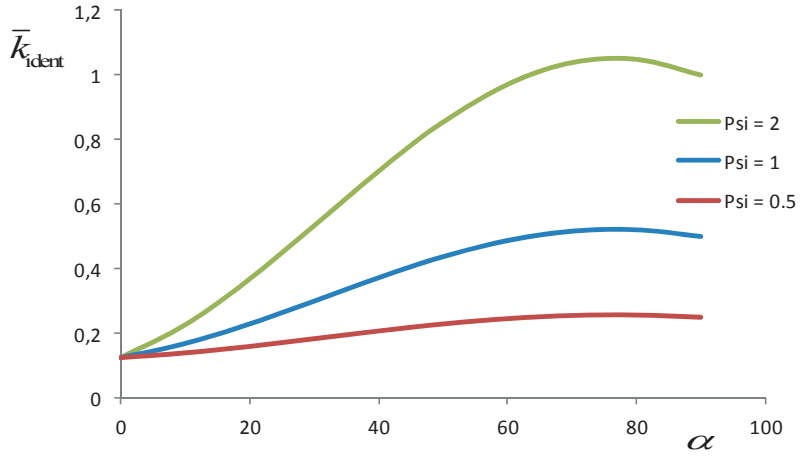

Fig. 5: The total joint stiffness $\overline{k}_{\text{ident}}$ versus the inclination angle α and the ratio between the axial stiffness and the embedment stiffness ψ_K (for parameters $l_{\text{thr},1}/l_1 = 1$ and $\mu = 0.5$).

Corresponding curves for the total stiffness, where the friction coefficient is varied, are shown in Fig. 6.

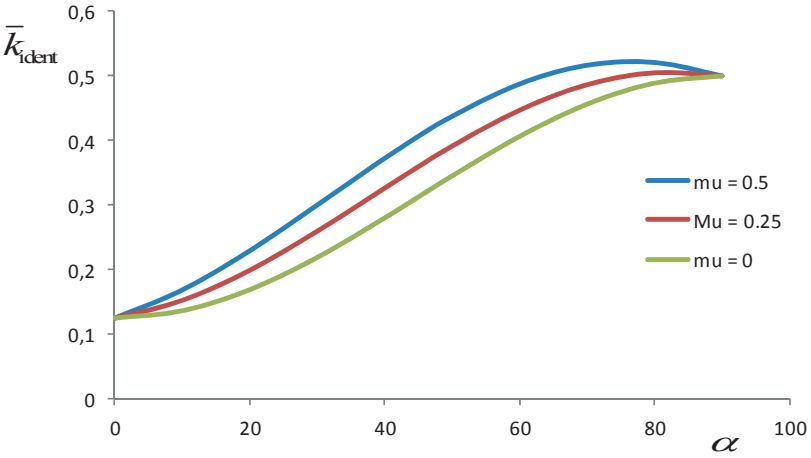

Fig. 6: The total joint stiffness $\overline{k}_{\text{ident}}$ versus the inclination angle α and the friction coefficient μ (for parameter $\psi_K = 1$ and $l_{\text{thr},1}/l_1 = 1$).

Eqs. (24) and (25) show the dependence of the inclination (α) on the stiffness value if the length of the screw (l) is kept constant. It means that the perpendicular depth of the screwing (s) is decreasing proportionally as the inclination increases. The following equation shows the corresponding dependence if the perpendicular depth of the screwing (s) is kept constant

in the variation of α, which means that the length of the screw needs to increase proportionally as the inclination increases:

$$k = d\, s_1 \left\{ \frac{1}{2} \left(\cos\alpha - \mu \sin\alpha \right) K_{\mathrm{h},\alpha,1} \frac{2 - s_1/x_1}{1 + x_2/x_1} + \sin\alpha \left(\tan\alpha + \mu \right) K_{\mathrm{ax,eff},1} \frac{l_{\mathrm{thr},1}/l_1}{1 + 1/\beta_{\mathrm{ax}}\beta_{l,\mathrm{thr}}} \right\} \tag{31}$$

and for identical conditions,

$$k_{\mathrm{ident}} = \frac{1}{2} d\, s_1 \left\{ \frac{1}{4} \left(\cos\alpha - \mu \sin\alpha \right) K_{\mathrm{h},\alpha,1} + \sin\alpha \left(\tan\alpha + \mu \right) K_{\mathrm{ax,eff},1} \frac{l_{\mathrm{thr},1}}{l_1} \right\} \tag{32}$$

In non-dimensional form, we have

$$\bar{k} = \left\{ \frac{1}{2} \left(\cos\alpha - \mu \sin\alpha \right) \frac{2 - s_1/x_1}{1 + x_2/x_1} + \sin\alpha \left(\tan\alpha + \mu \right) \psi_K \frac{l_{\mathrm{thr},1}/l_1}{1 + 1/\beta_{\mathrm{ax}}\beta_{l,\mathrm{thr}}} \right\} \tag{33}$$

$$\bar{k}_{\mathrm{ident}} = \frac{1}{2} \left\{ \frac{1}{4} \left(\cos\alpha - \mu \sin\alpha \right) + \sin\alpha \left(\tan\alpha + \mu \right) \psi_K \frac{l_{\mathrm{thr},1}}{l_1} \right\} \tag{34}$$

where

$$\bar{k} = \frac{k}{K_{\mathrm{h},\alpha,1} d\, s_1}; \quad \bar{k}_{\mathrm{ident}} = \frac{k_{\mathrm{ident}}}{K_{\mathrm{h},\alpha,1} d\, s_1} \tag{35}$$

Eq. (34) is illustrated in Fig. 7 using the same parameters as in Fig. 4.

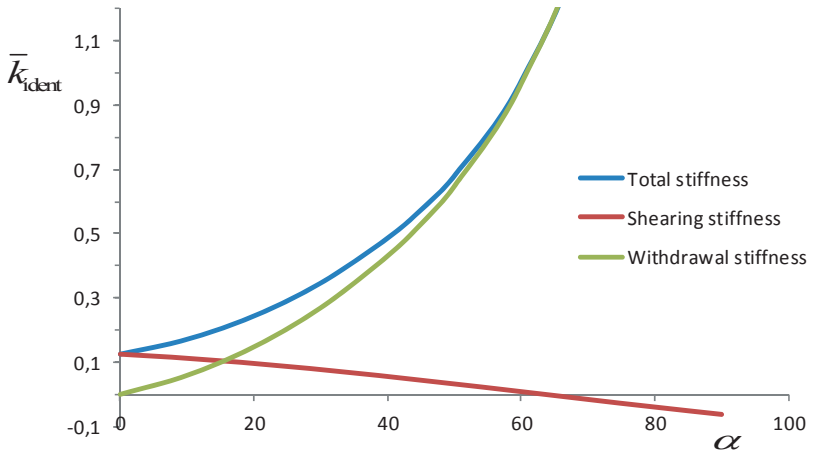

Fig. 7: Total joint stiffness $\bar{k}_{\mathrm{ident}}$ versus inclination angle α, when the perpendicular embedment depth *s* is kept constant (for parameters $\psi_K = 1$, $l_{\mathrm{thr},1}/l_1 = 1$ and $\mu = 0.5$). The corresponding shearing and withdrawal parts are also shown.

This equation is monotonically increasing indefinitely for increasing inclinations. Again, for larger inclinations, the results are not practically interesting. It is obvious that it is not possible to approach an inclination of $\alpha = 90°$ and still keep a constant perpendicular depth of the screwing (s) or, theoretically, it takes an infinitely long screw to approach that angle.

2.1 Limit of no hinge formed in the screw

The present model is applicable in the serviceability limit state or as long as secant values for the different stiffnesses can be used. It is also limited up to the point when a hinge (h) is formed in the screw.

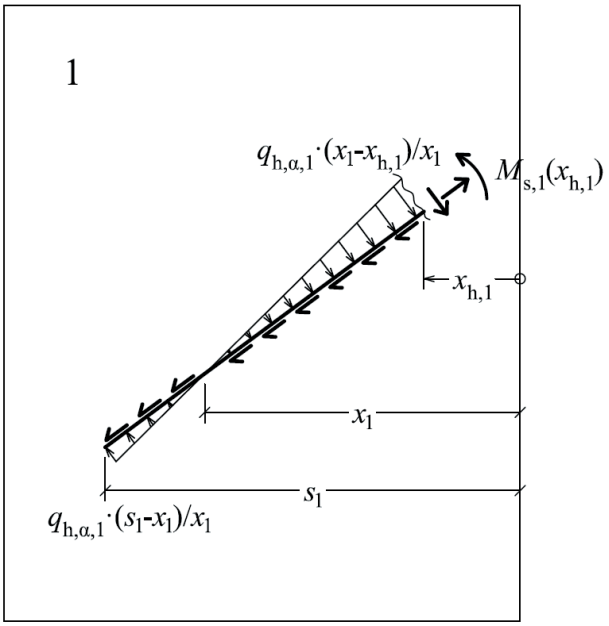

Fig. 8: Evaluation of the moment in the screw as a function of the perpendicular depth, $x_{h,1}$. The corresponding value $x_{l,1}$ along the axis of the screw is $x_{l,1} = x_{h,1}/\cos\alpha$.

The moment in the screw can according to Fig. 8 be written as

$$M_{s,1} = \frac{1}{6} q_{h,\alpha,1}[2\frac{(s_1 - x_1)^3}{x_1 \cos^2\alpha} + 3\frac{(s_1 - x_1)^2}{x_1 \cos\alpha}\frac{x_1 - x_{h,1}}{\cos\alpha} - \frac{(x_1 - x_{h,1})^3}{x_1 \cos^2\alpha}] \tag{36}$$

This equation holds true for variations of the rotation point between $s_1 \le x_1 < x_{h,1,max}$ or, in other words, variations of β_h and $\beta_{s,l}$ values that satisfy $\beta_{s,l,limit}$ according to Eqs (15) – (17). The maximum moment is attained at $x_{h,1,max} = s_1(2x_1/s_1 - 1)$ and using Eqs (2) and (4), the maximum moment is given by

$$M_{\mathrm{s},1,\max} = \frac{2}{3} q_{\mathrm{h},\alpha,1} l_1^2 \frac{s_1}{x_1}(1-\frac{x_1}{s_1})^3 = \frac{2}{3} K_{\mathrm{h},\alpha,1} d\, l_1^2 \frac{s_1}{x_1}(1-\frac{x_1}{s_1})^3 \delta_{\mathrm{lat},1} = \frac{2}{3} K_{\mathrm{h},\alpha,1} d \frac{l_1^3}{x_{l,1}}(1-\frac{x_{l,1}}{l_1})^3 \delta_{\mathrm{lat},1} \quad (37)$$

Using Eqs (12) - (14), the lateral displacement in terms of the joint slip can be written as

$$\delta_{\mathrm{lat},1} = \frac{\cos\alpha}{1+x_2/x_1}\delta \quad (38)$$

and then

$$M_{\mathrm{s},1,\max} = \frac{2}{3}\frac{K_{\mathrm{h},\alpha,1} d\, l_1^2 \cos\alpha}{1+x_2/x_1}\frac{s_1}{x_1}(1-\frac{x_1}{s_1})^3 \delta = m_{\mathrm{s},1,\max}\delta \quad (39)$$

where $m_{\mathrm{s},1,\max}$ is a convenience factor (bending moment stiffness [Nm/m]). For identical conditions, we get

$$M_{\mathrm{s},1,\max,\mathrm{ident}} = \frac{1}{54} K_{\mathrm{h},\alpha,1} d\, l_1^2 \cos\alpha \cdot \delta = m_{\mathrm{s},1,\max,\mathrm{ident}}\delta \quad (40)$$

The axial force is given by Eq. (9) and the axial deformation by Eq. (19) and Eq. (38), so then

$$\begin{aligned} F_{\mathrm{ax},1} &= \frac{K_{\mathrm{ax,eff},1} d\, l_{\mathrm{thr},1} \sin\alpha}{1+1/\beta_{\mathrm{ax}}\beta_{l,\mathrm{thr}}}\delta = f_{\mathrm{ax},1}\,\delta \\ F_{\mathrm{ax},1,\mathrm{ident}} &= \frac{1}{2} K_{\mathrm{ax,eff},1} d\, l_{\mathrm{thr},1} \sin\alpha \cdot \delta = f_{\mathrm{ax},1,\mathrm{ident}}\delta \end{aligned} \quad (41)$$

where $f_{\mathrm{ax},1}$ is a convenience factor (axial force stiffness [N/m]). Assuming a linear elastic interaction relationship between the moment and the axial tension force, the slip of the joint when yielding or plastic hinge is obtained in the screw is given by

$$\delta_{\mathrm{y}} = (\frac{m_{\mathrm{s},1,\max}}{M_{\mathrm{y}}} + \frac{f_{\mathrm{ax},1}}{F_{\mathrm{y}}})^{-1} \quad (42)$$

where $M_{\mathrm{y}}, F_{\mathrm{y}}$ are the yielding or plastic capacity of moment and axial tension force of the screw, respectively. For identical conditions, $M_{\mathrm{y}} = 24000$ Nmm, $F_{\mathrm{y}} = 29000$ N, $l_{\mathrm{thr},1} = l_1 = 100$ mm, $\psi_K = 2$, $K_{\mathrm{h},\alpha,1} d\, l_1 = 11.9$ kN/mm and otherwise using the same parameters as in earlier illustrations, the slip varies between $1.1 < \delta_{\mathrm{y}} < 2.9$ mm when the inclination varies between $0 < \alpha < 67.5°$, if only the bending capacity is taking into account, and correspondingly between $1.1 < \delta_{\mathrm{y}} < 1.4$ mm, if both the bending and tension capacity is accounted for. Further illustrations of the distribution of the moment and the hinge forming along the screw are given in the second companion paper [11].

3 Comparisons with other stiffness models

3.1 Tomasi et al. model (2010)

Tomasi et al. [6] presented a model that is semi-empirical with respect to the shearing part of the joint stiffness for inclined screws. They did not derive any expression for the dowel action, but only for the withdrawal effect, which is the same in both models. Their model does not explicitly demonstrate the consistency between the modelling of the shearing and withdrawal parts and the equilibrium of the system. They are showing a deformed screw with plastic hinges, but assume linear elastic conditions in the serviceability limit state. They just used the experimentally based slip modulus according to Eurocode 5. This means that their expression for the joint stiffness is not capable of taking into account different properties and geometries, e.g. the penetration length of the screws with respect to the dowel action. In case of dissimilar timber properties for the two components, Eurocode 5 suggests that the slip modulus is evaluated as the geometric mean value of the two moduli.

The present model is general in nature; it models also the shearing effect and can take dissimilar properties and geometries into account. The influence of the shearing effect is negligible compared to the withdrawal effect in the total stiffness of the joint for larger inclinations, but for smaller inclinations the effect can be rather substantial.

For the embedment stiffness, the following parameters are introduced in the model

$$k_{\mathrm{h},\alpha,i} = K_{\mathrm{h},\alpha,i} d \; ; \quad i = 1,\ 2 \tag{43}$$

$$k_{\mathrm{ax,eff},i} = K_{\mathrm{ax,eff},i} d \; ; \quad i = 1,\ 2 \tag{44}$$

i.e. the stiffness parameters $K_{\mathrm{h},\alpha,i}, K_{\mathrm{ax,eff},i}$ are assumed proportional to the diameter *d*, which needs to be experimentally verified. In some studies concerning the parameter, $k_{\mathrm{h},\alpha,i}$, there was found no significant dependence upon the diameter (see for example Gelfi et al. [9], but this study is not clear). The subscript 'effective' refers to the fact that there is a difference between the conventionally evaluated withdrawal strength or stiffness values in pure withdrawal tests and those values obtained for simultaneous withdrawal and lateral loading; cf. Bejtka and Blass [2]. Here it also, for convenience, include possible influence of the inclination, α. However, the model works whether $K_{\mathrm{h},\alpha,i}, K_{\mathrm{ax,eff},i}$ or $k_{\mathrm{h},\alpha,i}, k_{\mathrm{ax,eff},i}$ is used and both types of values need to be experimentally determined. These things will be discussed somewhat in the second companion paper [11].

Comparing the present model with that of Tomasi et al. by assuming pure shear effect for $\alpha = 0$ and pure axial effect for $\alpha = 90°$ for a symmetrical joint, the following relationships are found according to Eq. (25), respectively,

$$K_{\mathrm{h},\alpha,1} d\, l_1 = 8 K_{\perp,\mathrm{Tom}} = 8 K_{\mathrm{ser,EC5}} = \frac{8 \rho_{\mathrm{m}}^{1.5} d_{\mathrm{h}}}{23} \; ; \; [\mathrm{N/mm}] \tag{45}$$

$$K_{\mathrm{ax,eff},1} d\, l_{\mathrm{thr},1} = 2 K_{/\!/,\mathrm{Tom}} = \frac{2}{1/K_{\mathrm{ax},1,\mathrm{ser,DIBt}} + 1/K_{\mathrm{ax},2,\mathrm{ser,DIBt}}} = K_{\mathrm{ax},1,\mathrm{ser,DIBt}} = 30 l_1 d_{\mathrm{ax}} \; ; \; [\mathrm{N/mm}] \tag{46}$$

where the notation EC5 = Eurocode 5 [1] and DIBt = Deutsches Institut für Bautechnik [10] has been used, and where the mean density of the timber ρ_{m} is given in [kg/m^3], the diameter

d in [mm] and the embedment length l_1 (or threaded length, $l_{\text{thr},1}$, in [mm]). Here it is distinguished between the diameter used for embedment stiffness (d_{h}) and for withdrawal stiffness (d_{ax}) in the prescribed expressions. The relationship between the withdrawal and embedment stiffnesses is then given by

$$\psi_K = \frac{K_{\text{ax,eff},1}}{K_{\text{h},\alpha,1}} = \frac{K_{\text{ax,eff},1} d\, l_{\text{thr},1}}{K_{\text{h},\alpha,1} d\, l_1} = \frac{K_{\text{ax,1,ser,DIB}}}{8K_{\text{ser,EC5}}} = 86.3 \frac{l_{\text{thr},1} d_{\text{ax}}}{\rho_{\text{m}}^{1.5} d_{\text{h}}};\ [\text{N/mm}] \tag{47}$$

For the test specimens used in the paper of Tomasi et al., this ratio varies approximately between $1 < \psi_K < 1.5$. The parameter values in the two models are generally speaking determined experimentally in different ways. These things will be addressed in the second companion paper [11] by discussing different test methods.

If the substitution according to Eqs (45) and (46) is made, the Tomasi et al. model and the present model coincide as they should. However, if dissimilar properties are used the two models deviate as illustrated below. We assume $\mu = 0.5$, $\beta_{s,l} = 1.4$ and $\beta_{\text{h}} = 2$, which gives $\beta_{s,l,\text{limit}} \le 1.48$. Equation (26) is used for the present model, but only the shearing part for illustration purposes, and for comparison reasons and as suggested by Eurocode 5, the corresponding geometric mean value of the embedment stiffness is used in the Tomasi et al. model, in this case non-dimensionally given by

$$\frac{K_{\perp,\text{Tom,mean}}}{\sqrt{K_{\perp,\text{Tom},1}}} = \frac{K_{\text{ser,EC5,mean}}}{\sqrt{K_{\text{ser,EC5},1}}} = \sqrt{\beta_{\text{h}}} \tag{48}$$

The two curves for respective shearing stiffness are shown in Fig. 9.

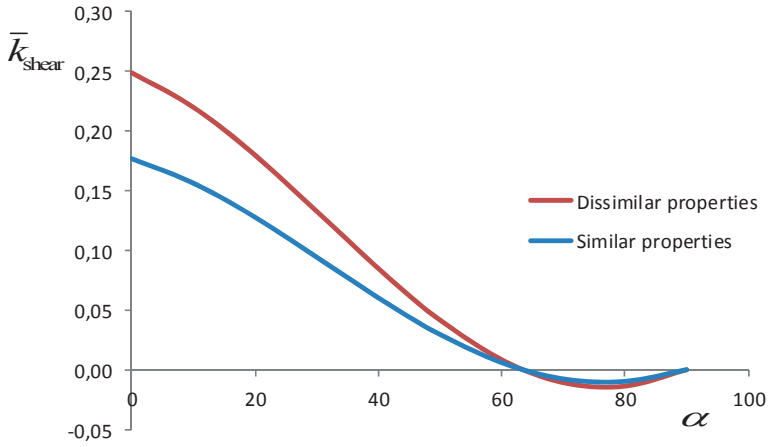

Fig. 9: The shearing part of the joint stiffness $\overline{k}_{\text{shear}}$ versus the inclination angle α for the cases of similar and dissimilar properties for the two joint components, respectively (for parameters, $\beta_{s,l} = 1.4$, $\beta_{\text{h}} = 2$ and $\mu = 0.5$).

In this case, the difference in shear stiffness or slip modulus of the joint is as much as 40 % between the two models for screws perpendicular to the shear plane ($\alpha = 0$).

With respect to withdrawal action, it should be noted that the withdrawal stiffness for the head part of the screw can be smaller than the tip part because the timber in the head part is penetrated twice with a screw that has possible different thread patterns and thread diameters in the different parts and that can damage the timber around the head part of the screw. Tomasi et al. [6] report that experimental results showed in various cases that, when the specimens were opened after their collapse, the head of the screw had penetrated the timber side member by up to 4 cm, while the tip had remained in their initial position. This led them to suggest that the withdrawal stiffness was much higher in the tip part of the screw than that of the head part. If we assume that the withdrawal stiffness in the head part of the screw is reduced to 50 % of that of the tip part, i.e. the β_{ax} -value changes from $\beta_{ax} = 1$ to $\beta_{ax} = 0.5$, the effect is shown in Fig. 10.

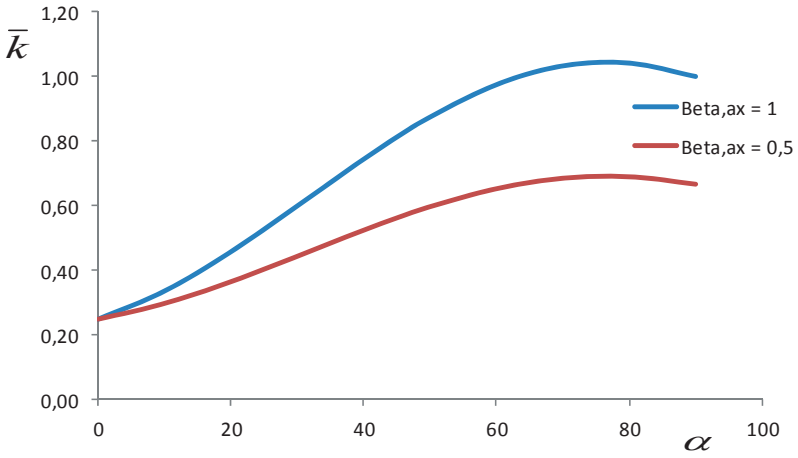

Fig. 10: The total joint stiffness $\overline{k}$ versus the inclination angle α and different ratios between the axial stiffnesses, β_{ax} (for parameters, $\psi_K = 2$, $l_{thr,1}/l_1 = 1$, $\mu = 0.5$, $\beta_{s,l} = 1.4$ and $\beta_h = 2$).

In this case, the difference in total stiffness or slip modulus of the joint is as much as 50 % between the two cases for a screw inclination of $\alpha = 60°$.

3.2 Symons et al. model (2010)

Symons et al. [7] developed a model for inclined screws. They assumed a model where bending and axial deformations of the screw are taken into account. They based their model on the theory of elastic foundation in two dimensions, using foundation stiffness parallel (k_p) and perpendicular to grain (k_t) per unit length of the screw [N/m^2], respectively. They are not explicitly modelling the withdrawal effect, but in a way axial effects are included through the

axial deformations of the screw together with the stiffness parameters in the two directions. To illustrate, if we account only for the axial displacements along the screw within the timber (v), they express the differential force parallel to grain as $\delta F_{\mathrm{p}} = v \sin\alpha \cdot k_{\mathrm{p}} (\delta x)_{\mathrm{ax}} \cos\alpha$ and perpendicular to grain as $\delta F_{\mathrm{t}} = v \cos\alpha \cdot k_{\mathrm{t}} (\delta x)_{\mathrm{ax}} \sin\alpha$, where $(\delta x)_{\mathrm{ax}}$ is the differential length along the screw (x is a distance from the shear plane). (It is noted that the length perpendicular to grain is $(\delta x)_{\mathrm{ax}} \cos\alpha$ and parallel to grain is $(\delta x)_{\mathrm{ax}} \sin\alpha$). The corresponding axial force along the screw can then be written as $\delta F_{\mathrm{ax}} = v[(k_{\mathrm{p}} \sin\alpha + k_{\mathrm{t}} \cos\alpha)\sin\alpha\cos\alpha](\delta x)_{\mathrm{ax}}$. The expression in the brackets can be interpreted as a type of "withdrawal or shear" stiffness, but the parameter does not contain any withdrawal type of stiffness values.

Their way of modelling renders zero stiffness with respect to the axial effects for both the inclinations $\alpha = 0°$ and $\alpha = 90°$. For large inclinations, the screw will act more in a shearing mode with respect to the timber and axial deformations, but still they are using foundation modulus valid for compression. Their model including bending and extension of the screw is closer to reality than the present model, which assumes a rigid screw, both with respect to bending and tension. However on the other hand, Symons et al. use some other simplifying assumptions in order to find explicit solutions to their problem. Also, as mentioned, it is questionable to use stiffness parameters that are applicable to compression also for some kind of shearing or withdrawal stresses.

With their model they are capable of estimating the practical limit for the embedment depth with respect to the shearing action and an optimum value for the inclination (α) of long screws for which the stiffness is maximum and the behaviour is dominated by axial deformations. They are studying a concrete-timber composite element and they assume that the screw is fixed in the concrete. The only deformations that occur are those in the timber component.

In order to compare with Symons et al. model, some changes need to be made in the present model. We will evaluate two different alternatives. First, if we still use the assumption of a totally rigid screw and accept their assumption of fixity in the concrete, no rotation takes place of the screw in the timber member. It means that the screw acts as a "plow" with an evenly distributed embedment load on it. Proceeding as in section 2, we then arrive at the following expression for the stiffness,

$$k = d\, l_{\mathrm{l}} \cos\alpha \left\{ \left(\cos\alpha - \mu \sin\alpha\right) K_{\mathrm{h},\alpha,1} + \sin\alpha \left(\tan\alpha + \mu\right) K_{\mathrm{ax,eff,1}} \frac{l_{\mathrm{thr,1}}}{l_{\mathrm{l}}} \right\} \tag{49}$$

This equation represents some kind of an upper value.

Second, for a model more on the lower end, we assume that the screw can bend as a cantilever and rotate elastically in the fixing point at the shear plane. If we calculate the spring stiffness of that moment, $k_{\mathrm{m}} = M_{\mathrm{m}} / \theta$, as the deflection at the tip of the screw and the rotation corresponding to that deflection divided by the length of the screw, $\theta = \delta_{\mathrm{l}} / l_{\mathrm{l}}$, we arrive at $k_{\mathrm{m}} = 4EI / l_{\mathrm{l}}$, where EI is the bending stiffness of the screw. (If we assume a point load at the tip of the screw, evenly or triangularly distributed load over the screw length, the rotational stiffness varies between, $3EI / l_{\mathrm{l}} \le k_{\mathrm{m}} \le 5EI / l_{\mathrm{l}}$. A mean value is chosen in the relation above.)

The moment according to Eq. (3) should then be equal the moment, M_{m}. Using the Eqs (2), (4) and (12), the distance to the rotation point can be expressed as

$$x_1 = \frac{2}{3} s_1 \left(\frac{2k_{\mathrm{m}} \cos^2 \alpha}{K_{\mathrm{h},\alpha,1} d\, s_1^3} + 1 \right)^{-1} = \frac{2}{3} l_1 \cos\alpha \left(\frac{2k_{\mathrm{m}}}{K_{\mathrm{h},\alpha,1} d\, l_1^3 \cos\alpha} + 1 \right)^{-1} \tag{50}$$

Using a moment stiffness value of $k_{\mathrm{m}} = 1.7 \times 10^6$ Nmm for the example screw type used in this paper, we find that $x_1 \approx (2/3) s_1 = (2/3) l_1 \cos\alpha$ (for inclination values, $0° \le \alpha \le 67.5°$, the deviation from the approximate x_1-value is 1.6 % – 4.0 %). Eqs (7), (9), (12), (17) and (21) give the following stiffness value ($k = F_1 / \delta_1$)

$$k = d\, l_1 \cos\alpha \left\{ \frac{1}{4} \left(\cos\alpha - \mu \sin\alpha \right) K_{\mathrm{h},\alpha,1} + \sin\alpha \left(\tan\alpha + \mu \right) K_{\mathrm{ax,eff},1} \frac{l_{\mathrm{thr},1}}{l_1} \right\} \tag{51}$$

This equation represents some kind of a lower value.

Symons et al. present a stiffness expression for the limiting case of a perpendicular driven screw ($\alpha = 0°$). For small embedment lengths ($l_1 < 2.3\, d$), there is negligible bending of the screw and the stiffness is given by $k_{\mathrm{Symons}} = k_{\mathrm{p}} l_1$ [N/m], where k_{p} [N/m^2] is the foundation modulus parallel to grain used in their model, i.e. the stiffness is proportional to the length of the screw (consequently, no bending stiffness of the screw appears in the expression) . According to Eq. (49), which is the equation relevant in this case because there is no bending of the screw, the corresponding stiffness is given by $k = K_{\mathrm{h},\alpha,1} d\, l_1$ [N/m], which is also proportional to the embedment length. The relationship between the two stiffnesses is then

$$K_{\mathrm{h},\alpha,1} d\, l_1 = k_{\mathrm{Symons}} = k_{\mathrm{p}} l_1 \quad \text{or} \quad K_{\mathrm{h},\alpha,1} d = k_{\mathrm{p}} \tag{52}$$

Symons et al. use a foundation modulus value of $k_{\mathrm{p}} = 1100$ N/mm^2. These things are indirectly addressed in part 2 of the companion papers [11].

Symons et al. also present a stiffness expression for the limiting case of a very long screw ($l_1 \to \infty$). For inclination values of the order of $\alpha = 60°$, maximum stiffness values are obtained and the stiffness is proportional to $k_{\mathrm{Symons}} \to \sqrt{k_{\mathrm{p}} (EA)_{\mathrm{screw}}} \to d \sqrt{k_{\mathrm{p}} E_{\mathrm{screw}}}$, where *EA* is the axial stiffness of the screw. It is noted that the foundation modulus parallel to grain appear in the expression even though the stiffness is governed mainly by axial deformations and, therefore, by shearing or withdrawal type of stresses in the timber. This is a questionable way of modelling of the axial effect. For a rigid screw in tension, the stiffness tends to infinity.

Both Symons et al. model and the present model do not predict the stiffness of the joint in an accurate way for large inclinations, but for different reasons. However, large inclinations are not practical.

4 Conclusions

The model presented in this paper can predict the slip modulus of inclined screws in shear-tension in timber-to-timber connections. It models both dowel and withdrawal action. It is valid in the elastic or linearized stage of the load-slip relationship in the serviceability limit state. The two parts of the joint can be of different properties (different embedment and withdrawal stiffnesses) and different geometries (embedment lengths or timber member thicknesses), the screw can be fully or partially threaded and friction between the members can be included. The screw is assumed rigid and the withdrawal stress uniform. The model is capable of predicting the effect of embedment lengths and optimum inclination angle for dissimilar properties and geometries of the two parts of the connection. Also, the criteria for the applicability of the model are also presented.

As expected, the withdrawal effect is dominant for large inclinations, while the dowel effect dominates the behaviour for screws installed with inclinations close to perpendicular to the shear plane. For ordinary conditions, the embedment stiffness can be neglected for inclinations $\alpha > 45°$, but the withdrawal stiffness have an effect already from rather small inclinations.

The effect of taking dissimilar properties and geometries between the two parts of the joint into account is large for different embedment stiffnesses and small inclinations with respect to dowel action. With respect to withdrawal action, it should be noted that the withdrawal stiffness for the head part of the screw can be substantially smaller than the tip part. This effect of dissimilar withdrawal properties should generally be taken into account, but the difference between the stiffness of the head and tip need to be experimentally verified first.

Acknowledgements

The authors would like to express their sincere appreciation for valuable comments and contributions to the paper by Professor Bo Källsner, Linnaeus University, Department of Building Technology, Växjö, Sweden.

They also would like to give their sincere thanks for the financial support from the County Administrative Board in Norrbotten, the Regional Council of Västerbotten, the European Union's Structural Funds – The Regional Fund, the centre for Lean Wood Engineering, and the Swedish governmental agency for innovation systems (VINNOVA).

References

[1] European Committe for Standardization (CEN). EN 1995-1-1:2004 (E). Eurocode 5 Design of timber structures: CEN; 2004.

[2] Bejtka I, Blass HJ. Joints with Inclined Screws. Proceedings of the CIB-W18 Timber Structures Meeting, Japan, 2002, Paper 35-7-5.

[3] Johansen KW. Theory of Timber Connections. International Association of Bridge and Structural Engineering. 1949;9:249-62.

[4] Kevarinmäki A. Joints with Inclined Screws. Proceedings of the CIB-W18 Timber Structures Meeting, Japan, 2002, Paper 35-7-4.

[5] Blaß HJ, Bejtka I, Uibel T. Trägfähigkeit von Verbindung mit selbst bohrenden Holzschrauben mit Vollgewinde. Karlsruher Berichte zum Ingenieurholzbau: Lehrstuhl für Ingenieurholzbau und Baukonstruktionen; 2006.

[6] Tomasi R, Crosatti A, Piazza M. Theoretical and experimental analysis of timber-to-timber joints connected with inclined screws. Construction and Building Materials. 2010;24(9):1560-71.

[7] Symons D, Persaud R, Stanislaus H. Slip modulus of inclined screws in timber-concrete floors. Proceedings of the Institution of Civil Engineers: Structures and Buildings. 2010;163(4):245-55.

[8] Ellingsbo P, Malo KA. Withdrawal capacity of long self-tapping screws parallel to grain direction. 12th World Conference on Timber Engineering, Auckland, New Zealand, 15-19 July 2012.

[9] Gelfi P, Giuriani E, Marini A. Stud shear connection design for composite concrete slab and wood beams. Journal of Structural Engineering. 2002;128(12):1544-50.

[10] Deutsches Institut für Bautechnik (DIBt). Zulassung Z-9.1-472 - SFS Befestiger WT-T-6,5, WT-T-8,2 und WR-T-8,9 als Holzverbindungsmittel. 2006.

[11] Jacquier N. Stiffness model for inclined screws in shear-tension in timber-to-timber joints – Part 2: Evaluation and parameter study

Appendix A: Second order expression for axial displacements of the screw

For the rigid fastener in a deformed state, consider Fig. 2, cf. Bejtka and Blass [2]. In the general case when the two components differ with respect to material properties and geometry, the axial displacements may move the fastener across the interface between the two components.

The total axial displacement of the screw can be expressed as

$$\begin{aligned}\delta_{ax} &= \delta_{ax,1} + \delta_{ax,2} = \sqrt{(x_1+x_2)^2 + (x_1\tan\alpha + \delta_1 + x_2\tan\alpha + \delta_2)^2} - \frac{x_1+x_2}{\cos\alpha} \\ &= \frac{x_1+x_2}{\cos\alpha}\left\{\sqrt{1+(\frac{\delta_1+\delta_2}{x_1+x_2}+\tan\alpha)^2}\cos\alpha - 1\right\} = (l_1+l_2)\left\{\sqrt{\cos^2\alpha + (\frac{\delta}{l_1+l_2}+\sin\alpha)^2} - 1\right\}\end{aligned} \tag{53}$$

For comparisons with Eq. (18), assume an ordinary screw, $l_1 = l_2 = 100$ mm and $\alpha = 45°$. We then have

$$\begin{aligned}&\delta_{ax} = 200\left\{\sqrt{\frac{1}{2} + (\frac{\delta}{200} + \frac{1}{\sqrt{2}})^2} - 1\right\}; \quad \text{Second order} \\ &\delta_{ax} = \frac{\delta}{\sqrt{2}}; \quad \text{First order}\end{aligned} \tag{54}$$

The comparison between the first and second order is shown in Table A.1.

Table A.1 Comparison between first and second order axial displacements

δ [mm]	Second order δ_{ax} [mm]	First order δ_{ax} [mm]	Difference [%]
0.5	0.354	0.354	0
1	0.708	0.707	0.1
2	1.42	1.41	0.4
3	2.13	2.12	0.5
5	3.57	3.54	0.9

It is obvious that the first order approach is adequate in the present model.

Paper V

Stiffness model for inclined screws in shear-tension in timber-to-timber joints – Part 2: Evaluation and parameter study

by Nicolas Jacquier

Draft to be Submitted

Stiffness model for inclined screws in shear-tension in timber-to-timber joints – Part 2: Evaluation and parameter study

Nicolas Jacquier
Division of Structural and Construction Engineering – Timber Structures, Luleå University of Technology, SE-971 87 Luleå, Sweden

Abstract

Stiffness of joints with inclined screws is important due to its widespread use in timber construction. In the serviceability limit state modelling of joint stiffness is crucial to properly capture mechanical behaviour. A new prediction model for the stiffness of joints with inclined screws was derived in the companion paper (Part 1). The model captures the contributions from embedding, withdrawal, and friction in the joint. The input parameters for the embedding and withdrawal stiffness for this model are not directly available in literature. This is due to the fact that some of them are not possible to test using the standards of today. The aim of this research is to propose possible test set-ups for these parameters and evaluating their impact through a parameter study. The parameter study is made analytically and the results are compared to test results available in literature. The results show that the parameters needed to confirm the proposed model are not fully available and thus the fit with experimental results is not convincing.

1 Introduction

Joints with inclined screws are increasingly used in timber structures, both in renovations and new constructions. Inclined screws can be used for assemblies between different timber building components or within building components, i.e. in mechanically jointed timber composite members. The load-displacement or stiffness behaviour in the serviceability limit state (e.g. with respect to deflection and vibration) is an important aspect which needs to be further investigated for the case of inclined screw joints due to the different phenomena taking place simultaneously in the load transfer.

A detailed elastic calculation model for the slip modulus of timber-to-timber joints with inclined screws in shear-tension was derived in the first companion paper [1]. The model requires specific input parameters for the embedment and withdrawal behaviour of the screw at different inclination angles. It is also considered that these values are affected by the simultaneous embedment and withdrawal actions. One of the aims of this paper is to discuss the possible test setups for determining

experimentally these parameters. Also this paper aims at evaluating with a parameter study the order of magnitude for theses parameters based on existing results presented in the literature and how sensitive the model is when different values are used. The values taken from the literature are based on existing standard testing methods and do not exactly match the test setups prescribed in this paper and the differences are discussed. This evaluation will allow to judge upon the applicability of the model by comparing the predicted values to some existing test results.

2 Experimental test setup for the stiffness parameters

The model requires the following parameters:

- The screw embedding stiffness parameter per unit area at an angle to the grain $K_{h,\alpha}$ [N/m^3];
- The screw effective withdrawal stiffness parameter per unit area $K_{ax,eff}$ [N/m^3], where the word effective accounts for both the effect due to the withdrawal displacement and possible combined lateral displacement. For convenience, the dependence on the inclination is also included.

The possible tests setups which can be used to obtain theses values are discussed in this section. These tests have not been carried out. This section presents the tests as they should be performed ideally. Some of these tests might however be difficult to carry out from a practical point of view. In all these proposed tests, the main interest is to evaluate the load-deformation or stiffness behaviour.

2.1 Embedding stiffness of partially threaded screws at an angle to the grain

The test setups shown in Fig. 1 and Fig. 2 are proposed to determine the load-displacement response of a half-screw inserted in a timber member and subjected to a force perpendicular to its axis at the intersection between the screw axis and the joint shear plane. The first test setup, Fig. 1, should be used for a screw inserted perpendicular to the shear plane ($\alpha = 0°$). The second test setup, see Fig. 2, can be used to obtain the load-deformation behaviour of the screw for inclination angles up to 60° (ideally tests at different angles with 15° interval should be performed). The limit of 60° is justified by the practical angle application range of joints with inclined screws in shear tension. Eurocode 5 [2] requires an inclination of $\alpha \leq 60°$.The measurement of the displacement perpendicular to the screw axis at the point of load application gives the embedment response at the shear plane position. Two additional measurement of the displacement on the external part of the screw may be used to estimate the rotation of the screw. For rigid type of screws, these measurements can show the rotation angle of the screw within the timber member for a given slip in the shear plane.

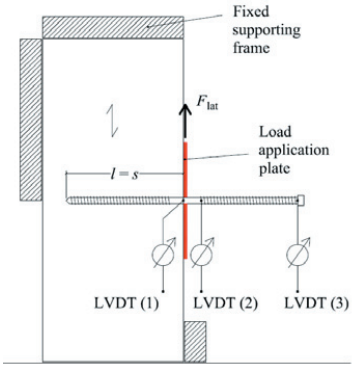

Fig. 1: Test setup for the embedding stiffness $K_{h,\alpha}$ parallel to the grain, $\alpha = 0°$

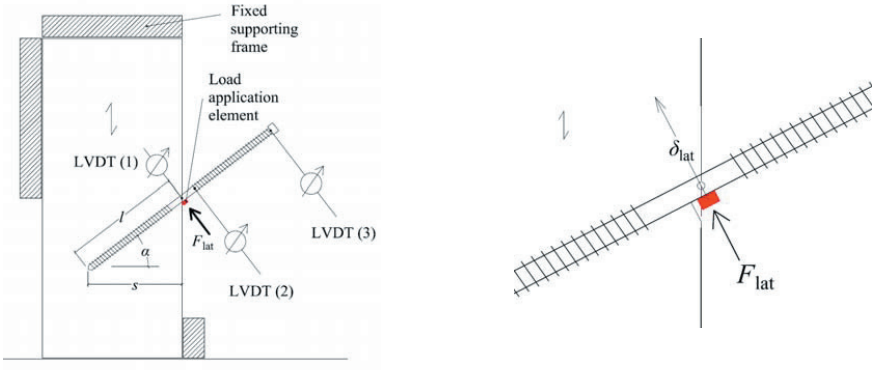

(a) (b)

Fig. 2: (a) Test setup for the embedding stiffness parameter $K_{h,\alpha}$ at an angle to the grain for $0° \leq \alpha \leq 60°$, (b) Needed indentation in the timber below the screw for the load application.

In Fig. 1, the load can be applied on the screw using a perforated steel plate with dimensions such that the screw may be able to rotate when the displacement increases. The plate should be as thin as possible to minimise the eccentricity of the load application (distance between the point of load application and the shear plane). Measures to minimise the friction between the steel plate and the timber member should be used. For inclined screws, a special steel piece should be used to apply the load directly on the screw, see Fig. 2-a. For lower inclination angles, it might also be necessary to make a small indent in the timber member in order to place the steel piece so that the intersection between the load application direction, the screw axis and the shear plane meet at the same point, see Fig. 2-b.

In the first companion paper [1], equations for the moment in the screw and force equilibrium perpendicular to the screw were derived at the shear plane position. These expressions are reported in Eq. (1) and Eq. (2) in terms of $K_{h,\alpha}$, respectively:

$$M = \frac{1}{6} K_{h,\alpha} d \, \delta_{lat} \frac{s^2}{\cos^2 \alpha} \left(2\frac{s}{x} - 3\right); \tag{1}$$

$$F_{lat} = \frac{1}{2} K_{h,\alpha} d \frac{s}{\cos \alpha} \left(2 - \frac{s}{x}\right) \delta_{lat}; \tag{2}$$

where α is the screw inclination according to Fig. 2, s is the distance perpendicular to the slip plane to the screw tip, and x is the perpendicular distance perpendicular from the slip plane to the rotational point of the screw. For more details about the parameters, the reader should refer to the companion paper.

From Eq. (1) and (2), under the assumption of a rigid screw and noting that the moment in the screw is zero at the point of application of the load, the embedment stiffness parameter $K_{h,\alpha}$ [N/m^3], as defined in the companion paper, can be obtained from the load-displacement curve obtained from the test setup shown in Fig. 1 or Fig. 2:

$$K_{h,\alpha} = \frac{4 \cdot F_{lat}}{d \cdot l \cdot \delta_{lat}} \tag{3}$$

where F_{lat} is the lateral applied force, l = s/cos(α) is the length of the screw part inserted in the timber member and δ_{lat} is the embedment measured perpendicular to the screw (LVDT (1) in Fig. 1 and Fig. 2). Testing different screw lengths, diameters and inclination angle, a regression analysis may allow to determine how $K_{h,\alpha}$ varies depending on these parameters.

2.2 Withdrawal stiffness of partially threaded screws at an angle to the grain

The withdrawal tests to obtain the effective withdrawal stiffness parameter should be performed on half-screws inserted in a timber member. Fig. 3a and Fig. 3b show the test setups for a screw under pure withdrawal ($F_{lat} = 0$) and for the screw under combined withdrawal and embedment forces ($F_{lat} \neq 0$), respectively. The angle α should vary from α = 0° to α = 60°, which comprises most of the practical angles of inclined screw joints (ideally with 15° interval). With this test configuration, the effect of different screw lengths, diameters, and ratios of thread lengths over screw lengths could be evaluated.

The withdrawal displacement is measured near the shear plane, directly or deduced from the different measurements presented in Fig. 3. The elongation of the screw may also be measured on the screw part outside of the timber member or in a separated test setup.

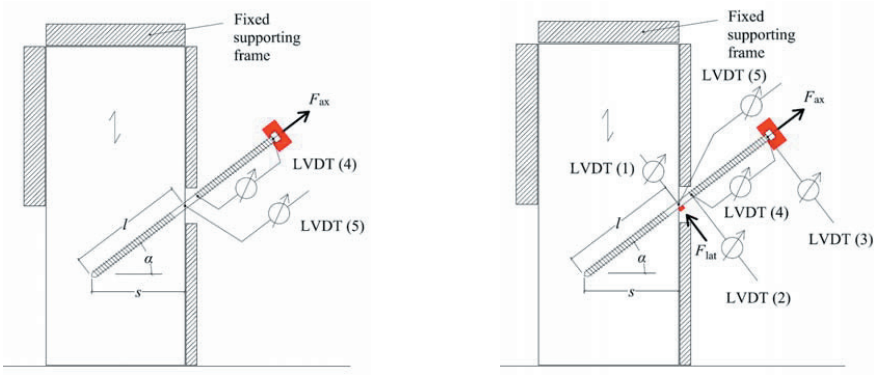

(a) (b)

Fig. 3: Test setup for the effective withdrawal stiffness parameter $K_{ax,\alpha}$ at an angle to the grain for $0° \leq \alpha \leq 60°$

Bejtka and Blass [3] have evaluated experimentally the influence of the embedment due to a lateral force on the withdrawal strength of screws, showing that the withdrawal strength parameter decreases when the combined lateral displacement (embedment) increases. In a similar manner for the stiffness parameters, the test setups shown in Fig. 2 and Fig. 3-a can be combined in order to evaluate the influence of the combined axial force and lateral force application on the withdrawal and embedding stiffness Fig. 3-b.

With $F_{lat} = 0$, the test setup corresponding to Fig. 3-a aims at obtaining the data to determine $K_{ax,\alpha}$. When $F_{lat} \neq 0$, (Fig. 3-b), the data obtained will allow to determine the withdrawal stiffness parameter $K_{ax,\alpha}$ considering both the influence of the screw inclination and the embedment displacement. In practice and to simplify the analysis, $K_{ax,\alpha}$ is not defined explicitly as a function of the lateral displacement, but rather as a reduced value, $K_{ax,eff}$, in line with the suggestion by Bejtka et al. [3] with respect to the withdrawal strength parameter. The subscript 'effective' then refers, in a simplified way, to the effect of the embedment displacement and here also, for convenience, to the influence of the inclination.

The effective withdrawal stiffness parameter is determined based on the applied load F_{ax} and displacement δ_{ax} measured from the LVDT (5) in Fig. 3 according to the companion paper [1] as:

$$K_{\text{ax,eff}} = \frac{F_{\text{ax}}}{\delta_{\text{ax}} \cdot d \cdot l_{\text{thr}}} \tag{4}$$

Double threaded screws (partially threaded), as shown in Fig. 3, can have different thread patterns (pitch) and diameters ($d_{\text{head-side}} > d_{\text{tip-side}}$) on the head and tip side of the screw. The reason why different pitch and outer thread diameter are used is to help tightening the two timber member together when assembling the members. However, during the screwing process, the fact that two different thread patterns pass through one of the timber members (member where the head of the screw is located) can have an influence on the withdrawal behaviour, as the timber around the screw may have been somewhat damaged. Additional investigations should therefore be carried out to determine whether there is a difference between the withdrawal stiffness of the two different threaded parts of the screws. Tomasi et al. [4] report that experimental results showed in various cases that, when the specimens were opened after their collapse, the head of the screw had penetrated the timber side member by up to 4 cm, while the tip had remained in their initial position. This led them to suggest what they call a single stiffness model that will be discussed later in section 5. With the same type of screws (SFS Intec WT-T) Jacquier and Girhammar [5], [6] observed however in shear tests between glulam and CLT members assembled with screws inclined at 45° that the withdrawal of the screw could occur in both timber members, with a tendency to be initiated more often in the glulam member (where the tip of the screw was located), indicating a different result than what was observed by Tomas et al.

To evaluate the withdrawal stiffness on the head side to the screw the same test setup than in Fig. 3-a and Fig. 3-b can be used, inserting the screw from the bottom left side. The thickness of the timber member may be chosen so that the screw head only reaches the outer surface of the timber member. Alternatively the screw head can be further driven in the timber, as it is sometimes done to protect the joint against fire. In order to apply the withdrawal force on the screw a different gripping device than in Fig. 3 must be used. Carrying out these tests is also interesting in order to evaluate the influence on the screw head contribution on the withdrawal stiffness.

3 Determination of stiffness parameters from the literature

The experimental studies suggested in section 2 have not been performed yet. However, the order of magnitude of the stiffness parameters can be estimated based on other similar experimental results available in the literature.

3.1 Foundation modulus

The embedding stiffness parameter $K_{h,\alpha}$ [N/m^3] corresponds in a way to the foundation modulus, noted $K_{f,s}$ [N/m^3] in this paper, which can be obtained using standard methods for determining the embedding strength of dowel type fasteners. The standard methods commonly used are based on the EN 383 [7] and ASTM D5764 [8]. The two methods differ by the way the load is applied. In the EN 383, see Fig. 4-a, the fastener is installed through a full hole in the timber member. The load is applied on the fastener on each side of the timber member. This configuration generates some bending moment in the fastener, but still the stress distribution is usually assumed uniform. The thickness of the timber member is therefore limited to 1.5*d* - 4*d* to reduce this effect. In the ASTM D5764, Fig. 4-b, the fastener is installed in a half-hole. The load can in this way be applied directly over the fastener, avoiding the creation of the bending moment in the fastener and the stress distribution will become uniform. Embedment tests for screws are less common and are not within the scope of EN 383 while they are covered by the ASTM D5764 standard.

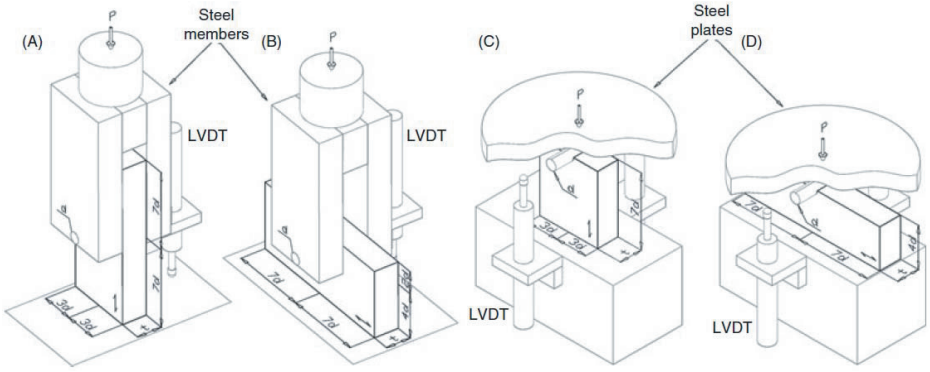

Fig. 4: Embedding test configurations for (a) EN 383 standard: (A) longitudinal compression; (B) radial compression; (c) ASTM D5764 standard: (C) longitudinal compression; (D) radial compression. [9]

Based on the load-deformation data recorded in these tests, the foundation modulus $K_{f,s}$ can be determined according to the EN 383 [7] with Eq. (5):

$$K_{f,s} = \frac{0.4 f_{h,est}}{w_{i,mod}} \tag{5}$$

where $f_{h,est}$ [N/m^2] is the estimated embedding strength and $w_{i,mod}$ is the so called modified initial deformation calculated according to Eq. (6) and Eq. (7), respectively:

$$f_{h,est} = \frac{F_{max,est}}{d \cdot t} \tag{6}$$

where $F_{max,est}$ is the estimated maximum load according to EN 383 [7], d is the fastener diameter and t the timber member thickness, as indicated in Fig. 4;

$$w_{i,mod} = \frac{4}{3}(w_{04} - w_{01}) \quad (7)$$

where w_{01} and w_{04} are the deformations measured at the load $0.1 \cdot F_{max,est}$ and $0.4 \cdot F_{max,est}$ respectively.

The elastic foundation modulus $K_{f,e}$ and the initial foundation modulus $K_{f,i}$ can also be calculated according to EN 383 [7]. However, the foundation modulus $K_{f,s}$ is often the value considered to characterise the stiffness of the connections. The determination of the foundation modulus based on the ASTM D5764 standard is similar and calculated, based on slope of the straight fit line on the linear portion of the load-deformation curve, using also the projected dowel area $d \cdot t$, therefore leading to a value comparable to the foundation modulus $K_{f,s}$ of the EN 383.

Embedment tests for screws are rare and most of the test results available concern dowels. Table 1 shows foundation modulus values obtained from embedding test results available in the literature for various dowel diameters and wood species.

Table 1: Values found in the literature for the foundation modulus parallel $K_{f,s,0}$ and perpendicular $K_{f,s,90}$ to the grain from embedment tests results in the literature.

				Foundation modulus		
	Fastener type / diameter d	Timber	Standard	$K_{f,s,0}$ (St. dev.)	$K_{f,s,90}$ (St. dev.)	Notes
				[N/mm^3]	[N/mm^3]	
Gattesco (1998) [10]	Dowel / 16 mm	Eastern Alps spruce glulam 469 kg/m^3 E_0 = 13117 N/mm^2 E_{90} = 304 N/mm^2	EN 383 modified	73.8 (U) [(a)] 77.3 (C) [(a)]	40.0 (U) [(a)] 55.4 (C) [(a)]	(a)
Gattesco et al. (2004) [11]	Dowel / 16 mm	Eastern Alps spruce glulam 442 kg/m^3 E_0 = 13947 N/mm^2 E_{90} = 288 N/mm^2	EN 383	82.4	45.7	(b)
Gelfi et al. (2002)	Dowel / 12 mm 16 mm 20 mm 48 mm	Alps spruce	-	108.3 81.2 65.0 27.1	-	(c)

Santos et al. (2010) [9]	Dowel / 14 mm	Pinus Pinaster, 550 – 570 kg/m^3	EN 383	113.3 (23.5)	37.2 (8.8)	-
	Dowel / 14 mm	Pinus Pinaster, 584 – 615 kg/m^3	ASTM D5764	120.9 (21.4)	36.0 (8.8)	-
Reynolds et al. (2013) [12]	Dowel / 12 mm 20 mm	Norway spruce	ASTM D5764	81.9 62.7	14.7 11.7	(d)
Reynolds et al. (2013) [12]	Screw / 7.5 mm	Norway spruce	ASTM D5764	72.2	23	(d) (e)

(a) Tests according to EN 383 for the tests with confinement noted (C). Tests without confinement are noted (U), see [10]. Number of tests: 8 parallel, 8 perpendicular.

(b) Number of tests: 30 parallel, 24 perpendicular.

(c) The experimental results for the foundation modulus are not detailed – a single stiffness value $k_w = 1300$ N/mm^2 is reported for all diameters considered (i.e. the foundation modulus expressed as $K_{f,s}$ [N/m^3] depends greatly on the diameter)

(d) Visco-elastic foundation modulus noted K_v in [12]. The authors present three different values for the foundation modulus: a dynamic, a viscoelastic and a total stiffness value. They mention that the so-called viscoelastic foundation modulus represents the stiffness appropriate to calculate the relative displacement due to short term static loading [12].

(e) 7.5 mm is the inner diameter of the screw; the outer thread diameter is 12 mm.

3.2 Withdrawal stiffness of screws

An estimate of the withdrawal stiffness parameter K_{ax} for the screws can be obtained from existing withdrawal tests. The commonly used standards concerning withdrawal tests are the EN 1382 [13] and the ASTM 1761 [14]. Although the test setups in these standards are used essentially to determine the load-carrying capacity of axially loaded screws, it is possible to determine the withdrawal stiffness parameter K_{ax} from the linear part of the load-displacement curve. The standards specify to carry out tests with screws inserted at 0° or 90° angle with respect to the timber grain direction, see Fig. 5 for EN 1383.

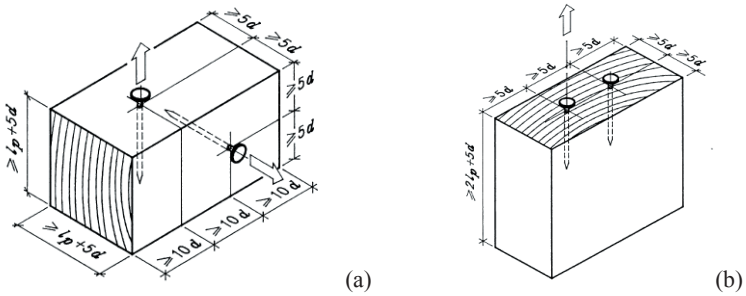

(a) (b)

Fig. 5: Withdrawal test pieces, (a) perpendiculr to the grain, (b) parallel to the grain in EN 1383 [13]

The tests are either carried out on a completely inserted screw in the timber or on a threaded portion of the screw only. In the latter configuration, the screw tip and head are sticking out of the timber member in order to measure the withdrawal behaviour on a homogeneous threaded part only. However, any non-linear distribution of the withdrawal stresses along the screw in a completely inserted screw cannot be captured by this test configuration.

Even though a large amount of withdrawal tests have been performed and reported in the literature, information about the load-displacement or stiffness behaviour remains rare. The displacement involved being very small, these tests are more sensitive to deformations occurring within the test setup, which might explain why these results are not systematically reported. A limited amount of studies has therefore been considered here to estimate the withdrawal stiffness parameter K_{ax}. Experimental results presented in the literature usually correspond to a certain configuration (screw type, thread length, diameter, timber…) and present the axial slip modulus value $k_{ax,test}$ [N/m]. The withdrawal stiffness parameter K_{ax} is estimated considering a uniform stress distribution along the thread with to Eq. (8).

$$K_{ax} = \frac{k_{ax,test}}{d \cdot l_{thr}} \tag{8}$$

Note that it can be argued that the stress distribution along the screw may not be uniform [15] and that the assumption behind Eq. (8) may become questionable. The uniform stress distribution is an assumption used here to simplify the calculation model. It can be mentioned that the model works as well using a stiffness parameter not explicitly depending on the diameter, $k_{ax} = K_{ax} d$ [N/m^2]. It should also be considered that the longer the screw, the higher the influence of the screw axial deformation.

The technical approvals (European Technical Approvals – ETA) of the screw manufacturers usually provide a general formula for calculating the slip modulus of mainly axially loaded screws, valid for

any inclination angle of the screw with respect to the grain direction. In the ETA for SFS-Intec WT-T screws [16], the expression for the axial slip modulus is $K_{ax,ser} = 25 \times l_{ef} \times d$ (in N/mm), where d (in mm) is the outer thread diameter and l_{ef} (in mm) is the effective thread length. In the former technical approval of the SFS-Intec WT-T screws [17] the expression was $K_{ax,ser} = 30 \times l_{ef} \times d$ (in N/mm) and is the value that was considered in Tomasi et al. [4]. These values correspond therefore to the withdrawal stiffness parameter K_{ax} equal to 25 and 30 N/mm^3 as defined in the companion paper [1] (due to lack of experimental data, we use here this value also for $K_{ax,eff}$). Other screw manufacturers recommend to calculate the axial slip modulus, independent of the inclination angle α, as $K_{ax,ser} = 780 \times d^{0.2} \times l_{ef}^{0.4}$ (in N/mm),where d the screw diameter and l_{ef} the penetration length in the timber member are in mm [18, 19], leading to much lower values of withdrawal stiffness than the ETA of SFS-Intec screws in general.

Blass et al. [20] have reported the withdrawal slip modulus for a large variety of screw types and inserted at different angle to the grain. The scatter from the different test results was large and the formula obtained by regression analysis ($K_{ax} = 234 \cdot (d \cdot \rho)^{0.2} \cdot l_{ef}^{0.4}$) leads to low withdrawal slip modulus values compared to the values given in the ETA for SFS Intec screws [16, 17], but comparable to the values obtained according to the ETA for self-tapping screws of Rothoblass [18] and and Spax [19]. It can be noted that the withdrawal test setup used in [20] involved a very small portion of the screw thread and that it is recognised that the obtained values were low [21].

Other authors have reported withdrawal tests results in studies focused on the load carrying capacity of axially loaded screws, therefore not explicitly presenting axial stiffness values. However, from observations on the load-deformation curves presented by Gehloff [22] the withdrawal foundation modulus could be estimated for inclinations angles α = 0°, 45° and 60°. The withdrawal foundation modulus K_{ax} estimated according to Eq. (8) was between 37 N/mm^3 and 16 N/mm^3 for screw diameters between 6 and 8 mm, with effective thread length between 4d and 10d, and for angles α between 0° and 45°. The highest withdrawal foundation modulus values were generally obtained for the screw installed at α = 0°. The values obtained for 60° were significantly lower. In this study, the general trend was that the smaller the diameter, the higher is the withdrawal foundation modulus. The withdrawal foundation modulus was also found to decrease when the effective thread length increases.

Different test setups have been used to consider other angles between the grain direction and the screw axis. Blass and Krüger [23] carried out withdrawal tests on self-drilling screws inserted at 45° angle with respect to the grain direction, see Fig. 6. The screws had 8 mm nominal diameter and the effective thread length in the timber was 80 mm. Thirteen withdrawal tests gave an average

withdrawal slip modulus of $k_{ax,test}$ = 25.4 kN/mm with a coefficient of variation of 25 %, corresponding to a value for the withdrawal stiffness parameter of $K_{ax,45}$ = 39.7 N/mm^3.

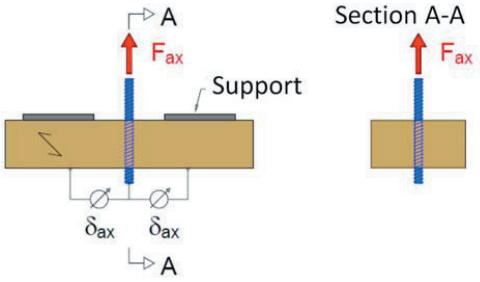

Fig. 6: Withdrawal test setup for self-tapping screws used in Blass and Krüger [23] (the inclination is 45° as indicated in the left figure)

It can be mentioned that as for the embedment stiffness parameter, a value varying depending on the inclination angle may be considered for the withdrawal stiffness parameter as well. It is however assumed that the effect of the angle between the screw axis and grain direction for the withdrawal of screw in joints with inclined screws in shear tension might not be very important. Also, due to the current lack of available results in the literature, only a single value for any angle is considered at the moment.

4 Parameter study

This section presents a parameter study where the influence of the magnitude of each of the parameters $K_{h,\alpha}$, $K_{ax,eff}$, and μ in the new stiffness model is evaluated. First the influence of the magnitude of these parameters is evaluated by modifying one input value at the time for identical conditions in both timber members. In a second part, the influence of varying the input parameters in one of the timber members only is evaluated.

4.1 Reference joint configuration

A reference joint configuration is used with chosen input values based on the review of test results reported in section 3 and discussion below. The input values considered in the parameter study are summarised in Table 2.

The reference joint is a joint with identical conditions in both timber members. The geometrical parameters for the reference configuration are chosen in that way because they match one of the configurations tested by Tomasi et al. [4], which can therefore be used for comparison with 30° and 45° inclination angles. The diameter d considered is the nominal outer thread diameter because other

parameters dependent on the screw diameter were also determined based on the nominal diameter. The choice of the reference friction coefficient is based on values reported in Möhler [24], ranging from 0.25 to 1.0 depending on the surface conditions of the members in contact and of the moisture content of the timber. For spruce and planed surfaces, an average value of 0.3 was measured with a minimum value of 0.223 and a maximum value of 0.675.

The withdrawal stiffness parameter $K_{ax,eff}$ considered is 40 N/mm^3 based on the results reported by Blass and Krüger [23].

Table 2: Input values considered as the reference case for the parameter study

Screw diameter	d	8.2	mm
Total screw length	$l_{ref} = l_{1,ref} + l_{2,ref}$	220	mm
Half screw length	$l_{1,ref} = l_{2,ref}$	110	mm
Thread length in each member	$l_{thr,1,ref} = l_{thr,2,ref}$	95	mm
Friction coefficient	μ_{ref}	0.3	-
Effective withdrawal stiffness parameter	$K_{ax,eff,ref}$	40	N/mm^3
Embedment stiffness parameter parallel to the grain	$K_{h,0,ref}$	60	N/mm^3
Embedment stiffness parameter perpendicular to the grain	$K_{h,90,ref}$	30	N/mm^3

The value selection for the embedment stiffness parameter is more complicated. There is first a certain variation in the values reported in Table 1 depending on the diameter and timber species. Also most of the tests concern dowels with significantly larger diameter than the screw diameter considered in the reference case. To estimate the corresponding embedment stiffness for a screw, the values for dowels should be reduced by a 0.7 factor so that the calculations can be performed using the screw nominal diameter d (outer thread diameter). The value 0.7 corresponds approximately to the ratio d_{ef} / d, with $d_{ef} = 1.1 \cdot d_{core}$ according to Eurocode 5 [2]. Concerning the embedding test result for the screw, the value from Table 1 may be divided by 1.1 to obtain a comparable value. The estimated reference foundation modulus parallel to the grain considering these aspects can therefore be estimated approximately as $K_{h,0,ref} = 60$ N/mm^3.

The results reported in Table 1 indicate also that different values should be considered for the embedment stiffness parameter parallel and perpendicular to the grain. A factor $\lambda_{K,h} = K_{h,0,ref} / K_{h,90,ref}$ [choose another parameter than beta, which we have used before] approximately between 2 and 3 can be found from the values in Table 1. $\lambda_{K,h} = 2$ is considered for the reference case, therefore $K_{h,90,ref}$ = 30 N/mm^3.

The foundation modulus at an angle to the grain $K_{h,\alpha}$ is calculated by analogy with the Hankinson formula as:

$$K_{h,\alpha} = \frac{K_{h,0} \cdot K_{h,90}}{K_{h,90} \cdot \cos^2(\alpha) + K_{h,0} \cdot \sin^2(\alpha)} \tag{9}$$

where $K_{h,0}$ and $K_{h,90}$ are the withdrawal stiffness parameters (or foundation moduli) parallel and perpendicular to the grain, respectively.

4.2 Influence of the magnitude of the main parameters for identical conditions in both timber members

The embedment stiffness and withdrawal stiffness parameters are varied from 0.5 to 1.5 times the reference value. The influence of the friction coefficient is evaluated by varying μ between 0 and 0.6. For all these variations, a diagram of the total joint slip modulus k as a function of the inclination of the screw α is presented. Additionally the ratios k / k_{ref} are plotted.

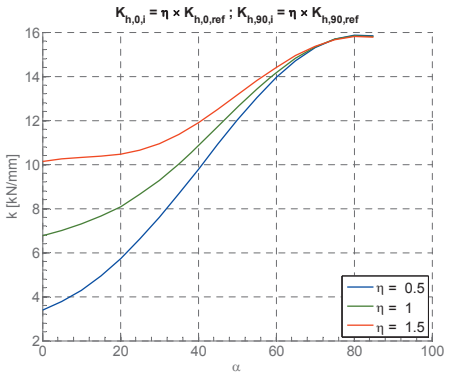

(a)

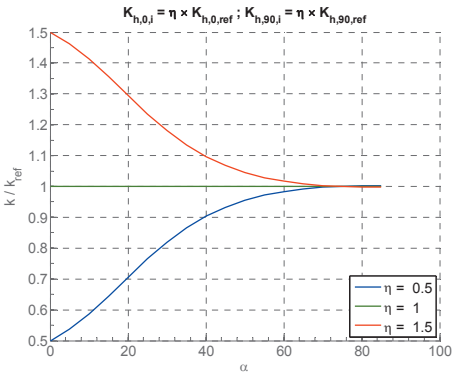

(b)

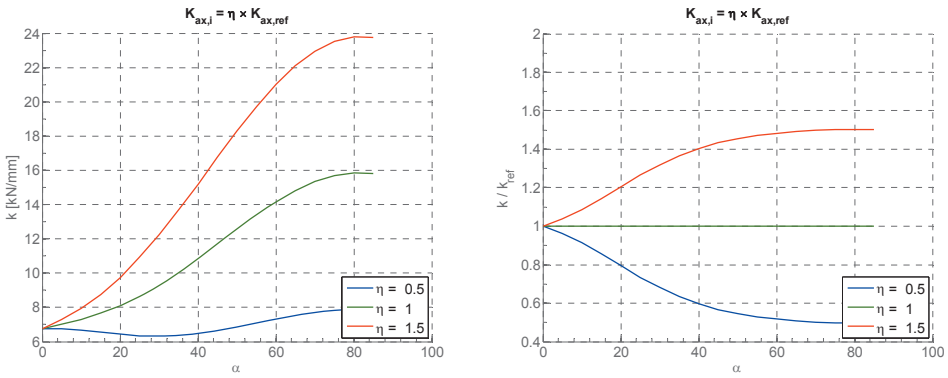

(c) (d)

Fig. 7: Variation of the embedment stiffness parameter $K_{h,ref}$: (a) joint slip modulus k, (b) ratio k / k_{ref} ; Variation of the withdrawal stiffness parameter $K_{ax,ref}$: (c) joint slip modulus k, (b) ratio k / k_{ref} ; where k_{ref} is the slip modulus for the reference case (η = 1)

Fig. 7 indicates that with the order of magnitude of the input values, the effect of an increase or decrease of the withdrawal slip modulus is more important than a change in the same proportions for the embedment stiffness parameter. For the practical range of inclination of inclined screws joints, (between 30 and 45 degrees), the effect of variation of the withdrawal stiffness parameter is already close to the maximum.

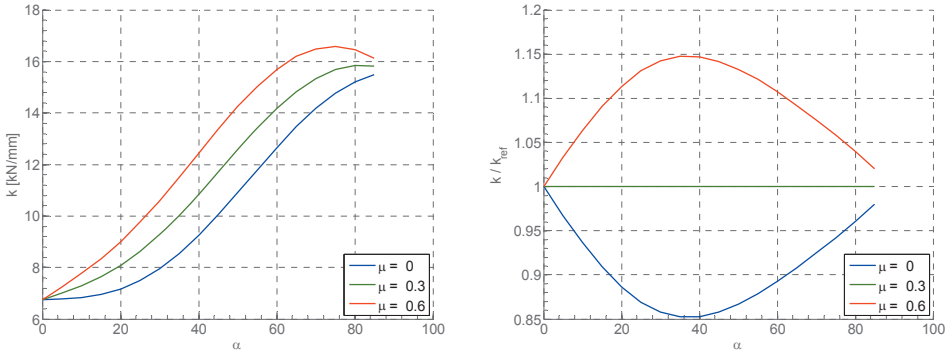

(a) (b)

Fig. 8: Variation of the friction coefficient μ: (a) joint slip modulus $k(\alpha)$, (b) ratio $k(\alpha)$/ $k_{ref}(\alpha)$

The effect of the friction is maximum for an inclination of about 40° for the reference case considered. The angle for which the effect of friction is maximum varies depending on the input values for the withdrawal and embedment stiffness parameters. For the present case, the order of magnitude for the effect of the friction coefficient is within +/- 15 %.

4.2.1 Moment in the screw for the reference case and different inclination angles

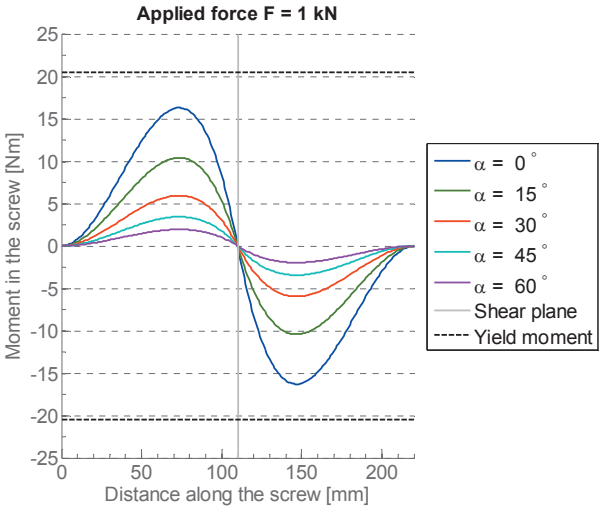

Fig. 9: Bending moment in the screw along the screw axis for an applied load of 1 kN.

Fig. 9 indicates that for the same applied force in the joint F = 1 kN, the magnitude of the yield moment in the screw varies strongly depending on the inclination angle. For the reference case with identical conditions in both timber members, the moment is maximum at a fixed distance from the shear plane in both timber members for any inclination angle. The stiffness model is based on the assumption that the screw is rigid. It can be argued that this assumption can be considered valid until the yield moment in the screw is reached. The yield moment limit shown in Fig. 9 is $M_{y,m}$ = 20.5 N·m (estimated mean value based on the value $M_{y,k}$ = 19.5 N·m given in the ETA for SFS Intec WT-T screw [16] and considering a coefficient of variation of 3 %).

The applied shear force in the joint to reach the yield moment in the screw is shown in Fig. 10 as a function of the angle α. This load level represents the maximum load under which the model is considered valid. The corresponding maximum slip at this load level is also plotted in Fig. 10. The maximum slip values for the reference case range approximately between 0.2 to 0.65 mm, for inclination between 0° to 60°. Note that the axial force contribution in the screw is not considered in this evaluation. While these limit values are relatively low, they are nevertheless close to the yield slip observed for inclined screws at higher inclinations angle ($\alpha \geq 45°$) [6]. The limit slip values for lower inclination angles ($\alpha < 45°$) are considered relatively low.

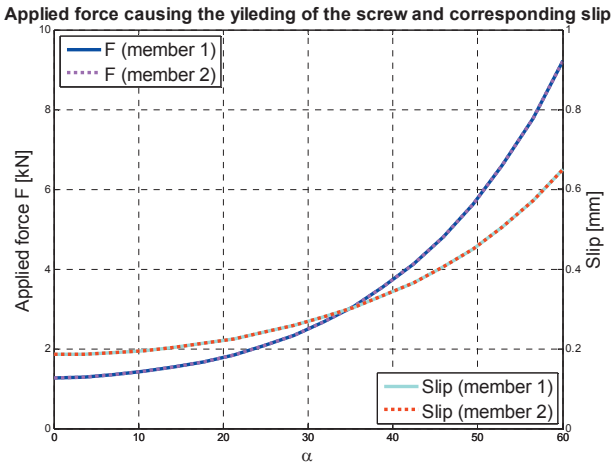

Fig. 10: Force needed to reach the yield moment in the screw and corresponding slip, depending on the inclination angle α.

4.3 Influence of different conditions in the timber members

When varying the embedment and withdrawal stiffness parameters from the reference case in one of the timber members at the time only between 0.5 and 1.5 times the reference value, the diagrams of the joint slip modulus *k* as a function of the screw inclination angle, see Fig. 11, vary in a similar way as for identical conditions (cf. Fig. 7) but with a lower magnitude. The influence of the different embedding behaviour is relatively small in terms of joint slip modulus but affects significantly the moment distribution in the screw. The moment distribution is however not affected when the withdrawal stiffness parameter differ in both member. The same behaviour would be obtained using the double stiffness model Tomasi et al. [4].

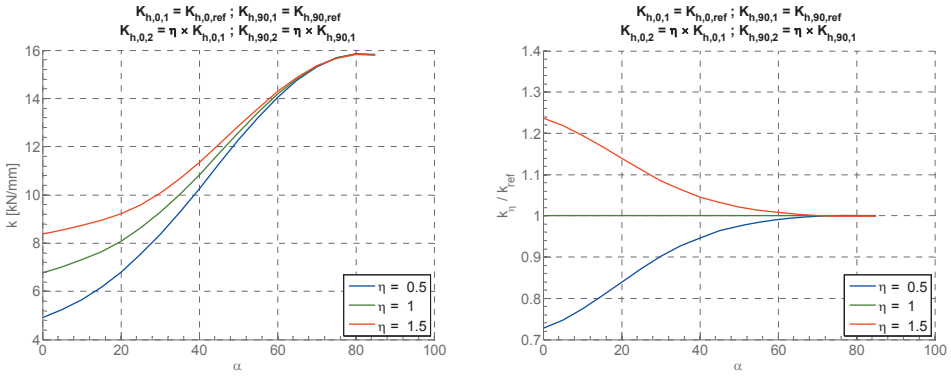

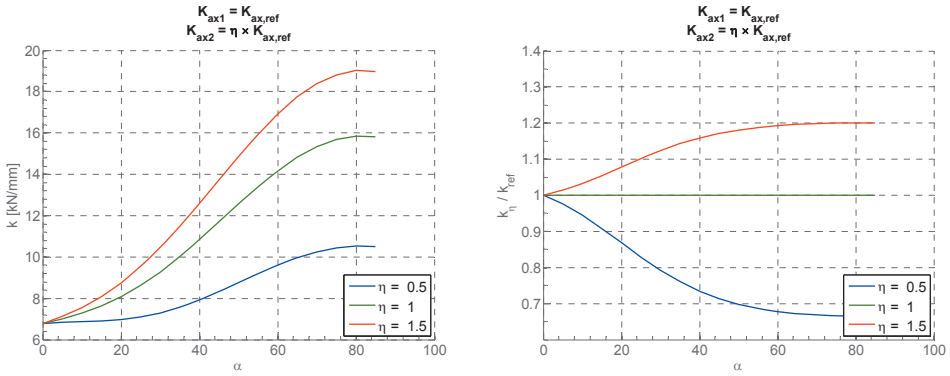

(c) (d)

Fig. 11: Variation of $K_{h,\alpha,2}$ with $K_{h,\alpha,1} \neq K_{h,\alpha,2}$: (a) Joint slip modulus k, (b) Ratio k / k_{ref} where k_{ref} is k for $\eta = 1$; Variation $K_{ax,eff,2}$ with $K_{ax,eff,1} \neq K_{ax,eff,2}$: (c) Joint slip modulus k, (d) Ratio k / k_{ref} where k_{ref} is k for $\eta = 1$

Having different material parameters in each timber member, the moment is different from 0 at the interface (see Fig. 12). The bending moment can reach higher values in one of the members for the same applied load than when conditions are identical, therefore reducing the range of validity of the model.

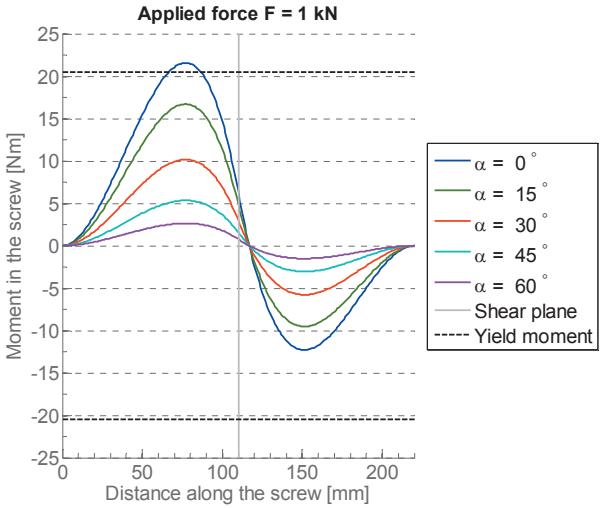

Fig. 12: Bending moment in the screw along the screw axis for an applied load of 1 kN depending on the inclination angle α, for $K_{h,\alpha,2} = \eta \cdot K_{h,\alpha,1}$, and $\eta = 1.5$.

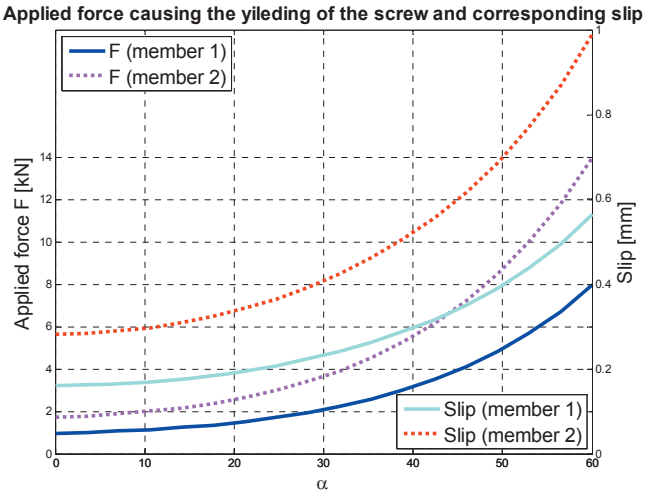

Fig. 13: Force needed to reach the yield moment in the screw and corresponding slip, depending on the inclination angle α, for $K_{h,\alpha,2} = \eta \cdot K_{h,\alpha,1}$, with $\eta = 1.5$.

With non-identical embedding stiffness parameters, the yield limit decreases compared to the case with identical conditions case. In the present case, the limit is below 1 kN for α = 0°. This is partly due to the fact that the screw considered is rather slender. A similar diagram with the same parameters but a shorter screw (l = 160 mm) can be found in Appendix A. The load limit in the timber member 1 is then about 1.5 kN at α = 0°. This indicates that the use of the model for low inclination angle might be limited.

5 Comparison with test results and discussion

Experimental results on inclined screw joints from Tomasi et al. [4] and Jacquier and Girhammar [6] are compared to the new stiffness model and to the stiffness models proposed by Tomasi et al. [4] (double stiffness model (DSM) and single stiffness model (SSM); the difference between these models is briefly summarised below). The test results and calculated values are presented in Table 3 for different joint configurations. The experimental study from Tomasi et al. [4] concerned timber-to-timber joints made with glulam GL24h, while the study from Jacquier and Girhammar [6] concerned an assembly made of glulam GL32h and Cross Laminated Timber (CLT) members. In both studies, the same screw type was used, SFS Intec WT-T screws.

It should be noted that the stiffness values calculated for the new model and for Tomasi et al. models are not directly comparable due to the different input values considered. The stiffness $k_{UAG,NJ}$ is calculated using the stiffness parameter and friction coefficient considered for the reference case in

section 4.1, cf. Table 2. The stiffness k_{DSM} and k_{SSM} according to Tomasi et al. are calculated using the input values considered in the original publication of Tomasi et al., i.e. using the empirical value from the Eurocode 5 for the stiffness of dowel type fasteners for the dowel action and the withdrawal stiffness value given in the technical approval for SFS Intec WT-T screws [17]. Tomasi proposed two different models, the so-called "single stiffness model" and the "double stiffness model". The difference between these models is way the withdrawal stiffness is considered. In the double-stiffness model, the withdrawal is considered to take place simultaneously in the two timber members, as it is also considered in the new model presented here. This assumption seems theoretically correct. The single stiffness model is proposed by Tomasi based on failure observations, revealing that the screws were withdrawn from one member only and seemed not to have moved in the other member. Based on this observation, Tomasi et al. considered that in the serviceability limit state, the screw could be considered fixed in one of the timber members with respect to the withdrawal action. This is equivalent in the new model presented in the companion paper to assume that $K_{ax,eff,1}$ or $K_{ax,eff,2}$ tends towards infinity, which is equivalent to globally multiplying by two the withdrawal stiffness in the joint (springs in series). Despite the fact that this assumption is questionable, the calculations according to this model are presented as well since the agreement with the test results is the best with this assumption, see Table 3.

Whether the assumption of the single stiffness model or if the new model with carefully determined input stiffness parameter should be preferred requires additional work.

Table 3: Comparison between experimental results ($k_{s,test}$) for the joint stiffness and calculated values based on Girhammar and Jacquier [1] ($k_{UAG,NJ}$) and Tomasi et al. models [4] (k_{DSM} and k_{SSM})

		Tomasi et al. [4]				Jacquier et al. [6]	
d	[mm]	8.2	8.2	8.2	8.2	6.5	8.2
l_{tot}	[mm]	190	190	220	220	160	160
α	[°]	0	15	30	45	45	45
$k_{UAG,NJ}$	[kN/mm]	5.84	6.44	9.09	11.62	6.36	8.02
k_{DSM}	[kN/mm]	2.27	3.25	5.64	8.15	4.68	5.95
k_{SSM}	[kN/mm]	2.27	4.53	9.83	15.46	8.64	10.95
$k_{s,test}$	[kN/mm]	2.08	6.18	9.14	16.84	9.70	12.71
$k_{UAG,NJ} / k_{s,test}$		2.80	1.04	0.99	0.69	0.66	0.63
$k_{DSM} / k_{s,test}$		1.09	0.53	0.62	0.48	0.48	0.47
$k_{SSM} / k_{s,test}$		1.09	0.73	1.08	0.92	0.89	0.86

The best agreement between the new model ($k_{UAG,NJ}$) and experimental results is obtained for inclination angles between 15° and 30°. At 0° degree, this model overestimates the stiffness using the stiffness parameters from Table 2. This is due to the fact that when the screw is perpendicular to the shear plane, the dowel action governs and the assumption of a rigid screw is questionable for this screw length. Empirically determined values according to the test setups discussed in this paper may improve the agreement between tests results and calculation for low inclination.

In general it can be mentioned that the values with the new model are lying in between the values obtained from the single stiffness and the double stiffness models, but that with the input parameters considered the new model is not able to predict well the stiffness for screws inclined at 45°. The calculated values are then about 30-35% below the experimental results. For inclinations of 15° and higher the prediction is better than that of Tomasi's double stiffness model, which is comparable.

It can be noted that the value chosen for the withdrawal stiffness parameter was not dependent on the angle α due to the lack of available data in the literature. This might be an effect to be considered in the future. At the moment, only the test results concerning the embedment indicate that the effect of grain direction is important.

It has been shown by Pirnbacher et al. [25] that the withdrawal strength of partially threaded screws is increased by 15% when the thread starts at a distance of at least 2*d* under the timber surface (shear plane). A similar configuration is found for timber-to-timber joints when using SFS Intec WT-T partially threaded screws. While this has been verified with respect to strength, it may be expected to see some increase in terms of stiffness as well. It can be noted also that withdrawal tests are often performed on a small threaded portion of the screw only, which may explain why most of the values present in the literature are somewhat low for the withdrawal stiffness parameter. The withdrawal stiffness parameter obtained from Blass et al. [23] may for example be increased for screws where the thread starts below the timber surface.

Conclusions

In this paper, the principles for new test setups were proposed in order to obtain experimentally the stiffness parameters necessary in the model for inclined screw joints derived in the companion paper. These tests have not been carried out. Approximate values for the stiffness parameters were estimated from the literature based on available results from similar standard tests. It should be noted that there is a difference in the stress distributions and in the behaviour of the screw between what is assumed in the present model and what is obtained from standard tests. The embedding stiffness for screws was

mostly estimated based on embedding test results on dowels parallel and perpendicular to the grain since embedding tests with screws are rare. In the literature, withdrawal tests for screws mostly concern the withdrawal strength; the stiffness is not often reported and values are found to vary significantly between different studies. Formulas for estimating the withdrawal stiffness from different standards for self-tapping screws also provide different values. This might be due to the fact that different proprietary screws do behave differently or that some of the values presented are chosen to be rather conservative.

Considering an ordinary inclined screw joint configuration, several of the input values in the stiffness model were varied around an estimated reference value in order to observe the influence of the parameters on the joint stiffness. As expected, the contribution to the joint stiffness from embedment, withdrawal action and friction varies depending on the inclination of the screw. The withdrawal stiffness parameter has the strongest influence for ordinary inclination angles (between 30° and 60°).

The assumption of a rigid screw in the model combined with using foundation modulus from the literature for the embedding stiffness parameter leads to an overestimation of the slip modulus at low inclinations with this model. The load or slip causing the formation of a hinge in the screw is considered as one of the limits for the validity for the present model. Due to the assumption of a rigid screw this limit is reached at low load levels for screws inserted at angles below 30°. The longer the screw, the stronger is this effect. A more detailed model based on beam on elastic foundation may improve the behaviour of the model in that respect. The present model, which is primarily applicable to connections with screws of shorter lengths and larger diameters, contains a consistent model for the dowel action, which is the dominant behaviour for small inclinations. For inclinations larger than, say 30°, this dowel action less pronounced and the behaviour is mainly dependent on the withdrawal action.

In order to improve the prediction of the slip modulus of inclined screws in shear-tension, a more detailed evaluation of the withdrawal and embedding stiffness parameters are necessary.
Future work should include determining the stiffness parameters experimentally as described tentatively in this paper. With respect to embedment stiffness, the test set-up should allow a stress distribution and a screw behaviour close to the model assumptions and with respect to withdrawal stiffness. The influence of a simultaneous lateral load application on the withdrawal stiffness value obtained from pure withdrawal tests should be accounted for. The dependence on the screw diameter, penetration length, inclination angle and density for the withdrawal and embedment stiffness parameters should be evaluated.

References

[1] Girhammar UA, Jacquier N. Stiffness model for inclined screws in shear-tension in timber-to-timber joints – Part 1: Derivation of the model.
[2] CEN. EN 1995-1-1:2004/A2:2014. Eurocode 5 - Design of timber structures - Part 1-1: General - Common rules and rules for buildings. Brussels, Belgium: European Committe for Standardization; 2014.
[3] Bejtka I, Blass HJ. Joints With Inclined Screws. CIB W18. Japan2002.
[4] Tomasi R, Crosatti A, Piazza M. Theoretical and experimental analysis of timber-to-timber joints connected with inclined screws. Construction and Building Materials. 2010;24(9):1560-71.
[5] Jacquier N. Shear tests on glulam-CLT joints with double-sided punched metal plate fasteners and inclined screws. Luleå Univeristy of Technology2014.
[6] Jacquier N, Girhammar UA. Tests on glulam-CLT shear connections with double-sided punched metal plate fasteners and inclined screws. Construction and Building Materials. 2014;72:444-57.
[7] European Committe for Standardization (CEN). SS-EN 383:2007 - Timber Structures - Test methods - Determination of embedding strength and foundation values for dowel type fasteners.
[8] ASTM International. ASTM D5764 -97a Standard Test Method for Evaluating Dowel-Bearing Strength of Wood and Wood-Based Products (Reapproved 2007).
[9] Santos CL, De Jesus AMP, Morais JJL, Lousada JLPC. A comparison between the en 383 and ASTM D5764 test methods for dowel-bearing strength assessment of wood: Experimental and numerical investigations. Strain. 2010;46(2):159-74.
[10] Gattesco N. Strength and Local Deformability of Wood Beneath Bolted Connectors. Journal of Structural Engineering. 1998;124(2):195-202.
[11] Gattesco N, Toffolo I. Experimental study on multiple-bolt steel-to-timber tension joints. Materials and Structures/Materiaux et Constructions. 2004;37(266):129-38.
[12] Reynolds T, Harris R, Chang W-S. Viscoelastic embedment behaviour of dowels and screws in timber under in-service vibration. Eur J Wood Wood Prod. 2013;71(5):623-34.
[13] European Committe for Standardization (CEN). SS-EN 1382 - Timber structures - Test methods - Withdrawal capacity of timber fasteners. 2000.
[14] ASTM International. ASTM D1761 - 12 - Standard Test Methods for Mechanical Fasteners in Wood. 2012.
[15] Ellingsbo P, Malo KA. Withdrawal capacity of long self-tapping screws parallel to grain direction. World Conference on Timber Engineering (WCTE), Auckland, New Zealand (July 2012)2012.
[16] Österreichisches Institut für Bautechnik (OIB) MoE. European technical approval ETA-12/0063 - SFS self-tapping screws WT. 2012.
[17] Deutsches Institut für Bautechnik (DIBt). Zulassung Z-9.1-472 - SFS Befestiger WT-T-6,5, WT-T-8,2 und WR-T-8,9 als Holzverbindungsmittel. 2006.
[18] ETA-Danmark MoE. European Technical Approval ETA-11/0030 - Rotho Blaas Self-tapping screws. 2012.
[19] ETA-Danmark MoE. European Technical Approval ETA-12/01114, SPAX self-tapping screws. 2012.
[20] Blaß HJ, Bejtka I, Uibel T. Trägfähigkeit von Verbindung mit selbst bohrenden Holzschrauben mit Vollgewinde. Karlsruher Berichte zum Ingenieurholzbau: Lehrstuhl für Ingenieurholzbau und Baukonstruktionen; 2006.
[21] Blass HJ. Private e-mail communation concerning the publication "Trägfähigkeit von Verbindung mit selbst bohrenden Holzschrauben mit Vollgewinde, by Blaß, H. J., Bejtka, I. and Uibel, T. (2006)". 2014.
[22] Gehloff M. Pull-out resistance of self-tapping wood screws with continuous thread: The University of British COlumbia; 2011.
[23] Blaß HJ, Krüger O. Schubverstärkung von Holz mit Holzschrauben und Gewindestangen 2010.
[24] Möhler K, Maier G. Der Reibbeiwert bei Fichtenholz im Hinblick auf die Wirksamkeit reibschlüssiger Holzerbindungen. HOLZ als Roh-und Werkstoff. 1969;27(8):303-7.

[25] Pirnbacher G, Brandner R, Schickhofer G. Base Parameters of self-tapping Screws. Proceedings CIB-W18 Meeting2009.

Appendix

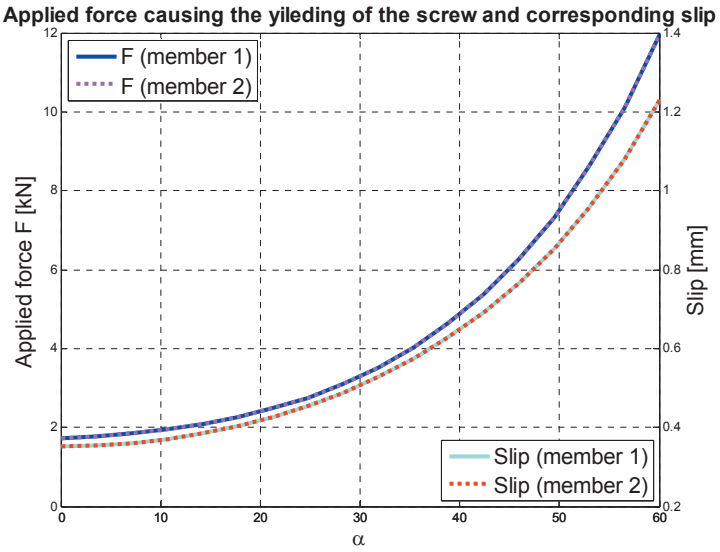

(a)

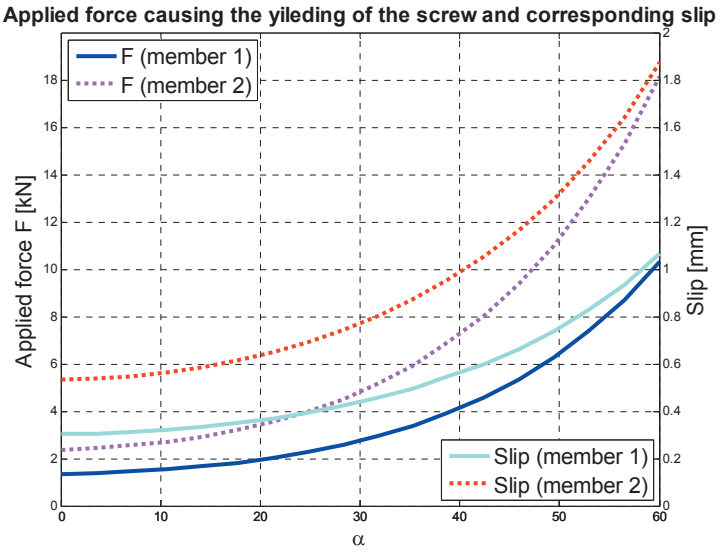

(b)

Figure 14: Yield limit load, and yield limit slip for a SFS-Intec WT-T 8.2 mm diameter screw, *l* = 160mm (a) identical, (b) non-identical